



University of  
**Sheffield**

**Novel functions of UPF1 in  
safeguarding DNA replication  
fidelity in S-phase and beyond**

Thomas Joseph Walne

A thesis submitted in partial fulfilment of the requirements for the degree  
of Doctor of Philosophy.

The University of Sheffield  
Division of Clinical Medicine and Population Health

June 2025

# Table of Contents

<b>List of Figures</b> .....	<b>viii</b>
<b>Abbreviations</b> .....	<b>xiii</b>
<b>Acknowledgements</b> .....	<b>xvi</b>
<b>Abstract</b> .....	<b>xvii</b>
<b>Chapter 1: Introduction</b> .....	<b>18</b>
1.1 DNA replication.....	18
1.1.1 Origin Licensing and Firing .....	18
1.1.2 Fork Elongation .....	19
1.1.3 Replication barriers .....	22
1.2 Transcription.....	23
1.3 Transcription-dependent DNA replication stalling .....	25
1.3.1 Transcription-dependent chromatin accessibility changes.....	25
1.3.2 non-B form DNA structure formation .....	26
1.3.3 Direct transcription-replication collisions (TRCs).....	28
1.4 Molecular mechanisms to prevent or recover stalled replication forks at R-loops and TRCs .....	28
1.4.1 Fork bypass and restart.....	29
1.4.2 Non-B form DNA structure resolution.....	29
1.4.3 Removal of a transcriptional barrier .....	30
1.4.4 Fork reversal .....	31
1.4.5 Origin Firing.....	32
1.5 Common Fragile Sites.....	34
1.5.1 The emergence of under-replicated DNA at common fragile sites .....	35

1.5.2	Under-replicated DNA is processed in G2 or mitosis by distinct DNA synthesis processes .....	37
1.6	Mitotic Checkpoints .....	39
1.6.1	Spindle Assembly Checkpoint.....	39
1.6.2	DNA damage promotes mitotic delay.....	42
1.6.2.1	UPF1 is required for a delay in mitosis following DNA damage...	43
1.7	UPF1 .....	44
1.7.1	Structure and Biochemical Activity .....	44
1.7.2	Nonsense-mediated mRNA Decay .....	46
1.7.2.1	NMD Target Recognition.....	46
1.7.2.1.1	EJC-dependent NMD.....	46
1.7.2.1.2	EJC-independent NMD.....	47
1.7.2.2	UPF1 activation and target degradation .....	48
1.7.3	Alternative RNA Decay Pathways.....	50
1.7.4	Non-canonical roles of UPF1 .....	51
1.7.4.1	DNA replication, repair and the maintenance of genomic stability	51
1.7.4.2	Telomere Homeostasis .....	52
1.7.5	UPF1 in Cancer.....	53
1.8	Aims and Hypothesis.....	54
<b>Chapter 2: Materials and Methods.....</b>		<b>55</b>
2.1	Materials .....	55
2.1.1	Reagents.....	55
2.1.2	Mammalian Cell Lines .....	57
2.1.3	Buffers and Stock Solutions .....	57
2.1.4	Treatment Compounds .....	61
2.1.5	Short interfering ribonucleic acid (siRNA) .....	63
2.1.6	Plasmids.....	64

2.1.7	Antibodies.....	64
2.1.7.1	Primary antibodies .....	64
2.1.7.2	Secondary antibodies .....	66
2.2	Methods.....	67
2.2.1	Mammalian tissue culture.....	67
2.2.1.1	Culture conditions and passaging.....	67
2.2.1.2	Cell freezing and thawing.....	67
2.2.2	Gene manipulation .....	68
2.2.2.1	siRNA transfection .....	68
2.2.2.2	Double transfection of siRNA and cDNA with Dharmafect Duo ...	68
2.2.3	Bacterial culture and plasmid preparation.....	68
2.2.3.1	Bacterial stab inoculation .....	68
2.2.3.2	Transformation of <i>E.coli</i> strain DH5 $\alpha$ .....	68
2.2.3.3	Plasmid purification .....	69
2.2.4	Protein assays.....	69
2.2.4.1	Cell harvesting for SDS-PAGE.....	69
2.2.4.2	Lysate preparation .....	69
2.2.4.3	Protein quantification .....	70
2.2.4.4	SDS-PAGE and western blotting .....	70
2.2.5	Fluorescence-activated cell sorting (FACS).....	71
2.2.5.1	Sample preparation.....	71
2.2.5.2	Propidium Iodide (PI) and BrdU co-staining.....	72
2.2.5.3	Analysis.....	72
2.2.6	Immunofluorescence assays.....	74
2.2.6.1	R-loop quantification interphase .....	74
2.2.6.1.1	S9.6 staining method .....	74
2.2.6.2	R-loop quantification, V5-RNaseH1 <sup>D210N</sup> .....	74

2.2.6.3	Mitotic DNA synthesis (MiDAS) assay .....	75
2.2.6.3.1	Cell plating and treatment .....	75
2.2.6.3.2	Staining method .....	76
2.2.6.3.3	Analysis .....	76
2.2.6.4	53BP1 nuclear body assay .....	76
2.2.6.4.1	Cell plating and treatment .....	76
2.2.6.4.2	Staining method .....	77
2.2.6.4.3	Analysis .....	77
2.2.6.5	DNA replication runover assay .....	78
2.2.6.5.1	Cell plating and treatment .....	78
2.2.6.5.2	Staining method .....	78
2.2.6.5.3	Analysis .....	79
2.2.6.6	DNA fibre analysis.....	79
2.2.6.6.1	Cell plating and treatment .....	79
2.2.6.6.2	DNA extraction and fibre combing .....	79
2.2.6.6.3	Immunodetection of replication tracts .....	81
2.2.6.6.4	Imaging .....	81
2.2.6.6.5	Analysis .....	81
2.2.7	Live cell microscopy .....	82
2.2.7.1	Cell plating and treatment .....	82
2.2.7.2	Imaging .....	82
2.2.7.3	Analysis.....	82
2.2.8	Statistical analysis .....	83
<b>Chapter 3: UPF1 regulates mitotic progression following DNA damage .....</b>		<b>85</b>
3.1	Introduction, aims and hypothesis .....	85
3.2	Results.....	86

3.2.1	UPF1-associated decay factors required for mitotic delay following DNA damage	86
3.2.2	Functionalities required for UPF1 mitotic delay	91
3.2.3	UPF1 inhibitor - VG1, mimics siRNA-mediated UPF1 knockdown with loss of mitotic delay phenotype	95
3.2.4	ATR $\alpha$ Promotes UPF1-dependent mitotic delay	97
3.2.5	UPF1 promotes mitotic delay in an R-loop- and transcription-dependent manner	100
3.2.6	UPF1 <sup>S42A</sup> induced and SMG6-depletion induced mitotic delay are transcription- and R-loop-dependent	103
3.3	Discussion	105
3.3.1	UPF1-dependent mitotic delay likely occurs independently of NMD	106
3.3.1.1	NMD following genotoxic stress and alternative splicing	107
3.3.1.2	SMG1 and the regulation of p53	108
3.3.2	mRNA decay-independent functions of UPF1 affect mitotic timing	109
3.3.2.1	Transcription is required for centromeric identity and faithful mitotic progression	109
3.3.2.2	Centromeric R-loops regulate mitotic progression	110
3.3.3	UPF1 could facilitate DNA replication or repair in mitosis	110
3.3.4	Limitations	112
<b>Chapter 4:</b>	<b>UPF1 in mitotic and interphase DNA replication</b>	<b>115</b>
4.1	Introduction	115
4.2	Results	116
4.2.1	UPF1 promotes mitotic DNA synthesis following replicative stress	116
4.2.2	UPF1 is not required for the occurrence of unscheduled DNA synthesis in G2 prior to mitotic entry of HeLa cells	122
4.2.3	RPE <sup>UPF1 KO</sup> cells also have reduced EdU incorporation in S-phase	128

4.2.4	Validation of replication deficit in UPF1 deficient RPE cells by flow cytometry .....	132
4.2.5	DNA fibre analysis reveals UPF1-deficiency promotes DNA replication fork stalling.....	134
4.2.6	Transcriptional inhibition by DRB rescues DSBs induced by loss of UPF1 in RPE cells .....	138
4.2.7	Transcriptional inhibition prevents the loss of sister fork symmetry in RPE <sup>UPF1 KO</sup> cells .....	142
4.3	Discussion .....	144
4.3.1	Depletion of UPF1 in unperturbed conditions promotes DNA replication fork stalling and DNA damage.....	145
4.3.2	Replication stress induced by loss of UPF1 is transcription-dependent and suggests UPF1-deficiency promotes transcriptional defects that inflict DNA replication stress.....	147
4.3.3	Loss of UPF1 reduces MiDAS frequency under conditions of mild replicative stress .....	148
4.3.4	UPF1 depletion could reduce UR-DNA persisting outside of S-phase, removing a requirement for MiDAS and G2 DNA replication runover .....	150
4.3.5	Limitations .....	152
<b>Chapter 5: Attempt to Quantify R-Loop Levels by Immunofluorescence.....</b>		<b>154</b>
5.1	Introduction.....	154
5.2	Results.....	155
5.2.1	Interphase S9.6.....	155
5.2.2	Metaphase spreads S9.6 .....	158
5.2.3	Interphase D210N RNaseH1 .....	158
5.3	Discussion .....	162
5.3.1	UPF1 prevents spontaneous R-loop formation .....	164
5.3.2	Limitations .....	166
<b>Chapter 6: Discussion .....</b>		<b>167</b>

6.1	A novel function or consequence of UPF1 deficiency .....	167
6.2	UPF1, a predictive clinical biomarker for replication-targeting chemotherapeutics or a therapeutic target.....	169
6.3	Future Work.....	170
<b>References .....</b>		<b>175</b>
<b>Appendix.....</b>		<b>211</b>

# List of Figures

Figure 1.1.1: DNA Replication initiation and elongation .....	21
Figure 1.1.2: Transcription initiation and elongation .....	24
Figure 1.1.3: Transcription-replication collisions, causes and resolution mechanisms .....	34
Figure 1.1.4: The emergence of UR-DNA at CFS following low-level replication stress. .....	36
Figure 1.1.5: The mitotic checkpoint complex governs controls prevents mitotic progression until microtubule attachment. ....	42
Figure 1.1.6: Identification of proteins involved in the regulation of mitotic duration following DNA damage. ....	43
Figure 1.1.7: UPF1 has a conserved helicase domain with unique accessory domains that mediate UPF1-specific functions. ....	46
Figure 1.1.8: UPF1 is the master regulator of Nonsense-mediated decay pathways. .....	49
Figure 2.2.1: FACS gating strategy. ....	73
Figure 2.2.2: Live Cell Microscopy Analysis Strategy .....	83
Figure 3.2.1: siRNA-mediated knockdown of UPF1-associated decay factors. ....	87
Figure 3.2.2: Live cell microscopy analysis of mean mitotic transit time of HeLa cells treated with 1 $\mu$ M carboplatin transfected with UPF1-associated decay factors. ....	91
Figure 3.2.3: Live cell microscopy analysis of mean mitotic transit time of FLP-IN TreX HeLa cells treated with 1 $\mu$ M carboplatin.....	95

Figure 3.2.4: Live cell microscopy analysis of mean mitotic transit time of HeLa cells treated with 1.25 $\mu$ M VG1 in combination with 1 $\mu$ M carboplatin.....	97
Figure 3.2.5: Live cell microscopy analysis of mean mitotic transit time of HeLa cells treated with ATRi or ATMi in combination with carboplatin following depletion of UPF1. ....	99
Figure 3.2.7: Live cell microscopy analysis of mean mitotic transit time of UPF1 <sup>S42A</sup> expressing or SMG6-depleted HeLa cells following treatment with 2 $\mu$ g/ml $\alpha$ -amanitin or RNaseH1. ....	104
Figure 4.2.1: Analysis of UPF1 mutant rescue on the occurrence of Mitotic DNA synthesis following low-dose replicative stress.....	119
Figure 4.2.2: Analysis of 53BP1 nuclear bodies in G1 of HeLa cells treated with low dose aphidicolin. ....	122
Figure 4.2.3: Segregation of asynchronous populations into G1, S and G2 by immunofluorescence.....	124
Figure 4.2.4: Analysis of G2 DNA synthesis in HeLa cells siRNA depleted for UPF1 and treated with 0.4 $\mu$ M Aphidicolin for 24hrs.....	128
Figure 4.2.5: Segregation of asynchronous populations into G1, S and G2 by immunofluorescence in RPE cells. ....	129
Figure 4.2.5: Segregation of asynchronous populations into G1, S and G2 by immunofluorescence in RPE cells. ....	130
Figure 4.2.6: Analysis of EdU and FANCD2 dynamics in RPE <sup>WT</sup> and RPE <sup>UPF1 KO</sup> cells treated with 0.4 $\mu$ M Aphidicolin for 24hrs.....	132

Figure 4.2.7: RPE <sup>WT</sup> and RPE <sup>UPF1 KO</sup> cell cycle distribution with and without treatment of 0.4µM aphidicolin for 24hrs.....	134
Figure 4.2.8: DNA fibre analysis of HeLa cells mock treated, or siRNA depleted for UPF1 with or without treatment with 0.4µM aphidicolin for 24hrs.....	137
Figure 4.2.9: Western blot analysis of RPE cells in response to acute DRB treatment. ....	139
Figure 4.2.10: Western blot analysis of RPE <sup>WT</sup> and RPE <sup>UPF1 KO</sup> cells in response to combination treatments of 0.4µM aphidicolin and 100µM DRB.....	142
Figure 4.2.11: DNA fibre analysis of RPE <sup>WT</sup> and RPE <sup>UPF1 KO</sup> cells untreated or treated with 0.4µM aphidicolin for 24hrs or 100µM DRB for 2hrs. ....	144
Figure 5.2.1: Optimisation and validation of RNaseH1 plasmid by immunofluorescence staining for S9.6 in HeLa cells. ....	157
Figure 5.2.2: Western blot of transfected V5-tagged RNaseH1 <sup>D210N</sup> in SiCtrl and SiUPF1 treated HeLa cells .....	160
Figure 5.2.3: Immunofluorescence microscopy for RPA and V5 in HeLa cells transfected with V5-tagged RNaseH1 <sup>D210N</sup> . ....	162
Figure 6.1.1: Proposed model for spontaneous replication fork stalling and DNA damage, following loss of UPF1. ....	169
Figure A1: Table of p-values for One-way ANOVA analysis of live cell microscopy in Figure 3.2.2.....	211
Figure A2: Table of p-values for One-way ANOVA analysis of live cell microscopy in Figure 3.2.2 continued. ....	212

Figure A3: Table of p-values for One-way ANOVA analysis of live cell microscopy in Figure 3.2.3C. ....	213
Figure A4: Table of p-values for One-way ANOVA analysis of live cell microscopy in Figure 3.2.3D. ....	214
Figure A5: Table of p-values for One-way ANOVA analysis of live cell microscopy in Figure 3.2.5B. ....	215
Figure A6: Table of p-values for One-way ANOVA analysis of live cell microscopy in Figure 3.2.6A. ....	215
Figure A7: Table of p-values for One-way ANOVA analysis of live cell microscopy in Figure 3.2.6B. ....	216
Figure A8: Table of p-values for One-way ANOVA analysis of live cell microscopy in Figure 3.2.7A. ....	216
Figure A9: Table of p-values for One-way ANOVA analysis of live cell microscopy in Figure 3.2.7B. ....	217
Figure A10: Table of p-values for One-way ANOVA analysis of live cell microscopy in Figure 3.2.7C. ....	217
Figure A11: Table of p-values for One-way ANOVA analysis of G1 population changes in Figure 4.2.7. ....	218
Figure A12: Table of p-values for One-way ANOVA analysis of Early S-phase population changes in Figure 4.2.7. ....	218
Figure A13: Table of p-values for One-way ANOVA analysis of Mid-Late S-phase population changes in Figure 4.2.7. ....	219

Figure A14: Table of p-values for One-way ANOVA analysis of G2 population changes in Figure 4.2.7.....	219
Figure A15: FACS Gating for Figure 4.2.7.....	220
Figure A16: Table of p-values for One-way ANOVA analysis of $\gamma$ -H2AX protein changes in Figure 4.2.10. ....	221
Figure A17: Table of p-values for One-way ANOVA analysis of P-Chk1 (Ser345) protein changes in Figure 4.2.10. ....	222
Figure A18: Table of p-values for One-way ANOVA analysis of P-RNAPII CTD (Ser2) protein changes in Figure 4.2.10. ....	223

# Abbreviations

53BP1	TP53-binding protein 1
APC/C	Anaphase promoting complex/ cyclosome
APS	Ammonium persulfate
AS	Alternative splicing
ATM	Ataxia-telangiectasia mutated
ATR	ATM- and Rad3-related
BrdU	Bromodeoxyuridine
Bub	Budding uninhibited by benzimidazole
BubR1	Budding uninhibited by benzimidazole-related 1
Cdc20	Cell division cycle 20
CDK	Cyclin dependent kinase
CFS	Common fragile site
CldU	Chloro-2'-deoxyuridine
CRC	Colorectal cancer
DDR	DNA damage response
DECID	Decay inducing
DMEM	Dulbecco's Modified Eagle's Medium
DMSO	Dimethyl sulfoxide
DNA-PKcs	DNA-dependent protein kinase, catalytic subunit
Dox	Doxycycline
DSB	Double-stranded break
EDTA	Ethylenediaminetetraacetic acid
EdU	Ethyl-2'-deoxyuridine
eIF	Eukaryotic translation initiation factor
EJC	Exon-junction complex
eRF	Eukaryotic translation termination factor
FCS	Foetal calf serum
H2AX	H2A histone family, member X
HCC	Hepatocellular carcinoma
HMD	Histone-mediated decay
HRP	Horseradish peroxidase

IdU	Iodo-2'-deoxyuridine
IF	Immunofluorescence
KNL1	Kinetochore scaffold 1
LADC	Lung adenocarcinoma
MAD	Mitotic arrest deficient
MCC	Mitotic checkpoint complex
MDC1	Mediator of DNA damage checkpoint 1
MELT	Methionine-glutamic acid-leucine-threonine
MiDAS	Mitotic DNA synthesis
MPS1	Monopolar spindle 1
MRN complex	MRE11-Rad50-NBS1 complex
mRNA	Messenger RNA
NHEJ	Non-homologous end joining
NMD	Nonsense-mediated decay
ORC2	Origin recognition complex subunit 2
PABPC1	Poly(A) binding protein cytoplasmic 1
PBS	Phosphate buffered saline
PFA	Paraformaldehyde
Plk1	Polo-like kinase 1
PP2A	Protein phosphatase 2A
PTC	Premature termination codon
RNAP	RNA Polymerase
RNP	Ribonucleoprotein
SAC	Spindle assembly checkpoint
SBS	Staufen-binding site
SDS-PAGE	Sodium dodecyl sulphate polyacrylamide gel electrophoresis
SETX	Senataxin
SMD	Staufen-mediated decay
SMG	Suppressor of morphogenesis in genitalia
SOD1	Superoxide dismutase 1
SSB	Single-stranded break
STAU1	Staufen-1
SURF complex	SMG1-UPF1-eRF1-eRF3 complex

TEMED	Tetramethylethylenediamine
TERRA	Telomeric repeat-containing RNA
TopBP1	DNA topoisomerase II binding protein 1
UR-DNA	Under-replicated DNA
UPF	Up frameshift suppressor

# Acknowledgements

First and foremost, I would like to express my heartfelt thanks to my supervisor, Dr Ruth Thompson, for her unwavering guidance and support throughout my PhD. Your belief in me, and the opportunity you gave me to independently plan and conduct my own research, have been instrumental in helping me develop both professionally and personally. I've grown in confidence and ability more than I ever thought possible. I am also deeply grateful to Professor Carl Smythe for his support and encouragement. Without your belief in me, I would not have had the chance to pursue this opportunity or achieve this milestone. Our long conversations were often a welcome respite from the whirlwind of academic life, I will always appreciate your insight and perspective.

This work would also not have been possible without the generous funding provided by The Humane Research Trust and the continued support of all those who contribute to their vital mission.

To the past and present members of the Thompson, Bryant and Collis labs, thank you for your knowledge, support and the many engaging discussions (and pub lunches!) that enriched both my work and my time here. A special thanks to Dr Nan Li, our brilliant post-doc, for keeping the lab running smoothly, for your vast technical knowledge and for patiently enduring my endless ramblings about UPF1. Thank you to Morgan for the shared bakes, coffee breaks and sweet treats that brightened so many days. Your kindness and company helped me navigate this journey with my sanity intact.

Finally, to my family: thank you to my parents, Robert and Angela, for your unconditional love and endless support and to my brothers, Matt and Alex, for always being there. I am especially grateful to Will, whose love, patience and understanding have been a constant pillar of strength, helping me be my best self through the most challenging moments.

# Abstract

Maintaining DNA replication fidelity is required to allow for the successful duplication of genetic information that will be passed on to the next generation of daughter cells. Interfering with this process leads to replication stress that can promote mutagenesis, double-stranded DNA breaks and loss of genetic stability. The fundamental process of transcription is a well described promotor of DNA replication stress through changes in chromatin dynamics, DNA structure and direct transcription-replication collisions (TRCs). In this thesis, we have identified a novel function for the RNA/DNA helicase UPF1 in preventing harmful consequences between the DNA replicative and transcriptional machineries. Loss of UPF1 resulted in an increase in spontaneous transcription-dependent replication fork stalling, double stranded breaks and an accumulation of R-loops. UPF1-deficient cells following mild replicative stress show a reduced frequency of replication fork stalling, mitotic delay and the DNA replication salvage pathway of mitotic DNA synthesis (MiDAS). However, no increase in markers of under-replicated DNA such as 53BP1 nuclear bodies in the subsequent G1 is observed, suggesting that cells deficient for UPF1 are able to fully replicate their DNA prior to mitotic entry under such conditions. Together these data demonstrate UPF1 as vital for protecting the genome from spontaneous TRCs, most likely through its role in regulating the dissociation of nascent R-loop associated-mRNAs. Loss or down-regulation of UPF1 also represents a potential mechanism whereby cells could display resistance to DNA replication-targeting chemotherapeutics. Targeting UPF1-deficient cancers or UPF1 inhibition with drugs known to synergize with high levels of TRCs such as PARP inhibitors, could be a promising therapeutic approach.

# Chapter 1: Introduction

DNA replication is a fundamental process essential for the faithful transmission of genetic information from one generation to the next. It involves the duplication of the entire genome to ensure accurate inheritance of genetic material during cell division. The complete and accurate duplication of DNA in S-phase is required for the maintenance of genomic stability in actively dividing cells, errors during DNA replication are associated with various human diseases, including cancer and neurodegenerative disorders. Thus, understanding the mechanisms that safeguard DNA replication integrity is of paramount importance for research and clinical applications.

## 1.1 DNA replication

### 1.1.1 Origin Licensing and Firing

Eukaryotic DNA replication begins at numerous sites within the genome known as origins of replication. Due to this, numerous replication complexes, termed replisomes, exist on template DNA simultaneously, requiring precise control to prevent the duplication of sections of the genome more than once. Eukaryotic cells achieve this by dividing replication licensing, the process by which replication origins are defined, and firing, the activation and initiation of DNA replication, in two temporally separate phases (Bleichert, Botchan and Berger, 2017). Licensing occurs during late mitosis and G1, whilst origin firing only occurs once the cells have entered S-phase.

The Origin Recognition Complex (ORC) consisting of ORC1-6, marks sites of replication origins for the precise assembly of pre-replication complexes (pre-RC) which serve as sites of DNA replication initiation. Recruitment of CDC6 and CDT1 in G1 together facilitate the ATP-dependent loading of MCM2-7 which encircles double-stranded DNA (dsDNA), forming the pre-RC (See **Figure 1.1.1.1**) (Dutta and Bell, 1997; Waga and Stillman, 1998; Moyer, Lewis and Botchan, 2006; Bleichert, Botchan and Berger, 2017; Zhai and Tye, 2017; Li *et al.*, 2018). The MCM2-7 double hexamer is the catalytic core of the replicative helicase which establishes the bidirectionality of DNA replication, however it is loaded in an inactive state. As cells enter S-phase, activation of key kinases CDK2-Cyclin E and DDK phosphorylate different members

of the MCM2-7 complex leading to the further recruitment of key replisome components and activation of the MCM helicase complex, whilst also simultaneously preventing further licensing events from taking place (Heller *et al.*, 2011; Kang, Warner and Bell, 2014). These phosphorylation events promote the recruitment of proteins required to form the pre-initiation complex (pre-IC) (see **Figure 1.1.1.2**). Components in mammalian cells include helicase accessory subunits Cdc45 and GINS; firing factors REQL4, Treslin and TopBP1 as well as Pol  $\epsilon$  and MCM10 (Ilves *et al.*, 2010; Kumagai *et al.*, 2010, 2011). Formation of the pre-IC is a key step for the activation of DNA replication, as together they promote the formation of the CMG complex which confers the DNA helicase activity required for DNA replication (see **Figure 1.1.1.3**) (Costa *et al.*, 2011; Yuan *et al.*, 2016).

### 1.1.2 Fork Elongation

Following the initiation of DNA replication and firing of replication origins, the CMG complex facilitates the unwinding of the parental DNA strands to allow for the initiation of DNA replication and generation of ssDNA coated by RPA. This provides a site for DNA replication priming by DNA polymerase  $\alpha$  (Pol $\alpha$ )-RNA primase complex from which DNA synthesis can begin (see **Figure 1.1.1.4**) (Uchiyama and Wang, 2004). Due to DNA polymerases only being able to catalyse the addition of nucleotides in a 5'-3' direction along DNA, the leading strand can be replicated continuously, whilst the lagging strand must be replication discontinuously (Stodola and Burgers, 2017; Aria and Yeeles, 2019). As a result Pol $\alpha$  must catalyse the addition of several RNA primers for lagging strand synthesis, whilst only one primer is required on the leading strand (Collins and Kelly, 1991).

On the leading strand, DNA synthesis is carried out continuously by the highly processive DNA polymerase  $\epsilon$  (Pol $\epsilon$ ), together with accessory factors and the eukaryotic sliding clamp Proliferating Cell Nuclear Antigen (PCNA) in a complex with CMG (see **Figure 1.1.1.5**) (Daigaku *et al.*, 2015; Yeeles *et al.*, 2017). On the lagging strand, DNA synthesis is carried out discontinuously by the DNA polymerase  $\delta$  (Pol $\delta$ ) (see **Figure 1.1.1.5**). Compared to Pol $\epsilon$ , Pol $\delta$  has much lower intrinsic processivity, however this is stimulated to a much greater extent through its interaction with PCNA (Khandagale, Thakur and Acharya, 2020). Pol $\delta$  also possess strand displacement

activity which Pol $\epsilon$  does not which is essential for efficient maturation of Okazaki fragments (Garg *et al.*, 2004). This absence of strand displacement activity of Pol $\epsilon$  seems to be due to its high 3' exonuclease activity which confers a proofreading ability making Pol $\epsilon$  synthesise DNA more accurately than both Pol $\alpha$  and Pol $\delta$ .

For lagging strand synthesis, Pol $\alpha$  synthesises numerous primers along the lagging strand which are extended by Pol $\delta$  to produce short sections of replicated DNA termed Okazaki fragments (see **Figure 1.1.1.5**). When Pol $\delta$  reaches the 5'-end of the preceding Okazaki fragment, it initiates strand displacement synthesis, resulting in the production of a 5' DNA flap containing the RNA primer. Pol $\delta$  limits 5' flaps to a minimal size through DNA synthesis inhibition following successive nucleotide displacement. Additionally, Pol $\delta$  switches between an DNA replication elongation and exonuclease activated form, successively degrading and polymerising the 5' flap. Recruitment of Flap Endonuclease 1 (FEN1), results in the endonucleolytic degradation of the 5' flap, and strand displacement synthesis restarts in order to remove the RNA primer through a process known as nick translation (see **Figure 1.1.1.6**) (Balakrishnan and Bambara, 2013). Excessive strand displacement synthesis can promote the formation of long 5' flaps that can form secondary DNA structures or become coated by RPA, making them resistant to FEN1. In these cases, the 5' endonuclease activity of DNA2 is required to promote the processing of these long flaps to short flaps, that can then be processed by FEN1 (see **Figure 1.1.1.6**) (Masuda-Sasa, Imamura and Campbell, 2006). Once all RNA primers have been removed, the resulting DNA-DNA nick is ligated to form a continuous DNA strand by DNA ligase (Howes and Tomkinson, 2012).

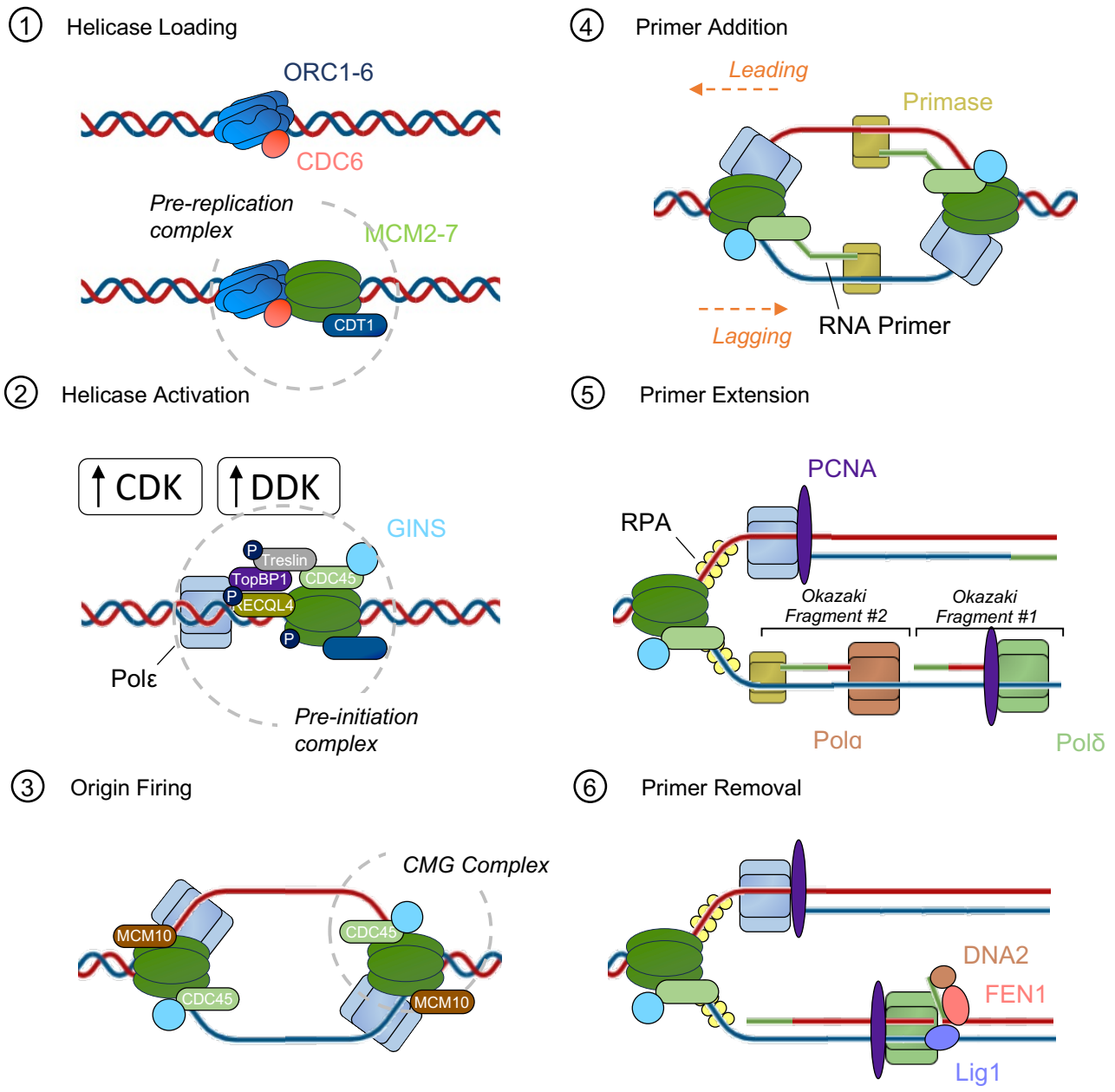


**Figure 1.1.1: DNA Replication initiation and elongation**

(1) Replication origins marked by the ORC complex. ATP-dependent loading of the MCM2-7 double hexamer is facilitated by CDC6 and CDT1, forming the pre-replication complex (pre-RC) in G1. (2) Following S-phase entry increased CDK and DDK activities results in the phosphorylation of Treslin, RECQL4 and the MCM2-7 complex promotes the recruitment of TopBP1, CDC45, GINS and Pol $\epsilon$ , forming the pre-initiation complex (pre-IC). (3) Recruitment of MCM10 to the pre-IC results in the formation of the CMG complex, initiating DNA unwinding. (4) Recruitment of PRIMPOL results in the synthesis of a short RNA primer, initial extension of the RNA primer is carried out by Pol $\alpha$ . (5) Pol $\epsilon$  or Pol $\delta$  then carries out the continuous or discontinuous replication of the leading and lagging strand respectively. (6) Flap processing by FEN1 or DNA2 allows for ligation by DNA Ligase.

### 1.1.3 Replication barriers

Once replication forks have been established there are numerous obstacles they could face before successfully completing DNA replication. These include direct physical barriers to DNA replication, such as DNA lesions or adducts which can arise due to both endogenous and exogenous sources but also dysregulated replication fork progression and origin firing. Generally, anything that poses a risk to the fidelity of DNA synthesis is regarded as DNA replication stress. This can be a hindrance to replication fork progression and can promote replication fork stalling, collapse, and DSB formation.

Ongoing transcription, whereby RNA is directly synthesised from template DNA, can pose as one such block to DNA replication, resulting in transcription-dependent replication stalling (St Germain, Zhao and Barlow, 2021). Transcription is a vital cellular process required for the conversion of information contained within DNA into the RNA for gene expression. All protein-coding mRNAs and most non-coding RNAs including microRNAs (Lee *et al.*, 2004), piwi-interacting RNAs (Li *et al.*, 2013) and long noncoding RNAs (Guttman *et al.*, 2009) are transcribed by RNA polymerase II (RNAPII). RNAPII consists of 12 subunits of Rbp1-12, the largest subunit Rbp1, possesses a highly repetitive carboxy-terminal domain (CTD) consisting of 52 repeats of Tyr1-Ser2-Pro3-Thr4-Ser5-Pro6-Ser7 in humans (Phatnani and Greenleaf, 2006). The CTD is critical in controlling RNAPII function, regulated by phosphorylation at residues Ser2 and Ser5 during transcription (Komarnitsky, Cho and Buratowski, 2000; Morris, Michelotti and Schwinn, 2005).

Whilst transcription and DNA replication share the same template DNA, mammalian cells spatially and temporally separate the two processes. Most transcription occurs in G1 prior to DNA replication initiation, as well as DNA replication and transcription demonstrating physical separation during S-phase, collisions between transcriptional machinery and the replisome still occur (Natsume and Tanaka, 2010; Razin *et al.*, 2011; Meryet-Figuere *et al.*, 2014; Rivera-Mulia and Gilbert, 2016; Marchal, Sima and Gilbert, 2019). Whilst this stalling can occur anywhere across the genome, a subset of large genes, that are over 800Kb in length, are specifically prone to collisions. On these genes, that initiate transcription in G2/M and finish transcription in the subsequent S-Phase, transcription-dependent fork stalling is unavoidable (Helmrich,

Ballarino and Tora, 2011). Transcription-dependent fork stalling occurs frequently in these regions of the genome and potentiate DSB formation due to replicative stress.

## 1.2 Transcription

Transcription initiation typically begins with the loading of general transcription factors (GTFs) prior to RNAPII recruitment to transcription start sites (TSSs) which exist in a promotor region at the 5' end of a gene (Hampsey, 1998) (see **Figure 1.1.2A**). Promotor regions are sufficient to promote transcription initiation though generally have low basal activity, therefore rely on regulatory elements called enhancers binding with transcription factors to promote gene expression. Regulatory elements called repressors, as well as changes in the local chromatin environment can also limit gene expression from a promotor region (Haberle and Stark, 2018). Formation of the preinitiation complex (PIC) at the promotor and subsequent RNAPII activation is required for transcription initiation.

The PIC consists of six GTFs which serve to recruit RNAPII to promotor regions. TFIID recognises core promotor elements, which recruits TFIIA and TFIIB. This allows for the recruitment of TFIIF in complex with RNAPII which allows for the subsequent binding of TFIIE and TFIIH. These proteins constitute the PIC (Zhang *et al.*, 2016) (see **Figure 1.1.2A**). Binding of TFIIH results in the activation of the PIC leading to the unwinding of DNA and phosphorylation of RNAPII at Ser5 in its C-terminal domain (CTD) by CDK7 (see **Figure 1.1.2A**). The RNAPII complex then facilitates the synthesis of a short RNA transcript before undergoing promoter-proximal pausing around 30-60bp downstream of the transcription start site, this occurs due to the interaction of two negative elongation factors, DSIF and NELF (Wada *et al.*, 1998; Yamaguchi *et al.*, 1999; Core and Adelman, 2019). This pausing is thought to allow for 5' end capping and allows for abortive transcription if RNAPII is not converted to an elongation competent form (Ho and Shuman, 1999; Fabrega *et al.*, 2003; Guenther *et al.*, 2007; Haberle and Stark, 2018). RNAPII pausing has also been suggested to be an alternative method of regulating gene expression, by providing an opportunity for the dissociation of engaged RNAPII and through relaxation of the chromatin structure around the core promotor region, allowing for initiation factors to more easily assemble (Gilchrist *et al.*, 2008; Henriques *et al.*, 2013). Phosphorylation of RNAPII

Ser2, NELF and DSIF by the kinase subunit of P-TEFb, CDK9, allows for the dissociation of NELF and the conversion of DSIF into a positive elongation factor and the recruitment of transcription elongation factors and RNA processing factors required for productive elongation (Yamada *et al.*, 2006; Cheng and Price, 2007; Saponaro *et al.*, 2014; Gressel *et al.*, 2017) (see **Figure 1.1.2B-C**).

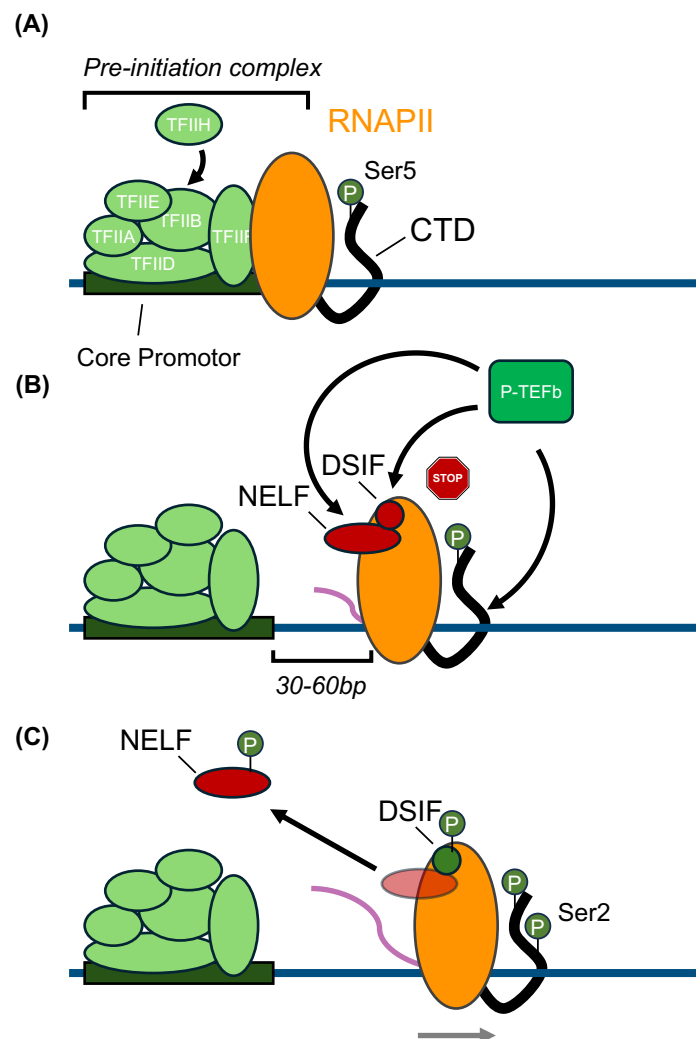


**Figure 1.1.2: Transcription initiation and elongation**

**(A)** Transcription initiation begins through the formation of the pre-initiation complex consisting of six GTFs along with RNAPII at core promoter region and transcription start site. Binding of TFIIH results in RNAPII CTD (Ser5) phosphorylation, DNA unwinding and transcription initiation. **(B)** Promoter-proximal pausing induced by NELF and DSIF 3-60bp downstream of the transcription start site. Phosphorylation of RNAP CTD (Ser2), NELF and DSIF promotes productive elongation. **(C)** Dissociation of NELF and conversion of DSIF into a positive elongation factor promotes RNAPII to continue transcription.

Whilst transcription preinitiation complexes can be effectively bypassed by the replisome, once an RNAP complex enters elongation or termination, the hybridisation of the nascent RNA within the RNAP to the template DNA results in the tight association between the two. This complex is not easily bypassed by the replisome and frequently results in DNA replication fork stalling.

### **1.3 Transcription-dependent DNA replication stalling**

Transcription can be both a direct and indirect block to DNA replication (García-Muse and Aguilera, 2016). Transcription- and associated chromatin modifying-factors can physically block DNA replication through their tight association to DNA. Alternatively, positive supercoiling ahead of transcriptional and replication machineries, or the presence of nascent RNA as a result of ongoing or stalled transcription, which can facilitate the formation of secondary DNA structures, can also impede replication fork progression (see **Figure 1.1.3**).

#### **1.3.1 Transcription-dependent chromatin accessibility changes**

The process of transcription can indirectly block DNA replication by affecting the chromatin accessibility state of DNA or by inflicting topological constraints through negative and positive supercoiling. Unwinding of the DNA duplex results in the accumulation of positive supercoiling ahead of and negative supercoiling behind the RNAPII (Liu and Wang, 1987). This positive supercoiling prevents further unwinding of the DNA duplex, stalling the RNAP (Gartenberg and Wang, 1992; Joshi, Pīa and Roca, 2010), whilst negative supercoiling results in the destabilisation of the DNA duplex which can lead to the formation of secondary DNA structures, capable of impeding replication fork progression (Stolz *et al.*, 2019; Chedin and Benham, 2020).

Cells possess specialised enzymes, termed topoisomerases (Top), which through the formation of transient single-stranded or double-stranded breaks, allow the passage of DNA strands through one another to relieve torsional stress and prevent genomic instability as a result of replication fork stalling and DNA damage (Promonet *et al.*, 2020; Pommier *et al.*, 2022). Top1 is responsible for the resolution of negative supercoiling behind the RNAP, whilst Top2 facilitates the relaxation of positive supercoiling ahead of the RNAP. However, in cases of converging RNAPII complexes

with the replisome, the torsional stress is thought to be too great to be overcome by topoisomerases, resulting in DNA replication fork stalling (Tuduri *et al.*, 2009).

Transcription is greatly affected by changes in chromatin accessibility. Chromatin allows DNA to be packaged within the nucleus but also functions to regulate gene expression. Transcription is impeded by tightly wound regions of the genome, referred to as heterochromatin, which are packaged into nucleosomes and marked by methylation of histone H3 lysine 9 and 27 (Liu, Ali and Zhou, 2020). Whereas, actively transcribed regions of the genome, referred to as euchromatin, are associated with acetylation of histone H3 and H4 as well as di- or tri-methylation of Lys4 of histone H3 (Morrison and Thakur, 2021). In order to overcome the constraints of histone compaction on transcription elongation, RNAPII frequently associates with chromatin remodellers, modifiers and chaperones (Bandau *et al.*, 2024). Whilst chromatin compaction equally impedes replication fork progression in the same manner as it does transcription. The formation of transcription-dependent DNA-RNA hybrid structures induce chromatin compaction, RNAP stalling and transcriptional silencing (Castellano-Pozo *et al.*, 2013; Groh *et al.*, 2014).

### **1.3.2 non-B form DNA structure formation**

DNA typically exists as a canonical B form structure, a double helix consisting of two anti-parallel strands of DNA held together by hydrogen bonding. However, DNA is capable of forming various non-B form or secondary DNA structures, some which are more stable than double-stranded DNA, when unwound during processes such as DNA replication and transcription (Lopes *et al.*, 2011). Such structures include hairpins, triplexes, G-quadruplexes (G4s) and DNA-RNA hybrids. The exact structure which forms depends on the DNA sequence, repetitive tracts and GC content (Treangen and Salzberg, 2011). Trinucleotide repeats, long regions of DNA that possess a three-nucleotide sequence repeated numerous times are known to form secondary structures such as hairpins and triplexes (Lilley, 1980; Panayotatos and Wells, 1981; Mirkin *et al.*, 1987). Regions of the genome which have GC-rich DNA such as telomeres and transcriptional regulatory regions have been shown to form R-loops and G-quadruplexes which can act as a barrier to replication if not properly resolved (Gellert, Lipsett and Davies, 1962).

The coordinated formation of non-B form DNA structures can occur in regions where they carry out a specific physiological function in processes such as immunoglobulin class switching in B cells, mitochondrial and nuclear DNA replication, numerous stages of transcriptional regulation and telomeric homeostasis (Yu *et al.*, 2003; Azzalin *et al.*, 2007; Balk *et al.*, 2013; Arora *et al.*, 2014; Cloutier *et al.*, 2016; Valton and Prioleau, 2016; Dumelie and Jaffrey, 2017; L. Chen *et al.*, 2017; Holt, 2022). However, spontaneous production of these structures, or a disruption to their homeostasis poses a severe threat to genomic stability through, replication stress, transcriptional inhibition, and associated DNA damage (Voineagu *et al.*, 2009; Wang *et al.*, 2011). Secondary DNA structures that impede the replicative helicases and polymerases can result in the uncoupling of the two, leading to the creation of long stretches of ssDNA (Amparo *et al.*, 2020; Kumar *et al.*, 2021; Williams *et al.*, 2023). Displaced ssDNA is highly susceptible to oxidative DNA damage, modifying enzymes and nucleases, as well as the formation of further non-B form DNA structures.

Transcription is a key driver of non-B form DNA structure formation, due to negative supercoiling and the creation of a ssDNA bubble (Jeon *et al.*, 2010; Stolz *et al.*, 2019). Transcription also contributes to secondary DNA structure formation through the creation of DNA-RNA hybrids, through the transient re-association of nascent mRNA with template DNA (Massé and Drolet, 1999; Santos-Pereira and Aguilera, 2015), this occurs frequently following RNAPII pausing or backtracking (Ginno *et al.*, 2012; Skourti-Stathaki, Kamieniarz-Gdula and Proudfoot, 2014) (see **Figure 1.1.3**). DNA-RNA hybrids result in the displacement of non-template strand DNA, forming a structure known as an R-loop (see **Figure 1.1.3C**). Non-B form DNA hinders DNA replication, increasing mutagenesis and genomic instability (Kotsantis *et al.*, 2016, 2020; Kumar *et al.*, 2021; St Germain, Zhao and Barlow, 2021). Mounting evidence suggests that genomic instability associated with R-loops and G-quadruplexes is due to reduced replication fork progression and associated DNA damage.

It is proposed that R-loops associated with deleterious collisions between transcription complexes and the replisome underly the genomic instability associated with R-loop formation.

### **1.3.3 Direct transcription-replication collisions (TRCs)**

Whilst transcription preinitiation complexes can be bypassed by approaching replisomes, conflicts between an elongating or terminating RNAP cannot be as easily avoided and thus result in TRCs. These can occur in two orientations. Co-directional (CD) collisions occur when an RNAP complex on the leading strand encounters the replisome moving in the same direction on DNA, whilst head-on (HO) collisions occur when the RNAP complex on the lagging strand and replisome are moving in opposite directions, towards each other (see **Figure 1.1.3**). In bacteria, CD-TRCs with a single RNAP complex can be bypassed by the replisome and utilise the nascent mRNA as a primer to reinitiate DNA replication (Pomerantz and O'Donnell, 2008; Brüning and Marians, 2021). Not all CD-TRCs can be bypassed in this manner, such as TRCs that occur due to DNA lesions on the template strand. In human cells, CD-TRCs that are encountered by the replicative helicase can be unwound or bypassed by CMG, if the 5' end of the DNA-RNA hybrid is or is not annealed to the template respectively, facilitating resolution of the CD-TRC (Hamperl *et al.*, 2017; Kumar *et al.*, 2021). A stabilised stalled RNAP through backtracking is also sufficient to result in more serious consequences as a result of CD-TRCs.

HO-TRCs are inherently far more deleterious which promote mutagenesis, fork stalling and DNA damage and require recruitment of accessory factors to resolve (Merrikh *et al.*, 2011; Hamperl *et al.*, 2017; Lang *et al.*, 2017; Chappidi *et al.*, 2020). The more severe phenotypes observed at HO-TRCs is attributed partially due to positive supercoiling ahead of both the replisome and transcriptional machinery as well as secondary DNA structure formation which impedes duplex unwinding and replication fork progression respectively (Lang and Merrikh, 2021). ATR-dependent replication fork pausing has been shown to occur at transcription termination sites of highly expressed genes which are enriched for DNA-RNA hybrid structures, to prevent TRCs and the emergence of DNA damage (Promonet *et al.*, 2020).

## **1.4 Molecular mechanisms to prevent or recover stalled replication forks at R-loops and TRCs**

Since TRCs and R-loops pose a serious risk to DNA replication fidelity and thus genomic stability, cells have developed numerous ways whereby they can limit the

occurrence of TRCs. However, in specific regions of the genome TRCs are unavoidable and therefore must be resolved. Some TRCs can be bypassed easily whilst others require the recruitment of specialised protein complexes to facilitate removal of stalled RNAPII, R-loop resolution or replication restart (Lalonde *et al.*, 2021).

#### **1.4.1 Fork bypass and restart**

It has been demonstrated that ‘naked’ R-loops are not a significant replication block when encountered by the replisome alone (Brüning and Marians, 2020). In a CD-orientation, the CMG helicase can translocate over an DNA-RNA hybrid if the 5'-RNA end is flush with the DNA template strand. Additionally, if a free 3'-OH is present on the RNA strand, this can be utilised as a primer for the reinitiation of DNA synthesis by Pol  $\alpha$  (Pomerantz and O'Donnell, 2008). The CMG helicase can also unwind the RNA if it is present as a flap-like structure, with the 5'-end not annealed to the template DNA. DNA synthesis can also reinitiate by the recruitment of PRIMPOL to facilitate repriming of DNA replication after a stalled RNAPII or R-loop (Šviković *et al.*, 2019; Conti and Smogorzewska, 2020) (see **Figure 1.1.3**). Indeed PRIMPOL has been demonstrated to facilitate DNA replication past G4-associated R-loop structures in microsatellite repeats, as well as limiting further R-loop formation, most likely due to the resumption of DNA synthesis at an uncoupled CMG helicase (Šviković *et al.*, 2019). In a HO orientation, the CMG can also bypass ‘naked’ R-loops as long as no secondary DNA structures are present on the displaced ssDNA. If a structure does exist, replication can be reinitiated downstream of the replication block, resulting in the production of a gap. However, when RNAP is present at an R-loop, the manner in which cells deal with such collisions are more complex. R-loop and R-loop associated G-quadruplex formation and their prompt resolution is therefore vital to prevent transcription-dependent replication fork stalling.

#### **1.4.2 Non-B form DNA structure resolution**

Minimising co-transcriptional R-loop formation is vital to prevent rehybridization of nascent RNA with the template DNA and replication fork stalling. The coupling of RNA processing with transcription results in the coating of nascent RNAs with RNA-binding proteins in an attempt to prevent R-loop formation. Consistent with this, depletion of

several RNA processing and export factors leads to spontaneous *cis* R-loop formation (Huertas and Andres Aguilera, 2003; Li and Manley, 2005; Mischo *et al.*, 2011; Pfeiffer *et al.*, 2013; Chakraborty, Huang and Hiom, 2018; Cohen *et al.*, 2018; Cristini *et al.*, 2018; Wood *et al.*, 2020). The resolution of these structures can be facilitated by exoribonucleolytic removal of the RNA by the R-loop resolving enzyme RNase H1, unwinding of the DNA-RNA hybrids by RNA/DNA helicases or the resolution of topological stress by topoisomerases (Petermann, Lan and Zou, 2022) (see **Figure 1.1.3**). DNA-RNA hybrids can also form in *trans*, independent of active transcription (Wahba *et al.*, 2011; Wahba, Gore and Koshland, 2013). Several lncRNAs have been shown to coordinate gene expression through the formation of R-loops with complementary sequences in yeast, plants and human cells showing that this is a conserved mechanism of gene expression regulation (Cloutier *et al.*, 2016; Ariel *et al.*, 2020; Luo *et al.*, 2022).

The ability for an R-loop to directly impede replication fork progression on its own is debated, though R-loops are indeed associated with an increase in DNA replicative stress in a multitude of studies (Li and Manley, 2005; Kotsantis *et al.*, 2016; Chakraborty, Huang and Hiom, 2018). Since the replicative helicase, or several accessory helicases are able to unwind a DNA-RNA hybrid to the same degree as the usual DNA duplex it is unlikely that an R-loop alone is sufficient to block replication fork progression (Brüning and Marians, 2020). However the presence of secondary DNA structures on the displaced ssDNA of an R-loop, such as a G-quadruplex, are sufficient to prevent replication fork progression (Kumar *et al.*, 2021). RTEL1 and FANCI have been implicated in the resolution of G4-associated R-loops and the prevention of TRCs, necessary for replication fork progression (Kotsantis *et al.*, 2020; Sanchez *et al.*, 2020). In addition to this, whilst co-transcriptional R-loops may be passable by the CMG helicase, the associated stalled RNAPII complex, which forms a transcription bubble that encompasses both strands of DNA, is not (Barnes *et al.*, 2015).

### **1.4.3 Removal of a transcriptional barrier**

Whilst non-B form DNA structure resolution is one manner in which DNA replication and transcription can both resume following TRCs, cells will also initiate the removal

of the transcriptional barrier to maintain DNA replication fidelity at any cost. Increased RNAPII occupancy promotes TRCs, demonstrating that an inability for the cell to clear RNAPs can result in replication impediments in several species (Sanchez *et al.*, 2020; Šiková *et al.*, 2020; Hurst *et al.*, 2021). In budding yeast, the ATR ortholog Mec1 has been linked to the targeted degradation of RNAPII complexes following treatment with hydroxyurea, which is required for recovery from replication stress (Poli *et al.*, 2016; Hurst *et al.*, 2021). In mammalian cells, RNAPII removal occurs primarily through subsequent polyubiquitination and degradation of RPB1, the largest subunit of RNAPII (see **Figure 1.1.3**). This process is dependent on RNAPII-CTD S5 phosphorylation. Interfering with these phosphorylation events results in the failure to remove RNAPII from chromatin which promotes TRCs (Landsverk *et al.*, 2020). Ubiquitination of RNAPII also occurs during transcription-coupled nucleotide excision repair (TC-NER). Responsible for the repair of modified nucleotides encountered by RNAPII, TC-NER facilitates polyubiquitination by the Elongin-Cullin complex with Def1, to drive RNAPII removal (Wilson *et al.*, 2013). In lower organisms, the manner in which RNAPII removal is promoted occurs through diverse mechanisms demonstrating the importance of RNAPII removal for the prevention or resolution of TRCs (Lalonde *et al.*, 2021).

Mechanisms for premature termination of transcription also allows for the removal of a fork blocking transcription complex. Utilisation of upstream poly adenylation sites can result in the production of stable, poly-adenylated truncated transcripts. This occurs most likely due to reduced elongation, which increases the efficiency of usually low-efficiency poly-(A) sites. Together these observations support that the ability for a cell to remove stalled RNAPII complexes is a viable mechanism by which cells can actively prevent and promote recovery from DNA replication stress induced by TRCs.

#### **1.4.4 Fork reversal**

Replication fork reversal is an alternative method of TRC resolution when all other resolution mechanisms cannot occur. Fork reversal is a rare event in unperturbed conditions and is utilised particularly following uncoupling of the helicase and polymerase activities, resulting in the production of ssDNA which stimulates the process. Through ATP-dependent remodelling of the stalled replication fork, the two

newly synthesised DNA strands are annealed together forming a four-way 'chicken foot' structure (see **Figure 1.1.3**). Fork reversal is mediated by DNA translocases SMARCAL1, ZRANB3 and HLTF as well as the helicase FBH1 and the Rad51 recombinase (Zellweger *et al.*, 2015; Poole and Cortez, 2017; Joseph *et al.*, 2020). This process protects the stalled replication fork from nucleolytic degradation, providing more time for the transcriptional block to be resolved and the reinitiation of DNA synthesis or for the passive completion of DNA replication by a converging replication fork. These proteins are thought to function in redundant pathways that are able to promote fork reversal of diverse substrates. Fork restart can then occur through various mechanisms. RECQ1 promotes fork restart through branch migration, this process is restrained by PARP activity, preventing reinitiation of DNA synthesis in the presence of replication stress (Ray Chaudhuri *et al.*, 2012; Berti *et al.*, 2013). DNA2 has also been demonstrated to promote replication restart in conjunction with WRN by creating a ssDNA overhang which binds RPA and stimulates SMARCAL1- or Rad51-dependent DNA replication restart (Petermann *et al.*, 2010; Thangavel *et al.*, 2015; Zellweger *et al.*, 2015). Dysfunction in this pathway leads to the subsequent collapse of stalled replication forks promoting DSB formation, these must be repaired by repair pathways such as homologous recombination, non-homologous end joining, single strand annealing or alternative end joining (Oh and Myung, 2022). However, collapsed replication forks risk an incompleteness of DNA synthesis, driving the potential requirement for the activation of new replisomes.

#### **1.4.5 Origin Firing**

In the event that a TRC results in the collapse of a replication fork, dormant origin firing occurs to allow for the completion of DNA synthesis. Instead of directly resolving TRCs, origin firing events can either passively or actively allow for the completion of DNA synthesis.

The manner in which higher eukaryotic genomes are organised means that origins of replication are frequently observed upstream of promoter regions of highly expressed genes. As a result, CD-TRCs occur more frequently in these regions to reduce deleterious consequences of such collisions. In addition to this, since replication forks are initiated bi-directionally, an approaching fork from the opposite direction is able to

complete DNA replication in the case of an individual TRC occurring. The firing of usually dormant origins can also occur to initiate the formation of additional replisomes in an attempt to complete DNA replication even in cases of high levels of TRCs, which cannot be bypassed efficiently and result in collapse. However, regions of the genome that are sparse for dormant replication origins or rely on the replication of large stretches of DNA by individual replisomes are particularly susceptible to TRCs and other fork stalling events. In these regions, high amounts of replication fork stalling leads to the emergence under-replicated DNA (UR-DNA) which can pose a serious risk to genomic stability.

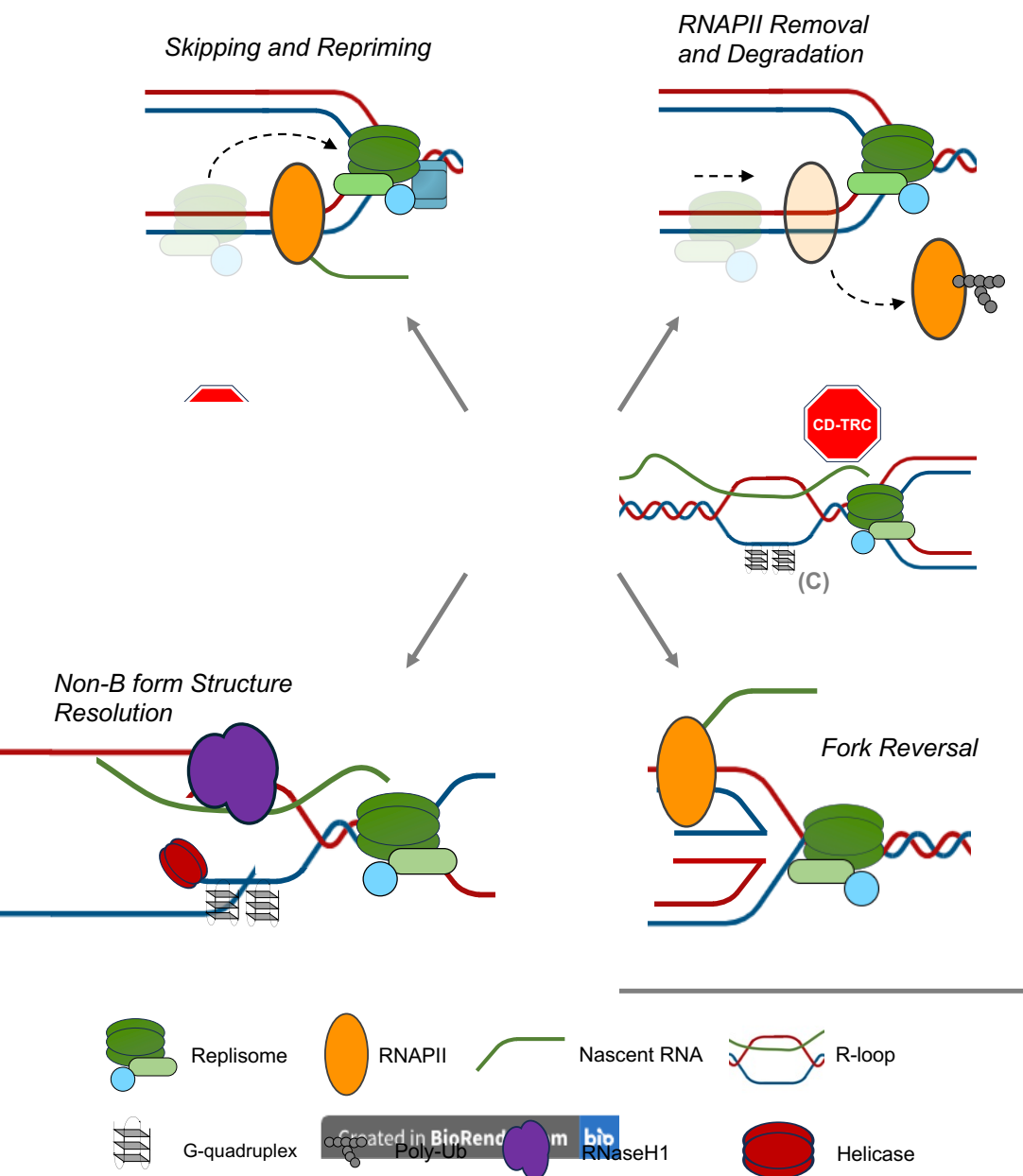


**Figure 1.1.3: Transcription-replication collisions, causes and resolution mechanisms**

*Legend on next page.*

### **Figure 1.1.3: Transcription-replication collisions, causes and resolution mechanisms**

Transcription-replication collisions (TRCs) can occur in a head-on (HO) or co-directional (CD) orientation as a result of **(A)** super-helical tension ahead of an elongating RNAPII, **(B)** direct collisions with a stalled RNAPII and **(C)** co-transcriptional secondary DNA structure formation such as R-loops and G-quadruplexes. Resolution of TRCs can occur through replisome skipping of a stalled transcriptional complex and repriming of DNA synthesis by PRIMPOL or the presence of nascent hybridised RNA. Removal of the transcription barrier by the phosphorylation and poly-ubiquitination of RNAPII results in dissociation and subsequent proteasomal degradation. Associated non-B form DNA structures such as R-loops and G-quadruplexes can be resolved through the recruitment of RNaseH1 for the degradation of RNA within DNA-RNA hybrid structures or through the recruitment of accessory helicases. The process of fork reversal which results in the formation of a 'chicken foot' structure through the annealing of nascent DNA strands, stabilises a stalled replication fork and can provide additional time for resolution of a TRC, bypass of the replisome and transcriptional complexes or facilitate the reinitiation of DNA synthesis. Adapted from (Lalonde *et al.*, 2021).

### **1.5 Common Fragile Sites**

Replication fork stalling has been shown to occur frequently at specific regions of the genome due to hard-to-replicate AT-rich repetitive sequences, active transcription during S-phase, association with large genes and inaccessible chromatin structure (Zhang and Freudenreich, 2007; Kaushal *et al.*, 2019; Sinai *et al.*, 2019). Termed common fragile sites (CFSs), CFSs are susceptible to mild replication stress due to reduced dormant origins, late replication timing and a propensity to form secondary DNA structures (Glover, Wilson and Arlt, 2017; Ji *et al.*, 2020; Macheret *et al.*, 2020). The delay in replication of these regions leads to a failure to condense properly during metaphase and therefore can be visualised as breaks or gaps on metaphase spreads (Glover *et al.*, 1984; Hellman *et al.*, 2000). Failure to properly replicate these regions leads to aberrant chromatid segregation and transmission of incorrectly replicated DNA to the daughter cells.

CFSs are associated with large-actively transcribed genes and the fragility of these regions have been frequently linked to TRC incidence (Helmrich, Ballarino and Tora, 2011; Wilson *et al.*, 2015; Brison *et al.*, 2019; Sanchez *et al.*, 2020). RTEL1 has been shown to be a key factor for the suppression of CFS fragility through the resolution of TRCs (W. Wu *et al.*, 2020). Additionally, RTEL1 depletion and low-dose aphidicolin

treatment (a common inducer of CFS fragility) promotes an accumulation of R-loops at CFSs suggesting that erroneous transcription, R-loop accumulation and TRCs are key drivers of CFS fragility. Transcriptional inhibition is associated with reduced CFS fragility though the precise mechanism for this is still debated (Saponaro *et al.*, 2014). Active transcription across these large genes has been shown to inhibit origin firing events at CFSs, driving a necessity for long-travelling replication forks (Brison *et al.*, 2019; Park *et al.*, 2021). Whilst TRCs are only one of many drivers of replication fork stalling in these regions, their incidence has been suggested to coincide with a failure to successfully complete DNA replication at CFSs.

### **1.5.1 The emergence of under-replicated DNA at common fragile sites**

Since CFSs are sparse for active and dormant replication origins, replication fork stalling in these regions frequently drives genomic instability due to the inability to fully replicate the DNA duplex. Specifically, double fork stalling events occurring in these regions can drive the emergence of under replicated DNA (UR-DNA), a key promoter of CFS fragility (Bertolin, Hoffmann and Gottifredi, 2020) (see **Figure 1.1.4**). When one irreversible fork stalling event occurs, a converging fork from the opposite direction is able to successfully complete DNA replication. However, when a double fork stalling event occurs, this converging fork is also impeded. As a result, the cell must elicit the firing of a dormant replication origin between the two stalled forks to allow for the full completion of DNA synthesis. At CFSs, these dormant origins are sparse and therefore when double fork stalling events occur there is no back up mechanism that allows for the completion of DNA replication during S-phase, which promotes the emergence of UR-DNA (Glover, Wilson and Arlt, 2017; Ji *et al.*, 2020; Macheret *et al.*, 2020).

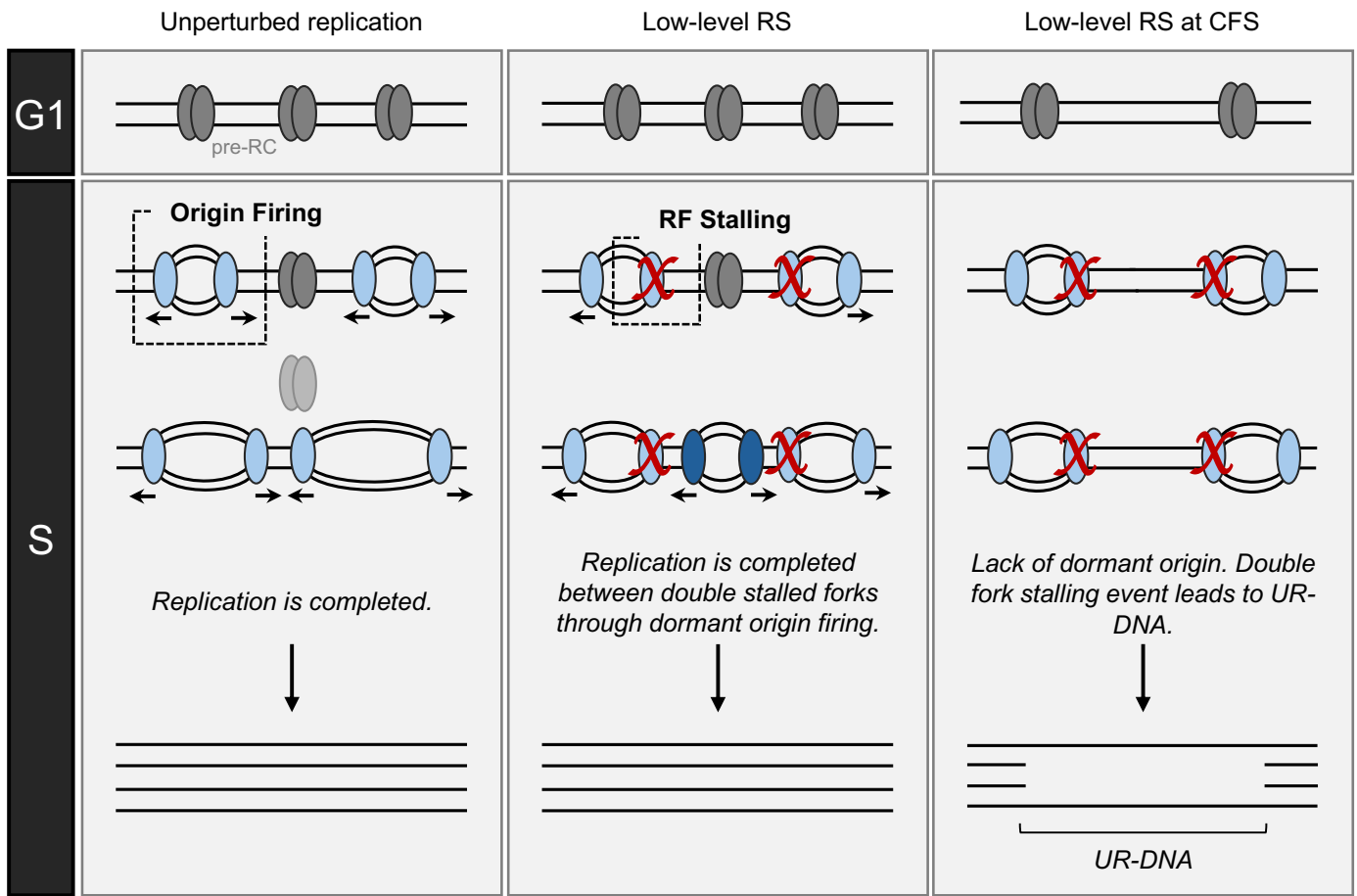


**Figure 1.1.4: The emergence of UR-DNA at CFS following low-level replication stress.**

During unperturbed DNA replication, dormant origins do not require firing in order to completely replicate DNA. Low-level replication stress (RS) can result in double DNA replication fork (RF) stalling which requires dormant origin firing to successfully replicate DNA between the two stalled replication forks. At common fragile sites (CFSs), lack of dormant origins between double replication fork stalling events results in the emergence of under-replicated DNA (UR-DNA) that persist outside of S-phase driving a necessity for mitotic DNA synthesis to complete DNA replication.

Whilst DNA damage checkpoint machinery can efficiently detect minimal double-stranded DNA breaks and is able to prevent cell cycle progression into G2/M through activation of the ATM/Chk2 signalling axis (van den Berg *et al.*, 2018). UR-DNA is not as easily detected by the ATR/Chk1 pathway, the activation of which relies on an accumulation of the single-stranded binding protein RPA. As a result, cells with UR-DNA are able to enter into mitosis (Torres-Rosell *et al.*, 2007; Minocherhomji *et al.*, 2015). It is possible that UR-DNA does not promote a sufficient RPA accumulation to

elicit global ATR activation and thus prevent G2/M entry through Chk1 activation. Alternatively, UR-DNA could be directly prevented from activating RPA. More work needs to be done in order to characterise how UR-DNA escapes G2 checkpoint activation. Since UR-DNA can progress out of S-phase without activating cell cycle checkpoints, it persists until mitosis where it is processed prior to cellular division.

### **1.5.2 Under-replicated DNA is processed in G2 or mitosis by distinct DNA synthesis processes**

The ability for UR-DNA to persist until mitosis means that cells have developed a mechanism to attempt to complete DNA replication of these regions. A process known as Mitotic DNA synthesis (MiDAS) has been reported to occur in prometaphase of mitosis, following the observation of active incorporation of the thymidine analogue EdU in early prophase when cells are exposed to mild replicative stress (Minocherhomji *et al.*, 2015; Bhowmick, Minocherhomji and Hickson Correspondence, 2016). This process has been shown to occur at regions that encompass all known common fragile sites (CFSs). Various studies have identified dependencies on numerous factors including MUS81, POLD3, RAD51 and RAD52 (Minocherhomji *et al.*, 2015; Bhowmick, Minocherhomji and Hickson Correspondence, 2016; Wassing *et al.*, 2021). It is proposed that the attempted condensation of under-replicated loci triggers MiDAS in early prophase. MiDAS is proposed to occur by a break-induced repair (BIR) -like mechanism, a homologous recombination-based pathway for the repair and restart of stalled replication forks marked by FANCD2.

Initially replisome disassembly of remaining stalled forks occurs as cells enter into mitosis, which is carried out by the E3-ubiquitin ligase TRAP1 (Deng *et al.*, 2019; Moreno *et al.*, 2019; Sonnevile *et al.*, 2019). Subsequently, cleavage of exposed DNA at stalled forks by MUS81 and SLX4 occurs, followed by the unwinding of any atypical DNA structures such as R-loops facilitated by RTEL1 (Minocherhomji *et al.*, 2015; Bhowmick, Minocherhomji and Hickson Correspondence, 2016; W. Wu *et al.*, 2020; Kim *et al.*, 2024). This then allows for DNA synthesis to occur aided by Rad51 and Rad52, gap filling synthesis by Rev1, Pol $\zeta$  and replicative DNA synthesis by Pol $\delta$  (Minocherhomji *et al.*, 2015; Bhowmick, Minocherhomji and Hickson Correspondence, 2016; Wassing *et al.*, 2021; Wu *et al.*, 2023).

This replication restart MiDAS model is still widely accepted, however Mocanu *et al.* has proposed an alternative mechanism for post-S-phase DNA replication (Mocanu *et al.*, 2022). It is suggested that the experimental conditions used to study MiDAS inadvertently compromise DNA synthesis, forcing cells to utilise a BIR-like mechanism to restart stalled replication forks (Mocanu *et al.*, 2022). Ro3306, used to arrest cells at G2-M for studying MiDAS was shown to have an off-target effect on CDK2, leading to replication inhibition that would cause replication fork stalling. It was shown that in the absence of Ro3306, DNA synthesis could indeed be detected in G2 and mitosis following treatment with low-dose aphidicolin (Mocanu *et al.*, 2022). This suggests that the canonical replication restart model for MiDAS could be incorrect. Continuous DNA synthesis through G2 also had reduced reliance on several 'characterised' MiDAS factors, specifically those involved in replication restart. Whilst these mechanisms of DNA replication could be distinct, both exist for the completion of DNA replication of UR-DNA outside of S-phase.

Compromising the process of MiDAS has been shown to result in an increase in ultra-fine bridges linking together daughter nuclei (Minocherhomji *et al.*, 2015; Bhowmick, Minocherhomji and Hickson Correspondence, 2016). These structures stain positive for several protein markers including BLM and PICH and represent uncondensed UR-DNA in mitosis (Baumann *et al.*, 2007; Chan, North and Hickson, 2007; Chan *et al.*, 2009). 53BP1 nuclear bodies have also been reported to mark UR-DNA in the subsequent G1 following mild replicative stress, which is increased following MiDAS inhibition (Harrigan *et al.*, 2011; Lukas *et al.*, 2011; Minocherhomji *et al.*, 2015; Bhowmick, Minocherhomji and Hickson Correspondence, 2016; Spies *et al.*, 2019).

Inhibition of MiDAS has also been suggested to result in anaphase delay as well as promoting centromere fragility, suggesting that the SAC could be able to sense and respond to incomplete DNA replication when MiDAS is dysfunctional (Wassing *et al.*, 2021). The reason for an observed mitotic delay could also be due to the sensing by the spindle assembly checkpoint (SAC) of acentric fragments that could be present due to a failure to completely replicate centromeric DNA. In line with this, mitotic cells also have been reported to exhibit DNA damage-dependent mitotic delay in response

to a range of DNA damaging and replicative stress agents (Gatenby, 2022; Gatenby *et al.*, 2022).

## **1.6 Mitotic Checkpoints**

The widely believed view is that there is no DNA damage or replication checkpoint that functions during mitosis. Due to the nature of condensed chromatin, DNA repair mechanisms represent a possible mechanism by which deleterious chromosomal fusion could occur if pathways such as NHEJ were activated. For this reason it was observed that these are downregulated by the cell following mitotic entry (Giunta, Belotserkovskaya and Jackson, 2010). In fact, the mitotic kinases CDK1 and Plk1 actively inhibit DSB repair and DNA damage checkpoints (Van Vugt *et al.*, 2010). Though a broad DNA damage response checkpoint has not been characterised in mitosis, the SAC is a checkpoint that mediates a delay in metaphase-anaphase transition until microtubule attachment has occurred. Regulation of the SAC in response to DNA damage or UR-DNA represents a possible mechanism by which cells could exhibit DNA damage- or replication stress-dependent mitotic delay.

### **1.6.1 Spindle Assembly Checkpoint**

The SAC functions during the metaphase-anaphase transition of mitosis and acts to ensure correct microtubule attachment to kinetochores of individual chromosomes, therefore preventing the incorrect separation of chromatids and the emergence of aneuploidy. Unlike DNA damage response checkpoints in interphase, such as the ATM/Chk2 and ATR/Chk1 signalling axes, which become activated in response to DNA damage, the SAC is automatically active in metaphase, until all kinetochore-microtubule attachments have occurred, at which point the SAC is turned off, allowing for mitotic progression.

The SAC involves the formation of the Mitotic Checkpoint Complex (MCC) at the chromosome kinetochore. The MCC is a multimeric protein complex composed of numerous SAC proteins including MAD2, BUBR1, BUB3 and CDC20, which negatively regulates the ability of CDC20 to activate the anaphase-promoting complex/ cyclosome (APC/C) (Musacchio and Salmon, 2007). APC/C inhibition prevents the polyubiquitination-mediated degradation of Cyclin B and securin

(Yamamoto *et al.*, 2005; Primorac and Musacchio, 2013). Securin, an inhibitor of the protease separase is responsible for cleavage of the cohesion complex that holds sister chromatids together, and thus progression into anaphase (Hornig *et al.*, 2002). Additionally, Cyclin B stabilisation results in prolonged activation of CDK1, the key mitotic kinase, preventing mitotic exit.

The MCC complex formation is initiated by the SAC kinase MPS1 which phosphorylates methionine-glutamic acid-leucine-threonine (MELT) repeat motifs of KNL1 and is shown in **Figure 1.1.5**. These phosphorylated MELT motifs recruit Bub1-Bub3 and BubR1-Bub3 complexes (Yamagishi *et al.*, 2012; Primorac *et al.*, 2013). BubR1 binds Cdc20 which facilitates the recruitment of closed-conformation of Mad2 through Mad1 (De Antoni *et al.*, 2005; Lischetti *et al.*, 2014). MPS1 binds open-conformation Mad2 resulting in the formation of Cdc20-C-Mad2 and completion of MCC recruitment (Hewitt *et al.*, 2010). When the SAC is satisfied, following all chromatids being correctly attached to microtubules, MPS1 dissociates from the kinetochore promoting BubR1-mediated recruitment of PP2A result in dephosphorylation of KNL1 MELT motifs leading to Bub3 and Mad1-Mad2 dissociation (Jelluma *et al.*, 2010; Espert *et al.*, 2014). This ultimately leads to Cdc20 release from the MCC allowing for the activation of the APC/C ubiquitin ligase activity. APC-C-mediated degradation of securin removes inhibition of separase protease activity, allowing for chromatid separation through the degradation of cohesion. The degradation of cyclin B by the APC/C also inhibits CDK1 activity facilitating anaphase progression and mitotic exit.

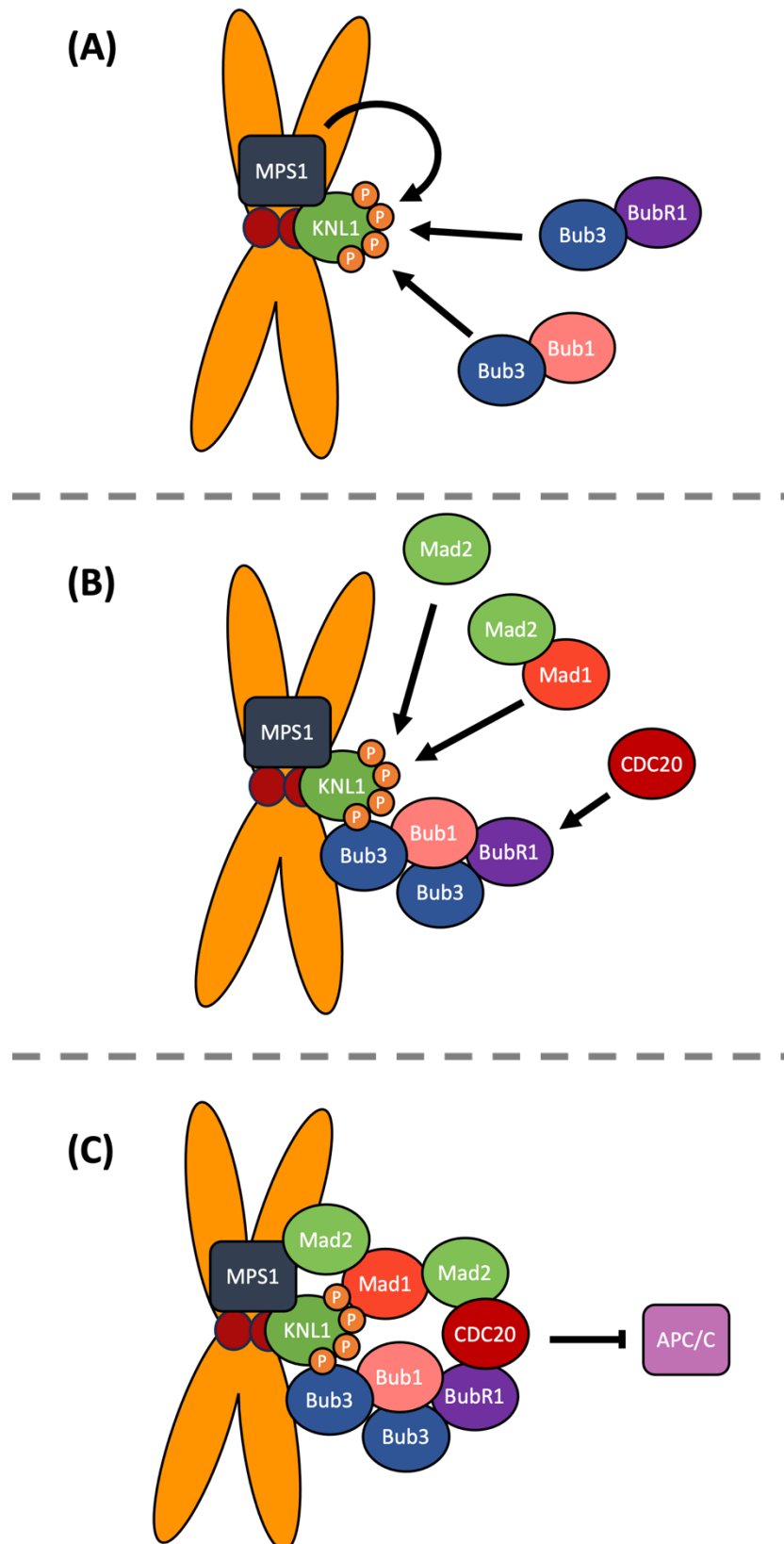


**Figure 1.1.5: The mitotic checkpoint complex prevents mitotic progression until microtubule attachment.**

*Legend on next page.*

**Figure 1.1.5: The mitotic checkpoint complex prevents mitotic progression until microtubule attachment.**

**(A)** MCC assembly begins by phosphorylation of MELT motifs on KNL1 which recruits Bub3-BubR1 and Bub3-Bub1 complexes. **(B)** Recruitment of Mad1-Mad2 as well as BubR1-mediated recruitment of CDC20 results in complete MCC assembly. **(C)** Sequestering of CDC20 results in the inhibition of the APC/C delaying mitotic progression until SAC satisfaction.

### **1.6.2 DNA damage promotes mitotic delay**

Despite an inhibition to the canonical DNA repair pathways in mitosis, there is emerging evidence that suggests mitotic cells do indeed respond to induced replication stress or DNA damage, both in mitosis and in interphase which can progress into mitosis due to defective interphase DDR checkpoints. In yeast, it was demonstrated that homologues of ATM (Tel1) and ATR (Mec1) promote metaphase arrest due to the stabilisation of securin (Pds1). This mitotic arrest was dependent on numerous SAC components including Mad1, Mad2, Mad3, Bub1 and Bub3, yet independent of a functional kinetochore (Kim and Burke, 2008).

A mitotic delay induced following DNA damage has been observed in human cells. U2OS osteosarcoma cells arrested with nocodazole remained in mitosis for 8 hours following nocodazole release when treated with IR. Whilst the untreated cells timely progressed into G1 (Smits *et al.*, 2000). HeLa and HCT116 cervical and colorectal cancer cells respectively arrested at metaphase for 10 hours following treatment with aphidicolin or IR, which then lead to mitotic catastrophe. Inhibition of BubR1 or Mad2 lead to the abrogation of this mitotic delay and resulted in abnormal mitosis (Nitta *et al.*, 2004). Furthermore, DNA damage or replication stress left unprocessed from interphase, that proceeds into mitosis through abrogation of interphase DDR checkpoints also prolongs mitotic duration (Thompson *et al.*, 2015; Gatenby, 2022; Gatenby *et al.*, 2022).

The occurrence of this mitotic delay in response to various DNA damaging agents suggests that mitotic cells can respond to genotoxic stress. The observation that this delay occurs at metaphase suggests that the DDR machinery can regulate normal

SAC function independent of kinetochore status. However, the differential requirement of SAC components raises uncertainty into how the delay is regulated.

### 1.6.2.1 UPF1 is required for a delay in mitosis following DNA damage

Previous work carried out in the Thompson laboratory investigated mitotic delay following genotoxic stress, specifically attempting to identify proteins that were required for this phenotype in human cells. Through a fluorescent microscopy siRNA screen, that assess mitotic population changes following irradiation, Up-frameshift Suppressor 1 (UPF1) was identified as being required for an observed increase in mitotic population following treatment with IR (see **Figure 1.1.6**).

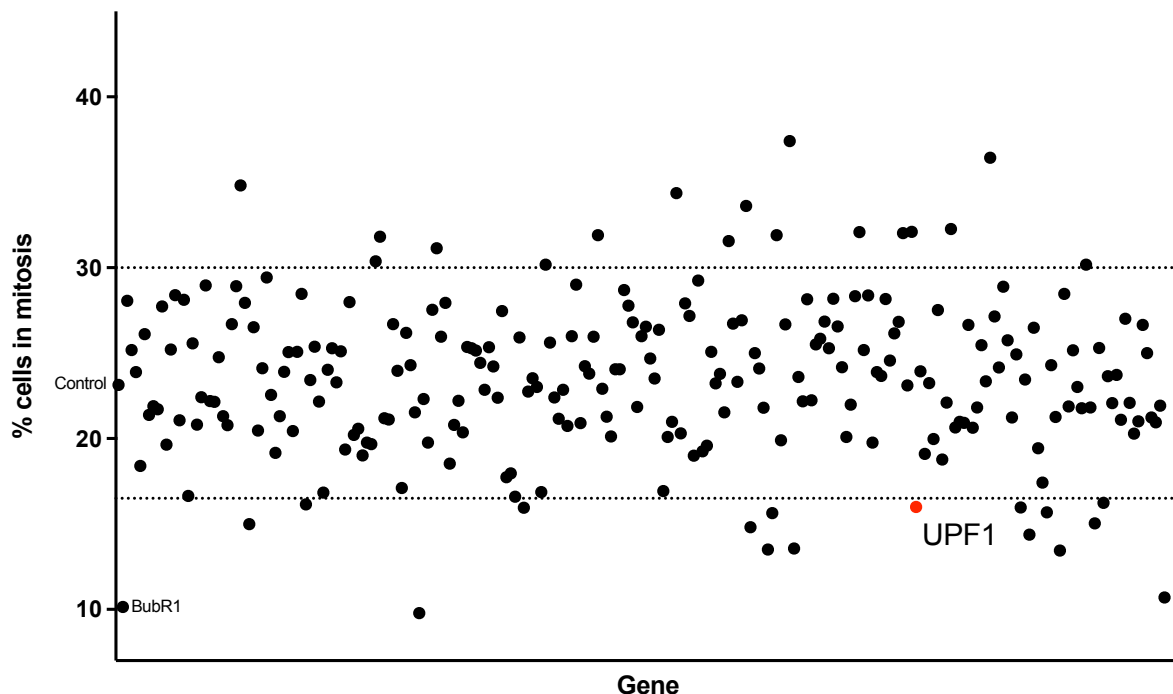


**Figure 1.1.6: Identification of proteins involved in the regulation of mitotic duration following DNA damage.**

High throughput fluorescent microscopy screen of mitotic population. siRNA screen using ON-TARGET<sup>plus</sup> DNA damage response siRNA library (Dharmacon) and cells treated with 10 Gy  $\gamma$ -radiation prior to fixation 16hrs later. Cells were stained for phosphor-histone H3 (Ser10) and DAPI and imaged on Molecular Devices ImageXpress Micro high content microscope using a Multi Wavelength Cell Scoring application on MetaXpress (v5.3) to analyse images. Data was rank-filtered by the mean ordered Z-score with a stringent Z-score cut off of 2, to identify siRNAs which significantly reduced the mitotic population (N=5). UPF1 is highlighted in red.

## 1.7 UPF1

Originally identified through genetic screening in *Saccharomyces Cerevisiae*, UPF1 deletion was shown to restabilise mRNAs containing a premature termination codon (PTC) through the process of nonsense-mediated decay (NMD) (Culbertson and Underbrink, 1980; Leeds *et al.*, 1991). Homologues of UPF1 have been identified in numerous species including, *Mus musculus* (RENT1), *Caenorhabditis elegans* (SMG2), *Drosophila Melanogaster* and *Homo sapiens* (hUPF1) (Culbertson and Underbrink, 1980; Applequist *et al.*, 1997).

### 1.7.1 Structure and Biochemical Activity

Structural and biochemical analysis revealed that UPF1 is an ATP-dependant RNA/ DNA helicase and the prototypical member of the UPF1-like helicases. UPF1 is recognised primarily as an RNA helicase belonging to the Superfamily 1, which have numerous roles in nucleic acid metabolism. It has a conserved helicase core consisting of two RecA-like domains (**Figure 1.1.7C**). It also possesses numerous auxiliary domains, an N-terminal cysteine- histidine rich (CH) domain that interacts with UPF2 and functions as an allosteric inhibitor of both RNA-binding and helicase activities (**Figure 1.1.7A**) (Kadlec *et al.*, 2006; Chamieh *et al.*, 2007; Chakrabarti *et al.*, 2011). A C-terminal serine-glutamine rich (SQ) domain also functions to impede helicase activity through a direct interaction, of which is regulated by phosphorylation of key residues known to be required for NMD (Fiorini, Boudvillain and Hir, 2013).

UPF1 can bind both RNA and DNA nucleic acids with a preference for single-stranded segments, most likely due to the size of the nucleic acid-binding channel present in UPF1 (Czaplinski *et al.*, 1995; Applequist *et al.*, 1997; Bhattacharya *et al.*, 2000; Dehghani-Tafti and Sanders, 2017). This channel is modulated by ATP-binding which promotes the dissociation of the mRNA or prevents further RNA binding (Weng, Czaplinski and Peltz, 1996; Cheng *et al.*, 2007). ATP-hydrolysis is therefore required for RNA-binding and thus helicase activity. UPF1 has been demonstrated to be able to unwind duplex RNA and DNA as well as numerous non-B form secondary DNA structures *in vitro*, including G-quadruplexes and triplex DNA structures (Dehghani-Tafti and Sanders, 2017). UPF1 has been demonstrated to be a uniquely highly

processive helicase, attributed to conserved structural variations that mediate tight nucleic acid binding (Fiorini *et al.*, 2015; Kanaan *et al.*, 2018). This high processivity allows UPF1 to remain bound to its substrate, effectively enabling it to scan across long distances on a target RNA to mediate decay.

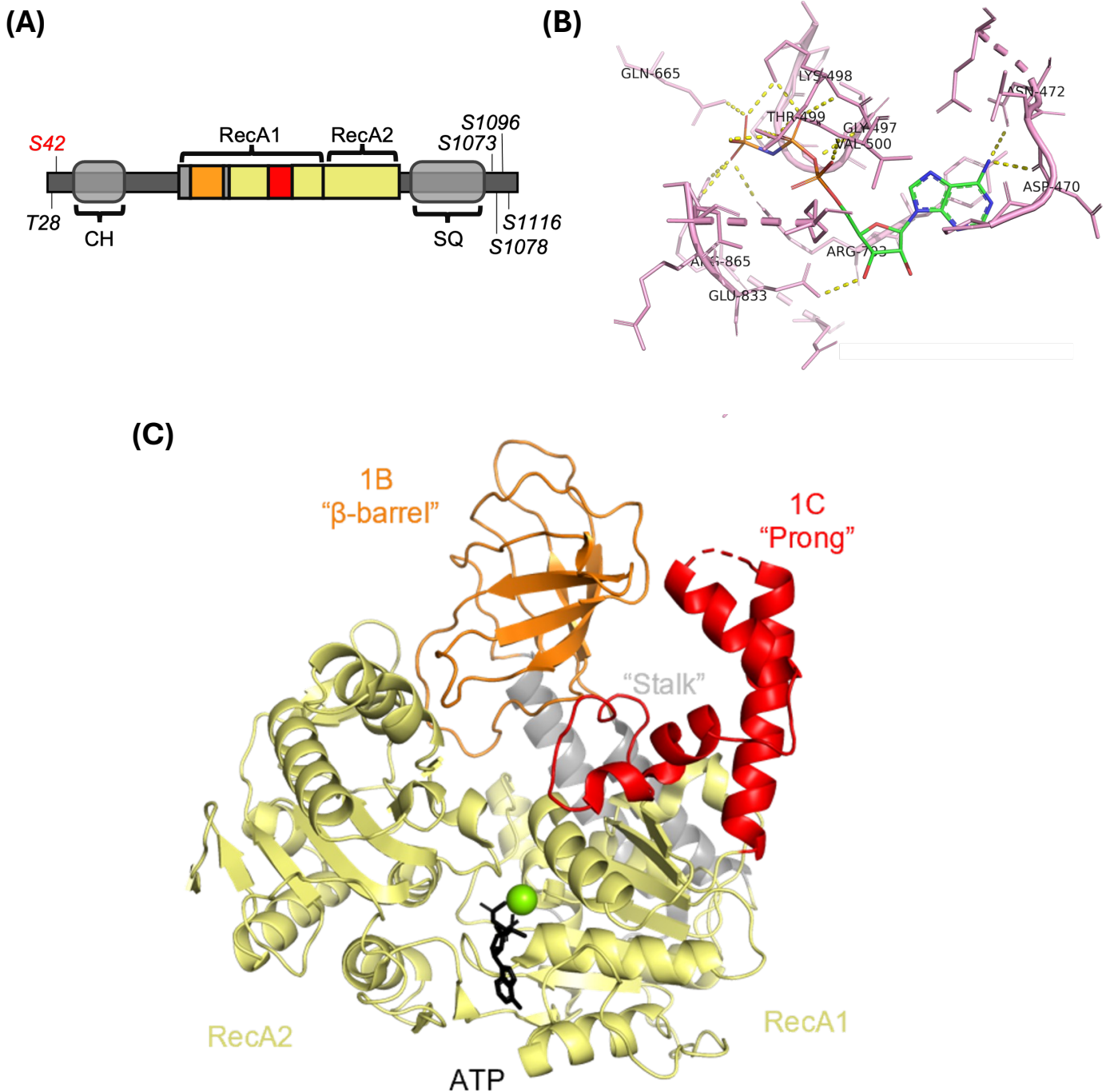


**Figure 1.1.7: UPF1 has a conserved helicase domain with unique accessory domains that mediate UPF1-specific functions.**

*Legend on next page.*

**Figure 1.1.7: UPF1 has a conserved helicase domain with unique accessory domains that mediate UPF1-specific functions.**

**(A)** Schematic depicting the conserved helicase domain of UPF1 consisting of two RecA-like domains with various auxiliary domains that modulate helicase activity. UPF1 also possess an N-terminal CH-domain and a C-terminal SQ domain that regulate UPF1 RNA-binding and helicase function. SMG1-dependent S/T-Q phosphorylation sites are depicted in black, in red the S42 site shown to mediate chromatin binding is shown. **(B)** UPF1 ATP-binding is facilitated by numerous residues between the RecA1 and RecA2 domains. **(C)** hUPF1 crystal structure showing conserved domains among UPF1-like helicases including RecA-like domains (yellow), stalk domain (grey), a prong structure (red) and  $\beta$ -barrel (orange).

UPF1 is a key mRNA surveillance protein and master regulator of numerous mRNA decay pathways, the best characterised being NMD. UPF1 also regulates other decay pathways including Staufen-mediated Decay (SMD) and Replication-dependant Histone-mediated Decay (HMD). NMD is a conserved surveillance pathway in eukaryotes, responsible for the degradation of transcripts harbouring premature termination codons (PTC), that would code for aberrant C-terminally truncated proteins. Deletion of UPF1, or deletion of the helicase domain has been shown to completely abolish NMD, demonstrating the necessity for catalytically active UPF1 for functioning mRNA decay pathways (Weng, Czaplinski and Peltz, 1996; Bhattacharya *et al.*, 2000). In addition to NMD having a role in maintaining the quality of mRNA expression, UPF1 has also been shown to regulate the expression of non-PTC containing, non-pathological transcripts, having an impact on a range of processes including, DNA replication, myoblast and neuronal differentiation, stress response and disease (Gong *et al.*, 2009; Bruno *et al.*, 2011).

## **1.7.2 Nonsense-mediated mRNA Decay**

### **1.7.2.1 NMD Target Recognition**

#### **1.7.2.1.1 EJC-dependent NMD**

The widely accepted model of NMD is depicted in **Figure 1.1.8**. Canonical NMD is a translation-coupled RNA decay pathway that is coupled with pre-mRNA splicing through the recognition of an exon-junction complex (EJC). Most newly transcribed protein coding RNAs are subjected to various post-transcriptional processing, these

include 5' capping, polyadenylation, and intron splicing. Most significant is intron splicing which, mediated by a ribonucleoprotein complex termed the spliceosome, removes non-coding segments (Introns) of an RNA and ligates together protein-coding segments (Exons), resulting in the formation of a mature, translatable mRNA. During this process a large protein complex known as the EJC, consisting of Y14, Btz, Magoh, eIF4AIII, UPF2, UPF3a/b is deposited around 20-24nt upstream of each exon-exon junction following splicing and serves to provide a memory of splicing events on a nascent mature mRNA even after it has left the nucleus to be translated (Kataoka *et al.*, 2000; Le Hir *et al.*, 2000; Chan *et al.*, 2004; Palacios *et al.*, 2004; Bono *et al.*, 2006).

Current understanding of mammalian NMD suggests that it occurs during the pioneering round of translation of a mature mRNA. This allows NMD to ensure that no truncated proteins are produced from any target PTC-containing RNAs. An EJC is typically removed by a translocating ribosome, then when the ribosome reaches a termination codon consisting of eRF1 and eRF3, translation termination occurs. However when an mRNA harbours a PTC, EJCs remain in the 3' UTR resulting in inefficient translation termination allowing for an interaction of eRF3 and UPF1 to occur which is sufficient to stimulate NMD (Czaplinski *et al.*, 1998; Kashima *et al.*, 2006).

#### **1.7.2.1.2 EJC-independent NMD**

Other EJC-independent mechanisms of NMD stimulation have been proposed which rely on an interaction of eRF3 with PABPC1 (see **Figure 1.1.8**) (Amrani *et al.*, 2004). PABPC1 is present in the 3' UTR of all mRNPs and acts to promote translation termination through an interaction with eRF3 (Ivanov *et al.*, 2016; C. Wu *et al.*, 2020). The existence of a PTC leads to the PABPC1 present in the 3' UTR being distal from the termination codon. The displacement of this factor due to a long 3' UTR results in ribosomal stalling at the termination codon, preventing efficient translation termination and therefore presents an opportunity for UPF1 to bind the eRF complex instead and stimulate NMD (Bühler *et al.*, 2006; Fatscher *et al.*, 2014). In these cases, the lack of an EJC means that the UPF proteins must be recruited by a distinct mechanism to canonical NMD. It is known that UPF1 binds significantly to GC-rich motifs in the 3' UTR of numerous mRNPs that are targets of NMD (Imamachi *et al.*, 2017). This

binding occurs in a length-dependant manner and altering the equilibrium of UPF1 binding can prevent NMD initiation (Hogg and Goff, 2010).

### **1.7.2.2 UPF1 activation and target degradation**

Regardless of how UPF1 is recruited to a target mRNA, once it has done so it then is required to promote the formation of a complex of proteins to initiate NMD. UPF1 is recruited to these PTC-containing mRNPs through an interaction with eRF1 and eRF3 at the stalled ribosome, along with the serine/threonine protein kinase SMG1 resulting in the formation of the **SMG1-UPF1, eRF1/3 (SURF)** complex in close proximity to the PTC (Kashima *et al.*, 2006). SMG1 is in complex with two regulatory subunits SMG8 and SMG9 which maintain SMG1 in an inactive state. The SURF complex, specifically UPF1, interacts with UPF2 and a downstream EJC component: UPF3B. UPF3B acts as a bridge between the UPF proteins allowing for the formation of the Decay-Inducing (DECID) Complex (Ivanov *et al.*, 2008). Activation of SMG1 results in the phosphorylation of UPF1 at numerous residues, *in vitro* SMG1 has shown to phosphorylate at least four S/T/Q residues. Activation of UPF1 results in the dissociation of eRF1 and eRF3, the interaction of UPF1 and UPF2 also results in the activation of UPF1 helicase activity due to conformational changes that remove allosteric inhibition by UPF1's CH domain. This helicase activity allows UPF1 to translocate along the target mRNA, resolving secondary DNA structures and facilitating the removal of bound-proteins to allow access to nucleases (Barbier *et al.*, 2007; Fiorini *et al.*, 2015). Phosphorylation of T28 and S1096 residues result in the phospho-specific recruitment of decay factors SMG6 and SMG5:SMG7 to the N-terminus and C-terminus of UPF1 respectively, as well as general degradation factors (Ohnishi *et al.*, 2003; Kurosaki *et al.*, 2014). UPF1 forms distinct complexes with UPF2 and SMG6, suggesting a necessity for the dissociation of UPF2 to facilitate SMG6 recruitment and mRNA decay (Langer *et al.*, 2024). PP2A-mediated dephosphorylation of UPF1 is then required for the dissociation of UPF1 from the mRNP, allowing for degradation. The RNA helicase MOV10 has been shown to promote decay in conjunction with UPF1 by acting as an RNA clearance factor to displace bound proteins and resolve secondary DNA structures (Gregersen *et al.*, 2014). SMG6 promotes endonucleolytic degradation in close proximity to the PTC whilst the SMG5:SMG7 heterodimer recruits POP2 and XRN2 to facilitate target

degradation through deadenylation (Unterholzner and Izaurralde, 2004; Loh, Jonas and Izaurralde, 2013; Ruiz-Gutierrez *et al.*, 2025). These two endo- and exonucleolytic pathways have previously been thought to function independently but recently it has been demonstrated that SMG5:SMG7 recruitment is required to authorise SMG6 activity for NMD target degradation (Boehm *et al.*, 2021).

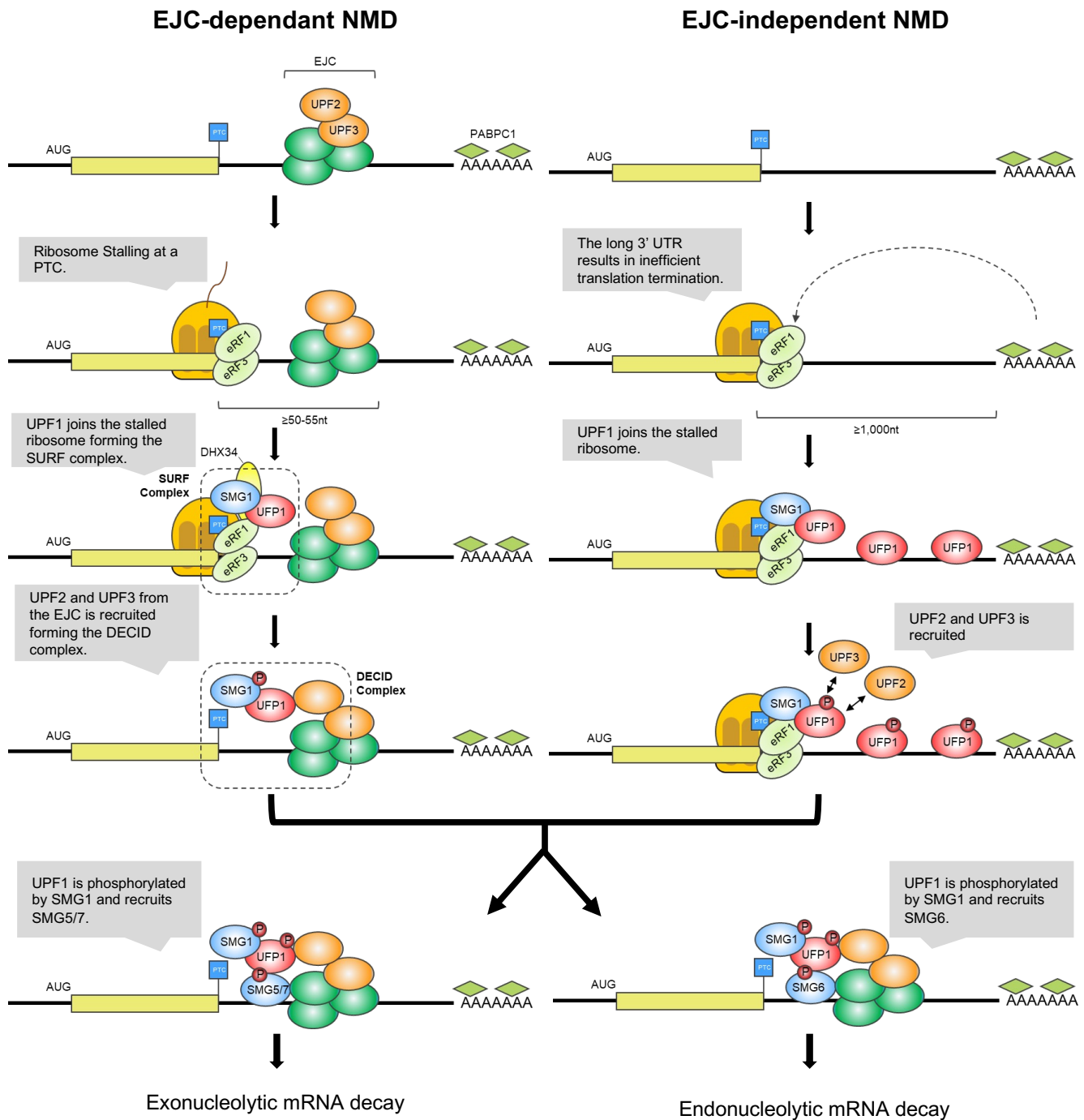


**Figure 1.1.8: UPF1 is the master regulator of Nonsense-mediated decay pathways.**

### 1.7.3 Alternative RNA Decay Pathways

Asides from NMD, UPF1 is also a key component of numerous other mRNA decay pathways that recruit UPF1 through distinct mechanisms. Recruitment of UPF1 to these decay pathways usually involves a direct interaction of UPF1 with an mRNA-binding protein. These RNA-binding proteins are differentially recruited by the signals for decay on an mRNA, which can range from a linear nucleotide sequence to more complex secondary DNA structures.

The pathway of Staufen-mediated decay is mediated by the binding of the double-stranded RNA-binding protein Staufen-1 (STAU1) to a STAU1-binding site (SBS), inter- and intra-RNA duplexes, within the 3'-UTR of a target mRNA (Gowravaram *et al.*, 2019). STAU1 directly interacts with UPF1, is independent of UPF2 and UPF3b and therefore SMD and NMD function as competitive pathways (Kim *et al.*, 2005; Gong *et al.*, 2009).

UPF1 has also been shown to function in the regulation of histone mRNA, specifically driving the gradual degradation of histone mRNA at the end of S-phase or in response to replicative stress. Coordinated expression of histone mRNAs is essential during S-phase to allow for the packaging of newly synthesised DNA into histones. The correct timely degradation of histone mRNA ensures correct histone protein production, efficient packaging of newly replicated DNA and the maintenance of genomic stability. The mRNA decay pathway of histone-mediated decay (HMD) functions through the recognition of a conserved 3'UTR stem-loop structure which exists on histone mRNA where all other mRNAs possess a poly(A) tail (Kaygun and Marzluff, 2005). This unique structure is recognised by Stem-loop Binding Protein (SLBP), demonstrated to be pivotal in regulating histone mRNA at several levels including pre-mRNA processing, export, translation and indeed degradation (Whitfield *et al.*, 2004; Sullivan *et al.*, 2009). Under normal conditions, SLBP associates with CBC-dependent translation initiation factor (CTIF) which acts to promote histone stability and allows for efficient translation to produce histone proteins (Choe *et al.*, 2013; Choe, Ahn and Kim, 2014). Following replicative stress, UPF1 is phosphorylated by ATR, SMG1 and/or DNA-PK promoting its preferential association with SLBP (Kaygun and Marzluff, 2005; Müller *et al.*, 2007; Choe, Ahn and Kim, 2014; Meaux, Holmquist and Marzluff, 2018). This disrupts the interaction of SLBP with CTIF resulting in reduced

translation efficiency, whilst UPF1 also promotes downstream exoribonucleolytic degradation of the histone mRNA through the recruitment of SMG5 and PNRC2. UPF1 has also been suggested to be negatively regulated by FBXO45 through the recruitment of a protein phosphatase, preventing UPF1 activation during S-phase and maintaining histone supplies (Li *et al.*, 2024).

Whilst NMD and most decay pathways are largely considered to be cytoplasmic processes, UPF1 has also been shown to associate co-transcriptionally on chromatin for surveillance (Hong, Park and Jeong, 2019; Singh *et al.*, 2019). Singh *et al.* demonstrates that in drosophila UPF1 is present at Pol II and Pol III transcription sites and required for release of mRNAs from their transcribed loci. This suggests that UPF1 could have a more comprehensive role in mRNA surveillance that occurs in the nucleus independently or in cooperation with cytoplasmic NMD.

#### **1.7.4 Non-canonical roles of UPF1**

Beyond the well described role that UPF1 plays in mRNA surveillance it has also been implicated in a range of other non-canonical functions including, telomeric homeostasis, DNA replication and repair and secondary DNA structure resolution.

##### **1.7.4.1 DNA replication, repair and the maintenance of genomic stability**

UPF1 has been implicated in the maintenance of genomic stability due to the emergence of spontaneous DNA damage observed following UPF1 depletion (Azzalin *et al.*, 2007; Chawla *et al.*, 2011; Turton, 2014). The observation that loss of UPF1 is embryonic lethal whereas loss of NMD is well tolerated in mice also supports a non-canonical function of UPF1 in the maintenance of genomic stability (Leeds *et al.*, 1991; Medghalchi *et al.*, 2001; Wittmann, Hol and Jäck, 2006; Ngo, Grimstead and Baird, 2021). Identification of a novel phosphorylation site in the N-terminus of UPF1 was shown to affect the chromatin-binding ability of UPF1 and be independent of its function in NMD (Turton, 2014). A mutant variant of UPF1 which was defective for chromatin binding was shown to be unable to rescue spontaneous DNA damage induced by loss of endogenous UPF1 (Turton, 2014). The chromatin recruitment of UPF1 is increased following irradiation or during S-phase and appears to be dependent on ATR (Lew, Enomoto and Berman, 1998; Azzalin and Lingner, 2006;

Turton, 2014). ATR depletion impairs UPF1 chromatin localisation, but no defects in NMD were observed, suggesting that the DNA damage-associated loading of UPF1 to chromatin is independent of the canonical NMD pathway.

UPF1 is also phosphorylated in response to genotoxic stress by SMG1, ATR and ATM, which has been shown to be independent of NMD (Brumbaugh *et al.*, 2004; Azzalin and Lingner, 2006; Matsuoka *et al.*, 2007; Xiao *et al.*, 2022). Due to its regulation by key DDR kinases UPF1 has been implicated in both DNA replication and repair. Further evidence for this role is an observed interaction of UPF1 with the p66 subunit of Pol  $\delta$ , an essential polymerase in eukaryotic lagging strand replication and repair (Carastro *et al.*, 2002; Azzalin and Lingner, 2006; Turton, 2014). The exact significance of this interaction has yet to be deciphered, beyond an implication in telomeric DNA replication (Chawla *et al.*, 2011).

UPF1 has also been reported to play a role in promoting resection at DSB sites induced in sub-telomeric regions in an NMD-independent manner, though with a dependence of UPF3b (Ngo, Grimstead and Baird, 2021). This process is suggested to drive homologous recombination, microhomology-mediated end joining and DNA damage checkpoint activation. This data presented contrary data on UPF1 as a driver of DNA-RNA hybrid structures at DSB sites, whereas numerous helicases, many a member of UPF1-like helicases have been demonstrated to resolve R-loops. UPF1 has been demonstrated to resolve R-loops *in vitro*, DNA and RNA helicases have been implicated in both resolution and formation of these structures (Mischo *et al.*, 2011; Dehghani-Tafti and Sanders, 2017; Chakraborty, Huang and Hiom, 2018; Cohen *et al.*, 2018; Cristini *et al.*, 2018; Cheruiyot *et al.*, 2021; Ngo, Grimstead and Baird, 2021). Indeed, UPF1 has been shown to be required for the resolution of R-loop-associated nascent mRNAs which rehybridize to their transcribed loci. This function has been shown to occur globally in drosophila and at telomeres in mammalian cells (Azzalin *et al.*, 2007; Porro *et al.*, 2014; Singh *et al.*, 2019).

#### **1.7.4.2 Telomere Homeostasis**

As mentioned, UPF1 has been shown to associate with telomeres and is required for the displacement and degradation of a long non-coding RNA TERRA (telomeric

repeat-containing RNA), which most likely rehybridizes at the telomere as an R-loop (Chawla *et al.*, 2011; Turton, 2014). UPF1 has been suggested to have other roles in telomeric homeostasis beyond R-loop dynamics and the dissociation of TERRA. UPF1 has been shown to interact with TPP1 and telomerase during telomeric replication in S-phase and G2/M where it is suggested to sustain leading-strand telomeric replication (Chawla *et al.*, 2011). Additionally, UPF1 has been shown to be part of a telomeric protective complex which prevents DNA damage, telomeric loss and chromosomal fusions (Bottoni *et al.*, 2019). UPF1 has also been suggested to promote DNA repair within telomeric repeats by promoting DNA resection through the formation of R-loops (Ngo, Grimstead and Baird, 2021). DNA repair within telomeres has also been demonstrated to be regulated by TERRA expression levels (Porro *et al.*, 2014). This function is suggested to be independent of NMD but dependent on UPF3b. Interestingly, overexpression of the NMD downstream endonuclease factor SMG6 has also been shown to promote anaphase bridge formation and telomere end fusions, suggesting it too has a role in telomeric homeostasis (Snow *et al.*, 2003). Therefore, it is possible that certain components of the NMD machinery have distinct roles in the maintenance of telomeres, independent of NMD.

### **1.7.5 UPF1 in Cancer**

Due to its involvement in the regulation of gene expression as well as implications in the maintenance of genomic stability, UPF1 dysregulation is a prominent feature of many human cancers including hepatocellular carcinoma (HCC) (Chang *et al.*, 2016; Zhou *et al.*, 2019; Li *et al.*, 2022), colorectal cancer (CRC) (Bokhari *et al.*, 2018), breast cancer (Yuan *et al.*, 2025) and lung adenocarcinoma (LADC) (Cao *et al.*, 2017; Han *et al.*, 2020). Several studies have reported that UPF1 acts as a tumour-suppressor and is frequently downregulated. UPF1 has also been shown to be overexpressed and function as an oncogene in HCC and LADC (Bokhari *et al.*, 2018; Han *et al.*, 2020), meaning that targeting UPF1 in LADC or HCC could be a potential treatment option (Fang *et al.*, 2024). UPF1 has also been shown to promote a stem cell-like phenotype in LADC (Wang *et al.*, 2020). Further understanding the NMD-dependent and NMD-independent functions of UPF1 is critical in overcoming cancer cell resistance in UPF1 overexpressing tumours and targeting UPF1 for therapeutic intervention.

## 1.8 Aims and Hypothesis

As previously described, preliminary data in the Thompson laboratory (University of Sheffield) showed that following DNA damage, mitotic cells experience prolonged mitotic transit. Through an siRNA screen analysing mitotic population changes following DNA damage, UPF1 was implicated in being required for this delay to occur, without having any effect on unperturbed mitotic progression (**Figure 1.1.6**).

The hypothesis of this thesis is that UPF1 has a role in the regulation of mitosis in response to DNA damage or replication stress.

The aims of this thesis are:

1. Validate the requirement of UPF1 in the regulation of mitosis following DNA damage
2. Characterise the role by which UPF1 regulates mitosis
3. Investigate implicated pathways of UPF1 in the regulation of mitosis following DNA damage or replication stress

# Chapter 2: Materials and Methods

## 2.1 Materials

### 2.1.1 Reagents

Reagent	Supplier
4',6-Diamidino-2-phenylindole dihydrochloride (DAPI)	Life technologies
Agar	Melford
Ammonium persulfate (APS)	Sigma-Aldrich
Ampicillin	Thermo Fisher Scientific
Block Aid	Invitrogen
Bovine serum albumin (BSA)	Sigma-Aldrich
Bromophenol blue	Sigma Aldrich
DharmaFECT 1 transfection reagent	Horizon Dharmacon
Dharmafect duo	Horizon Dharmacon
Dimethyl sulfoxide (DMSO)	Thermo Fisher Scientific
DNA Fibre Combing Kit	Genomic Visions
Doxycycline hyclate	Sigma-Aldrich
Dried skimmed milk powder	Marvel
Dulbecco's Modified Eagle's Medium (DMEM)	Sigma-Aldrich
EdU Click-iT Reaction Kit	Thermo Fisher Scientific
Enhanced chemiluminescence (ECL)	Thermo Fisher Scientific
Epredia™ Immu-mount™	Thermo Fisher Scientific
Ethanol	Thermo Fisher Scientific
Ethylene glycol tetraacetic acid (EGTA)	Sigma-Aldrich
Ethylenediaminetetraacetic acid (EDTA)	Sigma-Aldrich
Foetal calf serum (FCS)	Life Science Productions
Glycine	Thermo Fisher Scientific
HEPES	Sigma-Aldrich
Hydrochloric acid (HCL)	Thermo Fisher Scientific
Hygromycin B	Roche
Industrial methylated spirit (IMS)	Thermo Fisher Scientific
Luria broth base (LB), Millers Modified	Merck

<b>Reagent (Continued)</b>	<b>Supplier</b>
Magnesium chloride (MgCl <sub>2</sub> )	Thermo Fisher Scientific
Methanol	Thermo Fisher Scientific
Nuclease-free water	Invitrogen
Paraformaldehyde 4 %	Chem Cruz
PhosSTOP phosphatase inhibitor tablets	Roche
PIPES	Sigma-Aldrich
Precision plus molecular weight marker	Bio-Rad
Propidium iodide (PI)	Sigma-Aldrich
Protease cocktail inhibitor	Roche
ProtoGel 30 % Acrylamide mix	Geneflow
RNase A	Sigma-Aldrich
siRNA universal buffer	Dharmacon
Sodium chloride (NaCl)	Thermo Fisher Scientific
Sodium dodecyl sulfate (SDS)	Sigma-Aldrich
Sodium hydroxide (NaOH)	Thermo Fisher Scientific
β-Mercaptoethanol	Sigma-Aldrich
Sucrose	Sigma Aldrich
Tetramethylethylenediamine (TEMED)	Thermo Fisher Scientific
Tris base	Sigma-Aldrich
Triton-X 100	Alfa Aesar
Trypsin-EDTA	Sigma
Tween-20	Acros Organics
X-ray developer	Champion Photochemistry
X-ray fixer	Champion Photochemistry

### 2.1.2 Mammalian Cell Lines

Cell Line	Cell Type	Antibiotic Sensitivity	Supplier
<b>UPF1<sup>R843C</sup>-Flag HeLa</b>	HeLa Flp-In T-REx cell line	Hygromycin B and Blastidicin S Hydrochloride	A kind gift from Professor Carl Smythe (University of Sheffield)
<b>UPF1<sup>S42A</sup>-Flag HeLa</b>	HeLa Flp-In T-REx cell line	Hygromycin B and Blastidicin S Hydrochloride	A kind gift from Professor Carl Smythe (University of Sheffield)
<b>UPF1<sup>S42E</sup>-Flag HeLa</b>	HeLa Flp-In T-REx cell line	Hygromycin B and Blastidicin S Hydrochloride	A kind gift from Professor Carl Smythe (University of Sheffield)
<b>UPF1<sup>WT</sup>-Flag HeLa</b>	HeLa Flp-In T-REx cell line	Hygromycin B and Blastidicin S Hydrochloride	A kind gift from Professor Carl Smythe (University of Sheffield)
<b>RPE<sup>WT</sup></b>	Retinal Pigment Epithelium cell line	-	A kind gift from Dr Greg Ngo (Cardiff University)
<b>RPE<sup>UPF1 KO</sup></b>	Retinal Pigment Epithelium cell line	-	A kind gift from Dr Greg Ngo (Cardiff University)

### 2.1.3 Buffers and Stock Solutions

#### Phosphate buffered saline (PBS)

1x PBS was made by dissolving 1 PBS tablet (Oxoid) in dH<sub>2</sub>O (100 ml). The solution was made and autoclaved by departmental technical staff. PBS solution was stored at room temperature.

#### 1 M Tris (pH 6.8)

121.14 g tris base was dissolved in ddH<sub>2</sub>O and 10M HCL was added to achieve pH 6.8, then made up to 1 L with ddH<sub>2</sub>O and stored at room temperature.

### **1.5 M Tris (pH 8.8)**

181.71 g tris base was dissolved in dH<sub>2</sub>O and 10M HCL was added to achieve pH 8.8, then made up to 1 L with dH<sub>2</sub>O and stored at room temperature.

### **10 % APS**

0.5 g APS was dissolved in 5 mL dH<sub>2</sub>O and stored at 4 °C. 10 % APS was made fresh each week.

### **10 % SDS**

50 g SDS was dissolved in 500 ml dH<sub>2</sub>O and stored at room temperature.

### **5x Radioimmunoprecipitation assay (RIPA) lysis buffer**

25 ml 1 M Tris pH 8.0 (250 mM), 15 mL 5M NaCl (750 mM), 5 mL 10 % SDS (0.5 %), 5 ml NP-40 alternative (5 %), 2.5 g sodium deoxychorate (2.5 %), and made to 100 ml in dH<sub>2</sub>O. 5x RIPA lysis buffer and stored at room temperature. This buffer was diluted to a 1x working solution in dH<sub>2</sub>O for each use.

### **10X PhosStop**

1 tablet of PhosStop (Roche) was dissolved in 1ml of ddH<sub>2</sub>O. The solution was kept on ice then stored at -20°C.

### **10X Protease Inhibitor Cocktail**

1 tablet of cOmplete mini, EDTA-free protease inhibitor cocktail (SIGMA) was dissolved in 1ml of ddH<sub>2</sub>O. The solution was kept on ice then stored at -20°C.

### **5x Protein SDS-polyacrylamide gel electrophoresis (SDS-PAGE) loading dye**

25 ml 1 M Tris pH 6.8 (250 mM), 50 ml Glycerol (50 %), 5 ml β-Mercaptoethanol (5 %), 20 mg bromophenol blue (0.02 %), 10 g SDS (10 %) and made to 100 ml with dH<sub>2</sub>O. 5x protein SDS-PAGE loading dye was stored at room temperature.

### **1X SDS-PAGE running buffer**

10x SDS-PAGE running buffer was prepared by dissolving 30.3 g tris base (250 mM) and 144 g glycine (1.9 M) in 900 ml dH<sub>2</sub>O, 100 ml 10% SDS (1 %) was added for a

final volume of 1 L. The working solution of 1x SDS-PAGE running buffer was prepared by diluting 100 ml 10x SDS running buffer with dH<sub>2</sub>O to a total volume 1 L and stored at room temperature. Both buffers were stored at room temperature.

### **1X Transfer buffer**

10x transfer buffer was prepared by dissolving 30.3 g tris base (250 mM) and 144 g glycine (1.9 M) in 1 L dH<sub>2</sub>O. 10x transfer buffer was stored at room temperature. The working solution of 1x transfer buffer was prepared by diluting 100 mL 10x transfer buffer with 200 ml methanol and made to 1 L with dH<sub>2</sub>O. 1x transfer buffer was made on the day of use.

### **10x Tris-buffered saline (TBS) (pH 7.6)**

24.2 g tris base (200 mM) and 80 g NaCl (1.4 M) dissolved in dH<sub>2</sub>O and 10 M HCL added to achieve pH 7.6. Total volume was made to 1 L with dH<sub>2</sub>O and stored at room temperature.

### **1x TBS-Tween (TBS-T)**

100 ml 10x TBS stock was diluted with 900 ml dH<sub>2</sub>O with the addition of 1 ml Tween-20 (0.1 %). 1x TBS-T was stored at room temperature.

### **5 % Milk**

2.5 g milk powder was dissolved in 50 ml 1xTBS-T. 5 % Milk was stored at 4 °C.

### **5% BSA**

2.5g of BSA powder was dissolved in 50ml 1XTBS-T. 5% BSA was stored at 4°C.

### **LB Broth**

10 g LB broth (2.5%) was dissolved in 400ml of ddH<sub>2</sub>O. LB broth was autoclaved to sterilise before use and stored at room temperature.

### **LB Agar**

12 g agar (3%) and 10 g LB broth (2.5%) was dissolved in 400ml of ddH<sub>2</sub>O. LB Agar was autoclaved before use to sterilise and stored at room temperature.

### **PTMEF Buffer**

PTMEF buffer was prepared 10min prior to use for each experiment by combining 200 $\mu$ l 1M PIPES pH 6.8 (200mM), 200 $\mu$ l 1M MgCl<sub>2</sub> (200mM), 30 $\mu$ l 0.25M EGTA pH 8.0 (10mM), 400 $\mu$ l 10% PFA (4%), 2 $\mu$ l Triton X-100 (0.2%) and 160 $\mu$ l PBS.

### **0.1M Glycine**

1.50g of Glycine powder was dissolved in 200ml ddH<sub>2</sub>O.

### **Pre-extraction Buffer**

1.026g sucrose (300mM) dissolved in 9.1ml ddH<sub>2</sub>O along with 250 $\mu$ l 1M HEPES (pH 7.5) (25mM), 100 $\mu$ l 5M NaCl (50mM), 20 $\mu$ l 500mM EDTA (1mM), 30 $\mu$ l 1M MgCl<sub>2</sub> and 0.5ml 10% Triton X-100 in ddH<sub>2</sub>O (0.5%). Solution was made fresh on the day of use and stored on ice.

### **1M PIPES (pH 6.8)**

15.1g of PIPES was dissolved in 30ml of ddH<sub>2</sub>O then NaOH pellets were added to achieve a pH of 6.8. The solution was then made up to 50ml with ddH<sub>2</sub>O.

### **1M MgCl<sub>2</sub>**

4.76g of MgCl<sub>2</sub> was dissolved in 50ml of ddH<sub>2</sub>O.

### **0.25M EGTA (pH 8.0)**

0.95g of EGTA was dissolved in 5ml of ddH<sub>2</sub>O then the pH adjusted to 8.0 by addition of NaOH or HCl where appropriate. The solution was then made up to a final volume of 10ml.

### **1M HEPES (pH 7.5)**

23.83g of HEPES was dissolved in 60ml of ddH<sub>2</sub>O then 1M HCl was added to achieve a pH 7.5 then the solution was made up to 100ml with ddH<sub>2</sub>O.

### **5M NaCl**

146.1g of NaCl was dissolved in 500ml of ddH<sub>2</sub>O.

### 500mM EDTA

14.612g of EDTA was dissolved in 75ml of ddH<sub>2</sub>O, NaOH pellets were added whilst stirring until all precipitate had dissolved then the solution was made up to 100ml with ddH<sub>2</sub>O.

### DNA Fibre Denaturation Solution

50ml of denaturation solution was prepared by dissolving 1g of NaOH pellets and 2.93g of NaCl in 30ml of ddH<sub>2</sub>O until all precipitate had dissolved. The solution was then made up to 50ml with ddH<sub>2</sub>O.

#### 2.1.4 Treatment Compounds

Compound	Mechanism of action	Diluent	Supplier
<b><math>\alpha</math>-Amanitin</b>	RNA Polymerase II Inhibitor	H <sub>2</sub> O	Sigma-Aldrich
<b>Actinomycin D</b>	DNA intercalator	DMSO	Invitrogen
<b>Aphidicolin</b>	Inhibitor of eukaryotic nuclear DNA replication	DMSO	Scientific Laboratory Supplies
<b>AZD0156</b>	ATM Inhibitor	DMSO	Selleckchem
<b>AZD6738</b>	ATR Inhibitor	DMSO	Selleckchem
<b>BrdU</b>	Thymidine analogue	Serum-free DMEM	A kind gift from Professor Helen Bryant (University of Sheffield)
<b>Carboplatin</b>	Forms inter- and intra-DNA adducts	H <sub>2</sub> O	Sigma-Aldrich

<b>Compound (Continued)</b>	<b>Mechanism of Action</b>	<b>Diluent</b>	<b>Supplier</b>
<b>CldU</b>	Thymidine analogue	Serum-free DMEM	Merck Life Science
<b>Doxycycline</b>	Antibiotic	H <sub>2</sub> O	A kind gift from Dr Katie Myers (University of Sheffield)
<b>DRB</b>	CDK9 Inhibitor	DMSO	Scientific Laboratory Supplies
<b>EdU</b>	Thymidine analogue	DMSO	Fisher Scientific Ltd
<b>Hydroxyurea</b>	Inhibitor of eukaryotic nuclear DNA replication	H <sub>2</sub> O	Thermo Fisher Scientific
<b>Hygromycin B</b>	Antibiotic	H <sub>2</sub> O	Generon
<b>IdU</b>	Thymidine analogue	Serum-free DMEM	Merck Life Science
<b>RO-3306</b>	CDK1 Inhibitor	DMSO	Generon
<b>VG1</b>	Inhibits interaction between UPF1 and SMG5	DMSO	A kind gift from Professor Carl Smythe (University of Sheffield)

### 2.1.5 Short interfering ribonucleic acid (siRNA)

All siRNAs were made to a stock solution of 20 $\mu$ M with the manufacturer recommended buffer and stored at -20°C.

siRNA duplexes	Sequence (5'-3')	Resuspension Buffer	Supplier (cat number)
siGENOME non-targeting control pool 1	UAAUGUAUUGGAACGCA	1x siRNA buffer	Horizon (D-001206-13)
siSMG1 SMARTPool	Made of the 4-individual siRNA	Nuclease-free water	Dharmacon (L-005033-00)
siSMG5 SMARTPool	Made of the 4-individual siRNA	Nuclease-free water	Dharmacon (L-014023-00)
siSMG6 SMARTPool	Made of the 4-individual siRNA	Nuclease-free water	Dharmacon (L-017845-01)
siStau1 SMARTPool	Made of the 4-individual siRNA	Nuclease-free water	Dharmacon (M-011894-01)
siUPF1-1	GCUCCUACCUGGUGCAGUA	1x siRNA buffer	Dharmacon (D-011763-01)
siUPF1-Res	UUCUUCACACGAUCCGCUGUU	Nuclease-free water	Horizon
siUPF2 SMARTPool	Made of the 4-individual siRNA	Nuclease-free water	Dharmacon (M-012993-01)
siUPF3b SMARTPool	Made of the 4-individual siRNA	Nuclease-free water	Dharmacon (M-012871-00)
siBubR1	CAGATTTAGCACATTTACTAT	Nuclease-free water	Qiagen (SI000605017)

## 2.1.6 Plasmids

Protein	Protein Tag	Plasmid	Antibiotic resistance	Supplier (cat number)
RNaseH1-D210N	V5-tag	ppyCAG	Hygromycin	Addgene (111904) a gift from Xiang-Dong Fu
RNaseH1-WT	V5-tag	ppyCAG	Hygromycin	Addgene (111906) a gift from Xiang-Dong Fu

## 2.1.7 Antibodies

### 2.1.7.1 Primary antibodies

Primary Antibody	Host Animal	Application and Dilution	Supplier (cat number)
$\beta$ -Actin	Mouse	WB (1:1000)	Santa Cruz (sc-47778)
$\gamma$ -H2AX (Ser139)	Rabbit	WB (1:500)	Novus Biologicals (NB100-74435)
53BP1	Rabbit	IF (1:200)	Abcam (ab36823)
Anti-BrdU (CldU)	Rat	IF (0.8:25)	Abcam (ab6326)
Anti-BrdU (IdU)	Mouse	IF (4:25)	BD Biosciences (347580)
Anti-DNA-RNA Hybrid, clone S9.6	Mouse	IF (1:100)	MERCK Millipore (MABE1095)
Cyclin A2	Mouse	IF (1:200)	Cell Signalling (4656S)
FANCD2	Rabbit	IF (1:200)	Novus Biologicals (NB100-182)
FLAG-M2	Mouse	WB (1:1000)	SIGMA (F1804)
Phospho-ATM (Ser1981)	Rabbit	WB (1:1000)	Epitomics (YH101212D)
Phospho-Chk1 (Ser345)	Rabbit	WB (1:1000)	Cell Signalling (2348S)
Phospho-Histone H3 (Ser10)	Mouse	IF (1:200)	Abcam (ab14955)

<b>Primary Antibody (Continued)</b>	<b>Host Animal</b>	<b>Application and Dilution</b>	<b>Supplier (cat number)</b>
<b>Phospho-RNAPII CTD (Ser2)</b>	Rat	WB (1:10000)	MERCK Millipore (3943321)
<b>Phospho-UPF1 (Ser1096)</b>	Rabbit	WB (1:1000)	EMD Millipore (07- 1016)
<b>RPA32/RPA2</b>	Mouse	IF (1:200)	Abcam (ab2175)
<b>SMG1</b>	Rabbit	WB (1:1000)	Cell Signalling (D42D5)
<b>SMG5</b>	Rabbit	WB (1:1000)	Proteintech (12694-1- AP)
<b>SMG6</b>	Rabbit	WB (1:1000)	GeneTex (GTX131919)
<b>STAU1 (C-4)</b>	Mouse	WB (1:1000)	Santa Cruz (SC- 390820)
<b>Total-Chk1</b>	Mouse	WB (1:1000)	Cell Signalling (2G1D5)
<b>Total-RNAPII</b>	Mouse	WB (1:10000)	Cell Signalling (2629S)
<b>UPF1</b>	Rabbit	WB (1:1000), IF (1:200)	Cell Signalling (D15G6)
<b>UPF3B</b>	Rabbit	WB (1:1000)	Cell Signalling (E5U4C)
<b>V5-Tag</b>	Rabbit	IF (1:200)	Cell Signalling (D3HEQ)

### 2.1.7.2 Secondary antibodies

Secondary Antibody	Host Animal	Application and Dilution	Supplier (cat number)
Alexa Fluor™ 647 goat anti-mouse IgG	Donkey	IF (1:200)	Thermo Fisher Scientific (A-31571)
Alexa Fluor™ 488 goat anti-mouse IgG	Goat	IF (1:200)	Invitrogen (A11017)
Alexa Fluor™ 594 goat anti-rabbit IgG	Goat	IF (1:200)	Invitrogen (A11012)
Alexa Fluor™ 647 goat anti-human IgG	Goat	IF (1:200)	Invitrogen (A21445)
Goat anti-mouse Cy3	Goat	IF (2:25)	Abcam (ab97035)
Goat anti-mouse horse radish peroxidase (HRP)	Goat	WB (1:5000)	Invitrogen (A16078)
Goat anti-rat IgG Cy5	Goat	IF (2:25)	Abcam (ab6565)
Polyclonal swine Anti-Rabbit Immunoglobulin HRP	Swine	WB (1:5000)	Dako (P0399)
StarBright Blue 520 goat anti-mouse IgG	Goat	WB (1:4000)	Bio-rad (12005867)
StarBright Blue 520 goat anti-rabbit IgG	Goat	WB (1:4000)	Bio-rad (12005870)
StarBright Blue 700 goat anti-mouse	Goat	WB (1:4000)	Bio-rad (12004158)
StarBright Blue 700 goat anti-rabbit	Goat	WB (1:4000)	Bio-rad (12004162)

## **2.2 Methods**

### **2.2.1 Mammalian tissue culture**

#### **2.2.1.1 Culture conditions and passaging**

All tissue culture was carried out using a class II A/B3 biological safety cabinet. HeLa and RPE cell lines were cultured in DMEM, supplemented with 10% FCS and incubated at 37°C with 5% CO<sub>2</sub>. All TREx HeLa lines were grown with antibiotic selection with Hygromycin B (200µg/ml) added to each flask. All cell lines were cultured in T75 flasks with 10ml total media volume.

Cells were passaged once they reached 70-80% confluency through the removal of media, gentle washing with sterile PBS and then incubated with 3ml trypsin-EDTA at 37°C for 5 minutes. Following cell detachment, the appropriate pre-warmed media (7ml) was added to each flask, cell suspension was then diluted in a new flask with fresh medium and selection reagents where appropriate.

For plating of cells, cell suspensions were counted on a haemocytometer and the desired number of cells used to plate for the experiment.

#### **2.2.1.2 Cell freezing and thawing**

The cell suspension was centrifuged at 180×g for 3 minutes in a benchtop centrifuge. The pellet was resuspended in 2ml fresh media with 20% FCS and 10% DMSO. The suspension was divided into cryovials (1ml) and stored in a Mr. Frosty™ freezing container at -80°C. For long term storage (> 1 year) cell stocks were transferred to liquid nitrogen.

Frozen cell stocks were defrosted at 37°C in a water bath, added to 9ml fresh media then centrifuged at 180×g for 3 minutes. The pellet was resuspended in 10ml fresh media then transferred to a T25 or T75 flask, depending on the number of cells frozen down. Cells were grown at 37°C and passaged at least 3 times in T75 flasks before being used for experimental work.

## **2.2.2 Gene manipulation**

### **2.2.2.1 siRNA transfection**

$1.5 \times 10^5$  cells were plated per well in a 6 well plate 4 hours prior to transfection. For each transfection reaction, 5ul siRNA (20 $\mu$ M stock) was added to 245 $\mu$ l SFM and 3 $\mu$ l DharmaFECT-1 added to 247 $\mu$ l. For double siRNA transfection 2.5 $\mu$ l of siRNA (20 $\mu$ M stock) was added for each siRNA and transfected with the same volume of DharmaFECT-1 and SFM as used for single transfections. These solutions were incubated for 5 minutes then mixed and incubated for a further 20 minutes. 500 $\mu$ l of the resulting transfection reaction was added drop wise to each plated well containing 1.5ml media, to give a final siRNA concentration of 50nM. siGENOME non-targeting control pool (Dharmacon) siRNAs were used in parallel to targeted siRNAs as a negative control.

### **2.2.2.2 Double transfection of siRNA and cDNA with Dharmafect Duo**

$2.5 \times 10^5$  cells were seeded into a 6 well plate and left to adhere overnight. cDNA concentration was used at 250ng for both RNaseH1<sup>WT</sup> and RNaseH1<sup>D210N</sup>. 5  $\mu$ L siRNA (20  $\mu$ M stock) was added along with the correct volume of cDNA and 200  $\mu$ L SFM. In a separate tube, 5  $\mu$ L Dharmafect duo transfection reagent was added to 200  $\mu$ L SFM. The reaction was incubated for 5 minutes, then mixed and incubated for 20 minutes at room temperature. The total 400  $\mu$ L of cDNA-siRNA-Dharmafect duo solution was added to each well dropwise. Cells were incubated for 48 hours post-transfection.

## **2.2.3 Bacterial culture and plasmid preparation**

### **2.2.3.1 Bacterial stab inoculation**

Purchased bacterial stabs of RNaseH1<sup>WT</sup> and RNaseH1<sup>D210N</sup> transformed bacteria were used to spread colonies on to LB-Agar plates containing 100 $\mu$ g/ml Ampicillin. The plates were left overnight at 37°C, then individual colonies were picked and used to inoculate 5ml of LB Broth with 200 $\mu$ g/ml Ampicillin.

### **2.2.3.2 Transformation of *E.coli* strain DH5 $\alpha$**

RNaseH1<sup>WT</sup> and RNaseH1<sup>D210N</sup> plasmids were transformed into chemically competent *E.coli* strain DH5 $\alpha$ . 0.5 $\mu$ l of plasmid was mixed with 45 $\mu$ l of chemically competent DH5 $\alpha$ . The solution was mixed and left on ice for 20mins before being heat shocked

at 42°C in a water bath for 45sec. The tube was then placed back on ice for 2mins before adding 500µl of prewarmed 42°C LB broth, then left for 1hr in a shaking incubator at 37°C. The bacterial culture was then centrifuged at 4000g for 5mins, most of the supernatant was removed and the bacterial pellet resuspended in the remaining solution. The bacterial solution was then streaked onto LB agar plates containing 100µg/ml Ampicillin. The plates were incubated at 37°C overnight to form discrete colonies. Several colonies were selected and used to inoculate 5ml LB broth containing 200µg/ml Ampicillin then left overnight at 37°C in a shaking incubator.

### **2.2.3.3 Plasmid purification**

Plasmid DNA was purified from the bacteria using the Qiagen spin miniprep kit following manufacturer instructions. The resultant plasmid concentrations were determined using the nanodrop spectrophotometer (ND-1000, Thermo Fisher) using the DNA-50 nucleic acid setting. Plasmid preparations were stored at -20°C.

## **2.2.4 Protein assays**

### **2.2.4.1 Cell harvesting for SDS-PAGE**

Cells were plated at the appropriate density for the time frame of an experiment into 6 well plates and treated accordingly.

### **2.2.4.2 Lysate preparation**

The media of each sample was removed, and each well was washed with PBS. Lysis buffer was prepared by the addition of 100µl of phosSTOP inhibitor (10x) and protein inhibitor cocktail (10x) to 1ml 1x RIPA buffer on ice. 50µl of lysis buffer was added to each well and incubated for 10 minutes on ice before being scraped using a cell scraper and the lysate transferred to a clean-labelled Eppendorf. The solution was left on ice for a further 10mins. The leftover lysis buffer was stored at -20°C.

Following incubation on ice each sample was centrifuged at 4°C for 15 minutes at 13,000 RPM. The resulting supernatants were collected and transferred into a new tube for quantification.

### **2.2.4.3 Protein quantification**

A Bradford assay was used to determine the concentration of protein in each sample. A protein standard curve was generated through the dilution of a 1mg/ml BSA stock solution to a range of concentrations (0-0.1mg/ml). Samples were diluted 1:100 then 40µl of each standard and sample was added in triplicate to a 96 well plate.

200µl of protein assay dye reagent (Bio-Rad) was added to each well, then the optical density (OD) for each sample and standard was measured at 595nm wavelength using the Multiscan™ FC microplate photometer. The protein standards were used to generate a standard curve by plotting the average OD against concentration. The sample concentrations were determined by interpreting the OD against the standard curve and accounting for the sample dilution factor.

All samples protein concentrations were standardised to the sample with the lowest protein content through the addition of a calculate volume of 1x protein SDS-PAGE loading dye. 5x protein SDS-PAGE loading dye was also added to each sample 1:4 then boiled at 70°C for 5 minutes and stored at -20°C.

### **2.2.4.4 SDS-PAGE and western blotting**

Polyacrylamide resolving gels were prepared at varying percentages with a 5% stacking gel. The components of which are described in **Table 2.2.1**. 10µl of a Bio-Rad Precision Plus molecular weight marker was loaded for every gel and 35-50µg of protein was loaded for each sample.

SDS-PAGE gels were run with 1x SDS Running Buffer at 120 V until the loading front had run off the gel. Protein was then wet transferred onto nitrocellulose membrane (GE healthcare) between Whattman filter paper with 1x transfer buffer at 94 V for 2-3 hours at 4°C. Membranes were blocked in either 5% milk or 5% BSA in TBS-T for 1 hour at room temperature then incubated overnight with primary antibodies at 4°C with gentle rocking. After this incubation the membrane was washed with 1x TBS-T 3 times for 5 minutes. The corresponding HRP-conjugated secondary antibody (1:5000) or StarBright Blue 520/700 secondary antibodies (1:4000) in the appropriate blocking

buffer was then incubated for 1 hour at room temperature on the rocker in the dark. The membrane was washed 3 times with TBS-T for 10 minutes.

For HRP-conjugated antibodies, activation of the conjugated HRP, to allow for visualisation of the protein, was carried out by preparing ECL reagent in equal volumes and putting on the membrane for 1 minute. The Kuiu medical x-ray film (Fujifilm) was exposed to the membrane in the dark room, developed and fixed using the RG universal x-ray developer and RG universal x-ray fixer in the SRX 101A film processor (Konica).

For StarBright secondary antibodies the blot was put in PBS and then the membranes were visualised on the Bio-rad Chemidoc MP imaging system with the appropriate detector.

Solution Components	Resolving Gel (10ml)			Stacking Gel (5ml)
	6%	10%	15%	5%
<i>H<sub>2</sub>O</i>	5.3ml	4ml	2.3ml	3.4ml
<i>30% Acrylamide mix</i>	2.0ml	3.3ml	5.0ml	0.83ml
<i>1.5M Tris (pH 8.8)/ 1M Tris (pH 6.8)</i>	2.5ml	2.5ml	2.5ml	0.63ml
<i>10% SDS</i>	100ul	100ul	100ul	50ul
<i>10% APS</i>	100ul	100ul	100ul	50ul
<i>TEMED</i>	8ul	4ul	4ul	5ul

**Table 2.2.1: SDS Gel Recipe**

## 2.2.5 Fluorescence-activated cell sorting (FACS)

### 2.2.5.1 Sample preparation

RPE<sup>WT</sup> and RPE<sup>UPF1<sup>KO</sup></sup> cells were seeded at 1x10<sup>6</sup> cells into a 10cm sterile dish and treated as required with 0.4µM aphidicolin for 4 and 24hrs. Prior to harvesting, cells were treated for 30mins with 5ml of 10µM BrdU in warm fresh media per 10cm dish. Each dish was then washed quickly with 5ml of pre-warmed PBS twice to remove BrdU and prevent nucleotide incorporation. The cells were detached by incubating

with 2ml trypsin for 5mins at 37°C before being diluted in 5ml of fresh media to neutralise trypsin and transferred to a 15ml falcon. The cells were centrifuged at 180g for 5mins to pellet and wash twice with PBS to remove residual FCS. After washing the resulting pellet was resuspended in a small volume of remaining PBS before being fixed by the gradual addition of 1ml ice-cold 70% ethanol. The fixed cells were then stored for up to 1 week at -20°C in the dark.

#### **2.2.5.2 Propidium Iodide (PI) and BrdU co-staining**

On the day of FACS analysis the cell pellet was centrifuged at 300g and the ethanol gently poured off before washing the pellet twice with 5ml PBS. To denature the DNA and allow for immunodetection of incorporated BrdU the cell pellet was resuspended with 10µl of 2M HCl and incubated at room temperature for 30mins. 5ml of PBS was added to each falcon tube and centrifuged to pellet and the supernatant removed. The pellet was then washed three times with 5ml of PBS followed by one wash with 5ml PBS-T solution (0.1% BSA, 0.2% Tween20 in PBS). To detect BrdU the cell pellet was then incubated with 10µl anti-BrdU solution (1:1, BrdU antibody: PBS) pipetted directly to the cell pellet and resuspended well before being left at room temperature in the dark for 30mins. The cell pellet was then washed twice with 5ml PBS-T solution before being incubated with 50µl of secondary antibody solution (1:10, anti-mouse AF488: PBS) for 20mins in the dark. After secondary antibody labelling the cell pellet was washed once in PBS then left in the fridge.

Prior to running the samples on the FACS machine, cell pellets were treated with 50µl of 100µg/ml RNaseA for 15mins at room temperature. They were then incubated with 200µl of 50µg/ml propidium iodide (PI) solution for 15mins. Samples were processed on the Aurora 3 Laser Spectral Flow Cytometer using the violet and blue lasers (Cytex Biosciences). An unstained control and single stain controls for PI and BrdU were also prepared to allow for autofluorescence extraction.

#### **2.2.5.3 Analysis**

Debris was excluded from the analysis by plotting the FSC-A against SSC-A and gating a clear cellular population (see **Figure 2.1**, *top left panel*). Doublet discrimination was then carried out by plotting PI-width against PI-area, doublets

appear as cells with double width, so we gated for low PI-width cells (see **Figure 2.1**, *top right panel*). 10,000 events were collected in this gate per condition to produce both a PI-area histogram and AF488-area against PI-area scatter plot. G1 and G2 proportions were defined as cells negative for AF488 but with differing PI content (see **Figure 2.1**, bottom right panel). To confirm this, a BrdU negative control was used in which cells were not incubated with BrdU but still stained (see **Figure 5.2.5H**). Early S-phase cells were gated as having G1 PI-area but staining positive for AF488 and mid-Late S-phase were dictated as having above G1 PI-area whilst still positive for AF488.

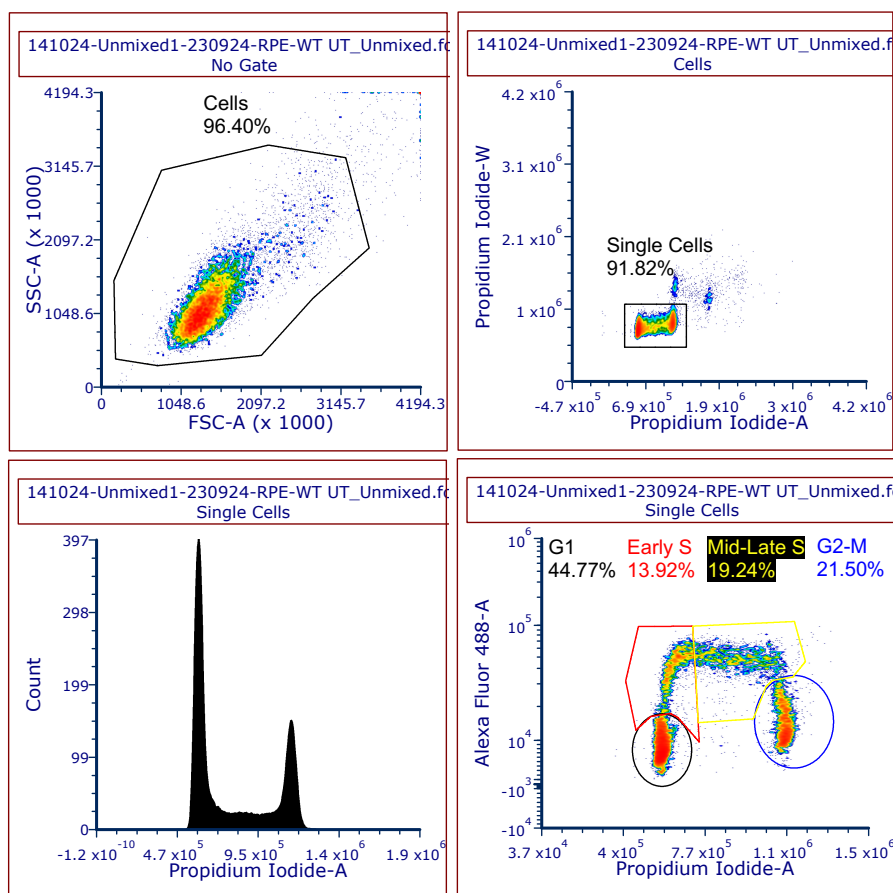


**Figure 2.2.1: FACS gating strategy.**

Cells were first gated for in the top left plot, removing any debris in the sample. Doublets were then excluded in the top right plot, the black box gates in single cells since doublets are visible as having greater PI width. This single cell population was used for subsequent cell cycle analysis.

## **2.2.6 Immunofluorescence assays**

### **2.2.6.1 R-loop quantification interphase**

#### **2.2.6.1.1 S9.6 staining method**

Forward transfection was carried out on HeLa cells with indicated siRNAs as previously described (**Section 2.2.2.2**). 48hrs post-transfection cells were treated as indicated with 0.4 $\mu$ M aphidicolin for 23hrs and 1 $\mu$ M carboplatin for 6hrs prior to fixation. Cells were fixed by addition of 2ml ice-cold 100% methanol for 7mins at -20°C. Cells were then subsequently rehydrated by removal of the methanol and washing with 2ml PBS three times for 5mins each. Each well was washed one at a time to avoid cells drying out at any point. Coverslips were then quenched by addition of 2ml freshly prepared 0.1M Glycine solution for 10mins at room temperature, followed by washing three times with PBS for 5mins each. Coverslips were then permeabilised by addition of 2ml 0.2% Triton-X solution for 7mins before being washed again for three times with PBS for 5mins. To detect R-loops, coverslips were then inverted onto 85 $\mu$ l mouse anti-S9.6 primary antibody diluted 1:250 in PBS, on parafilm, inside of a humid chamber. The chamber was covered and left in the dark for 1hr at room temperature. Coverslips were then transferred to a fresh 6 well plate and washed three times with PBS. The coverslips were then inverted onto 85 $\mu$ l AF488 anti-mouse secondary antibody diluted 1:1000 in PBS, on parafilm, inside of a humid chamber for 1hr at room temperature. The coverslips were then returned to the 6 well plate before being washed two times with PBS. Nuclei were then counterstained by incubating with 1:1000 DAPI-PBS solution for 5mins. Coverslips were then mounted with Immu-Mount onto microscope slides and allowed to set in the dark before being stored at 4°C prior to imaging.

#### **2.2.6.2 R-loop quantification, V5-RNaseH1<sup>D210N</sup>**

HeLa cells were transfected with V5-RNaseH1<sup>D210N</sup> plasmid with indicated siRNAs as described (**Section 2.2.2.2**). 48hrs post-transfection cells were treated as indicated with 0.4 $\mu$ M Aphidicolin for 23hrs and 1 $\mu$ M Carboplatin for 6hrs prior to fixation. Cells were then pre-extracted with freshly made ice-cold Pre-extraction buffer for 2mins on ice before being fixed for 10mins on ice with 4% PFA in PBS. Cells were then washed three times with PBS before being stored in PBS at 4°C until staining.

To detect R-loops cells were permeabilised for 10mins with 0.1% Triton-X 100 then blocked with 1% BSA in PBS for 1hr at room temperature. Coverslips were inverted onto 150µl of 1:200 rabbit anti-V5-Tag and mouse anti-RPA32 antibodies in blocking buffer and incubated for 1hr at room temperature. Coverslips were then washed with PBS for 5mins three times before being flipped onto 150µl of 1:200 anti-rabbit AF594 and anti-mouse AF488 secondary antibodies in blocking buffer and incubated for 1hr at room temperature. Coverslips were then returned to the plate and washed twice with PBS twice for 5mins each. Nuclei were then counterstained by incubating with 1:1000 DAPI-PBS solution for 5mins. Coverslips were then mounted with Immu-Mount onto microscope slides and allowed to set in the dark before being stored at 4°C prior to imaging.

### **2.2.6.3 Mitotic DNA synthesis (MiDAS) assay**

#### **2.2.6.3.1 Cell plating and treatment**

Forward transfection was carried out as previously described (**Section 2.2.2.1**) on UPF1 FLP-IN HeLa mutant cell lines and where appropriate cells were induced with 1µM Doxycycline. 48hrs post-transfection cells were treated with 0.4µM Aphidicolin in 2ml fresh media for 23hrs prior to harvesting. All conditions were treated with 9µM RO3306 for 5hrs prior to harvesting. Media was aspirated and then cells subsequently washed with pre-warmed PBS three times for 3mins each. 1ml fresh media containing 20µM EdU was added and incubated with the cells for 25mins. Mitotic cells were collected through mitotic shake-off by gently vortexing the 6 well plate and collecting the resultant cell suspension. The cell suspension was pelleted in a 15ml falcon tube at 300g for 5mins and most of the resultant supernatant discarded. The pellet was gently resuspended in 100µl of remaining media by gently pipetting up and down and then seeded onto a poly-L-lysine coated coverslip in a new 6 well plate. The cells were left to adhere for 5mins before the media was gently poured off the coverslip and aspirated. Cells were fixed with 100µl of freshly made PTMEF buffer for 10mins in a fume hood. Fixative was then removed, and the coverslips washed three times with PBS. Coverslips were then stored in PBS at 4°C until being stained.

### **2.2.6.3.2 Staining method**

To detect EdU, slides were blocked in 3% BSA-PBS solution for 30mins at RT then permeabilised with 0.5% Triton X-100 in PBS for 20mins. Coverslips were then inverted onto 50 $\mu$ l of EdU Click-iT Reaction Mix (Fisher Scientific Ltd) according to manufacture instructions and incubated for 1hr at RT in the dark. The coverslips were then returned to a 6 well plate and washed three times with 3% BSA in 0.5% Triton-X 100 in PBS for 20mins each. Then coverslips were washed for 5mins with 1:1000 DAPI in PBS then mounted onto a microscope slide using Immu-Mount and allowed to set in the dark before being stored at 4°C prior to imaging.

### **2.2.6.3.3 Analysis**

Z-stack images were taken of each slide on a Nikon W1 Spinning Disk Confocal microscope using a 63X lens. FIJI Image J software was used to count the number of EdU foci per prophase cell which were identified by their ring-shaped condensed DNA.

First the Z-stack images were converted into single images by carrying out a maximum projection. The DAPI stain was made binary and used to create as mask for the nuclei of each cell. The find maxima function with a prominence of 500 was used to pick out individual foci and then the integrated density of each cell was used to calculate the number of foci by dividing by 255.

## **2.2.6.4 53BP1 nuclear body assay**

### **2.2.6.4.1 Cell plating and treatment**

Forward transfection was carried out as previously described (**Section 2.2.2.1**) on UPF1 FLP-IN HeLa mutant cell lines and where appropriate cells were induced with 1 $\mu$ M Doxycycline. 48hrs post-transfection cells were treated with 0.4 $\mu$ M Aphidicolin in 2ml fresh media for 23hrs. All conditions were treated with 9 $\mu$ M RO3306 for 5hrs prior to harvesting. Media was aspirated and then cells subsequently washed with pre-warmed PBS three times for 3mins each. Mitotic cells were collected through mitotic shake-off by gently vortexing the plate and collecting the resultant cell suspension. The cell suspension was pelleted in a 15ml falcon tube at 300g for 5mins and most of the resultant supernatant discarded. The pellet was gently resuspended in 100 $\mu$ l of remaining media by gently pipetting up and down and then seeded onto a poly-L-lysine

coated coverslip in a new 6 well plate. The cells were left to adhere for 5mins before the 2ml of fresh media was gently pipetted into the well. The plate was returned to the incubator and incubated for 2.5hrs before being fixed with 4% PFA for 10mins on ice in a fume hood. Fixative was then removed, and the coverslips washed three times with PBS. Coverslips were then stored in PBS at 4°C until being stained.

#### **2.2.6.4.2 Staining method**

Slides were blocked in 3% BSA-PBS solution for 30mins at RT then permeabilised with 0.5% Triton X-100 in PBS for 20mins. Coverslips were then inverted onto 200µl of 1:200 rabbit anti-53BP1 and mouse anti-Cyclin A2 primary antibodies and incubated O/N at 4°C. The coverslips were then returned to a 6 well plate and washed three times with 0.5% Triton-X 100 in PBS for 10mins each. Coverslips were then inverted onto 150µl 1:200 AF594 goat anti-rabbit and AF488 goat anti-mouse secondary antibodies in Blocking Buffer. Coverslips were incubated for 1hr in the dark at room temperature. Coverslips were then returned to the 6 well plate and washed three times with 0.5% Triton X-100 in PBS for 10mins then incubated with 1:1000 DAPI-PBS solution for a further 5mins. Coverslips were mounted using Immu-Mount onto microscope slides and allowed to set in the dark before being stored at 4°C prior to imaging.

#### **2.2.6.4.3 Analysis**

Z-stack images were taken of each slide on a Zeiss LSM980 confocal microscope using a 63X lens.

FIJI Image J software was used to count the number of 53BP1 foci per G1 cell which were identified by being Cyclin A negative. First the Z-stack images were converted into single images by carrying out a maximum projection. The DAPI stain was made binary and used to create as mask for the nuclei of each cell. The find maxima function was used to pick out individual foci and then the integrated density of each cell was used to calculate the number of foci by dividing by 255. Cyclin A mean nuclear intensities were also measured for each nuclei as to confirm cells were indeed in G1.

For quantification in Cell Profiler, DAPI and 53BP1 channels were manually thresholded prior to import into cell profiler. In cell profiler we then were able to identify foci as regions of interest, quantifying their area, allowing us to distinguish large and small foci. Measurements of small and large foci per nuclei were then able to be quantified as well as summing together total area of 53BP1 foci within each cell. Cyclin A mean nuclear intensity was again used to confirm the presence of G1 cells and to remove any non-G1 cells from the analysis.

## **2.2.6.5 DNA replication runover assay**

### **2.2.6.5.1 Cell plating and treatment**

Forward transfection was carried out as previously described (**Section 2.2.2.1**) on HeLa cells. 16hrs post-transfection cells were replated 1:4 into 6 well plates containing sterilised coverslips. 48hrs post-transfection cells were treated with 0.4 $\mu$ M Aphidicolin in 2ml fresh media for 23hrs. After 23hrs media was aspirated and 1ml fresh media containing 20 $\mu$ M EdU was added and incubated with the cells for **25mins**. Cells were subsequently fixed in 1ml ice-cold methanol before being washed three times with PBS and storing at 4°C until staining.

### **2.2.6.5.2 Staining method**

To stain for FANCD2 and p-histone H3 (Ser10) cells were blocked for 1hr at room temperature in 5% BSA, 0.5% Triton-X in PBS. Subsequently coverslips were inverted into 6 well plates containing 200 $\mu$ l 1:100 mouse anti-p-histone H3 (Ser10) and 1:100 rabbit anti-FANCD2 in blocking buffer. The plates were wrapped in parafilm and incubated overnight at 4°C in the dark. The following day the coverslips were then turned face up, antibody solution removed and washed with 2ml 0.5% Triton-X in PBS for 10mins each three times. The coverslips were then inverted onto 150 $\mu$ l secondary antibody solution, containing 1:200 AF647 anti-mouse and 1:200 AF594 anti-rabbit on parafilm for 1hr at room temperature in the dark. The coverslips were then washed with 0.5% Triton-X in PBS for 10mins each three times.

Following antibody detection for FANCD2 and p-histone H3 (Ser10), cells were detected for EdU. The coverslips were incubated with 50 $\mu$ l Click-iT reaction mix (Fisher Scientific Ltd) according to manufacturer's instructions and incubated for 1hr

in the dark. The coverslips were then returned to a 6 well plate and washed three times with 3% BSA in 0.5% Triton-X 100 in PBS for 20mins each. Then coverslips were washed for 5mins with 1:1000 DAPI in PBS then mounted onto a microscope slide using Immu-Mount and allowed to set in the dark before being stored at 4°C prior to imaging.

### **2.2.6.5.3 Analysis**

Z-stack images were taken of each slide on a Zeiss LSM980 Confocal microscope using a 40X lens. FIJI Image J software was used to analyse the images.

First the Z-stack images were converted into single images by carrying out a maximum projection. The DAPI stain was made binary and used to create as mask for the nuclei of each cell. The find maxima function with a prominence of 1000 and 10,000 was used to pick out individual EdU and FANCD2 foci. The integrated density of each cell was used to calculate the number of foci by dividing by 255. The mean, IntDen and RawIntDen were all also measured for each channel using the nuclei mask.

### **2.2.6.6 DNA fibre analysis**

#### **2.2.6.6.1 Cell plating and treatment**

Forward transfection was carried out in a 6 well plate as previously described (**Section 2.2.2.1**) on HeLa cells where appropriate. 16hrs post-transfection cells were replated into 10cm dishes. 48hrs post-transfection cells were treated with 0.4 $\mu$ M Aphidicolin for 23hrs. After 23hrs Aphidicolin containing media was aspirated and replaced with 5ml fresh media containing 100 $\mu$ M CldU for 20mins followed by the addition of 5ml 1mM IdU giving a final concentration of 500 $\mu$ M IdU in 10ml of media for a further 20mins. Cells were then washed three times with PBS before being trypsinised and pelleted for DNA extraction.

#### **2.2.6.6.2 DNA extraction and fibre combing**

The following steps were carried out on a fresh cell pellet using the DNA Fibre Combing Kit (Genomic Vision) according to manufacturer's instructions. The cell pellet was gently resuspended in 45 $\mu$ l of Buffer 1 by pipetting up and down 10 before being warmed to 50°C in a water bath. Then the pellet was mixed with 45 $\mu$ l of melted Buffer

2 and pipetted up and down gently until no visible clumps were observed. The resulting mixture was then pipetted into a plug mould and stored in the dark for 1hr at 4°C or until solid. The plugs were then removed from the moulds and gently placed into a 15ml falcon containing 250µl of complete protease digestion buffer (225µl Buffer 3 + 25µl Component 3). The tubes were warmed to 50°C for 30mins before being gently swirled to homogenise the solution, then left for 16hrs at 50°C.

The following day, Buffer 4 was prepared by diluting it in a 1:100 proportion with newly sterilised water. The plugs were removed from the digestion buffer and placed in a 15ml flacon containing 14ml of diluted Buffer 4 and washed for 1hr with rocking three times. At this point the plugs were moved into a 2ml Eppendorf containing 1ml of Buffer 5 and kept in the fridge until DNA combing was required.

Prior to carrying out agarose digestion if the plug had been stored in Buffer 5 the plugs were subjected to another round of washing in diluted Buffer 4 for a further 3hrs as previously described. After washing, the plug was moved to a 2ml Eppendorf containing 1ml of Buffer 6 and warmed to 68°C for 20mins in a water bath to melt the agarose. Prior to this the tubes were quickly and gently moved to a heat block equilibrated at 42°C and incubated for another 10mins. Following this time 1.5µl of Component 6 was added slowly and at the surface to prevent any shearing of the DNA from occurring. The tube was also not mixed at any point after melting of the agarose plug. The tubes were incubated overnight at 42°C. At this point the DNA solution can be stored in the fridge for up to a week.

Prior to DNA combing the prepared DNA solution should be gently poured into a disposable DNA reservoir containing 1.2ml of Buffer 6 and allowed to come to room temperature for at least 30mins. After this point the DNA solution can be combed onto a silanized coverslip using the FibreComb® Molecular Combing System. After combing coverslips were baked in a 65°C oven. If the fibres were not subject to immunodetection immediately, the coverslips were stored in the dark at -20°C in a sealed box.

### 2.2.6.6.3 Immunodetection of replication tracts

If coverslips had been stored at -20°C they were first allowed to defrost at room temperature before being sequentially dehydrated by submersing the coverslip in 70%, 90% and 100% ethanol for 3mins each before being allowed to dry in a hood in the dark.

To denature the combed fibres, coverslips were submerged in a 0.5M NaOH, 1M NaCl solution for 8mins at room temperature before being washed three times in PBS for 10sec with gentle agitation. The coverslips were then dehydrated as previously described in ethanol before being allowed to dry in a hood. Once dry coverslips were incubated facedown with 25µl Block Aid (Invitrogen) containing 0.8µl rat anti-BrdU and 4µl mouse anti-BrdU per coverslip and incubated in the dark at 37°C for 1hr in a humidified chamber. The coverslips were then washed three times for 3mins with a solution of 0.05% Tween20 in PBS. Coverslips were then incubated with 25µl Block Aid containing 2µl goat anti-rat Cy5 and 2µl goat anti-mouse Cy3 secondary antibodies for in the dark at 37°C for 45mins in a humidified chamber. After incubation the coverslips were washed three times with 0.05% Tween20 in PBS for 3mins each before washing once in PBS. The coverslips were then mounted onto microscope slides using Immu-mount and allowed to set at 4°C in the dark overnight prior to imaging.

### 2.2.6.6.4 Imaging

Images of each slide were taken on a Zeiss LSM980 Confocal Microscope using a 63X lens.

### 2.2.6.6.5 Analysis

Quantification of replication tracts was carried out manually in FIJI and measured in µM. To quantify replication fork speed (Kb/min) and sister fork symmetry scores, the following equations were used:

$$\text{Fork Speed (Kb/min)} = \frac{(\text{Tract Length } (\mu\text{M})_{\text{clau}} + \text{Tract Length } (\mu\text{M})_{\text{ldu}}) \times 2.59}{\text{Length of Pulse (min)}_{\text{clau}} + \text{Length of Pulse (min)}_{\text{ldu}}}$$

$$\text{Fork Symmetry Score (A.U)} = \frac{\text{Smaller Sister Fork Length}}{\text{Larger Sister Fork Length}}$$

## **2.2.7 Live cell microscopy**

### **2.2.7.1 Cell plating and treatment**

Forward transfection was carried out as previously described (**Section 2.2.2.1**) and cultured at 37°C and 5 % CO<sub>2</sub>. 48 hours post-transfection cells were replated in duplicate at 5x10<sup>4</sup> cells in a 24 well plate. One well of each condition was treated with 1µM Carboplatin 2 hours prior to imaging.

### **2.2.7.2 Imaging**

The cells were imaged on the Zeiss Cell Discoverer 7 for 20 hours with conditions maintained at 37°C and 5% CO<sub>2</sub>. The plate was imaged using oblique contrast using a 10x objective lens. 5 images were captured at different positions of each well, every 5 minutes.

### **2.2.7.3 Analysis**

FIJI Image J software was used to visualise the time-lapse video produced at each position. Rounding up and clear breakdown of the nuclear envelope was defined as a cell entering mitosis, whilst a clear division between two daughter cells defined the end of mitosis (see **Figure 2.2.2**). From this, the time required for a mitotic transit was measured for 50 cells per condition per repeat.

$$\text{Mitotic Transit Time (min)} = (\text{Mitotic Exit Frame} - \text{Mitotic Entry Frame}) \times 5$$

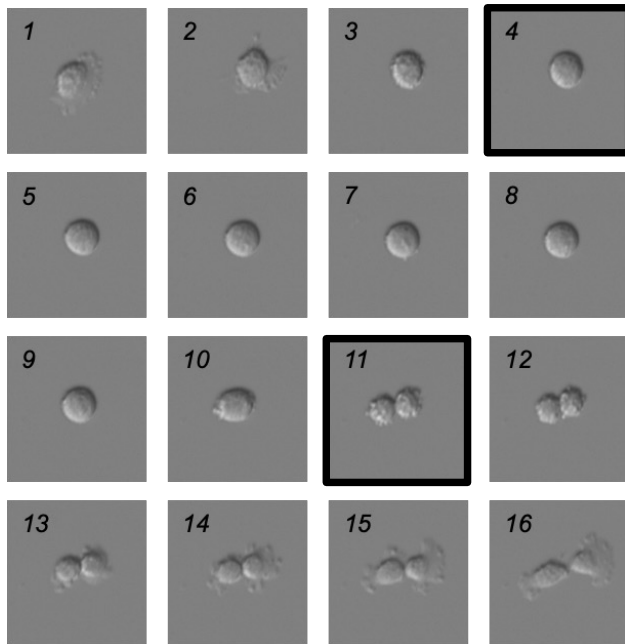


**Figure 2.2.2: Live cell microscopy analysis strategy**

Equation for the determination of mitotic transit time. Representative images taken from live cell microscopy for the analysis of mitotic transit time. To quantify mitotic duration, mitotic onset is defined by the rounding up of the cell as shown in **Frame 4**. Mitotic exit or cytokinesis is shown by the physical separation of the daughter cells as shown in **Frame 11**.

### 2.2.8 Statistical analysis

Graphing and statistical analysis was carried out using GraphPad Prism (version 10) software. Where data has been shown of single data points from an independent experimental repeat, the data is represented by the mean +/- standard deviation (SD). Data that has been graphed by displaying the mean value from each independent biological replicate, the data is represented by the mean of means +/- standard error of the mean (SEM). To aid in the visualisation of presented data, some significance bars have been removed, though all statistical data is available in the attached p-value tables.

Statistical significance was determined between means for parametric data by One-way ANOVA with Dunnett correction test for multiple comparisons. For non-parametric data statistical significance between means was determined using Kruskal-Wallis test

with Dunn's multiple comparisons. A p value  $\leq 0.05$  was regarded significant (\* p  $\leq 0.05$ , \*\* p  $\leq 0.01$ , \*\*\* p  $\leq 0.001$ , \*\*\*\* p  $\leq 0.0001$ ).

# Chapter 3: UPF1 regulates mitotic progression following DNA damage

## 3.1 Introduction, aims and hypothesis

The Thompson lab has demonstrated that cells exhibit mitotic delay in response to a range of genotoxic insults, indicating the ability and necessity of mitotic cells to sense and respond to DNA damage (Smits *et al.*, 2000; Nitta *et al.*, 2004; Thompson *et al.*, 2015; Gatenby, 2022; Gatenby *et al.*, 2022). However, the reason for this delay and the mechanism by which these distinct proteins operate to mediate a response to DNA damage in mitosis is unknown. Previously, ATR has been demonstrated to localise to RPA-coated centromeric R-loops, where by it promotes faithful chromosomal segregation in mitosis, however this pathway is not DNA damage specific (Kabeche *et al.*, 2018). Dysregulation of this pathway could lead to DNA damage-dependent mitotic delay, alternatively, ongoing DNA replication in mitosis seems to correlate with changes in mitotic duration (Wassing *et al.*, 2021). The Thompson lab has demonstrated that a DNA damage-dependent increase in mitotic delay is dependent on several proteins including UPF1 (Gatenby, 2022; Gatenby *et al.*, 2022).

UPF1 is an RNA/ DNA helicase and a key mediator of mRNA decay pathways that regulate both the quality and quantity of mRNA expression of a wide range of genes. The most characterised decay pathway UPF1 mediates is nonsense-mediated decay (NMD), which regulates the expression of mRNAs that harbour premature termination codons, however, has also been shown to impact on several other cellular processes. UPF1 has also been implicated to have a role in the maintenance of genomic stability, telomeric and R-loop homeostasis and DNA replication/repair, though the exact manner by which UPF1 carries out these diverse functions is currently unknown. In this chapter, an investigation into the manner through which UPF1 directly promotes mitotic delay is studied.

The aims of this chapter are to assess the following to determine the manner by which UPF1 mediates DNA damage-dependent mitotic delay:

1. What UPF1-interacting proteins are required for DNA damage-dependent mitotic delay
2. How UPF1 mutants defective for RNA- or DNA-binding effect mitotic delay
3. The effect of UPF1 inhibition by VG1 on mitotic delay
4. The effect of inhibition of PIKKs ATR and ATM on mitotic delay
5. The effect of RNaseH1 on mitotic delay
6. The effect of transcription inhibition by  $\alpha$ -amanitin on mitotic delay

The hypothesis of this chapter is:

UPF1 mediates mitotic delay independently of canonical NMD.

## **3.2 Results**

### **3.2.1 UPF1-associated decay factors required for mitotic delay following DNA damage**

UPF1 was first identified as potentially playing a role in the mitotic response to DNA damage through a siRNA DNA damage screen conducted in the Thompson Laboratory (see **Figure 1.1.6**). Further work into characterising this checkpoint was carried out including a mass spectrometry screen to identify interactors with BUBR1 following DNA damage. This screen reported UPF1 as being an enriched interactor with BUBR1 following irradiation. UPF1 being a hit in both screens, as well as its implications in genomic stability, prompted further investigation into UPF1's role in promoting a DNA damage-dependent mitotic delay.

To investigate the role that UPF1 plays in the regulation of mitosis following DNA damage, live cell microscopy was conducted to allow for the analysis of mitotic progression. For these studies a small panel of UPF1-associated decay factors (UPF2, UPF3b, STAU1, SMG1, SMG5 and SMG6) were chosen to assess their relative involvement in mediating DNA-damage associated mitotic delay. First siRNAs against each of these factors were validated by western blot (see **Figure 3.2.1**). Whilst

we demonstrated clear knockdown of UPF1, UPF3b, SMG1 and SMG6 for the tested siRNAs due to issues with antibodies against the remaining factors we were unable to validate their direct protein knockdown by western blot. It is worth mentioning that though UPF2 was one of these proteins we were unable to blot for, UPF2 siRNA treatment resulted in a significant upregulation of UPF1, consistent with what would be observed following UPF2 depletion. We then conducted live cell microscopy as carried out previously to assess the relative involvement of each of these proteins in promoting DNA damage-dependent mitotic delay.

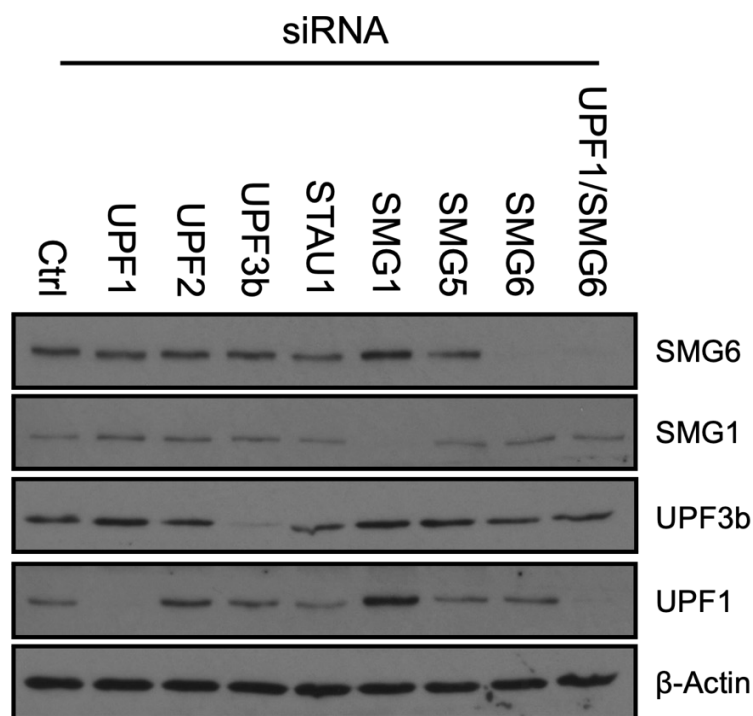


**Figure 3.2.1: siRNA-mediated knockdown of UPF1-associated decay factors.**

Representative western blot for  $\beta$ -actin, UPF1, UPF3b, SMG1 and SMG6 of HeLa cell lysates transfected with indicated siRNAs for 48hrs. (N=3)

I replicated the previous work carried out in the Thompson laboratory, confirming the requirement of UPF1 for mitotic delay following DNA damage induction, in a HeLa cell line using an engineered UPF1 siRNA (see **Figure 3.2.2A**) (Gatenby, 2022; Gatenby *et al.*, 2022). This data shows that in the absence of exogenous DNA damage, siRNA-mediated depletion of UPF1 has no effect on mitotic progression compared to the SiCtrl. However, when cells are exposed to exogenous genotoxic stress, mediated

through the addition of 1 $\mu$ M Carboplatin 3hrs prior to commencing live cell microscopy, an increase in mitotic transit time is observed (see **Figure 3.2.2A**). UPF1 depletion then results in a significant reduction in mitotic transit time compared to the SiCtrl treated condition, confirming UPF1 is required for this mitotic delay. To demonstrate that the changes observed in mitotic duration are not consistent with a dysfunctional SAC we also assessed the effect of siRNA-mediated depletion of BubR1 on mitotic duration (see **Figure 3.2.2D**). Following siRNA-mediated depletion of BubR1 a significant reduction in mitotic duration was observed even in untreated conditions with an average duration of ~17mins. This reduction in mitotic duration is also observed following treatment with 1 $\mu$ M carboplatin compared to the SiCtrl carboplatin treated condition. Interestingly, even in the BubR1 depleted conditions, we did observe a small but reproducible increase in mitotic duration following treatment with carboplatin which fell just short of statistical significance. This could suggest that even in the absence of a functional SAC, DNA damage-dependent mitotic delay can still be observed, implying that this delay occurs independently of metaphase arrest.

To begin understanding the mechanism by which UPF1 promotes mitotic delay, I tested several other factors that are known to function in conjunction with UPF1, and their respective effects on mitotic progression. UPF2, a cofactor of UPF1, required for enhancing helicase and ATPase activities was shown to have the same effect on mitotic progression as observed with UPF1 (see **Figure 3.2.2A**). siRNA-mediated depletion of UPF2 had no effect in the absence of DNA damage. But UPF2 depletion following carboplatin treatment resulted in a significant reduction in mitotic transit time compared to the SiCtrl treated condition. Another canonical NMD factor was also tested, UPF3b, an EJC component that recruits UPF1 to PTC-containing mRNAs. UPF3b depletion appeared to have no effect on mitotic progression in the absence of DNA damage and following carboplatin treatment, a significant increase in mitotic transit time is observed, similar to that of the SiCtrl condition. This suggests that UPF3b may have no role in mediating mitotic duration increases following treatment with carboplatin and that UPF1 could be acting independently of the canonical NMD pathway (**Figure 3.2B**). Staufen-mediated decay (SMD) is another mRNA decay pathway which requires UPF1. For SMD, UPF1 is recruited to target mRNAs by the RNA-binding protein STAU1. As with UPF3b, STAU1 depletion had no effect on mitotic

progression. STAU1 depletion had no effect on mitotic progression under any condition. This suggests that STAU1, like UPF3b, has no role in mediating mitotic duration changes following treatment with carboplatin. Together it suggests that the role that UPF1 plays in promoting DNA damage-dependent mitotic delay could be independent of both NMD and SMD (**Figure 3.2.2B**).

As the UPF1 binding partner and regulator, UPF2 was also found to be required for DNA damage-induced mitotic delay, we wanted to examine whether reducing UPF1 activity, this time by depleting SMG1, a key kinase that regulates UPF1, had a similar effect. Unlike UPF1 and UPF2, siRNA-mediated depletion of SMG1 led to a significant reduction in mitotic transit time in the untreated condition to ~32.6min compared to the SiCtrl untreated (see **Figure 3.2.2C**). Depletion of SMG1 also led to a significant reduction in mitotic transit time following treatment with carboplatin compared to the SiCtrl carboplatin treated condition. This could suggest that UPF1 phosphorylation by SMG1 is required for promoting DNA damage-dependent mitotic delay. Alternatively, it could be that SMG1 has a UPF1-independent role in controlling SAC function in an unperturbed cell cycle.

Since it seemed that upstream factors required for recruiting UPF1 for NMD and SMD played no role in mediating the mitotic delay observed, we wished to test whether any downstream endo- or exo-nuclease components known to interact with UPF1 had any effects. The endonuclease activity is stimulated by SMG6, whilst the exonuclease function is promoted by a dimer of SMG5 and SMG7. We found that SMG5 siRNA transfection had no impact on mitotic progression in the absence or presence of DNA damage suggesting that exonuclease activity is not required by UPF1 to promote DNA damage-dependent mitotic delay. However, depletion of the endonuclease factor SMG6 resulted in an increase in mitotic transit time, comparable to that following DNA damage even in the absence of exogenous DNA damage (see **Figure 3.2.2C**). SMG6 depletion did not however promote further mitotic delay when combined with carboplatin treatment. Suggesting that carboplatin induced mitotic delay, that is dependent on UPF1, could act with SMG6 to mediate mitotic delay. These data suggest that unlike UPF1 and UPF2, which are both required to promote mitotic delay following induction of DNA damage, SMG6 suppresses mitotic delay.

To assess whether SMG6 depletion-induced mitotic delay is functionally related to UPF1, we carried out a double knockdown of both factors and observed the resulting mitotic phenotype. Depletion of UPF1 was found to suppress SMG6 depletion-induced mitotic delay (see **Figure 3.2.2C**). Together these data suggest that SMG6 depletion-dependent mitotic delay requires UPF1, implying that these two proteins function together and regulate mitotic duration in the same pathway.

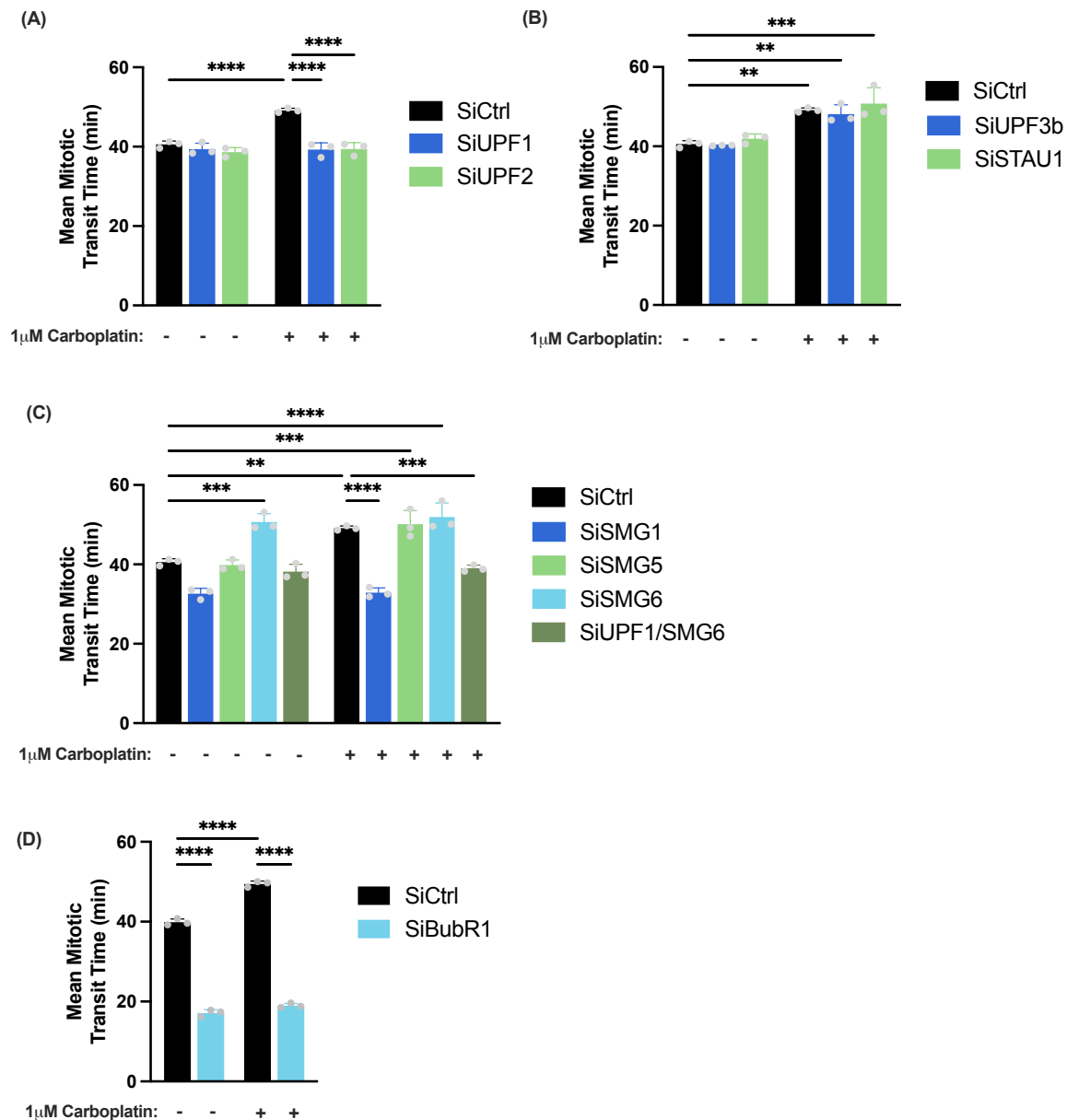


**Figure 3.2.2: Live cell microscopy analysis of mean mitotic transit time of HeLa cells treated with 1µM carboplatin transfected with UPF1-associated decay factors.**

*Legend on next page.*

**Figure 3.2.2: Live cell microscopy analysis of mean mitotic transit time of HeLa cells treated with 1 $\mu$ M carboplatin transfected with UPF1-associated decay factors.**

**(A-D)** Time-lapse live cell microscopy analysis for the mean time taken to complete mitosis. HeLa cells transfected with the indicated siRNAs and treated with 1 $\mu$ M Carboplatin as shown. 50 cells for each condition were counted and the data illustrated represents the overall mean of each independent experiment  $\pm$  SEM (N=3). To aid visualisation some statistical significance bars have been removed, though all statistical data can be found in table of p-values from One-way ANOVA test with Dunnett's correction test for multiple comparisons for each individual panels of siRNAs against SiCtrl can be found in **Figure A1**.

Together the involvement of UPF1 interacting proteins UPF2 and SMG6 in mediating mitotic delay confirms a specific requirement of the UPF1 signalling axis in mediating DNA damage-dependent mitotic delay. The lack of a necessity for canonical NMD factor UPF3b, or SMD factor STAU1 suggests at least in part that UPF1 could be promoting delay in a non-canonical manner independent of at least these mRNA decay pathways.

### **3.2.2 Functionalities required for UPF1 mitotic delay**

To further characterise the manner through which UPF1 is acting we wanted to examine which functionalities of UPF1 were required for promoting mitotic delay. To do this we carried out rescue experiments using exogenously expressed mutant proteins, testing the abilities of various UPF1 mutants to rescue DNA damage-dependent mitotic delay, in the absence of endogenous UPF1. Using TreX HeLa FLP-IN UPF1 mutant cell lines we can deplete endogenous UPF1 using an engineered siRNA, then add back siRNA-resistant exogenous UPF1 through the induction of these cell lines using doxycycline. For these experiments we used several UPF1 variants: WT (Wild-type), R843C (RNA-binding deficient), S42A (Chromatin-binding deficient), S42E (Chromatin-binding enhanced), all of which are stably transfected into the TreX HeLa cell lines under the control of a tetracycline responsive promoter. The induction of these cell lines had been previously optimised for endogenous rescue experiments (Turton, 2014).

**Figure 3.2.3B** shows knockdown of endogenous UPF1 as well as rescue of UPF1 levels with exogenous UPF1 expression of exogenous in each of the engineered cell lines. We also observed FLAG expression in the S42A, S42E and R843C cell lines. Curiously we did not detect FLAG expression in the WT cell line, most likely this was due to a mislabelled aliquot of cells lacking the FLAG tag as we can see clear rescue of UPF1 levels in this cell line. Whilst the expression of these mutants differed among cell lines, we were able to reproducibly rescue UPF1 to at least endogenous level.

All cell lines showed the same mitotic progression phenotypes as in the HeLa cell line when uninduced (see **Figure 3.2.3C**). Demonstrating that these mutant cell lines behave like the un-engineered HeLa line and therefore any changes following addition of doxycycline are specific to the presence of exogenous UPF1. We also carried out an additional control to show that the addition of 1µg/ml doxycycline had no effect on mitotic progression in an un-engineered HeLa cell line (see **Figure 3.2.3A**). This showed that doxycycline had no effect on mitotic duration itself, or on the ability for siRNA-mediated UPF1 depletion to rescue DNA damage-dependent mitotic delay. This confirms again that any changes observed in our induced cell lines are due to a specific phenotype induced by mutant exogenous UPF1 constructs.

Overexpression of UPF1<sup>WT</sup> had no effect on mitotic duration in the untreated condition, as cells progressed normally through mitosis in both SiCtrl and SiUPF1 conditions. When cells expressing siRNA-resistant UPF1<sup>WT</sup> were treated with carboplatin a significant increase in mitotic duration was observed compared to the untreated conditions. When endogenous UPF1 was depleted, these cells still showed a significant increase in mitotic transit time compared to untreated SiCtrl or SiUPF1 conditions demonstrating that the impact of SiUPF1 on mitotic progression is not due to off-target effects of the siRNA (see **Figure 3.2.3D**).

The R843C mutant of UPF1 is deficient for RNA-binding. Live cell microscopy of a FLP-IN TreX HeLa cell line expressing this mutant form of UPF1 revealed that the exogenous UPF1<sup>R843C</sup> is incapable of rescuing carboplatin-induced mitotic delay suggesting that the RNA-binding ability of UPF1 is necessary in mediating DNA damage-dependent mitotic delay (see **Figure 3.2.3D**).

UPF1 has been implicated to have a novel role in the maintenance of genomic stability through its ability to associate with chromatin. We observed that expression of a chromatin-binding defective mutant of UPF1 (UPF1<sup>S42A</sup>) caused a significant increase in mitotic duration compared to the WT untreated line even in the absence of any exogenous DNA damage induction which was independent of UPF1 knockdown (see **Figure 3.2.3D**). This suggests that the S42A mutation is dominant over endogenous UPF1 in promoting a mitotic delay phenotype. Analysis of the chromatin-binding enriched UPF1<sup>S42E</sup> mutant showed no changes in mitotic transit time in untreated conditions, as observed with the S42A mutant. Unlike the S42A which would promote mitotic delay, the S42E mutant was incapable of rescuing DNA damage-dependent mitotic delay following loss of endogenous UPF1.

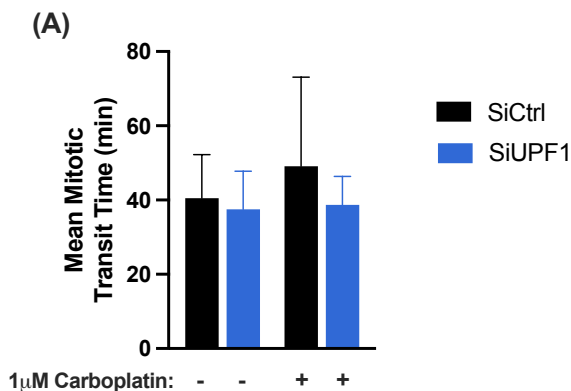


**Figure 3.2.3: Live cell microscopy analysis of mean mitotic transit time of FLP-IN TreX HeLa cells treated with 1 $\mu$ M carboplatin.**

*Legend on page 84.*

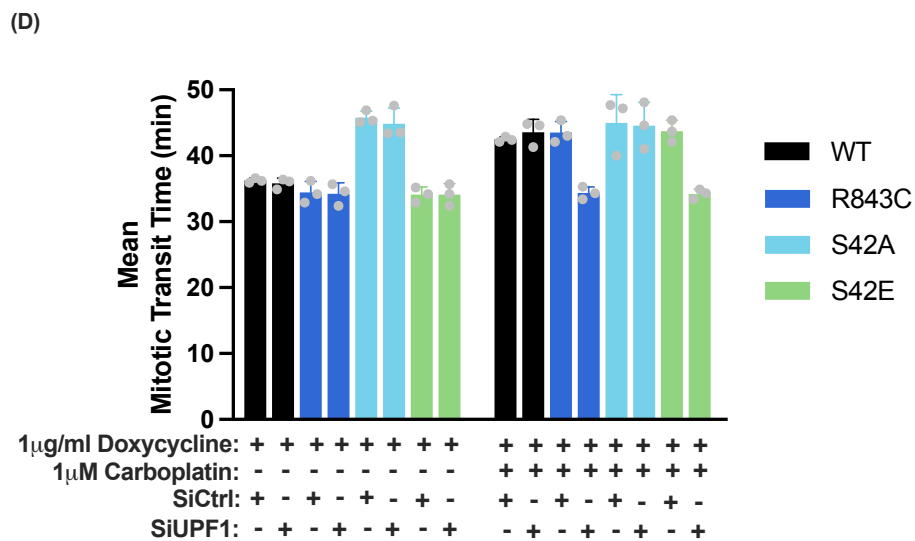
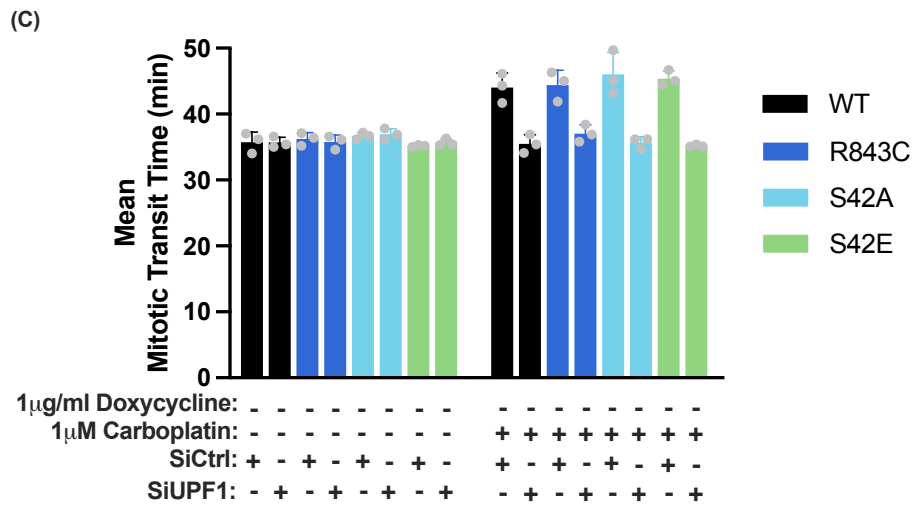
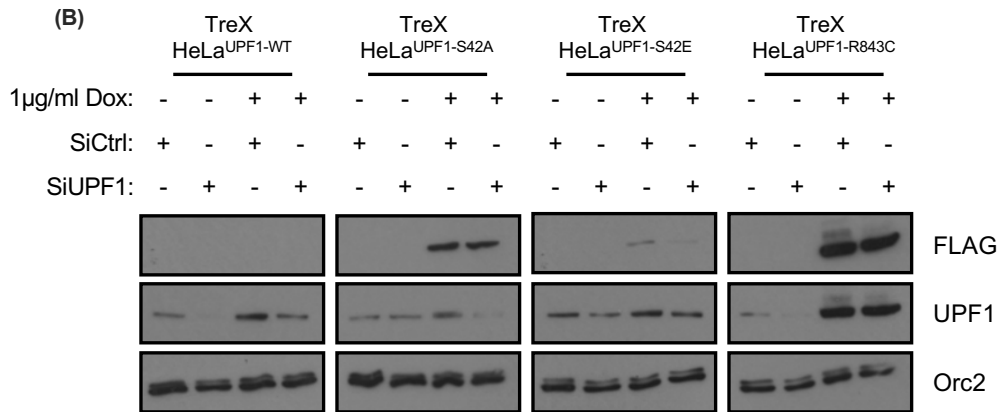


Figure 3.2.3: Live cell microscopy analysis of mean mitotic transit time of FLP-IN TreX HeLa cells treated with 1µM carboplatin. Legend on next page.

**Figure 3.2.3: Live cell microscopy analysis of mean mitotic transit time of FLP-IN TreX HeLa cells treated with 1 $\mu$ M carboplatin.**

**(A)** Time-lapse live cell microscopy analysis for the mean time taken to complete mitosis. HeLa cells were treated with 1 $\mu$ g/ml Doxycycline and transfected with the indicated siRNAs for 48hrs and treated with 1 $\mu$ M carboplatin as indicated. (N=1) **(B)** Representative western blot for FLAG, UPF1 and Orc2 of FLP-IN TreX HeLa cell lysates transfected with SiCtrl or SiUPF1 and treated with and without 1 $\mu$ g/ml doxycycline for 48hrs as indicated. **(C)** Time-lapse live cell microscopy analysis for the mean time taken to complete mitosis. UPF1 FLP-IN HeLa cells were transfected with the indicated siRNAs, without doxycycline and treated with 1 $\mu$ M Carboplatin as indicated. **(D)** Same as **(C)** except all cells were treated with 1 $\mu$ g/ml doxycycline as indicated for 48 hours prior to imaging. 50 cells for each condition were counted and the data illustrated represents the overall mean of each independent experiment +/- SEM (N=3). One way ANOVA with Dunnett's correction test for multiple comparisons was performed to determine statistical significance and the resultant p values are displayed in **Figure A3-4** for the uninduced and doxycycline induced experiments respectively. *Dox* = doxycycline, *C* = SiCtrl, *U* = SiUPF1.

Together these results show a specific role for UPF1 in promoting mitotic delay following the induction of DNA damage. We have also shown that both RNA-binding and chromatin-binding abilities of UPF1 are important in correctly mediating mitotic delay both following genotoxic stress but also in unperturbed conditions.

**3.2.3 UPF1 inhibitor - VG1, mimics siRNA-mediated UPF1 knockdown with loss of mitotic delay phenotype**

Since we have shown that UPF1 promotes mitotic delay following DNA damage induction by carboplatin, and that UPF2 and SMG1, two proteins that promote UPF1 activity, also seem to promote delay. We wanted to examine whether a UPF1 inhibitor, which would reduce UPF1 activity, would mimic UPF1 knockdown and its effect on mitotic delay following DNA damage. VG1 is a specific UPF1 inhibitor that prevents the interaction of SMG5:SMG7 with UPF1, as a result PP2A cannot be recruited for dephosphorylation and UPF1 remains in a hyperphosphorylated state (Gotham *et al.*, 2016). UPF1 dephosphorylation by PP2A has been shown to be required for UPF1

dissociation from an mRNP and to allow for subsequent target degradation during NMD (Ohnishi *et al.*, 2003).

Firstly, the inhibitor was tested by western blot to optimise a concentration that resulted in a significant increase in phosphorylated UPF1 (see **Figure 3.2.4A**). The PP2A inhibitor, Okadaic Acid was used as a positive control and shows an increase in phosphorylated UPF1 (S1127) but not total levels of UPF1 compared to the control. This shows that we can indeed detect hyperphosphorylated forms of UPF1. At all concentrations tested, an increase in p-UPF1 was also observed therefore a concentration of 1.25µM was chosen at which there was minimal cytotoxicity (Data not shown).

Live cell microscopy was then carried out as previously described apart from being treated with 1.25µM VG1 3 hours prior to imaging commencing, in combination with carboplatin as indicated. This data shows that inhibition of UPF1 by VG1 has no effect on mitotic progression in the absence of DNA damage induction by carboplatin (see **Figure 3.2.4B**). Following treatment with carboplatin a significant increase in mitotic transit time is observed in the vehicle control condition. However, when HeLa cells are treated with a combination of carboplatin and VG1 a significant reduction in mitotic delay is observed compared to the carboplatin alone condition.

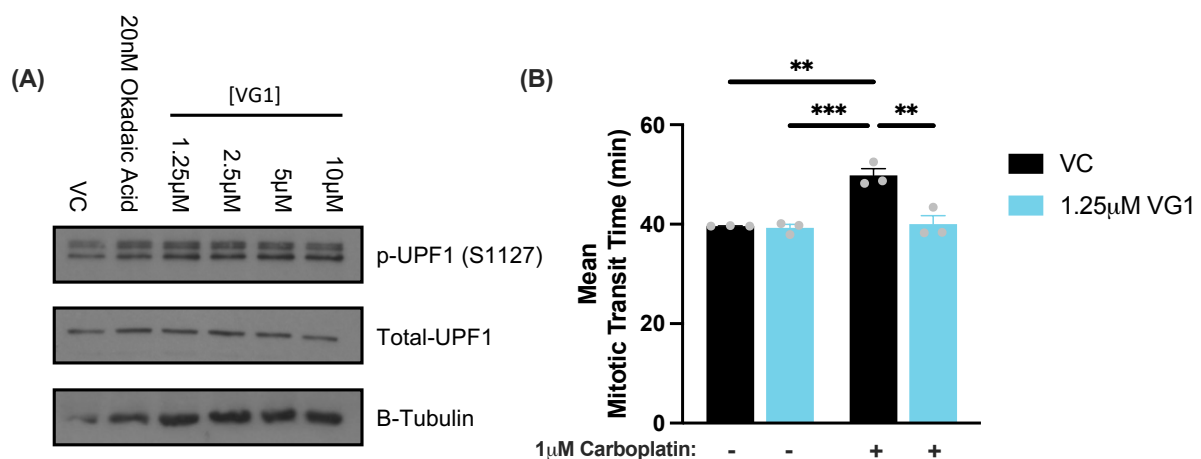


**Figure 3.2.4: Live cell microscopy analysis of mean mitotic transit time of HeLa cells treated with 1.25µM VG1 in combination with 1µM carboplatin. Legend on next page.**

**Figure 3.2.4: Live cell microscopy analysis of mean mitotic transit time of HeLa cells treated with 1.25 $\mu$ M VG1 in combination with 1 $\mu$ M carboplatin.**

**(A)** Representative western blot for P-UPF1 (Ser1127), UPF1 and  $\beta$ -tubulin of HeLa cell lysates treated with the indicated concentration of VG1 or Okadaic acid as indicated. **(B)** HeLa cells were treated with 1.25 $\mu$ M of VG1 4hrs prior to live cell microscopy in the presence or absence of 1 $\mu$ M carboplatin as indicated. 50 cells for each condition were counted and the data illustrated represents the overall mean of each independent experiment +/- SEM. One way ANOVA with Dunnett's correction test for multiple comparisons was performed to determine statistical significance (N=3).

This suggests that interfering with the UPF1 phosphorylation cycle by preventing its dephosphorylation by PP2A with VG1 is sufficient to prevent DNA damage-induced mitotic delay through UPF1.

### **3.2.4 ATRi Promotes UPF1-dependent mitotic delay**

Since we had found that UPF1 chromatin function, through the S42 site, was important in mediating mitotic delay we wanted to examine whether any known proteins that have also been shown to be important for mediating UPF1 chromatin binding, had any effect on mitotic duration. UPF1 chromatin binding has been suggested to be driven by the key replication stress PIKK, ATR, that directly phosphorylates UPF1 for its activation. ATR depletion has been shown to diminish UPF1 chromatin binding in S-phase or following  $\gamma$ -irradiation of HeLa cells (Azzalin and Lingner, 2006). Since we had shown that the chromatin-binding defective UPF1<sup>S42A</sup> mutant promoted mitotic delay, we hypothesised that by inhibiting ATR, we would also reduce UPF1 chromatin binding, that should lead to the occurrence of a mitotic delay, even in the absence of DNA damage. To investigate this, we utilised the small molecular inhibitor AZD6738, a potent and selective ATP-competitive inhibitor of ATR (hereon referred to as ATRi). We observed that following 6hrs treatment with 1 $\mu$ M ATRi a complete loss of P-Chk1 (Ser345) induced following depletion of either UPF1 or UPF2 (see **Figure 3.2.5A**) demonstrating effective ATR inhibition. We also observed an induction of P-ATM (Ser1981) following treatment with ATRi. ATRi leads to a compensatory activation of the ATM pathway and ATM phosphorylation that is dependent on UPF2 (O'Leary *et*

*al.*, 2022; Turchick *et al.*, 2023). The same dependence on UPF1 or UPF2 was not observed in our cell line.

Consistent with our hypothesis, we observed that following treatment with 1 $\mu$ M ATRi, there was a significant increase in mitotic transit time compared to the untreated SiCtrl condition (see **Figure 3.2.5B**). Furthermore, we found that siRNA-mediated depletion of UPF1 led to a significant reduction in mitotic duration in ATRi treated cells, suggesting that UPF1 is required for promoting ATRi-dependent mitotic delay in a similar manner to carboplatin-induced delay. The combination treatment of ATRi and carboplatin did not lead to a cumulative increase in mitotic duration, whilst it did lead to an increase compared to the untreated, suggesting that both of these drugs were likely promoting DNA damage-dependent mitotic delay through the same process. This combination also was completely rescued by depletion of UPF1, leading to a significant reduction in mitotic duration to an untreated level.

In order to confirm that the observed phenotype was not due to an increase in endogenous DNA damage as a result of a defective key DDR kinase, we also investigated the effect of ATM inhibition (ATMi) under the same conditions. Whilst ATMi did appear to lead to a small increase in mitotic duration in all conditions, the effects observed were not significant and appeared not to be dependent on UPF1 (see **Figure 3.2.5B**). This suggested that the effect induced by ATMi was likely distinct from the specific effect of ATRi treatment. The ATMi treated conditions displayed the same pattern of mitotic duration as untreated cells, displaying a significant increase following carboplatin treatment which could be rescued by depletion of UPF1. Suggesting that ATM is not required for UPF1 dependent mitotic delay

Together these results show that ATR inhibition by AZD6738 is sufficient to promote mitotic delay that is resolvable by UPF1 depletion in a similar manner to carboplatin induced mitotic delay. This highlights ATRi as either another stimulus, sufficient to induce delay or as potentially being involved in regulating UPF1 to prevent delay occurring even in the absence of DNA damage.

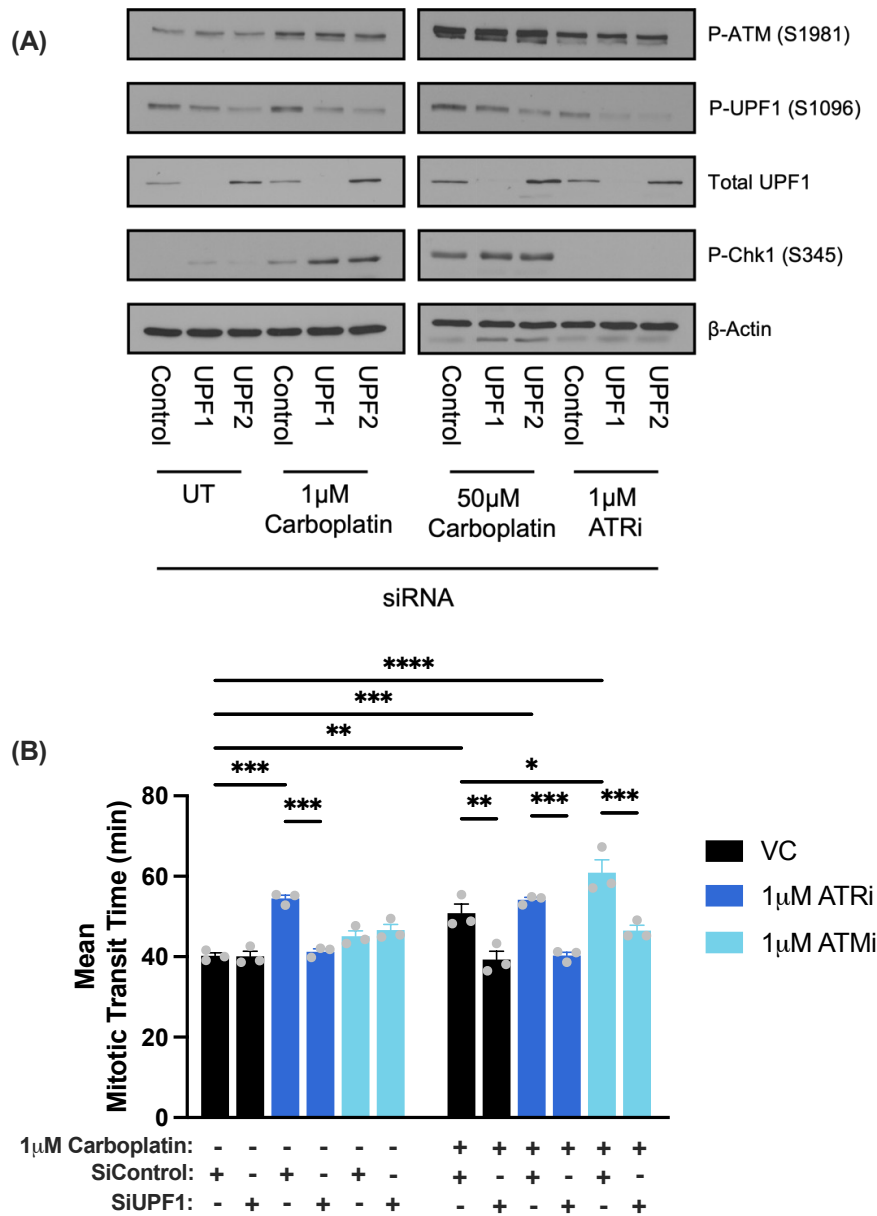


**Figure 3.2.5: Live cell microscopy analysis of mean mitotic transit time of HeLa cells treated with ATRi or ATMi in combination with carboplatin following depletion of UPF1.** (A) HeLa cells transfected with siRNAs and treated for 6hrs with Carboplatin, ATRi or ATMi as indicated then western blotted for P-ATM (S1981), Total-ATM, P-UPF1 (S1096), Total UPF1, P-Chk1 (S345), Total Chk1 and  $\beta$ -Actin (N=3). (B) Time-lapse live cell microscopy analysis for the mean time taken to complete mitosis. HeLa cells were transfected with the indicated siRNAs and treated with ATRi or ATMi as indicated. 50 cells for each condition were counted and the data illustrated represents the overall mean of each independent experiment  $\pm$  SEM (N=3). One way ANOVA with Dunnett's correction test for multiple comparisons was performed to determine statistical significance (\*\*\*) denotes  $p \leq 0.001$  and \*\*\*\* denotes  $p \leq 0.0001$ ). A table of p-values can be found in **Figure A5**.

### 3.2.5 UPF1 promotes mitotic delay in an R-loop- and transcription-dependent manner

Since we had determined that UPF1 was most likely acting in a non-NMD-related pathway to promote mitotic delay following DNA damage induction by carboplatin, we wished to assess other known roles of UPF1 in their ability to affect the mitotic delay phenotype. UPF1 has been recently implicated in having a role in secondary DNA structure homeostasis, specifically in the regulation of DNA-RNA hybrid structures known as R-loops. UPF1 has been demonstrated to bind to R-loops, but contradicting data on whether UPF1 promotes the formation of or resolves R-loops exists (Cristini *et al.*, 2018; Wang *et al.*, 2018; Cheruiyot *et al.*, 2021; Ngo, Grimstead and Baird, 2021).

To test whether DNA damage-induced mitotic delay was due to an accumulation of R-loop structures, we transfected cells with a plasmid that would overexpress RNaseH1, an enzyme that degrades RNA in DNA-RNA hybrids leading to the resolution of R-loops. As a control, cells were also transfected with a functionally dead RNaseH1<sup>D210N</sup> that can bind to R-loops but is catalytically inactive so is therefore unable to resolve these structures.

In untreated cells transfected with either the RNaseH1<sup>D210N</sup> or RNaseH1<sup>WT</sup>, no change in mitotic transit times were observed and cells proceeded through mitosis at a similar rate to non-transfected cells (see **Figure 3.2.6A**). As in un-transfected cells, cells transfected with RNaseH1<sup>D210N</sup> and treated with 1 $\mu$ M carboplatin showed a significantly increased mitotic transit time compared to the untreated control. By contrast, transfection of RNaseH1<sup>WT</sup> resulted in a significantly reduced mitotic delay compared to the treated RNaseH1<sup>D210N</sup> condition. We observed no changes in any conditions following siRNA-mediated depletion of UPF1, which is expected as both depletion of UPF1 and overexpression of RNaseH1 reduce mitotic transit times in the presence of DNA damage. This data shows that mitotic delay induced by treatment of carboplatin is entirely resolvable by RNaseH1 overexpression, suggesting this delay is R-loop dependent. This could also suggest that UPF1 mediates changes in mitotic duration by regulating the abundance of R-loops, though no direct link can be drawn from these experiments.

Since R-loops appear to be important in promoting mitotic delay, we also wished to test whether conditions under which R-loop homeostasis are known to be affected we could alter mitotic delay in the same manner. R-loops are known to form preferentially at sites undergoing active transcription due to the presence of a nascent RNA molecule and an unwound complementary DNA duplex. Therefore, we wished to examine the effect that acute transcriptional inhibition would have on mitotic progression. For this we used,  $\alpha$ -amanitin an RNA pol II inhibitor that prevents transcriptional initiation and elongation. The addition of 2 $\mu$ g/ml  $\alpha$ -amanitin led to a significant reduction in mitotic transit time following DNA damage-induction to the untreated level (see **figure 3.2.6B**). Suggesting that carboplatin-induced mitotic delay is also transcription dependent.

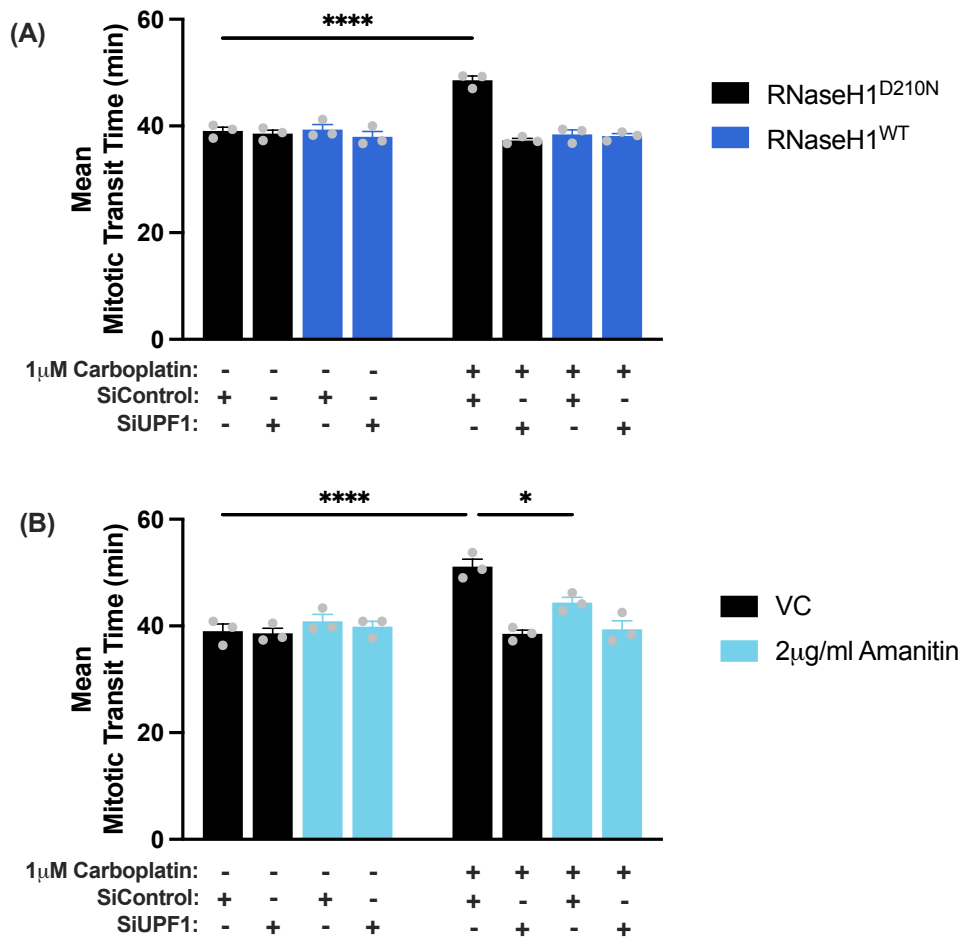


**Figure 3.2.6: DNA damage induced mitotic delay is an R-loop- and Transcription-dependent phenomenon.**

Time-lapse live cell microscopy analysis for the mean time taken to complete mitosis. HeLa cells were transfected with siRNAs in combination with **(A)** RNaseH1<sup>D210N</sup> or RNaseH1<sup>WT</sup> plasmid **(B)** or 2µg/ml α-Amanitin and treated with 1µM Carboplatin as indicated, 3hrs prior to beginning live cell. 50 cells for each condition were counted and the data illustrated represents the overall mean of each independent experiment +/- SEM (N=3). One way ANOVA with Dunnett's correction test for multiple comparisons was performed to determine statistical significance. A table of p values for RNaseH1 and amanitin experiments can be found in **Figure A6-7** respectively.

### 3.2.6 UPF1<sup>S42A</sup> induced and SMG6-depletion induced mitotic delay are transcription- and R-loop-dependent

Since we had shown that RNaseH1 and  $\alpha$ -amanitin treatment could effectively rescue DNA damage-induced mitotic delay, we wished to examine whether the delay that is induced by either the expression of the UPF1<sup>S42A</sup> protein or depletion of SMG6 could be rescued in the same manner.

Following treatment with 2 $\mu$ g/ml  $\alpha$ -amanitin or expression of RNaseH1<sup>WT</sup> we observe a significant reduction in S42A-induced mitotic delay compared to the untreated and RNaseH1<sup>D210N</sup> transfected conditions respectively (see **Figure 3.2.7A-B**). In the same way, carboplatin treatment did not extend mitotic duration any further than had already been done so by the expression of UPF1<sup>S42A</sup> and both  $\alpha$ -amanitin and RNaseH1<sup>WT</sup> were also able to significantly reduce mitotic transit times compared to carboplatin treated alone and RNaseH1<sup>D210N</sup> conditions respectively. Together this data provides evidence that the expression of UPF1<sup>S42A</sup> induces mitotic delay that is both R-loop and transcriptional-dependent, suggesting that this chromatin-binding defective UPF1 could lead to mitotic delay through an accumulation of transcriptional-associated R-loops.

Similarly, treatment with  $\alpha$ -amanitin or RNaseH1<sup>WT</sup> significantly reduced SMG6 depletion-induced mitotic delay compared to the untreated and the catalytically inactive RNaseH1<sup>D210N</sup> conditions respectively (see **Figure 3.2.7C**). As observed with UPF1<sup>S42A</sup>-induced mitotic delay, we found that transcriptional inhibition and RNaseH1<sup>WT</sup> expression were both sufficient to significantly reduce mitotic delay even when SMG6-depletion was combined with carboplatin treatment.

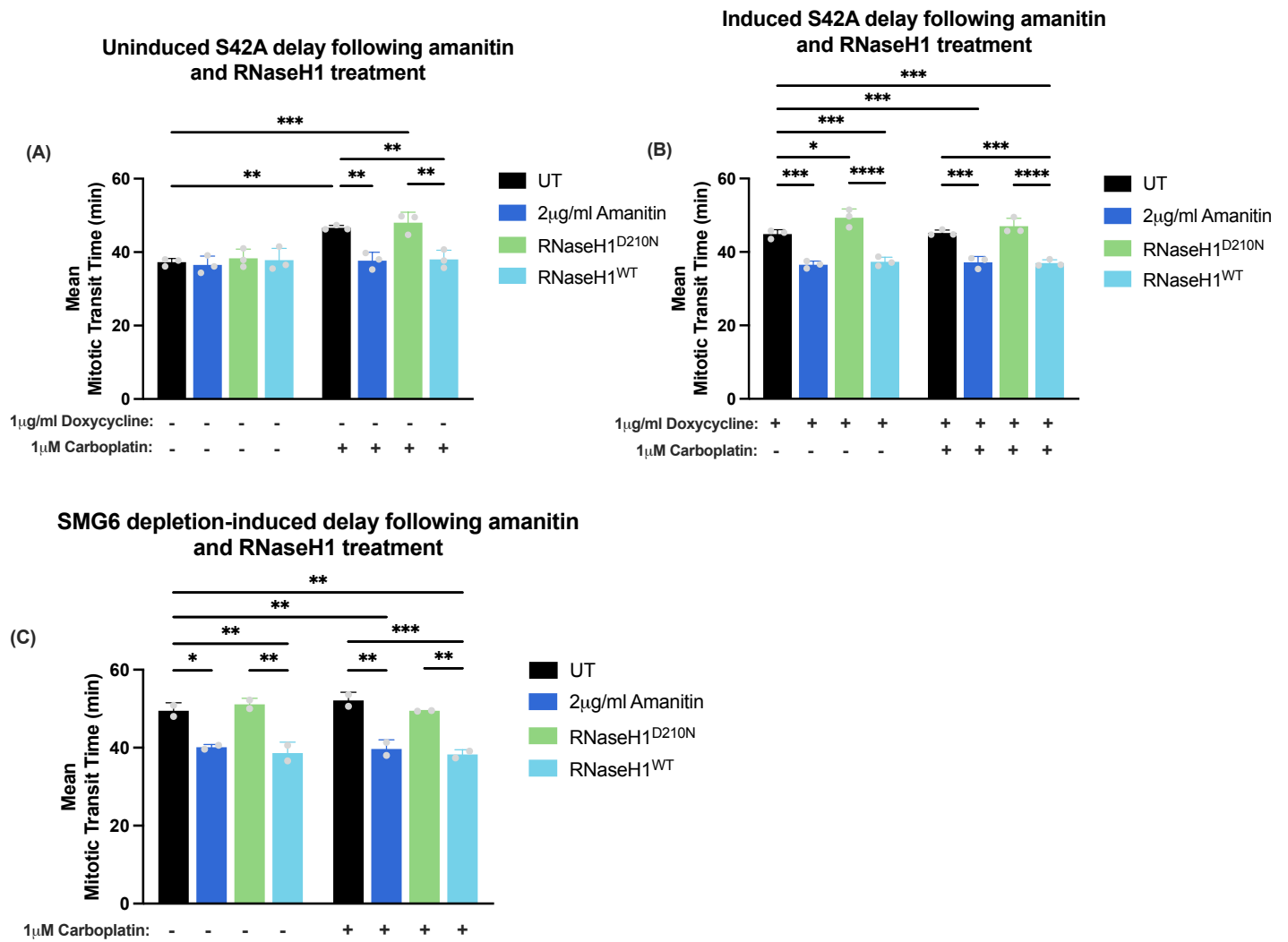


**Figure 3.2.7: Live cell microscopy analysis of mean mitotic transit time of UPF1<sup>S42A</sup> expressing or SMG6-depleted HeLa cells following treatment with 2 μg/ml α-amanitin or RNaseH1.**

(A-C) Time-lapse live cell microscopy analysis for the mean time taken to complete mitosis. (A,B) UPF1<sup>S42A</sup> FLP-IN HeLa cells were transfected with RNaseH1<sup>D210N</sup> or RNaseH1<sup>WT</sup> plasmid or treated with 2 μg/ml α-Amanitin and treated with 1 μM Carboplatin as indicated, 3hrs prior to live cell beginning. The cell lines were induced by the addition of 1 μg/ml doxycycline as shown. (C) HeLa cells were transfected with siSMG6 in combination with RNaseH1<sup>D210N</sup> or RNaseH1<sup>WT</sup> plasmid or treated with 2 μg/ml α-Amanitin and treated with 1 μM Carboplatin as indicated. 50 cells for each condition were counted and the data illustrated represents the overall mean of each independent experiment +/- SEM (N=3,3,2). One way ANOVA with Dunnett's correction test for multiple comparisons was performed to determine statistical significance. A table of p-values can be found at **Figure A8-10** for uninduced UPF1<sup>S42A</sup> FLP-IN HeLa cells, 1 μg/ml doxycycline treated UPF1<sup>S42A</sup> FLP-IN HeLa cells and SMG6-depleted HeLa cells respectively.

Together these data suggest that this mutant form of UPF1 could result in a build-up of transcriptional-associated R-loops which act to impede mitotic progression even in the absence of exogenous DNA damage. This also suggests that the role that UPF1 is playing in mediating delay is not necessarily specific to instances of DNA damage but could indeed be occurring in unperturbed cell cycle that become aggravated by the addition of replicative stress or DNA damage signalling. This is supported by the observation that SMG6 depletion induces delay which is too sensitive to RNaseH1 overexpression and transcriptional inhibition, suggesting requirement for a UPF1:SMG6 pathway even in the absence of DNA damage that is coupled both with R-loops and transcription.

### **3.3 Discussion**

UPF1 has been confirmed to play a role in the regulation of mitosis following DNA damage, both through previous work carried out in the Thompson laboratory, including mitotic population and progression assays (Gatenby, 2022), but also in this thesis through further mitotic progression and complementation experiments.

The data presented in this thesis suggests that whilst UPF1 depletion has no effect on unperturbed mitotic progression, in the presence of DNA damage or ATR inhibition, UPF1 is required for cells to exhibit a delay in mitosis. In concordance with this we further found depletion of a core regulatory factor of UPF1, UPF2 which is required for promoting its helicase and ATPase activities was also necessary to promote this mitotic delay (Chamieh *et al.*, 2007; Chakrabarti *et al.*, 2011; Fiorini, Boudvillain and Hir, 2013). This in combination with the ability of a UPF1 inhibitor VG1, which interferes with the phosphorylation cycle of UPF1, prevents the emergence of mitotic delay suggesting a requirement for active UPF1 to promote this phenotype (Gotham *et al.*, 2016). Depletion of key UPF1 recruitment factors UPF3b and STAU1 to target mRNAs for NMD or SMD had no impact on mitotic progression, suggesting a potential independence from canonical UPF1-associated decay pathways. We have also shown that DNA damage-dependent mitotic delay required both RNA- and DNA-binding activities of UPF1, and an abolishment of UPF1 ability to bind to chromatin is sufficient to induce mitotic delay even in the presence of endogenous UPF1, during an unperturbed cell cycle. Endonuclease activity downregulation by SMG6 depletion, but not exonuclease downregulation by SMG5 depletion, through siRNA-mediated

depletion of SMG6, promoted mitotic delay, demonstrating a requirement for active endonuclease decay to prevent spontaneous mitotic delay. Finally, we showed that carboplatin-, chromatin binding abolished UPF1- and SMG6 depletion-induced mitotic delay are all dependent on transcription and the presence of secondary DNA-RNA structures known as R-loops. Together this data suggests a novel transcription- and R-loop-dependent role of UPF1 and its binding partners, in preventing spontaneous and DNA damage-dependent mitotic delay.

### **3.3.1 UPF1-dependent mitotic delay likely occurs independently of NMD**

We have shown that UPF1 and UPF1-associated factors UPF2 and SMG1, that promote UPF1 helicase and or ATPase activities, are required for cells to promote a mitotic delay in response to DNA damage induction by carboplatin. One explanation for this phenotype would be due to a defect in UPF1's most described function, facilitating NMD. Consistent with this, UPF1 has recently been demonstrated to be required for the timely degradation of CENPF mRNA in G2 which serves to regulate SAC activity. Lack of this degradation by either PC2 or UPF1 depletion lead to spontaneous segregation errors, mitotic delay and mitotic catastrophe (Pan *et al.*, 2025). If this degradation event was present within our cells, then we would have observed spontaneous mitotic delay following UPF1 depletion. For their study the authors use a differentiated hepatocyte-derived carcinoma line Huh-7 (Pan *et al.*, 2025), it is possible that this could be a cell-type specific signalling pathway controlled by UPF1. Further evidence which suggests an NMD-independent function of UPF1 is the observation that depletion of the EJC factor UPF3b, which recruits UPF1 to NMD target mRNAs has no effect on mitotic duration. This was also true when we depleted STAU1, required for recruiting UPF1 to SMD target mRNAs (Kim *et al.*, 2005; Kashima *et al.*, 2006; Chamieh *et al.*, 2007; Gong *et al.*, 2009; Gowravaram *et al.*, 2019). It is important to mention that alternative models for UPF1 recruitment to NMD substrates have been suggested, which occur independently of UPF3b, through binding of UPF1 to the 3' UTR of a target mRNA (Bühler *et al.*, 2006; Fatscher *et al.*, 2014; Ivanov *et al.*, 2016; C. Wu *et al.*, 2020). A reliance on this could be investigated by examining the effect that depletion of PABPC1, which is required for promoting UPF1 3'-UTR association. It is therefore possible that UPF1 could be eliciting NMD independently of UPF3b.

We also have potentially observed that mitotic delay occurs independently of SMG5 and therefore exonucleolytic activity but not endonucleolytic activity of SMG6. Confirming knockdown of SMG5 is required to draw any solid conclusions from this live cell data. Exonucleolytic activity has been shown to be required for authorising SMG6 activity during NMD, the reliance on only one of these activities and an apparent independence of UPF3b, suggests that this could be a NMD-independent function of UPF1 (Boehm *et al.*, 2021). Whilst we do see a requirement for UPF2 in promoting DNA damage-dependent mitotic delay, UPF2's role in releasing UPF1's ATPase autoinhibition by its CH-domain has been shown to be required for RNA binding kinetics (Chapman *et al.*, 2024). It is likely that RNA-binding or the opening of the RNA-binding channel is still required for NMD-independent functions of UPF1 for recruitment to RNA or DNA.

### **3.3.1.1 NMD following genotoxic stress and alternative splicing**

We have shown that UPF1 depletion only affects mitotic duration in the presence of DNA damage. If this were due to dysregulation of NMD, then UPF1 depletion, even in the absence of DNA damage would lead to a mitotic progression defect, since depletion of UPF1 leads to a reduction in NMD efficiency and increase in NMD-target stability. Since NMD is a translation-coupled process, a global translational repression, inflicted by genotoxic stressors, has also been shown to downregulate NMD efficiency through eIF2 $\alpha$  and eIF2E phosphorylation (Gardner, 2008; Trivigno *et al.*, 2013; Usuki, Yamashita and Fujimura, 2019). DNA damage has also been shown to activate p38 MAPK to regulate gene expression changes through the inhibition of NMD (Nickless *et al.*, 2017). Under DNA damage conditions, it is therefore conceivable that NMD is already repressed, so depletion of UPF1 would be unlikely to have a further effect acting through NMD.

Alternative splicing, coupled with NMD, is a well-studied mechanism of gene expression changes following DNA damage (Lewis, Green and Brenner, 2003; Hansen *et al.*, 2009; Gabriel *et al.*, 2015; McCann *et al.*, 2023). It is possible that following DNA damage induction, mitotic regulators, such as APC/C components, which could be crucial for promoting this delay, become alternatively spliced making

them targets for NMD. A study in drosophila revealed that depletion of core NMD factors UPF1 and UPF2 and numerous SMG proteins resulted in the dysregulation of spliced isoforms of genes involved in mitotic regulation through NMD (Hansen *et al.*, 2009). The same group also demonstrated that depletion of these factors resulted in an increase in G2/M population (Rehwinkel *et al.*, 2005). This data is inconsistent with our observation that UPF1 depletion results in a reduced mitotic population. We hypothesise that this same regulation does not occur in human cells as if this were the case, then loss of UPF1 or UPF2 would affect mitotic progression even in the absence of genotoxic stressors. We have shown that VG1 treatment was able to phenocopy UPF1-depletion, in abolishing mitotic delay, with only 2hrs pre-treatment. NMD results in the degradation of mRNAs, therefore, the question is whether there is sufficient time for this to result in changes in protein expression, resulting in aberrant mitotic progression. Further investigation into this mechanic could help elucidate whether NMD is indeed the required pathway. It seems that in response to stress, NMD is largely inhibited either directly or indirectly. However, we have demonstrated that UPF1 is required for mitotic delay following DNA damage induction, therefore a loss of NMD efficiency does not explain the observed changes in mitotic progression.

### **3.3.1.2 SMG1 and the regulation of p53**

The depletion of a key kinase SMG1, that promotes UPF1 phosphorylation and activation, resulted in a significant reduction in mitotic duration following treatment with carboplatin, but also in the absence of DNA damage induction. This is inconsistent with our other UPF1 knockdown experiments which show loss of UPF1 has no effect on mitotic progression in the absence of DNA damage. No direct link between SMG1 and mitosis or SAC regulation has been suggested previously. This could be a result of a more effective way of abolishing UPF1 activity, since SMG1 is upstream of UPF1. Alternatively, this could be a result of an independent function of SMG1.

Depletion of SMG1 has been shown to regulate the well described tumour suppressor p53. Specifically, SMG1 induces alternate splicing of p53 and reduces p53 activity in response to DSBs, independently of NMD and UPF1 (Gewandter, Bambara and O'Reilly, 2011; J. Chen *et al.*, 2017; McCann *et al.*, 2023). P53 phosphorylation at Ser15 by ATM following mitotic entry has been suggested to maintain p53 in an

inactive state at centrosomes, when the spindle is correctly in place (Oricchio *et al.*, 2006). It is now proposed that p53 governs a mitotic surveillance pathway in combination with USP28 and 53BP1 (Fong *et al.*, 2016; Stracker, 2024). This suggests that SMG1 depletion could lead to the p53 pathway dysregulation, that could promote mitotic timing changes independent of UPF1.

### **3.3.2 mRNA decay-independent functions of UPF1 affect mitotic timing**

#### **3.3.2.1 Transcription is required for centromeric identity and faithful mitotic progression**

We have shown that both the RNA- and DNA-binding abilities of UPF1 seems crucial in regulating the requirement for a mitotic delay. Delay induced by the UPF1<sup>S42A</sup> mutant and depletion of the endonuclease SMG6 is also dependent on both ongoing transcription and R-loop accumulation. Whilst the chromatin localisation function of UPF1 is poorly characterised, it is known that chromatin-binding deficient UPF1 is unable to rescue spontaneous DSBs induced by depletion of endogenous UPF1 (Azzalin and Lingner, 2006; Azzalin *et al.*, 2007; Turton, 2014). UPF1 has been suggested to be required for regulating transcription, R-loop homeostasis or lncRNA release and degradation at specific genomic loci (Azzalin *et al.*, 2007; Chawla *et al.*, 2011; Hong, Park and Jeong, 2019; Singh *et al.*, 2019; De *et al.*, 2022).

Mitotic transcriptional activation has been shown to be required for the clearance of remaining RNAPII complexes in early prophase, blocking this has been shown to result in defective mitotic progression (Liang *et al.*, 2015). The requirement of *de novo* transcription in mitosis is widely debated, since global transcriptional repression is observed following mitotic entry through displacement of transcription factors and RNAPII complexes (Martínez-Balbás *et al.*, 1995; Novais-Cruz *et al.*, 2018). However, active transcription by RNAPII at the centromere in mitosis has also been suggested to be required to maintain centromeric identity and SAC functionality (Mena, Lam and Chatterjee, 2010; Chan *et al.*, 2012; Liu *et al.*, 2015; Blower, 2016; McNulty, Sullivan and Sullivan, 2017; Bobkov, Gilbert and Heun, 2018; Kang *et al.*, 2024). Mitotic regulation has also been demonstrated to be influenced by lncRNAs. Depletion of *linc00899* has been shown to promote mitotic delay through the transcriptional silencing of microtubule-binding protein TPPP/p25 (Stojic *et al.*, 2020). Since UPF1 is

required for the displacement and degradation of nascent lncRNAs in the telomeric regions, it is possible that UPF1 could possess a similar role at centromeres and other regions of the genome (Azzalin *et al.*, 2007; Arora *et al.*, 2014; Turton, 2014).

### **3.3.2.2 Centromeric R-loops regulate mitotic progression**

Centromeric RNAs (cenRNAs) are also vital in the maintenance of the kinetochore, like telomeres, centromeres require cenRNAs associating with the centromere through R-loops to maintain proper function. It is possible that UPF1 could play a similar role at centromeres, as it does at the telomere. UPF1 and numerous other UPF1-like helicases including the well described regulator of R-loops, SETX, have been demonstrated to have roles in the regulation of R-loop structures (Dehghani-Tafti and Sanders, 2017; Cohen *et al.*, 2018; Li *et al.*, 2020; Cheruiyot *et al.*, 2021; Ngo, Grimstead and Baird, 2021). R-loops mediate critical recruitment of centromeric factors, however also promote replication stress and genomic instability (Giunta *et al.*, 2021). Mitotic regulators BugZ and BUB3 have been implicated in the removal of these structures through an interaction with spliceosomal components similar to the action of UPF1 (Wan *et al.*, 2015; Cheruiyot *et al.*, 2021).

The existence of an R-loop driven mitotic checkpoint acting through ATR has also been proposed to function at centromeres, supporting this hypothesis (Kabeche *et al.*, 2018). This checkpoint is dependent on Aurora A association with CENP-F which allows ATR to interact with RPA-coated R-loop structures at the centromere. Acute degradation or inhibition of ATR leads to abnormal chromosome segregation, which is independent of the DDR or unscheduled DNA synthesis. It is possible that UPF1 could play a role in the regulation of these R-loop structures directly at the centromere, especially given our observation that mitotic delay can be induced by ATRi in a similar manner, which is dependent on UPF1. Suggesting that UPF1 could function upstream of ATR, facilitating ATR recruitment to R-loops to allow for correct checkpoint signalling.

### **3.3.3 UPF1 could facilitate DNA replication or repair in mitosis**

Since the mitotic delay that we observe seems to be independent of the canonical SAC and only occurs following DNA damage induction, UPF1 could be promoting an

alternative mitotic delay to allow for DNA replication or repair. Under conditions of mild replication stress, prometaphase mitotic cells are known to exhibit Mitotic DNA synthesis (MiDAS) (Minocherhomji *et al.*, 2015; Bhowmick, Minocherhomji and Hickson Correspondence, 2016). Whilst no direct links have been made discerning whether MiDAS activation or disruption affect mitotic delay, studies demonstrate a correlation between the occurrence of MiDAS and mitotic delay (Wassing *et al.*, 2021). It is important to mention that MiDAS has been shown to be dependent on both transcription and R-loop burden, of which we have also observed for our DNA damage and induced mitotic delay phenotypes studied in this thesis (Groelly *et al.*, 2022; Said *et al.*, 2022).

UPF1 has been suggested to facilitate telomeric DNA replication, an absence of which leads to telomeric DSBs and telomeric loss (Azzalin *et al.*, 2007; Chawla *et al.*, 2011). Telomeres are CFSs which undergo MiDAS in prometaphase due to their late replication. Since UPF1 appears to be required for this replication, maybe it has a more general role in CFS replication through MiDAS. MiDAS has been demonstrated to be dependent on p66 subunit of pol $\delta$ , which UPF1 has been shown to interact with previously (Carastro *et al.*, 2002; Azzalin and Lingner, 2006; Minocherhomji *et al.*, 2015; Wu *et al.*, 2023). Other DNA helicases have also been demonstrated to have a role in MiDAS such as RTEL1 and SETX (W. Wu *et al.*, 2020; Said *et al.*, 2022). RTEL1 recruits RAD52 and the p66 subunit of Pol  $\delta$ , through the resolution of G-quadruplex associated R-loops. Interestingly, RTEL1 has also been demonstrated to have other roles similar to that of UPF1, including the displacement of TERRA from telomeres, suggesting that these two helicases could act in a similar manner (Ghisays *et al.*, 2021).

CFSs are also sites that represent hotspots of transcription-replication collisions (TRCs) during S-phase, due to the requirement to replicate and transcribe these genes concomitantly (Helmrich, Ballarino and Tora, 2011). TRCs have been linked to MiDAS activation, due to occurring on late replicating sites in the genome and increasing R-loop burden, a known activator of MiDAS (W. Wu *et al.*, 2020; Bhowmick *et al.*, 2022; Groelly *et al.*, 2022). Replicative stress increases the frequency of such occurrences. Interestingly, other NMD factors, namely UPF2 and SMG1 modulators SMG8:SMG9

have both recently been identified as having roles in promoting the formation of these structures in the presence of an ATR inhibitor (Llorca-Cardenosa *et al.*, 2022; O’Leary *et al.*, 2022). Here depletion of UPF2 and SMG8:SMG9 were shown to prevent deleterious effects of ATRi on DNA replication and the DDR. We have shown that UPF1 only impacts mitotic delay following DNA damage treatment, therefore UPF1 could only have an accessory role in the regulation of these structures. It is possible that UPF1 is only required when transcription-replication collisions are induced by DNA damage or if repair is prevented. This is consistent with the fact that R-loops are known to associate preferentially during transcription when RNA Pol II stalls, whether this is due to bulky DNA lesions produced by platinum-based chemotherapy agents or through replication-transcription conflicts during S-Phase. Alternatively, since we can elicit a mitotic delay even in the absence of DNA damage, it is possible that lower levels of R-loops inflicted by depletion of UPF1, can be handled by the cell and is not at a sufficient level to promote mitotic delay.

In this chapter we have demonstrated that UPF1 promotes DNA damage-dependent mitotic delay independent of UPF3b-dependent NMD. The ability for DNA damage-dependent mitotic delay to be rescued by RNaseH1 overexpression and transcriptional inhibition implicate UPF1 in having a role in mitotic DNA replication or DNA damage-dependent regulation of the SAC.

### **3.3.4 Limitations**

To investigate the effect of various NMD factors on mitotic duration we have utilised siRNAs to deplete each target protein. Whilst this is an efficient and reliable way of knocking down a protein of interest, long-term loss of the protein can complicate the understanding of results obtained. In addition to this, siRNA have been demonstrated to exhibit off-target effects, whilst we have demonstrated that exogenous UPF1 expression rescues siRNA-mediated UPF1 loss to disprove this, rescue experiments for other components tested by siRNA should be carried out. To address these issues further, auxin-inducible degron cell lines could be developed to effectively and rapidly degrade targeted proteins, allowing for the assessment of the effect that loss has at various times within the cell cycle (Nishimura *et al.*, 2009; Yesbolatova *et al.*, 2020). This is combination with methods of cell synchronisation such as using a double

thymidine block to synchronise cells at G1 and monitor the time taken to enter into various cell cycle phases, will allow for a better determination for the time at which UPF1 and UPF1-associated proteins are required. Cell synchronisation would also have an added effect of ensuring that cells experience DNA damage or replicative stress in the same cell cycle phase and for an equal amount of time. Whilst we have been able to reliably quantify a ~10min average increase in mitotic duration of asynchronous populations, this data does not necessarily truly reflect the nature of the delay that is being studied. That is, in some cell's delays are observed for up to 150mins, compared to an untreated cell which can progress through mitosis in ~40mins. The reason for this discrepancy in cells responding to DNA damage is most likely due to the range of times in which they are exposed to carboplatin for. Synchronising cells does not come without its own limitations, since impairing the ability of a cell to cycle freely can promote spontaneous DNA damage as well as altering the balance of cyclin levels (Ligasová and Koberna, 2021). Since the use of thymidine for synchronisation promotes G1 arrest by depleting nucleotide pools, this is most likely to have an effect of subsequent DNA replication following release.

For these live cell studies, we employed bright field live cell microscopy to measure mitotic timing changes by measuring the time taken between mitotic rounding and cytokinesis. Whilst this is a reliable method for an approximation of mitotic timing, alternative methods of measuring mitotic timing using GFP-tagged lamin B and mCherry Histone H2B could be used to better determine stages of chromatin condensation and nuclear envelope breakdown (Wassing *et al.*, 2021). These methods of live cell imaging allow for the breakdown of mitosis into its distinct phases, providing us with data for the determination of where in mitosis DNA damage-dependent mitotic delay is occurring.

Use of the FLP-IN HeLa cell lines also bring in potential limitations. it is important to take into consideration the exact nature of the mutations tested. The UPF1<sup>R843C</sup> possesses a mutation in the RNA-binding channel that occludes the entrance, preventing RNA-binding. Whilst this canonically is described as an RNA-binding mutation, UPF1 also displays significant ssDNA-binding activity that also occurs through this channel, which could characterise this mutation more broadly as a single

stranded nucleic acid-binding mutant (Dehghani-Tafti and Sanders, 2017). To this end, this mutant could prevent an interaction between UPF1 and ssDNA or ssRNA. In addition, the chromatin-binding deficient S42A mutation, is an uncharacterised phosphorylation site that impairs chromatin localisation of UPF1 and results in a form of UPF1 unable to rescue spontaneous  $\gamma$ -H2AX resulting from endogenous UPF1 depletion. It is likely that preventing or mimicking the phosphorylation at this site, will result in dominant phenotypes due to the trapping of UPF1 in a specific state.

# Chapter 4: UPF1 in mitotic and interphase DNA replication

## 4.1 Introduction

UPF1 has been demonstrated to function on chromatin in a non-canonical manner to maintain genomic stability, however the exact significance of this function is yet to be understood. Numerous implications suggest a key role in mediating DNA replication and/or repair through an interaction with a subunit of p66 of Pol  $\delta$  (Carastro *et al.*, 2002; Azzalin and Lingner, 2006; Turton, 2014), as well as observing UPF1 chromatin recruitment in S-phase increasing in response to a range of DNA damage and replication stress stimuli. This recruitment has been shown to require the PIKK ATR, to drive the movement of UPF1 to chromatin following IR, however this is the extent which is known as to this role.

After determining that UPF1 promotes DNA damage-dependent mitotic delay in most likely a non-canonical fashion, that is independent of NMD but dependent on both active transcription and R-loop accumulation, we hypothesised that UPF1 could be driving the process of Mitotic DNA synthesis (MiDAS). MiDAS is a recently characterised DNA synthesis pathway that occurs during prophase of mitosis for the completion of under-replicated stretches of DNA (Minocherhomji *et al.*, 2015). MiDAS inhibition has been linked to delays in mitotic progression (Wassing *et al.*, 2021). R-loop accumulation and active transcription has also been shown to promote the underlying problem that MiDAS resolves, but also be required for the initiation of MiDAS (Li and Manley, 2005; W. Wu *et al.*, 2020; Said *et al.*, 2022). It is therefore possible that mitotic delay coincides with MiDAS occurrence, and therefore UPF1 could be promoting mitotic delay through MiDAS activation. In this chapter we aim to assess whether DNA replication dynamics and the response to DNA replication stress is altered in UPF1-deficient cells.

The aims of this chapter are to assess the following:

1. The effect of UPF1 deficiency on the occurrence of MiDAS or G2 runover replication following mild replicative stress in HeLa and RPE cell lines
2. The effect of UPF1 deficiency on cell cycle distribution of RPE cell lines following mild replicative stress
3. The effect of UPF1 deficiency on global DNA replication dynamics in unperturbed and mild replicative stress conditions
4. The ability of transcriptional inhibition by DRB to rescue replication fork stalling induced by UPF1 deficiency

The hypothesis of this chapter is:

UPF1 deficiency affects DNA replication stress response through altered DNA replication dynamics.

## **4.2 Results**

### **4.2.1 UPF1 promotes mitotic DNA synthesis following replicative stress**

We have reported an increase in mitotic transit time following treatment with DNA damage and replication stress agents, that is dependent on UPF1. We hypothesised that UPF1 could be crucial for promoting DNA replication or DNA damage repair during mitosis. In prometaphase of mitosis a phenomena termed Mitotic DNA synthesis (MiDAS) has been proposed to occur when cells are exposed to mild replication stress. This leads to a delay in DNA replication completion without activating the G2-M checkpoint (Minocherhomji *et al.*, 2015; Bhowmick, Minocherhomji and Hickson Correspondence, 2016). As a result, these cells exhibit ongoing DNA replication during prometaphase which can lead to chromosomal fragility during spindle pole segregation.

To detect this repair, cells are exposed to a mild replication stress agent, typically 0.4 $\mu$ M aphidicolin for 23hrs and then must be synchronised at the G2-M transition using the CDK1 inhibitor RO3306. These cells are then released into prometaphase and incubated with the thymidine analogue EdU to detect ongoing replication (see

**Figure 4.2.1A-B**). When cells have not been treated with replication stress or DNA damage they exhibit very limited MiDAS as DNA replication is typically confined to S-phase in unperturbed conditions (see **Figure 4.2.1C**). However, the addition of 0.4 $\mu$ M aphidicolin results in a significant increase in EdU foci observed in prometaphase cells (see **Figure 4.2.1B-C**). siRNA mediated depletion of UPF1 leads to these cells exhibiting a significant reduction in EdU foci, suggesting either a defective MiDAS pathway that is unable to occur, or a lack of requirement for activation of the pathway.

We aimed to also rescue the loss of UPF1 in these experiments using the FLP-IN TreX HeLa cell line from the previous chapter. UPF1<sup>WT</sup> is capable of rescuing the loss of endogenous UPF1, demonstrating a specific role for UPF1 in promoting the emergence of MiDAS following mild replicative stress (see **Figure 4.2.1C**). Both UPF1<sup>S42A</sup> and UPF1<sup>S42E</sup> mutants are capable of rescuing the loss of MiDAS following depletion of endogenous UPF1. This suggests that neither of these mutants appear to impede with the process of MiDAS itself, however UPF1 is indeed required for the occurrence of mitotic DNA replication.



**Figure 4.2.1: Analysis of UPF1 mutant rescue on the occurrence of Mitotic DNA synthesis following low-dose replicative stress.**

Immunofluorescence microscopy of HeLa cells incubated with 20 $\mu$ M EdU, subjected to mitotic shake off and stained for EdU. **(A)** Schematic depicting experimental outline. Cells were transfected with indicated siRNAs and induced with 1 $\mu$ g/ml doxycycline as described. Cells were treated with 0.4 $\mu$ M Aphidicolin as indicated for 23hrs prior to mitotic shake-off. **(B)** Representative immunofluorescence images showing EdU and DAPI of prophase cells. **(C)** Quantification of EdU foci per prometaphase cell. 50 cells for each condition were quantified and the data illustrated represents the EdU foci from one repeat. (N=3). One way ANOVA with Dunnett's correction test for multiple comparisons was performed to determine statistical significance (\*\* denotes  $p \leq 0.01$ , \*\*\* denotes  $p \leq 0.001$  and \*\*\*\* denotes  $p \leq 0.0001$ ).

UPF1 depletion significantly reduces the occurrence of MiDAS following treatment with aphidicolin suggesting that it could indeed be required for this process. Alternatively, the loss of UPF1 could improve the cells response to replicative stress, allowing for efficient replication even in the presence of replication stressors, removing the necessity for replicative runover into mitosis. To investigate whether this is the case we then chose to look at the occurrence of 53BP1 nuclear bodies under the same conditions. 53BP1 nuclear bodies mark sites of DNA under-replication post-mitosis and serve as a mark for the repair or replication prior to entering the subsequent S-phase. If UPF1 depletion is indeed compromising the pathway of MiDAS, we should observe a significant increase in 53BP1 nuclear bodies in the subsequent G1 of these cells.

For this assay we carried out a similar experiment to the MiDAS assay, but omitting EdU incorporation and allowing the cells to enter into G1 prior to mitotic shake-off. This assay allows us to quantify only cycling cells that have undergone mitosis in the presence of aphidicolin. A detailed schematic of the experimental outline can be found in **Figure 4.2.2A**. Even though this experimental plan enriches for post-mitotic G1 cells, as with the MiDAS assay, dying or poorly attached cells can be knocked off during mitotic shake-off. To confirm we were indeed quantifying G1 cells we immunostained with Cyclin A, whose expression is restricted to outside of G1. Indeed we observed that several cells did stain positive for Cyclin A and as a result these cells

were omitted from subsequent analysis (see **Figure 4.2.2C**). 53BP1 foci in untreated G1 cells were very minimal across all conditions tested, however following treatment with 0.4 $\mu$ m aphidicolin we saw a large increase in total 53BP1 foci in all SiCtrl FLP-IN TreX HeLa cell lines (see **Figure 4.2.2D**). Depletion of endogenous UPF1 caused no obvious change in 53BP1 foci in the UPF1<sup>WT</sup> cell line and neither did rescue of endogenous UPF1, by the addition of doxycycline. The only obvious change that was observed in this experiment was that expression of UPF1<sup>S42A</sup> appeared to lead to a large increase in 53BP1 foci in G1 cells.

The quantification of 53BP1 nuclear bodies is a highly debated topic, with many disagreeing over what defines a 53BP1 nuclear body. Specifically size has been a controversial topic, since 53BP1 forms both small and large foci that are clearly distinguishable from each other. To try and assess whether our oversimplistic quantification of 53BP1 foci was shrouding the analysis we chose to implement an alternative method of quantification using Cell Profiler. From this we were able to quantify again total foci, average 53BP1 area per cell, number of small and large foci and the percentage of cells that possessed 'large' 53BP1 nuclear bodies. In this manner we observed again relatively few total foci in the absence of replication stress (see **Figure 4.2.2E**). We found that UPF1 depletion in untreated conditions resulted in a subtle increase in total 53BP1 foci by this method of quantification. Low dose aphidicolin induced a large increase in total 53BP1 foci which was unchanged by UPF1 depletion. These same patterns were observed for small foci, large foci and percentage of cells with nuclear bodies in their respective conditions (see **Figure 4.2.2G-I**). Whilst this is only one repeat, it is a possible observation that UPF1 depletion in combination with low-dose aphidicolin treatment does not lead to an increase in under-replication, at least that marked by 53BP1 in G1 cells, whilst UPF1 depletion alone does potentially lead to under-replication spontaneously (see **Figure 4.2.2E-I**). Together this data suggests that UPF1 could not be directly involved in MiDAS, but does directly affect DNA replication dynamics prior to mitotic entry, which is required for driving the necessity for MiDAS.



**Figure 4.2.2: Analysis of 53BP1 nuclear bodies in G1 of HeLa cells treated with low dose aphidicolin.**

(A) Schematic of experimental outline for analysis of 53BP1 nuclear bodies. FLP-IN TreX HeLa cells were transfected with the indicated siRNAs for 48hrs with and without 1 $\mu$ g/ml doxycycline, before being incubated with 0.4 $\mu$ M aphidicolin as indicated, for 23hrs. All conditions were treated with 9 $\mu$ M Ro3306 for 5hrs. Washout of Ro3306 was followed by mitotic shake off, resultant cells were then allowed to enter into G1 for 2.5hrs before being fixed for immunofluorescence. (B) Representative immunofluorescence microscopy images of 53BP1, Cyclin A and DAPI in untreated and 0.4 $\mu$ M aphidicolin treated G1 cells. (C) Histogram of mean nuclear cyclin A intensity of all cells. The red dotted line represents the cut off used to dictate a Cyclin A negative population, indicative of cells in G1. (D) Quantification of 53BP1 foci of G1 cells of uninduced and induced FLP-IN TreX HeLa cell lines. Quantification of (E) Total 53BP1 foci, (F) Average 53BP1 area, (G) Small 53BP1 foci, (H) Large 53BP1 foci and (I) percentage of cell population with 53BP1 nuclear bodies of G1 cells. These analyses were conducted only on uninduced SiCtrl or SiUPF1 with and without 0.4 $\mu$ M aphidicolin (N=1).

**4.2.2 UPF1 is not required for the occurrence of unscheduled DNA synthesis in G2 prior to mitotic entry of HeLa cells**

It was observed that depletion of UPF1 led to a significantly reduced occurrence of MiDAS in prophase of mitosis. The traditional MiDAS model suggests that MiDAS is the restart of replication in mitosis at sites that exhibit replication fork stalling in late S-phase, when treated with mild replication stress. The assay used for several years to study this, as mentioned previously, relies on the synchronisation of cells in G2 with the CDK1 inhibitor Ro3306 (see **Figure 4.2.1A**). However, recently this drug has been suggested to interfere with DNA replication through an off-target effect on CDK2, therefore precluding the observation of DNA replication in G2 (Mocanu *et al.*, 2022). Mocanu *et al.* proposed that DNA replication which stalls in late S-phase continues replicating through G2 and into mitosis. They also demonstrated that this replication occurs independent of some 'known' MiDAS proteins, most likely due to the lack of restart required. We hypothesised that UPF1 could be required for both the traditional MiDAS model and for G2 runover DNA synthesis.

To study whether UPF1 does indeed impact this DNA replication runover outside of S-phase, asynchronous cultures were treated with 0.4 $\mu$ M Aphidicolin for 23hrs as with

the MiDAS experiments, omitting the use of Ro3306. 30mins prior to fixation they are incubated with 20 $\mu$ M EdU to allow for the detection of ongoing DNA replication. The cells were then subsequently stained for P-Histone H3 (S10), EdU and DAPI. The use of P-Histone H3 (Ser10) in combination with DAPI measurements allows us to quantitatively determine the cell cycle stage each cell is in at the time of EdU pulse. P-Histone H3 (Ser10) is a marker of chromatin condensation that begins at late replication regions in G2 (Van Hooser *et al.*, 1998; Mocanu *et al.*, 2022). By multiplying together P-Histone H3 (Ser10) and DAPI nuclear intensities you can distinguish G1 and G2 populations more easily than either one alone. This in combination with the mean nuclear EdU intensity allows us to segregate our asynchronous populations into three distinct sub populations (see **Figure 4.2.3**). In support of this being an effective way to determine cell cycle phase we can reproducibly determine G1, S and G2 populations of 49%, 40% and 11% respectively in our untreated SiCtrl conditions across our three biological replicates with little variation (see **Figure 4.2.3E**). When we treat these cells with the replication inhibitor aphidicolin we observe an accumulation of cells in S-phase with a resulting G1, S and G2 population of 9%, 82% and 8.6% respectively (see **Figure 4.2.3E**). This reduction in G1 population is consistent with an accumulation of cells in S-phase following aphidicolin treatment.

Since we were now able to reliably and reproducibly segregate cells imaged into three distinct populations, we wanted to examine whether we could indeed detect any changes in replication dynamics at any point throughout the cell cycle.

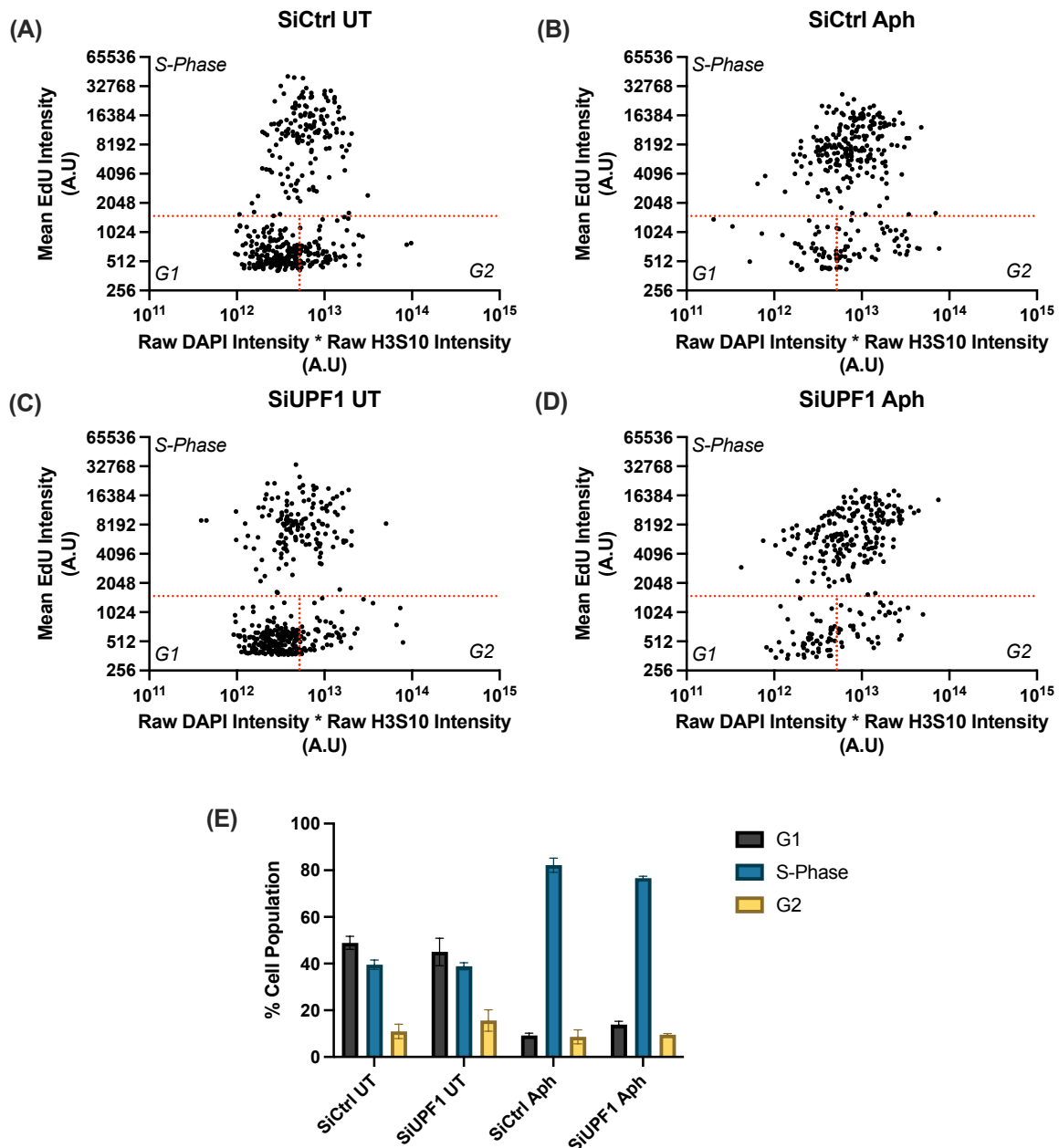


**Figure 4.2.3: Segregation of asynchronous populations into G1, S and G2 by immunofluorescence.**

**(A-D)** Representative X-Y plots for Mean EdU Intensity vs Raw DAPI Intensity  $\times$  Raw H3S10 Intensity in HeLa cells treated with SiCtrl or SiUPF1 with or without a 24hr treatment with 0.4 $\mu$ M Aphidicolin as stated. Gating for G1, S and G2 populations demonstrated with red dashed lines. A minimum of 150 individual cells imaged per biological repeat. **(E)** Mean cell cycle phase distribution of HeLa cells transfected with SiCtrl or SiUPF1 and treated with or without 0.4 $\mu$ M Aphidicolin for 24hrs prior to fixation. Data points represent mean cell cycle phase distribution  $\pm$  SEM (N=3). *Aph* = *Aphidicolin*,

To examine whether loss of UPF1 impacted the appearance of DNA replication run over in G2 we quantified EdU foci in cells gated for being part of the G2 population (see **Figure 4.2.4C**). In the absence of mild replication stress, we observed relatively few EdU foci per G2 cell. However, treatment with 0.4 $\mu$ M aphidicolin induces a significant increase in observable EdU foci compared to the untreated control. This is consistent with Mocanou *et. al.* and of a similar magnitude, as they observed an average number of EdU foci of ~50 in G2 cells whilst our data shows a mean EdU foci of 47.0 in G2 cells. When these cells are depleted for UPF1 we observed no significant change in EdU foci suggesting that in this HeLa cell line UPF1 does not play a role in facilitating DNA replication runover in G2.

One explanation for why we could observe no difference under these conditions is the presence of bulk DNA synthesis occurring in G2 in this cell line. We observed an increase in coincidence of pan EdU staining, indicative of an S-phase cell, and the cell being positive for P-Histone H3 (Ser10), a G2 marker (see **Figure 4.2.4D**). As a result, these G2 cells also cannot be used for quantification of EdU foci in G2, this presented problems in quantifying a sufficient number of G2 cells in this cell line. siRNA-mediated depletion of UPF1 appears to compromise DNA synthesis meaning that replication runs into G2, not just CFSs but bulk DNA synthesis that would normally be completed in S-phase.

Quantification of EdU foci in G1 revealed no significant changes under any conditions tested (see **Figure 4.2.4G**). Demonstrating that depletion of UPF1 did not lead to an increase in post-mitotic DNA damage. It is also possible that these sites mark ssDNA in G1, and therefore could be a marker of DNA under-replication. We also thought that if MiDAS was disrupted by siRNA-mediated depletion of UPF1 then we would expect to observe an increase in DNA synthesis occurring in the subsequent G1 after exiting mitosis as a result of mitotic aberrations and DNA breaks during mitosis. However, this is not observed suggesting that loss of UPF1 does not lead to enhanced CFS expression in mitosis, and potentially that UPF1 depletion does not lead to a defective MiDAS pathway.

Whilst looking at the X-Y plots we noticed that S-phase cells depleted for UPF1 appeared to have reduced mean nuclear EdU intensities (see **Figure 4.2.3A-D**). Suggesting that these cells could have problems with DNA synthesis in S-phase, we decided to plot the mean nuclear EdU intensity for the S-phase population of each condition. In order to aid comparison across repeats we decided to normalise the mean nuclear EdU intensity to the untreated SiCtrl and express each value as a fold-change. From this we did indeed observe that siRNA-mediated depletion of UPF1 led to a significant reduction in mean nuclear EdU intensity in S-phase cells even in the absence of aphidicolin, indicative of replication problems occurring in the absence of UPF1 (see **Figure 4.2.4E**). In support of this being a reliable quantification we also observed a significant reduction in mean nuclear EdU intensity when both SiCtrl and SiUPF1 cells were treated with 0.4 $\mu$ M aphidicolin for 24hrs compared to the untreated SiCtrl. It is possible that due to a change in cell cycle distribution, specifically during S-phase, that we would observe a reduction in mean nuclear EdU intensity. To check that this was not the case and that we were indeed seeing a reduction in EdU incorporation, rather than a shift in cell cycle distribution, we plotted the median nuclear EdU intensity from the three biological repeats (see **Figure 4.2.4F**). Depletion of UPF1 does also significantly reduce the median mean nuclear EdU intensity in S-phase cells, as well as the same reductions following treatment with aphidicolin in both SiCtrl and SiUPF1 conditions. Together these observations support the occurrence of a defect in EdU incorporation in S-phase cells that are depleted for UPF1.

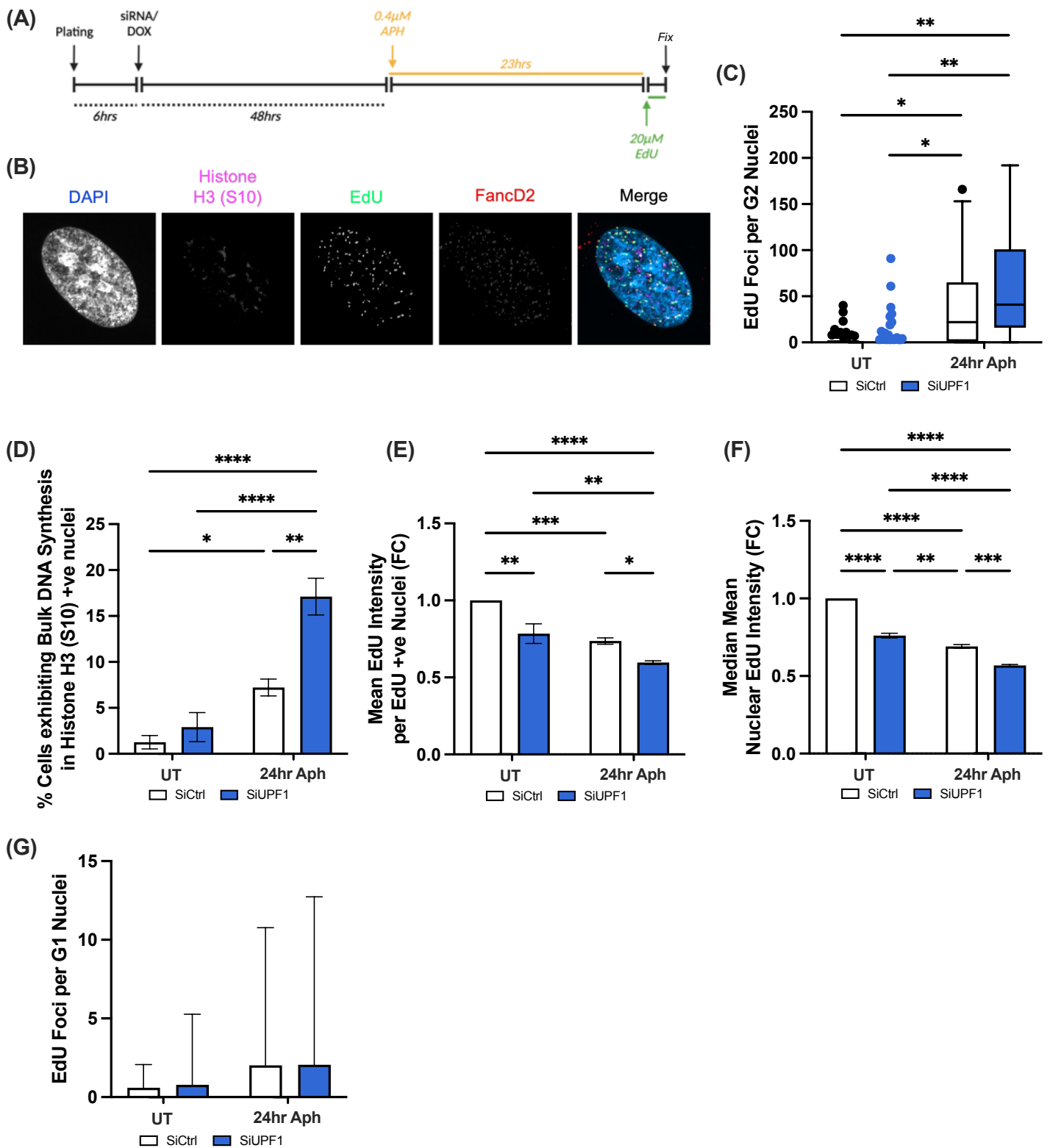


**Figure 4.2.4: Analysis of G2 DNA synthesis in HeLa cells siRNA depleted for UPF1 and treated with 0.4µM Aphidicolin for 24hrs.**

*Legend on next page.*

**Figure 4.2.4: Analysis of G2 DNA synthesis in HeLa cells siRNA depleted for UPF1 and treated with 0.4 $\mu$ M Aphidicolin for 24hrs.**

(A) Drugging schedule for G2 EdU incorporation assay. (B) Representative immunofluorescence images of HeLa cells treated with 0.4 $\mu$ M aphidicolin for 24hrs before being fixed and stained for EdU, Phospho-Histone H3 (Ser10), FANCD2 and DAPI. (C) Quantification of nuclear EdU foci per G2 cells. (D) Quantification of percentage of cells exhibiting bulk DNA synthesis in G2 cells. (E-F) Quantification of normalised mean and median EdU intensity of S-phase cells respectively. (G) Quantification of nuclear EdU foci per G1 cells. Data illustrated for E and G are representative graphs taken from one biological replicate, where each dot represents an individual cell. Data illustrated for D-F represent the mean of the three replicates +/- SEM. A One-way ANOVA with Dunnett's correction test for multiple comparisons was performed on the mean from each biological replicate to determine statistical significance (N=3) (\* denotes  $p \leq 0.05$ , \*\* denotes  $p \leq 0.01$ , \*\*\* denotes  $p \leq 0.001$ , \*\*\*\* denotes  $p \leq 0.0001$ ).

**4.2.3 RPE<sup>UPF1 KO</sup> cells also have reduced EdU incorporation in S-phase**

Since we had observed a reduction in EdU incorporation in S-phase of cells depleted for UPF1 we wanted to validate that this was a specific phenotype and not due to off target effects of the siRNA. To confirm this, we decided to use the non-cancerous RPE cell line that had been CRISPR engineered as a heterozygous knockdown for UPF1. This cell line is untransformed but immortalised through the expression of hTERT. **Figure 4.2.5A** confirms that UPF1 protein expression is significantly reduced in the RPE<sup>UPF1 KO</sup> cell line. We then wanted to repeat the DNA replication runover assay as mentioned previously to determine whether this RPE cell line, and this method of UPF1 knockdown exhibited the same replication phenotypes. By plotting X-Y of mean EdU intensity vs raw DAPI intensity  $\times$  raw H3S10 intensity we can determine G1, S and G2 populations of the imaged cells. As with the HeLa cell line we observe in these experiments an increase in the S-phase population following aphidicolin treatment (see **Figure 4.2.5 D-G**). We analysed the EdU dynamics in G1, S-Phase and G2-M, this time in combination with FANCD2, a known protein that colocalises to sites of MiDAS and a marker of stalled replication forks (see **Figure 4.2.5B-C**).

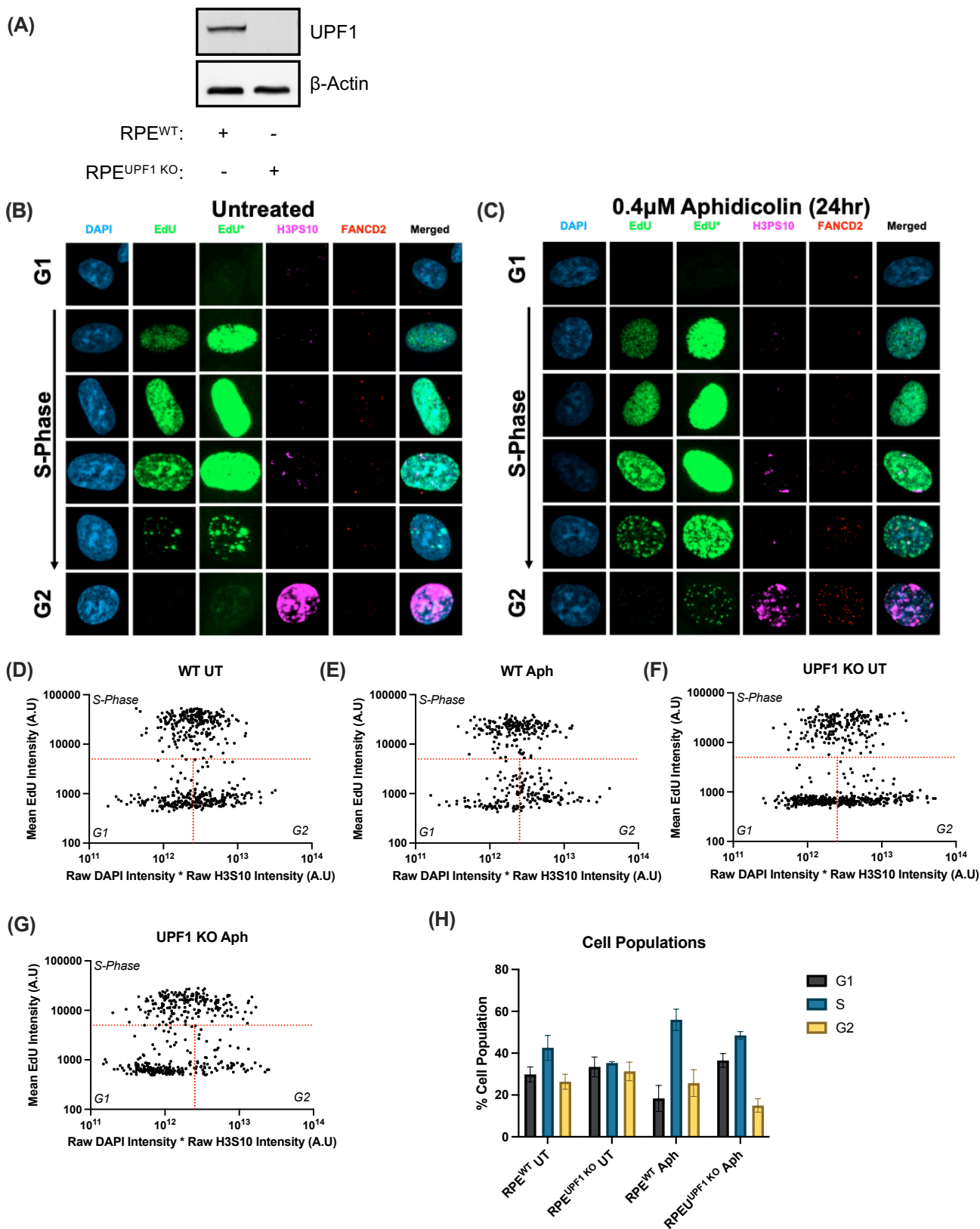


**Figure 4.2.5: Segregation of asynchronous populations into G1, S and G2 by immunofluorescence in RPE cells.**

*Legend on next page.*

**Figure 4.2.5: Segregation of asynchronous populations into G1, S and G2 by immunofluorescence in RPE cells.**

**(A)** Western blot analysis of RPE<sup>WT</sup> and RPE<sup>UPF1 KO</sup> cells for UPF1 and  $\beta$ -actin. **(B-C)** Representative immunofluorescence images for RPE<sup>WT</sup> cells at each stage of the cell cycle untreated and with 0.4 $\mu$ M aphidicolin for 24hrs before being stained for EdU, FANCD2, H3PS10 and DAPI. **(D-G)** Representative X-Y plots for Mean EdU Intensity vs Raw DAPI Intensity  $\times$  Raw H3S10 Intensity in RPE<sup>WT</sup> and RPE<sup>UPF1 KO</sup> cells treated with or without a 24hr treatment with 0.4 $\mu$ M Aphidicolin as stated. Gating for G1, S and G2 populations demonstrated with red dashed lines. A minimum of 250 individual cells imaged per biological repeat. **(H)** Mean cell cycle phase distribution determined by gating of X-Y plots in **D-G**. Data points represent mean cell cycle phase distribution  $\pm$  SEM (N=3).

We observed that loss of UPF1 resulted in a reproducible reduction in mean EdU intensity in S-phase compared to the untreated RPE<sup>WT</sup> (see **Figure 4.2.6A**). However, this fell short of being statistically significant. Consistent with UPF1 loss promoting a DNA replication problem in S-phase we also observed that there was a reproducible increase in FANCD2 foci in S-phase (see **Figure 4.2.6B**). Together this data demonstrates a replication defect occurring as a result of UPF1 loss most likely leading to an increase in spontaneous replication fork stalling as marked by FANCD2.

As with the HeLa cell line we consistently observed relatively few G2-M EdU foci in untreated conditions in both RPE<sup>WT</sup> and RPE<sup>UPF1 KO</sup> cell lines (see **Figure 4.2.5B** and **Figure 4.2.6C**). Treatment with 0.4 $\mu$ M aphidicolin increased the number of observable G2-M EdU foci significantly in both cell lines however the RPE<sup>UPF1 KO</sup> cell line also had significantly less EdU foci compared to the RPE<sup>WT</sup> line (see **Figure 4.2.5C** and **Figure 4.2.6C**). We observed colocalization between the EdU foci and FANCD2 in G2 following treatment with 0.4 $\mu$ M aphidicolin, consistent with the sites undergoing replication runover being 'MiDAS sites' which frequently exhibit replication fork stalling (see **Figure 4.2.5C**). FANCD2 foci also showed a very similar phenotype to that of the quantified EdU foci in G2-M (see **Figure 4.2.6D**). FANCD2 foci were also slightly increased in untreated G2 RPE<sup>UPF1 KO</sup> cells compared to the untreated RPE<sup>WT</sup> cells, which could suggest spontaneous DNA replication runover. A reduction in FANCD2 foci formation in RPE<sup>UPF1 KO</sup> G2-M cells compared to the RPE<sup>WT</sup> cells was also observed following treatment with aphidicolin, however this was also not statistically

significant. Overall G2-M DNA replication appears to be dependent on UPF1 in RPE cells, with loss of UPF1 also driving a modest amount of spontaneous DNA under-replication.

In untreated conditions, we observed very few EdU foci in G1 cells both in the presence and absence of UPF1 (see **Figure 4.2.6E**). However, treatment with 0.4 $\mu$ M aphidicolin for 24hrs induced a significant increase in observable G1 EdU foci. This increase in EdU foci was not observed however in G1 nuclei of RPE<sup>UPF1 KO</sup> cells treated with 0.4 $\mu$ M aphidicolin. Consistently, we also observed the same pattern of FANCD2 foci under these conditions (see **Figure 4.2.6F**). Together these data suggests that loss of UPF1 could prevent under-replicated DNA emerging and persisting into the subsequent cell cycle.

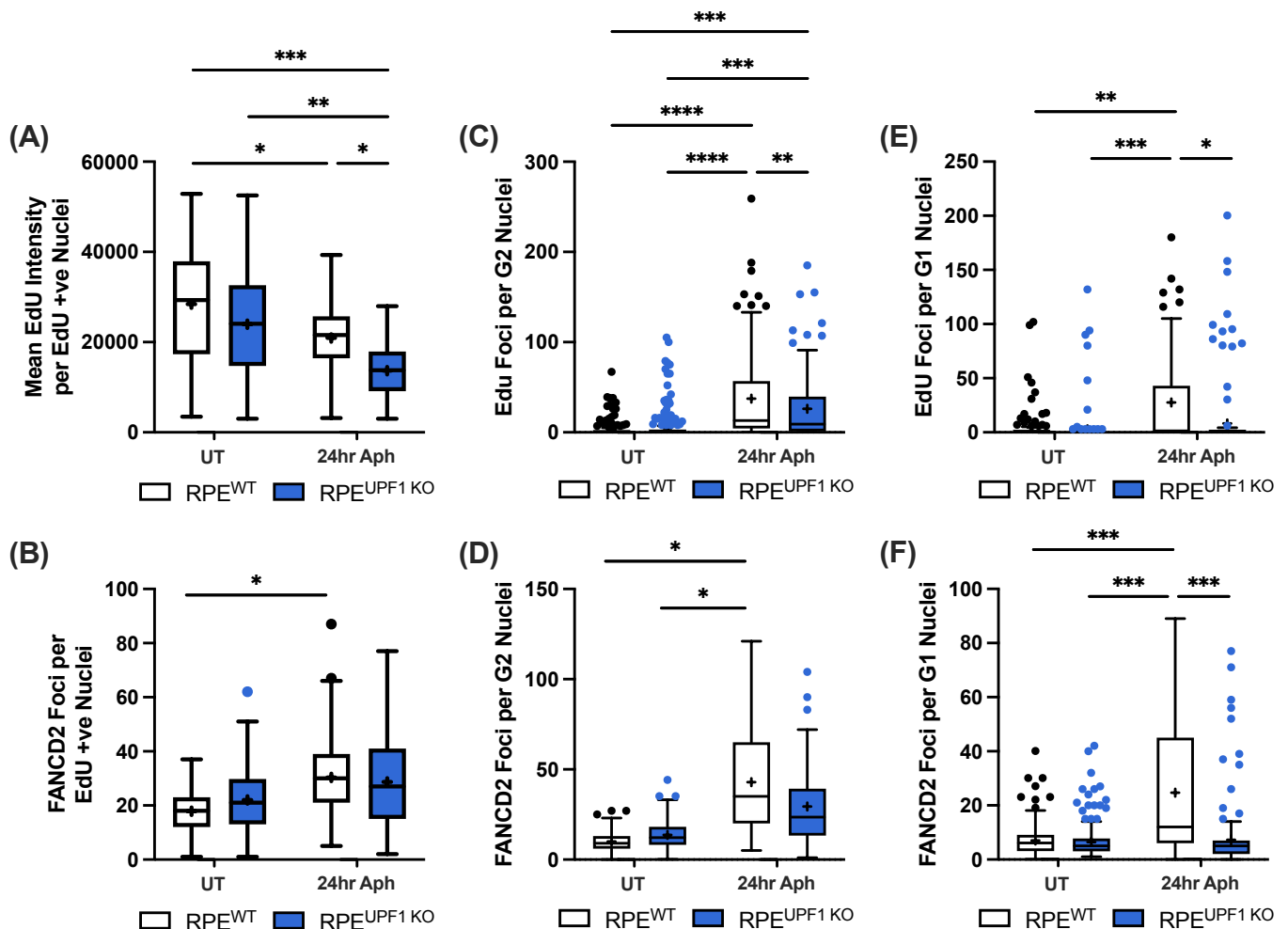


**Figure 4.2.6: Analysis of EdU and FANCD2 dynamics in RPE<sup>WT</sup> and RPE<sup>UPF1 KO</sup> cells treated with 0.4 $\mu$ M Aphidicolin for 24hrs.**

*Legend on next page.*

**Figure 4.2.6: Analysis of EdU and FANCD2 dynamics in RPE<sup>WT</sup> and RPE<sup>UPF1 KO</sup> cells treated with 0.4 $\mu$ M Aphidicolin for 24hrs.**

**(A)** Quantification of mean EdU intensity per EdU positive cells gated from **Figure 4.2.5.** **(B-F)** Quantification of nuclear EdU and FANCD2 foci per S-phase, G2 and G1 cells as indicated. Data illustrated are representative Tukey plots taken from one biological replicate. A horizontal black line indicates the median, whiskers indicate the interquartile range and black crosses indicate the mean. For EdU foci and FANCD2 foci in all cell cycle phases a One-way ANOVA with Dunnett's correction test for multiple comparisons was performed on the mean nuclear foci from each biological replicate to determine statistical significance (N=2) (\* denotes  $p \leq 0.05$ , \*\* denotes  $p \leq 0.01$ , \*\*\* denotes  $p \leq 0.001$ , \*\*\*\* denotes  $p \leq 0.0001$ ).

Together these data demonstrate that UPF1-deficiency impairs DNA replication processes in S-phase, G2 and mitosis. Loss of UPF1 whilst in unperturbed conditions promoting spontaneous replication problems in S-phase, appears to negatively regulate DNA replication outside of S-phase following mild replication stress.

#### **4.2.4 Validation of replication deficit in UPF1 deficient RPE cells by flow cytometry**

Since we have now observed that UPF1-depleted cells seem to exhibit a replication defect that results in reduced EdU incorporation, we wanted to attempt to validate the phenotype again. It has been demonstrated previously that shRNA-mediated knockdown of UPF1 resulted in the accumulation of cells with a slightly higher than  $2n$  DNA content, which was suggested to be a result of an early S-phase arrest (Azzalin and Lingner, 2006). However, unpublished data from the lab of Professor Carl Smythe and from the lab that generated the RPE<sup>UPF1 KO</sup> cell line, suggests this phenotype is not reproducible (Turton, 2014; Ngo, Grimstead and Baird, 2021).

To examine any changes in cell cycle progression we carried out fluorescent-activated cell sorting (FACS). Since we were interested specifically in S-phase we decided to incubate the cells with 10 $\mu$ M of the thymidine analogue BrdU for 30mins which allows for the detection of cells carrying out DNA synthesis at the time of fixation. Antibody-based immunodetection for BrdU in combination with propidium iodide (PI) for DNA content staining, means we were able to determine cell cycle profiles with a focus on

S-phase. We examined RPE<sup>WT</sup> and RPE<sup>UPF1 KO</sup> cells in untreated conditions but also following 4hrs and 24hrs treatment of 0.4 $\mu$ M aphidicolin.

We could not determine any cell cycle changes between the RPE<sup>WT</sup> and RPE<sup>UPF1 KO</sup> cell lines in untreated conditions. Consistent with *Ngo et.al.* we only observed a small increase in G1 population of the RPE<sup>UPF1 KO</sup> cells compared to the RPE<sup>WT</sup> (see **Figure 4.2.7A-B**). Following 4hr 0.4 $\mu$ M aphidicolin we observed an increase in the early S-phase population in the WT line, consistent with a slowing of DNA replication by DNA polymerase inhibition. However, this same increase could not be seen in the UPF1 KO cells. Only at 24hrs do we observe a modest but non-significant increase in the early S-phase population of the UPF1 KO cell line. At which point in the WT cell line ~43% of cells are in G2-M. This suggests that UPF1 KO cells could be slower to exhibit replication stress following aphidicolin treatment.

To validate the UPF1 loss-dependent replication defect that we observed in our immunofluorescence assays we decided to measure the median BrdU intensity for the S-phase population. We found that the untreated UPF1 KO S-phase population showed a significantly reduced median EdU intensity compared to the untreated WT S-phase population (see **Figure 4.2.7C**).

Together these data suggests that loss of UPF1 whilst not impeding cell cycle progression in untreated conditions seems to result in a DNA replication defect. Furthermore, loss of UPF1 seems to delay or prevent the response to DNA polymerase inhibition by low dose aphidicolin in RPE cells.

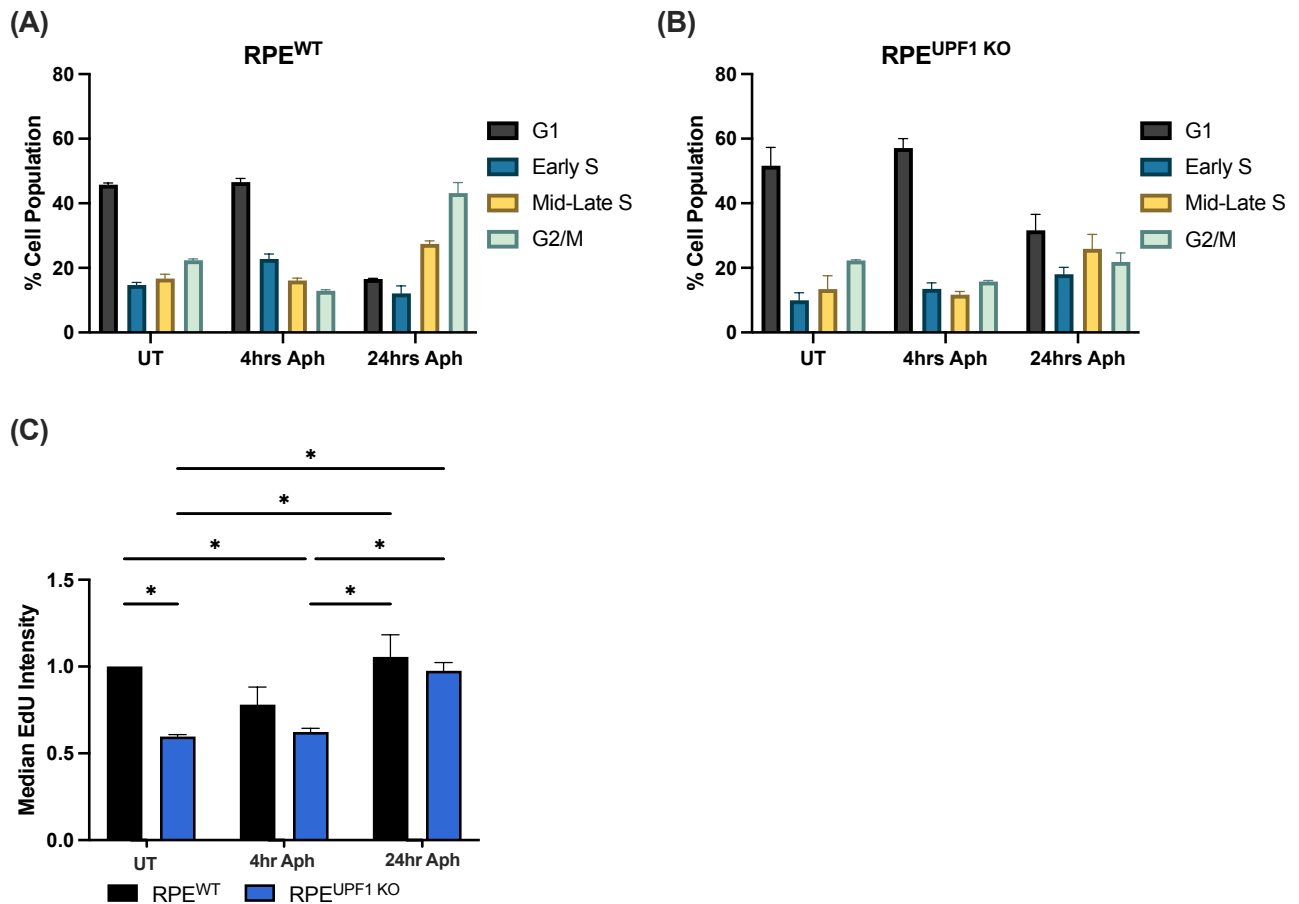


**Figure 4.2.7: RPE<sup>WT</sup> and RPE<sup>UPF1 KO</sup> cell cycle distribution with and without treatment of 0.4 $\mu$ M aphidicolin for 24hrs.**

**(A-B)** Mean cell cycle phase distribution of RPE<sup>WT</sup> and RPE<sup>UPF1 KO</sup> cells respectively. **(C)** Average normalised median EdU intensity of total S-phase population +/- SEM (N=3). One way ANOVA with Dunnett's correction test for multiple comparisons was performed to determine statistical significance (\* denotes  $p \leq 0.05$ ). Table of p-values from One-way ANOVA test for each individual cell cycle phase can be found in **Figure A11-13** for G1, Early S-phase, Mid-Late S-Phase and G2-M respectively.

#### 4.2.5 DNA fibre analysis reveals UPF1-deficiency promotes DNA replication fork stalling

In two cell lines we have observed following the removal of UPF1, either by CRISPR engineered knockdown or by siRNA, a reduction in EdU incorporation in S-phase cells as well as altered DNA replication stress pathway responses. UPF1 has been implicated in DNA replication previously. UPF1 has been demonstrated to interact with p66/ POLD3, the regulatory subunit of DNA polymerase  $\delta$  which is important in

modifying Pol $\delta$  for its role in homologous recombination and translesion DNA synthesis (Carastro *et al.*, 2002; Azzalin and Lingner, 2006). UPF1 has also been demonstrated to be required for telomeric leading-strand DNA replication through an interaction with TPP1 and telomerase (Chawla *et al.*, 2011). Whilst there is evidence for UPF1 being required for DNA replication it could also be interfering with DNA replication as a result of defective RNA homeostasis. Therefore, we hypothesised that UPF1 could be promoting a replication defect by one of two hypotheses:

- UPF1 is directly involved in DNA replication
- Removal of UPF1 leads to roadblocks on DNA that prevent efficient DNA replication

In order to test this hypothesis and directly measure whether DNA replication was indeed defective in the absence of UPF1 and in what manner, we utilised the DNA fibre assay. To begin we chose to analyse replication fork speeds to determine whether DNA replication was indeed perturbed in the absence of UPF1. For this analysis only dual colour DNA fibres are quantified (see **Figure 4.2.8A** (top panel)). In untreated conditions the HeLa cell line had an average fork speed of 0.84Kb/min, this is consistent with published literature that suggests fork speeds in a HeLa cell line are ~0.7Kb/min (Técher *et al.*, 2013) (see **Figure 4.2.8B**). siRNA-mediated depletion of UPF1 resulted in a significant reduction in fork speed by ~18% even in the absence of replication stress. Treatment with low dose aphidicolin for 24hrs in the SiCtrl and SiUPF1 condition also significantly reduced the progressing fork speed by ~46% and ~44% respectively compared to the untreated SiCtrl. This fork speed analysis reveals that indeed DNA replication is compromised in the absence of UPF1 in unperturbed conditions, but the reason for this is still unknown. DNA fibre tracts can be shorter for two reasons: (1) DNA replication rate is reduced or (2) an increase in replication fork stalling. In order to discern why DNA replication fork speeds are reduced in the absence of UPF1 we chose to quantify sister fork symmetry.

Sister fork symmetry is the analysis of replication origins and the symmetry in length of the replication forks emanating in opposite directions away from the origin. Replication forks from the same origin (sister forks) are known to travel with a similar

velocity and therefore during unperturbed DNA replication have a high degree of symmetry (Conti *et al.*, 2007). By analysing replication origins, we can determine whether DNA replication rates have reduced or if fork stalling has increased. If DNA replication rates have reduced then symmetry will still be maintained, as both forks will be equally shorter. But, if the incidence of fork stalling has increased then sister fork symmetry will be lost, as fork stalling will most likely not affect both forks equally. Representative images demonstrating symmetric and asymmetric sister forks are shown in **Figure 4.2.8A** (bottom panel).

In line with there being a high degree of sister fork symmetry during unperturbed DNA synthesis we observe that our untreated SiCtrl cells show an average symmetry score of 0.895 (see **Figure 4.2.8C**). siRNA-mediated depletion of UPF1 results in a significant loss of this symmetry with a score of 0.575. Treatment of SiCtrl cells with 0.4 $\mu$ M aphidicolin also results in a loss of symmetry with a score of 0.617. Whilst aphidicolin does indeed reduce replication rates, if not entirely stop at high concentrations, low dose aphidicolin induces a significant degree of replication fork stalling at CFSs. The treatment of low dose aphidicolin in HeLa cells siRNA-mediated depleted for UPF1 resulted in no significant reduction in sister fork symmetry compared to the untreated SiCtrl. This combination of loss of UPF1 and aphidicolin treatments results in a significantly increased symmetry of 0.819 compared to both untreated UPF1-depleted cells and low dose aphidicolin treated SiCtrl cells. Together this data reveals that loss of UPF1 leads to an increased frequency of spontaneous replication fork stalling that compromises unperturbed DNA synthesis. This UPF1 loss-dependent replication fork stalling also seems to be at least partly rescuable by slowing DNA replication rates through DNA polymerase inhibition by low dose aphidicolin.

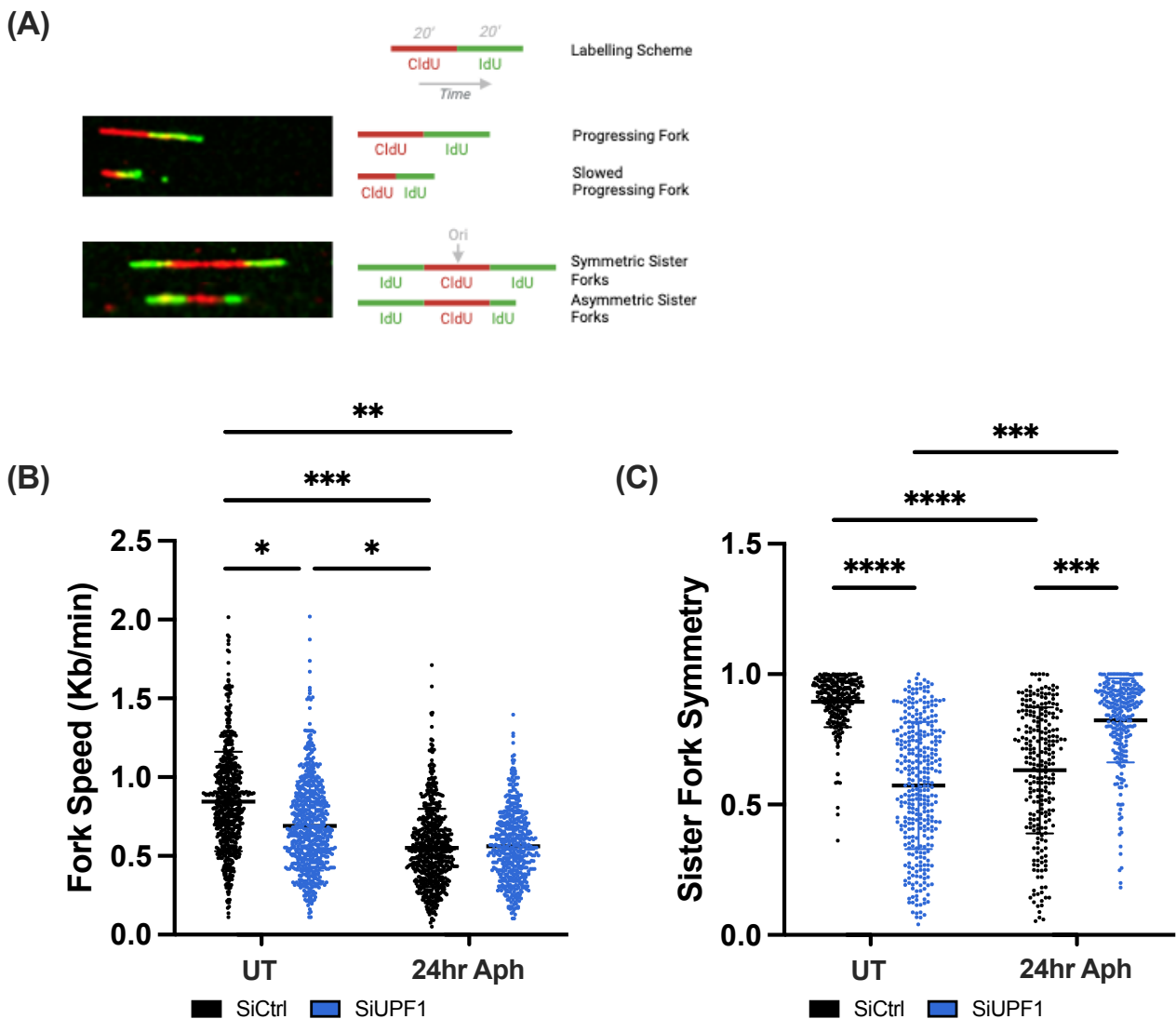


**Figure 4.2.8: DNA fibre analysis of HeLa cells mock treated, or siRNA depleted for UPF1 with or without treatment with 0.4 $\mu$ M aphidicolin for 24hrs.**

(A) Labelling scheme of 100 $\mu$ M CldU and 500 $\mu$ M IdU pulses of HeLa cells and the subsequent DNA fibre structures analysed for B-D. (B) Quantification of progressing fork speeds. (C) Quantification of sister fork symmetry. Data points represent individual DNA fibres analysed, the black line and error bars represent the mean  $\pm$  SD (N=3). A minimum of 200 individual DNA fibres were analysed per condition and a One-way ANOVA with Dunnett's correction test for multiple comparisons was performed on the mean of each biological replicate to determine statistical significance (\* denotes  $p \leq 0.05$ , \*\* denotes  $p \leq 0.01$ , \*\*\* denotes  $p \leq 0.001$ , \*\*\*\* denotes  $p \leq 0.0001$ ).

#### 4.2.6 Transcriptional inhibition by DRB rescues DSBs induced by loss of UPF1 in RPE cells

We have observed that the removal of UPF1 leads to an increase in replication fork stalling that can be rescued by treatment with low dose aphidicolin. Replication fork stalling can occur for a number of reasons including, encounters between replicative machinery, template damage, slow-moving or paused transcription complexes, unrelieved positive super helical tension, covalently bound protein-DNA complexes and as a result of cellular stress responses. These are all possible mechanisms through which UPF1 could be promoting replication fork stalling.

Since UPF1 is characterised as an RNA/DNA helicase and involved in RNA homeostasis, we hypothesised that UPF1 could indeed be impeding replication fork progression as a result of defective transcriptional processes. Interfering with transcription elongation or termination could lead to the existence of slowed or trapped RNAPII complexes which would block replication fork progression, leading to the formation of a transcription-replication collision (TRC). To test this hypothesis, we reasoned that inhibiting transcription would lead to the removal of RNAPII from DNA, relieve any transcriptional defect induced by loss of UPF1 and rescue the subsequent phenotypes associated with UPF1 loss.

To do this we utilised the CDK9 inhibitor 5,6-dichloro-1-beta-D-ribofuranosylbenzimidazole (DRB). This drug is a specific CDK9 inhibitor which prevents key regulatory phosphorylation events from occurring in the C-terminal domain of RNAPII. Specifically, DRB prevents RNAPII CTD (Ser2) phosphorylation, that is required for efficient transcriptional elongation. Since long-term transcriptional inhibition would lead to G1 arrest, prevent S-phase entry and therefore prevent any subsequent assessment of DNA replication, we knew we could only treat our cells with DRB for a relatively short amount of time. To see whether such a short drugging schedule would work, we exposed WT and UPF1 KO RPE cells to increasing concentrations of DRB for 2hrs and assessed the level of P-RNAPII CTD (Ser2) and Total-RNAPII by western blot (see **Figure 4.2.9**).

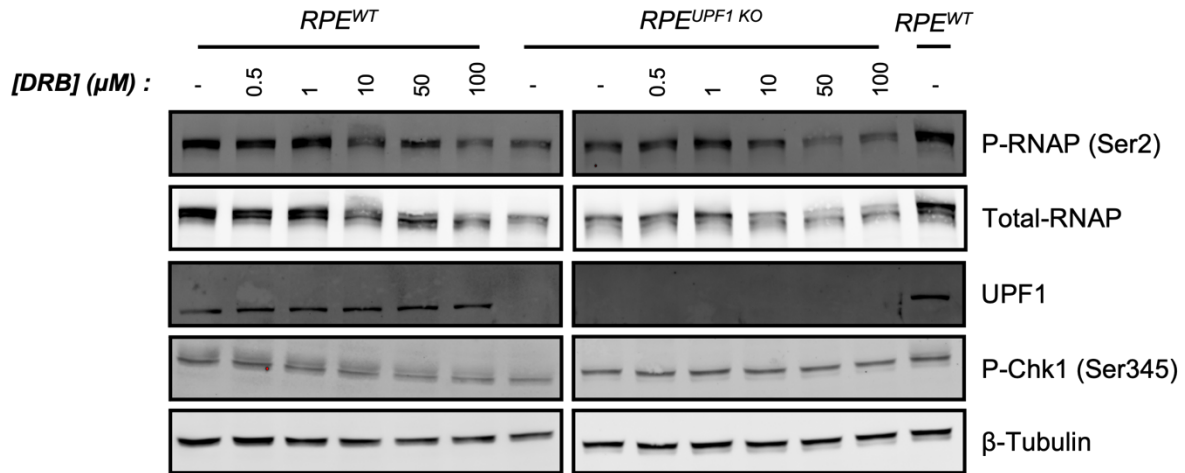


**Figure 4.2.9: Western blot analysis of RPE cells in response to acute DRB treatment.**

Western blot of RPE<sup>WT</sup> and RPE<sup>UPF1 KO</sup> cells treated with increasing concentrations of DRB for 2hrs before being blotted for P-RNAPII (Ser2), Total-RNAPII, UPF1, P-Chk1 (Ser345) and  $\beta$ -tubulin. The untreated control for each cell line was loaded on the end of each blot to allow for comparison between the samples ran on separate gels (N=1).

We observed a dose dependent reduction in both phospho-RNAPII CTD (Ser2) and total-RNAPII in both cell lines. It is also worth noting that no toxicity was observed at any of the concentrations tested after 2hrs, therefore we chose to use 100 $\mu$ M DRB for our subsequent experiments, since we observed the most dramatic reduction in phospho-RNAPII CTD (Ser2) levels. Now that we had optimised the drugging schedule for DRB we wanted to test whether we could indeed rescue any defects induced by loss of UPF1. To begin with, we examined a highly reproducible phenotype observed in cells depleted for UPF1, spontaneous DSBs (Azzalin and Lingner, 2006; Turton, 2014).

For these experiments we assessed the appearance of phosphorylation of the Ser139 residue of the histone variant H2AX which forms  $\gamma$ -H2AX, a sensitive and early marker of DSB induction. We tested this in RPE<sup>WT</sup> and RPE<sup>UPF1 KO</sup> cell lysates treated with 0.4 $\mu$ M aphidicolin for 24hrs and/or 100 $\mu$ M DRB for 2hrs (see **Figure 4.2.10A**). In the WT line we reproducibly observed that DRB treatment alone reduced spontaneous  $\gamma$ -

H2AX, whilst low dose aphidicolin induced  $\gamma$ -H2AX, all be it to no significant degree (see **Figure 4.2.10B**). The combination treatment has a similar  $\gamma$ -H2AX signal to that of the untreated suggesting that these two drugs appear to cancel each other out, most likely due to the relative induction and rescue of TRCs following aphidicolin and DRB treatment respectively. In the UPF1 KO cells we observed a statistically significant increase in spontaneous  $\gamma$ -H2AX compared to the untreated WT line (see **Figure 4.2.10B**). DRB treatment alone caused a reduction in the level of spontaneous  $\gamma$ -H2AX in UPF1 KO cells. Whilst statistical analysis fell short of a significant difference between the untreated and DRB treated UPF1 KO cells, UPF1 KO cells treated with DRB no longer had a significant increase compared to the untreated WT cells. Curiously, we did not observe a reduction in  $\gamma$ -H2AX in UPF1 KO cells following treatment with aphidicolin nor did we observe a significant reduction in the combination treatment. Demonstrating that DNA replication inhibition does not prevent UPF1 depletion-induced DSBs, whilst transcriptional inhibition does.

UPF1-deficiency has also been shown to promote a reduction in replication stress signalling through P-Chk1 (Ser345) (Ngo, Grimstead and Baird, 2021). Indeed, we did observe a small reduction in P-Chk1 signalling in the UPF1 KO compared to the WT line, though the change was not significant most likely due to the much large changes observed following induction of mild replication stress (see **Figure 4.2.10C**). We found no difference between the P-Chk1 (Ser345) between WT and RPE lines under any conditions tested, suggesting there were no changes in global DNA replication stress signalling through Chk1.

Finally, we examined changes in phospho-RNAPII CTD (Ser2) (see **Figure 4.2.10D**). We observed that UPF1 KO cells had a reduction in phosphorylation at this residue compared to the matched WT conditions. In untreated conditions, UPF1 KO cells had significantly reduced levels of phospho-RNAPII CTD (Ser2) compared to the untreated WT cells. No clear reduction in total RNAPII was observed, though this was not quantified, suggesting that it was only a reduction of this modification that was affected by loss of UPF1.

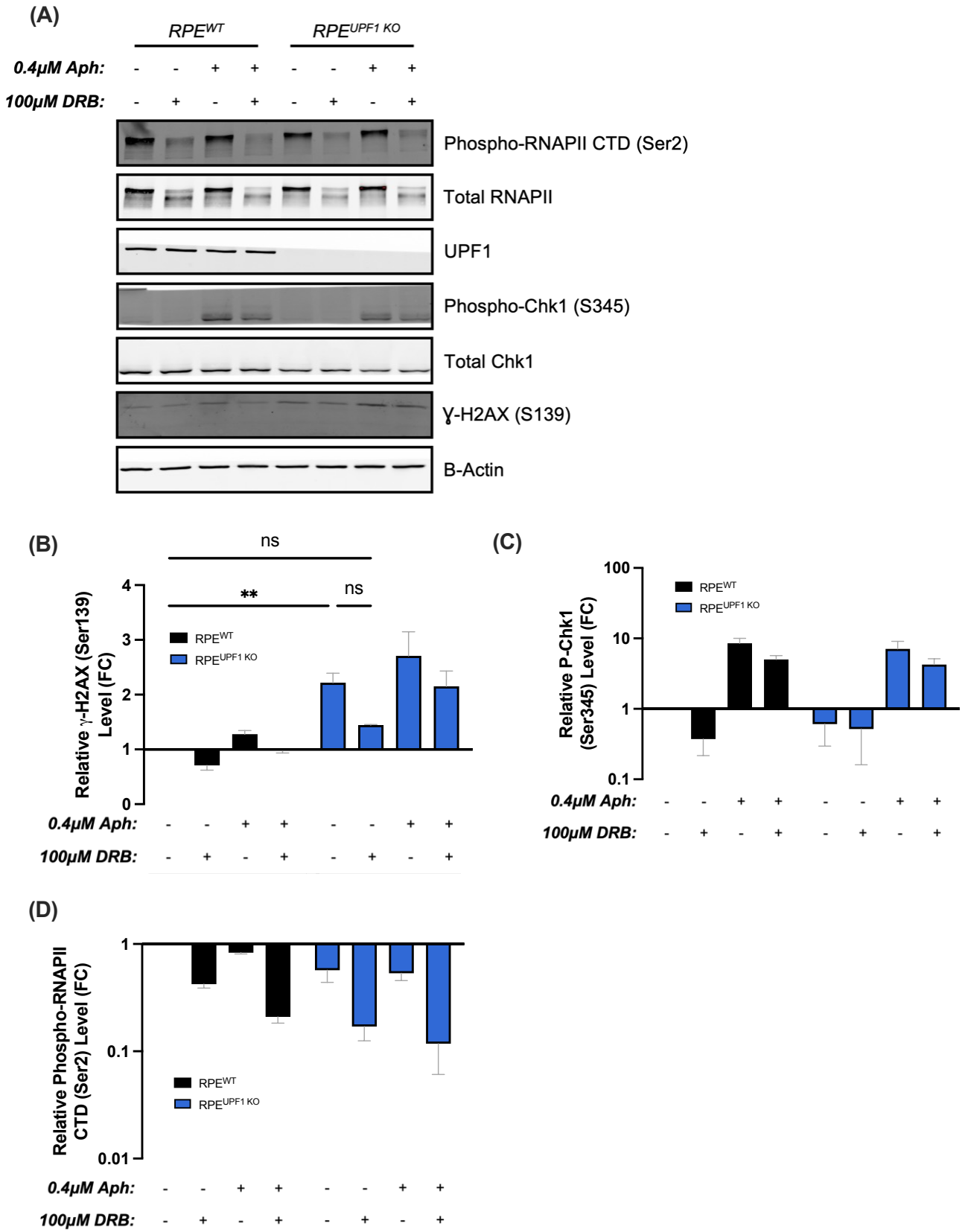


**Figure 4.2.10: Western blot analysis of *RPE<sup>WT</sup>* and *RPE<sup>UPF1 KO</sup>* cells in response to combination treatments of 0.4 $\mu$ M aphidicolin and 100 $\mu$ M DRB. Legend on page 138.**

**Figure 4.2.10: Western blot analysis of RPE<sup>WT</sup> and RPE<sup>UPF1 KO</sup> cells in response to combination treatments of 0.4 $\mu$ M aphidicolin and 100 $\mu$ M DRB.**

**(A)** Representative western blot for Phospho-RNAPII CTD (Ser2), Total RNAPII, UPF1, Phospho-Chk1 (Ser345), Total Chk1,  $\gamma$ -H2AX (Ser139) and  $\beta$ -actin in RPE<sup>WT</sup> and RPE<sup>UPF1 KO</sup> cells prior to treatment without or with 24hrs 0.4 $\mu$ M aphidicolin and 2hr 100 $\mu$ M DRB. **(B-D)** Quantification of  $\gamma$ -H2AX (Ser139), P-Chk1 (Ser345) or phospho-RNAPII CTD (Ser2) in response to treatments indicated, adjusted to  $\beta$ -actin levels to allow for loading variation and expressed as a fold-change of the untreated in RPE<sup>WT</sup> cells (N=3) Table of p-values from One-way ANOVA test with Dunnett's correction test for multiple comparisons (\*\* denotes  $p \leq 0.01$ , ns denotes  $p > 0.5$ ) for  $\gamma$ -H2AX (Ser139), phospho-Chk1 (Ser345) and phospho-RNAPII CTD (Ser2) in **Figure A16-18** respectively.

Together, these data show that UPF1-depletion induced DSBs are transcriptionally, but not DNA replication dependent. UPF1-depletion does appear to compromise RNAPII dynamics to some degree whilst not having any significant effect on global DNA replication stress signalling through Chk1.

#### **4.2.7 Transcriptional inhibition prevents the loss of sister fork symmetry in RPE<sup>UPF1 KO</sup> cells**

Since we have now shown that DSBs induced by loss of UPF1 can be rescued by transiently turning off transcription using DRB we hypothesised that the same was true for the replication fork stalling phenotype we have characterised. To assess this, we carried out the DNA fibre assay again, this time in the WT and UPF1 KO RPE lines and treated the cells with 0.4 $\mu$ M aphidicolin for 24hrs or 100 $\mu$ M DRB for 2hrs prior to CldU and IdU labelling. These DNA fibres were quantified in the same manner as previously described (see **Figure 4.2.8A**). The untreated WT RPE line had a high replication fork speed of  $\sim 1.5$ Kb/min, this was in comparison to the UPF1 KO cell line that had a significantly reduced fork speed of 1.0Kb/min as observed in our HeLa cell line following UPF1 depletion (see **Figure 4.2.11A**). Following treatment with 0.4 $\mu$ M aphidicolin both the WT and UPF1 KO cells exhibited a significantly reduced progression speed of  $\sim 0.7$ Kb/min compared to the untreated WT line. When treated with 100 $\mu$ M DRB the WT line showed a similar progressing fork speed to its matched untreated condition. However, the UPF1 KO cell line when treated with DRB showed

an increase in fork speed compared to the untreated UPF1 KO condition, similar to that of the untreated WT cells, though the effect was not statistically significant.

We then again assessed sister fork symmetry under the same conditions (see **Figure 4.2.11B**). As with the untreated HeLa line the untreated WT line shows a high degree of sister fork symmetry. The UPF1 KO cell line had significantly reduced symmetry in untreated conditions which phenocopies what was observed in the UPF1 depleted HeLa cell line. Following aphidicolin treatment, the WT line displayed a significant reduction in sister fork symmetry whilst the UPF1 KO line had an increase in symmetry that was statistically significant compared to the untreated UPF1 KO condition. Finally, treatment with DRB caused no significant change in the WT line, whilst promoting a statistically significant increase in sister fork symmetry in the UPF1 KO line compared to the untreated UPF1 KO condition.

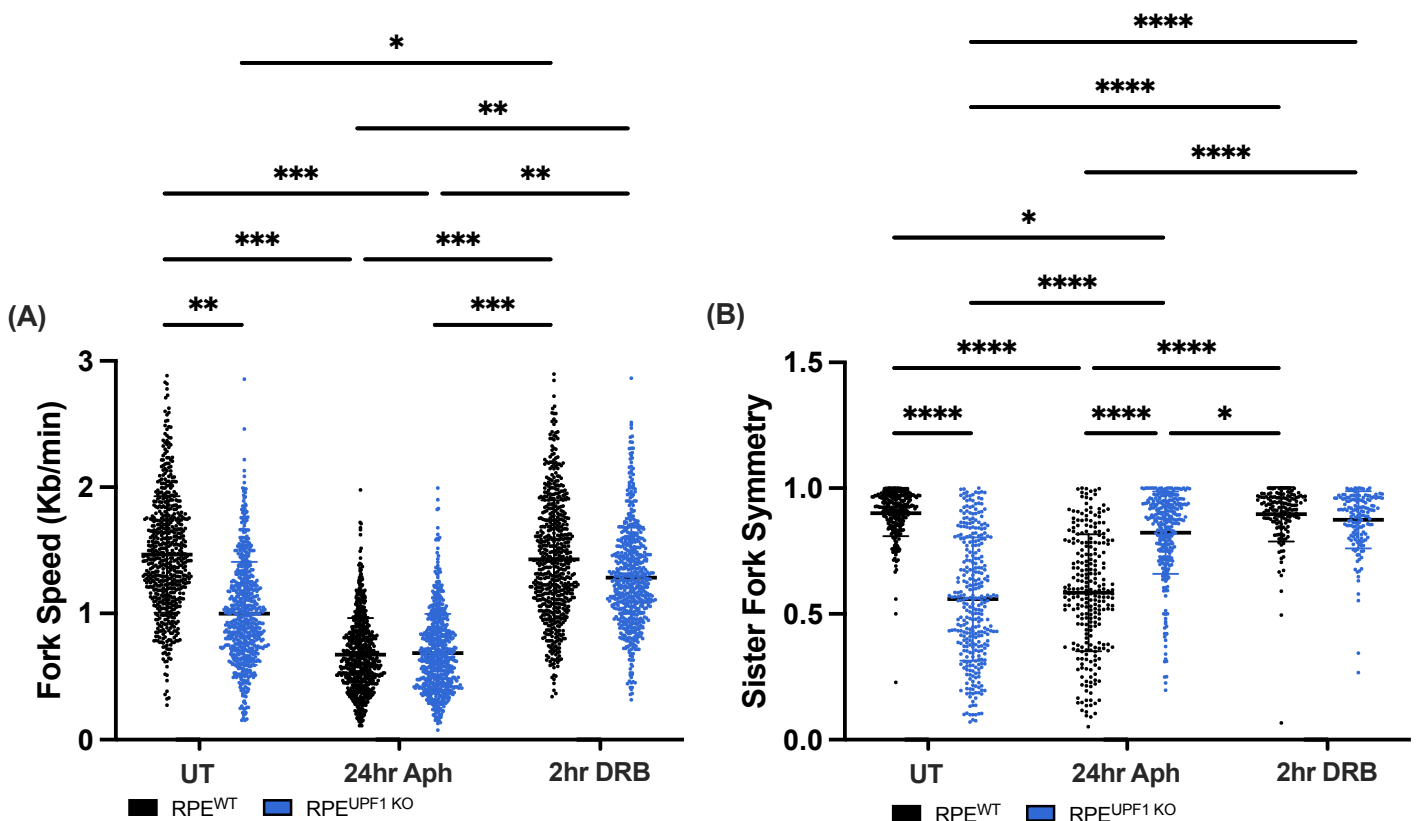


**Figure 4.2.11: DNA fibre analysis of RPE<sup>WT</sup> and RPE<sup>UPF1 KO</sup> cells untreated or treated with 0.4µM aphidicolin for 24hrs or 100µM DRB for 2hrs. Legend on next page.**

**Figure 4.2.11: DNA fibre analysis of RPE<sup>WT</sup> and RPE<sup>UPF1 KO</sup> cells untreated or treated with 0.4µM aphidicolin for 24hrs or 100µM DRB for 2hrs.**

**(A)** Quantification of progressing fork speeds. **(B)** Quantification of sister fork symmetry. Data points represent individual DNA fibres analysed, the black line and error bars represent the mean +/- SD (N=3). A minimum of 200 individual replication tracts were analysed per condition for fork speed analysis and 100 individual sister forks for symmetry analysis. For both a One-way ANOVA with Dunnett's correction test for multiple comparisons was performed on the mean of each biological replicate to determine statistical significance (\* denotes  $p \leq 0.05$ , \*\* denotes  $p \leq 0.01$ , \*\*\* denotes  $p \leq 0.001$ , \*\*\*\* denotes  $p \leq 0.0001$ ).

Together these experiments suggest that replication fork stalling that occurs following UPF1-deficiency relies on active transcription to occur. Given this phenotype and the role that UPF1 plays in mRNA metabolism it is possible that UPF1 deficiency gives rise to spontaneous transcription-replication collisions.

### **4.3 Discussion**

In this chapter we strived to uncover the mechanism by which UPF1 promotes the DNA-damage/ replication stress dependent mitotic delay identified in Chapter 3. In Chapter 3, we hypothesised that this phenotype could be due to a lack of ongoing DNA replication or repair during prometaphase, termed MiDAS. Indeed, we found that UPF1-deficient cells did not exhibit MiDAS following treatment with replication stress, induced by low-dose aphidicolin. Whilst investigating whether UPF1 has a key role in non-S-phase DNA replication we observed that cells lacking UPF1 have a DNA replication defect even during an unperturbed cell cycle. This defect leads to reduced replication fork progression, increased replication fork stalling and DNA damage. We found that replication fork stalling and DNA damage, induced by the absence of UPF1, was dependent on active transcription. This suggests that UPF1 could be vital in preventing spontaneous transcription-replication collisions from occurring.

Taken together we propose that in the absence of UPF1, a transcriptional barrier promotes DNA replication fork stalling, delays S-phase, preventing DNA under-replication in the presence of low-dose aphidicolin and the requirement for G2 DNA synthesis or MiDAS. This pathway could represent a mechanism whereby cancer cells

could show resistance to replication targeting chemotherapeutics that inflict DNA damage by interfering with the process of replication.

#### **4.3.1 Depletion of UPF1 in unperturbed conditions promotes DNA replication fork stalling and DNA damage**

We have shown that UPF1 depletion leads to a reduction in DNA replication fork progression, replication fork stalling and DNA damage in unperturbed conditions. These observations suggest that UPF1 is required to prevent the spontaneous emergence of replication stress.

Replication problems have been previously suggested following loss of UPF1. Azzalin and Lingner reported that shRNA-mediated depletion of UPF1 led to an accumulation of cells in early S-phase, defective replication and spontaneous DSBs in the absence of UPF1 that was dependent on ATR (Azzalin and Lingner, 2006). They proposed that UPF1 was required for S-phase progression and that due to an interaction with Pol $\delta$ , UPF1 was directly required for DNA replication or repair. However, the observation of an early S-phase arrest was not replicated by numerous other groups, including ourselves (Turton, 2014; Ngo, Grimstead and Baird, 2021). The same group also suggested that UPF1 is required to directly maintain leading-strand DNA replication at telomeres in HeLa cells, through an association with telomerase and TPP1 (Azzalin *et al.*, 2007; Chawla *et al.*, 2011). However, no direct quantification of telomeric replication was carried out by this group, these conclusions were drawn on the noted loss of telomeres in the absence of UPF1 and a proposed interaction observed between UPF1 and the regulatory subunit of Pol $\delta$  (Carastro *et al.*, 2002; Azzalin and Lingner, 2006; Turton, 2014). An alternative cause of telomeric loss could be due to a defect in DSB repair at sub-telomeric repeats following loss of UPF1 (Ngo, Grimstead and Baird, 2021). Whilst we show that loss of UPF1 appears to promote DNA replication fork stalling, rather than a direct reduction in DNA synthesis rates, a non-significant but modest reduction in fork progression is still observed even following rescue with DRB, in the UPF1 KO line compared to the WT untreated condition. This could be suggestive of a small replication issue persisting even following rescue of fork stalling with transcriptional inhibition though further work into this would be required.

UPF1 has also been linked to DNA replication through mRNA decay pathways. One such pathway is replication-dependent histone-mediated decay (HMD), which is an essential pathway responsible for degrading histone mRNA at the end of S-phase or in response to replication stress (Kaygun and Marzluff, 2005; Müller *et al.*, 2007; Sullivan *et al.*, 2009; Choe, Ahn and Kim, 2014). Depletion of FLASH or SLBP, required for the expression of and stability of histone mRNAs respectively, results in reduced replication fork speeds (Mejlvang *et al.*, 2014). It is conceivable that if dysregulation of histone mRNA was a result of UPF1 depletion, under our conditions, that DNA synthesis would be affected globally. This most likely would present as symmetric reductions in fork progression, which we did not observe. However, histone over abundance could also lead to non-specific binding of histones to DNA, interfering with DNA replication or transcriptional processes, promoting replication fork stalling (Singh, Paik and Gunjan, 2011). Long term loss of histone mRNA through SLBP depletion results in genomic stability as evidenced by spontaneous  $\gamma$ -H2AX, 48hrs after transfection (Mejlvang *et al.*, 2014).

Whilst UPF1 is involved in the regulation of histone levels, its role is in the timely degradation of histone mRNA through an interaction with SLBP. UPF1's depletion during S-phase would not result in a decrease or increase in histone levels, since its function is to degrade histone mRNA only at the end of S-phase or following DNA replication stress. Additionally, following our DRB rescue experiments, DRB treatment and the subsequent inhibition to transcriptional elongation would in theory reduce histone mRNA and protein levels. This would result in a further reduction in DNA replication rates due to reduced production of histone mRNA, however we observed an increase in DNA replication speeds following loss of UPF1, suggesting that the phenotypes being studied here are likely independent of UPF1's role in the maintenance of histone levels.

#### **4.3.2 Replication stress induced by loss of UPF1 is transcription-dependent and suggests UPF1-deficiency promotes transcriptional defects that inflict DNA replication stress**

We have observed that DNA replication fork stalling following the depletion of UPF1 could be rescued by DNA replication or transcriptional inhibition. Interestingly, we also observed that DSBs induced by the depletion of UPF1 could also be rescued by short term DRB treatment, whilst aphidicolin increased the appearance of DSBs likely due to increased levels of stalled and collapsed replication forks. Transcription-induced DNA damage following WRNIP1 depletion is consistent with this pattern of DNA damage and aphidicolin and transcription inhibition (Valenzisi *et al.*, 2024). Transcription-dependent DSBs, as observed following UPF1 depletion, have also been proposed as a consequence of SSBs arising from the trapped Top1 cleavage complexes in combination with the accumulation of SSBs on the displaced ssDNA of an R-loop (Sollier *et al.*, 2014). This phenotype is particularly detrimental in non-replicating cells, due to HR deficiency (Cristini, Gromak and Sordet, 2020). UPF1, through regulation of R-loop structures could affect the formation of these transcription-dependent DSBs, which directly impede DNA replication in cycling cells. Alternatively, the ability for this replication fork stalling and induction of DSBs to be rescued by turning off transcription suggests that UPF1 depletion could be leading to spontaneous transcription-replication collisions. UPF1-associated factors UPF2 and SMG1 modulating factors SMG8:SMG9 have been demonstrated to prevent spontaneous replication fork stalling and promote deleterious consequences such as TRCs, following treatment with an ATR inhibitor in a similar manner (Llorca-Cardenosa *et al.*, 2022; O'Leary *et al.*, 2022). This provides a potential basis whereby UPF1-associated factors can modulate DNA replication and promote replication fork stalling. The precise mechanism by which UPF1-associated factors have this affect is unknown.

Transcription can be a direct barrier to replication but can also promote numerous indirect replication barriers including increased torsional stress and secondary DNA structure formation, such as hairpins, triplexes, G-quadruplexes and DNA-RNA hybrids (Huertas and Andrés Aguilera, 2003; Paulsen *et al.*, 2009; Saponaro *et al.*, 2014; Rojas *et al.*, 2024). UPF1 could induce a direct transcription block, as a result of stalled or tethered RNAPII complexes that block DNA replication. In support of this,

UPF1 has been shown to associate with transcriptionally active genes independently of RNAPII (Singh *et al.*, 2019; De *et al.*, 2022), suggesting it plays a role in coordinating the transcriptional process through the association with nascent RNA. Loss of this function in UPF1-deficient *Schizosachharomyces pombe* results in an increase in RNAPII occupancy in the gene body or proximal to the transcription end site, at a subset of genes, suggesting transcriptional stalling or a defect in transcriptional termination (De *et al.*, 2022). Whether this is a conserved phenotype in eukaryotic cells has yet to be demonstrated. One hypothesis is that UPF1 interferes with DNA replication through the stabilisation of DNA-RNA hybrid structures that form *in cis* or *in trans* from nascent mRNAs. Such roles of UPF1 have been suggested at telomeric regions where UPF1 facilitates the removal and degradation of nascent rehybridized TERRA, which can promote DNA replication stalling and genomic instability (Azzalin *et al.*, 2007; Chawla *et al.*, 2011; Turton, 2014; Silva *et al.*, 2021). Whilst TERRA transcription is usually suppressed in S-phase to prevent this from occurring, a failure to remove TERRA that has been transcribed in the previous G1 phase can act as a DNA replication barrier (Porro *et al.*, 2010). It could be possible that this is a more global role of UPF1 in the release of nascent mRNAs, as observed in *Drosophila* (Singh *et al.*, 2019). In reality these two processes are not distinct. Since R-loops are a barrier to RNAPII elongation, as well as leading and lagging strand synthesis directly. In fact the indirect stalling of RNAPII at an R-loop has been demonstrated to pose a larger threat and require leading strand restart downstream of a stalled RNAPII complex in bacteria (Brüning and Marians, 2020, 2021). Interestingly sites which are known to be prone to TRCs encompass the same class of CFSs which are known to exhibit MiDAS.

#### **4.3.3 Loss of UPF1 reduces MiDAS frequency under conditions of mild replicative stress**

MiDAS is known to be driven by replication fork stalling in late S-phase at CFSs. Due to the sparsity of active and dormant replication origins, hard-to-replicate repetitive sequences and replication in late S-phase, double replication fork stalling in these regions frequently leads to the emergence of under-replicated DNA (UR-DNA) (see **Figure 1.1.3**) (Le Beau *et al.*, 1998; Hellman *et al.*, 2000; Letessier *et al.*, 2011; Sugimoto *et al.*, 2018; Macheret *et al.*, 2020). Unlike DSBs, which promote checkpoint

activation, UR-DNA can avoid G2 checkpoints, exit S-phase and then is replicated by either G2 DNA replication runover or in prophase by MiDAS (Minocherhomji *et al.*, 2015; Bhowmick *et al.*, 2022; Mocanu *et al.*, 2022).

We have demonstrated that UPF1 depletion results in a reduction in both restart-dependent MiDAS but also a reduction in G2 DNA replication runover when cells are inflicted with mild replication stress (Minocherhomji *et al.*, 2015; Mocanu *et al.*, 2022). UPF1 could be directly involved in DNA replication outside of S-phase, both in G2 and prometaphase, in the resolution of secondary DNA structures prior to restart, or the direct synthesis of DNA. UPF1 has been demonstrated to interact with the p66 regulatory subunit of Pol $\delta$  (Carastro *et al.*, 2002; Azzalin and Lingner, 2006; Turton, 2014), as such it is possible that UPF1 could be present at Pol $\delta$ -dependent replication in mitosis, or be important in directing Pol $\delta$  to sites of MiDAS (Wu *et al.*, 2023). Overexpression of the R-loop resolving enzyme RNaseH1 has been shown to prevent MiDAS occurrence, suggesting a link between the two either in S-phase or directly in mitosis (W. Wu *et al.*, 2020; Bhowmick *et al.*, 2022; Groelly *et al.*, 2022). UPF1 has also been shown to be involved in the homeostasis of R-loop structures (Cristini *et al.*, 2018; Wang *et al.*, 2018; Ngo, Grimstead and Baird, 2021). In agreement with this role, the UPF1-like helicase SETX has been demonstrated to be required to prevent spontaneous MiDAS in a R-loop dependent manner, whilst RTEL1 has been shown to be required for the process of MiDAS (W. Wu *et al.*, 2020; Said *et al.*, 2022; Rao *et al.*, 2024). Whilst we do observe an increase in spontaneous replication fork stalling in unperturbed conditions, we do not observe spontaneous MiDAS. It is possible that since UPF1-deficiency most likely results in a transcription-dependent DNA replication barrier, possibly due to an accumulation of R-loops, that this is insufficient to result in double replication fork stalling events, required for promoting MiDAS at CFSs (see **Figure 4.3.1**). UPF1 may also only promote replication fork stalling in regions of the genome that have sufficient dormant replication origins that can be fired to prevent the emergence of UR-DNA.

Transcription has been shown to directly affect DNA replication dynamics at CFSs including, initiation, fork progression and replication timing (Blin *et al.*, 2018). TRCs have also been directly linked to promoting MiDAS at early replicating transcribed loci

(Bhowmick *et al.*, 2022). An alternative mitotic DNA replication phenotype, distinct from MiDAS, has also been demonstrated to occur at transcription start sites in unperturbed conditions, termed G-MIDS (Wang *et al.*, 2021). Since we have observed that UPF1-depletion appears to reduce replication fork stalling in S-phase, in the presence of aphidicolin, it is possible that it is due to this, that we also no longer observe MiDAS.

#### **4.3.4 UPF1 depletion could reduce UR-DNA persisting outside of S-phase, removing a requirement for MiDAS and G2 DNA replication runover**

Both MiDAS and G2 DNA replication runover exist as pathways that deal with UR-DNA as a consequence of late replicating fork stalling, persisting through late S-phase, driving a necessity for DNA replication in G2 and mitosis (Minocherhomji *et al.*, 2015; Mocanu *et al.*, 2022). Since UPF1 depletion reduces the incidence of replication fork stalling in S-phase under conditions of mild replication stress, it is possible that this leads to a reduction of UR-DNA after S-phase, since it is due to double stalled replication forks specifically that drive the emergence of UR-DNA (Sonneville *et al.*, 2019). Consistent with this hypothesis, UPF1 depletion, though reducing the frequency of MiDAS, did not lead to an accumulation of UR-DNA in the subsequent G1, as marked by 53BP1 nuclear bodies in our individual repeat. Every other described MiDAS factor has been demonstrated to result in increased 53BP1 nuclear bodies in the subsequent G1 (Lukas *et al.*, 2011; Naim *et al.*, 2013; Ying *et al.*, 2013; Minocherhomji *et al.*, 2015; Pedersen *et al.*, 2015; Wu *et al.*, 2023). We also observed a reduction in G1 DNA synthesis in UPF1-deficient cells under conditions of replication stress, suggesting a reduction in post-mitotic DNA damage repair as well. In yeast, DNA replication in G1 has been shown to promote DNA over-replication, chromosomal breaks and an accumulation of ssDNA (Reuswig *et al.*, 2022). This supports the hypothesis that UPF1-depletion reduces UR-DNA in G2 and prometaphase under mild replication stress, rather than a direct defect in the process of MiDAS, though of course the 53BP1 assay needs to be replicated to draw firm conclusions on this matter. Indeed, transcription and TRCs in S-phase are a well-known driver of MiDAS (Groelly *et al.*, 2022; Said *et al.*, 2022) and G-MIDS (Wang *et al.*, 2021). So, it is conceivable that reducing DNA replication fork stalling, as observed under mild replicative stress

following UPF1 depletion, could result in a reduction in UR-DNA and therefore a reduced necessity for MiDAS.

An alternative reasoning for an observed reduction in UR-DNA, following UPF1 depletion, could be due to the dysregulation of replication-dependent histone RNA levels. UPF1 is required to promote histone mRNA decay following DNA replication stress or at the end of S-phase, therefore the loss of UPF1 could lead to continued DNA synthesis due to a maintained histone supply (Kaygun and Marzluff, 2005). Whilst the loss of histone synthesis is well known to impair DNA replication processes (Paul *et al.*, 2016; Strobino *et al.*, 2020), histone protein overexpression or expression outside of S-phase results in degradation by the proteasome, a failure to degrade excess histones promotes chromosome aggregation or loss and cellular toxicity (Singh *et al.*, 2009; Mei *et al.*, 2017). Overexpression of replication-dependent histone mRNAs has been shown to affect the sensitivity of tumour cells to replication-targeting chemotherapeutics (Jin *et al.*, 2023), suggesting it could confer an advantage to cells following replicative stress. Whether histone supply is sufficient to maintain DNA replication in the presence of replication stress is not described. Since numerous local and global mechanisms of DNA replication inhibition are mediated by the ATR-Chk1 axis (Ahmed-Seghir *et al.*, 2023), it is unlikely that histone overexpression alone could reinitiate DNA synthesis. In addition to this, uncontrolled histone overexpression as suggested here, would not prevent replication fork stalling from occurring, as we observe here. Outside of S-phase, histone transcription is drastically reduced (DeLisle *et al.*, 1983), suggesting a further potential inability to maintain DNA replication rates. Degradation of SLBP, required for recruitment of UPF1 to histone mRNAs, occurs at the end of S-phase which would mean UPF1 recruitment to histone mRNAs could not occur, as well as impairing histone RNA processing and therefore translation (Whitfield *et al.*, 2000; Zheng *et al.*, 2003; Koseoglu, Dong and Marzluff, 2010). Under these circumstances, histone decay is likely no longer dependent on UPF1. Histone decay also occurs at the end of S-phase, irrespective of the degradation of SLBP (Zheng *et al.*, 2003), further suggesting potential backup mechanisms to promptly shut-down histone biogenesis, independent of UPF1. Further work into examining histone dynamics following loss of UPF1 is required to firmly conclude an independence of this pathway being responsible for the replication fork stalling observed.

In this chapter, we have demonstrated a novel role of UPF1 in preventing transcription-dependent DNA replication fork stalling and DNA damage in unperturbed conditions. Endogenous transcription-dependent replication fork stalling in the absence of UPF1 reduces replication stress phenotypes, such as MiDAS and mitotic delay, following mild replication stress due to a hypothesised reduced frequency of TRCs. This effect of UPF1 depletion on both cancerous and non-cancerous human cells represents a novel mechanism whereby UPF1-deficiency could confer treatment resistance to DNA replication stress inducing chemotherapeutics.

#### **4.3.5 Limitations**

The DNA Fibre assay is a well-known experimental technique for the global analysis of DNA replication dynamics, however lack of spatial information in restricts interpretation of such experiments. Whilst it can be used in combination with fluorescent in-situ hybridisation (FISH) to monitor DNA replication at specific chromosomal loci, such experiments are very time consuming. Other methods of analysing DNA replication which do provide spatial information such as BrdU-seq, would allow us to determine whether UPF1 was promoting DNA replication fork stalling at specific regions of the genome, by overlaying BrdU-seq profiles with known genomic information such as CFS locations, transcriptional start or termination sites or other genomic regions (Rojas *et al.*, 2024).

Having optimised the drugging schedule of DRB and demonstrated a significant reduction in phosphorylation of RNAPII-CTD (Ser2) it is confirmed that transcription elongations has indeed been inhibited. However, the exact affect that this is having on RNAPII is not shown. It is known that this reduces ongoing transcription elongation, as indicated by a reduction in RNAPII-CTD Ser2 phosphorylation, a key phosphorylation event required for productive transcription elongation. Demonstrating that treatment of this drug does indeed result in a reduction in RNA synthesis and RNAPII occupation on chromatin can be demonstrated. 5-EU incubations which, similar to BrdU assays allow for the detection and quantification of incorporated 5-EU in nascent RNA, allowing for a measurement of global RNA synthesis levels. Furthermore, immunofluorescence of chromatin-bound RNAPII would allow us to

determine whether RNAPII is also being removed from chromatin or remaining stalled on template DNA.

It is important to mention that we faced issues during the analysis of G2 replication turnover in the HeLa cell line. Mocanu *et al.* carried out their assay using quantitative immunofluorescence-based cytometry (QIBC), this relied on them imaging over 1000 cells per condition (Mocanu *et al.*, 2022). We were not able to carry out the same approach and therefore have a much smaller number of quantified cells. In addition to this, the size of the HeLa cells and the lack of abundance of G2 cells following treatment, obtaining 50 cells per condition was not possible. We could have purposely looked for G2 cells by utilising phospho-histone H3 (Ser10) staining but also wanted to obtain an asynchronous population of cells for our analysis. This problem potentially has made the quantification of our G2 population for the HeLa experiments unreliable. It is important to mention however that the same problem was not encountered when using the much smaller RPE-1 cell line, that allowed for the imaging of a far greater number of cells, which also had a greater abundance of G2 cells. This makes the RPE data much more reliable for the quantification of G2 cells only, since we were able to quantify an abundance of S-phase and G1 cells in the HeLa cell line.

# Chapter 5: Attempt to Quantify R-Loop Levels by Immunofluorescence

## 5.1 Introduction

We have shown that UPF1 is required to promote a DNA damage induced mitotic delay. This delay we have also shown can be resolved by overexpression of the R-loop resolving enzyme RNase H1 or through transcriptional inhibition with  $\alpha$ -amanitin. This data could suggest that the delay observed in mitosis is due to an increase in R-loop levels following DNA damage that through some mechanism increases mitotic length duration. We have also shown that UPF1 depletion appears to promote replication stress and DNA replication fork stalling. This phenotype also appears to be dependent on active transcription as can be resolved by short-term treatment with the CDK9 inhibitor DRB, which prevents RNAPII-mediated transcriptional elongation. This could suggest UPF1 has a role in the prevention of TRCs by regulating transcription. UPF1 could prevent replication fork stalling by the dissociation of nascent mRNAs that rehybridize with their transcribed loci as DNA-RNA hybrids *in cis*, promoting the formation of R-loop structures (Azzalin *et al.*, 2007; Singh *et al.*, 2019).

R-loops are key inducers of replication stress during S-phase, and key drivers of mitotic DNA replication through MiDAS (Groelly *et al.*, 2022; Said *et al.*, 2022). R-loops have also been shown to regulate mitotic timing, specifically RPA-coated centromeric R-loops have been suggested to act as a binding platform for ATR, which stimulates Aurora B activity, preventing the mis-segregation of chromosomes, extending mitotic duration (Kabeche *et al.*, 2018). Centromeres are a hot spot of R-loop formation due to their highly repetitive nature and high levels of transcription by RNAPII which drives R-loop formation *in cis* (McNulty, Sullivan and Sullivan, 2017). These R-loops seem vital in maintaining centromere identity by promoting recruitment of numerous centromeric proteins including CENP-A (McNulty, Sullivan and Sullivan, 2017). BRCA1 has also been demonstrated to associate with R-loops at centromeres and loss of BRCA1 results in impaired CENP-A localisation (Racca *et al.*, 2021). Loss of

CENP-A in S-Phase has also been shown to result in the accumulation of R-loops, impeding replication fork progression (Giunta *et al.*, 2021). This promotes recombination at alpha-satellite repeats, unfinished replication and anaphase bridges in the subsequent mitosis. Together these data suggest R-loops must be kept in a fine balance to maintain centromeric identity, but also allow for correct response in mitosis to replication stress and DNA damage. In addition to this UPF1 has also been shown to be localised at DNA-RNA hybrids and having a role in the regulation of the abundance of R-loop structures across the genome (Cristini *et al.*, 2018; Wang *et al.*, 2018). However, conflicting data exists regarding whether UPF1 be responsible for the formation or the resolution of such structures (Ngo, Grimstead and Baird, 2021).

For this reason, in this chapter we attempt to quantify changes in R-loop structures following UPF1 depletion in conditions of replication stress in interphase and mitotic cells.

The aim of this chapter is to do the following:

1. Examine changes in R-loop abundance following depletion of UPF1 in unperturbed and DNA replication stress or damage conditions

The hypothesis of this chapter is:

UPF1 affects R-loop abundance across the genome.

## **5.2 Results**

### **5.2.1 Interphase S9.6**

Initially we attempted to assess a global change in R-loop abundance under our experimental conditions by utilising the monoclonal antibody S9.6 antibody. S9.6 binds to several dsRNA species including dsDNA-RNA structures that exist within R-loops. For this reason, it is used routinely to measure changes in R-loops both through immunofluorescence, DNA-RNA immunoprecipitation sequencing (DRIPseq) and dot blots. For our studies we attempted to carry out S9.6 immunofluorescence, since we also wanted to investigate whether we could detect UPF1 present at R-loop sites,

under conditions of DNA damage or replication stress. As mentioned, S9.6 recognises several dsRNA species but not solely R-loops, for this reason a negative control must be used that resolves only R-loops to demonstrate that changes in S9.6 signals are indeed R-loop specific. For this, the endonuclease RNaseH1 that specifically degrades RNA in DNA-RNA hybrids is used. Depletion of the R-loop resolving helicase SETX has also been used as a positive control in several studies. RNaseH1 can be used either by directly treating cells or DNA with purified RNaseH1 or through the plasmid-induced expression of exogenous RNaseH1 in live cells. Both methods have their pros and cons, for our studies we utilised a plasmid vector that overexpresses a V5-RNaseH1<sup>WT</sup>.

In conditions treated with RNaseH1 we expect to see a global reduction in S9.6 signal intensities, due to R-loop resolution. In our initial tests of the plasmid by immunofluorescence we detected that S9.6 nuclear intensity would reduce with increasing amounts of plasmid (see **Figure 5.2.1**). This data does demonstrate a dose dependent reduction in S9.6 staining following RNaseH1 transfection, it also shows that depletion of UPF1 results also in a reduction in S9.6 intensity, indicating UPF1 could promote R-loop formation in unperturbed conditions. However, closer inspection of the staining reveals largely cytoplasmic S9.6 signal with poor nuclear staining. It is also worth mentioning, that changes observed in S9.6 staining with increasing amounts of plasmid were not specific to the nucleus, as we observed an overall reduction in S9.6 staining in the cytoplasm as well. This would not be expected with treatment of RNaseH1. For this initial staining we used PFA as a fixative since this was our standard IF protocol. Literature suggests that methanol is a better fixative for S9.6 due to its less stable nature in comparison to proteins.

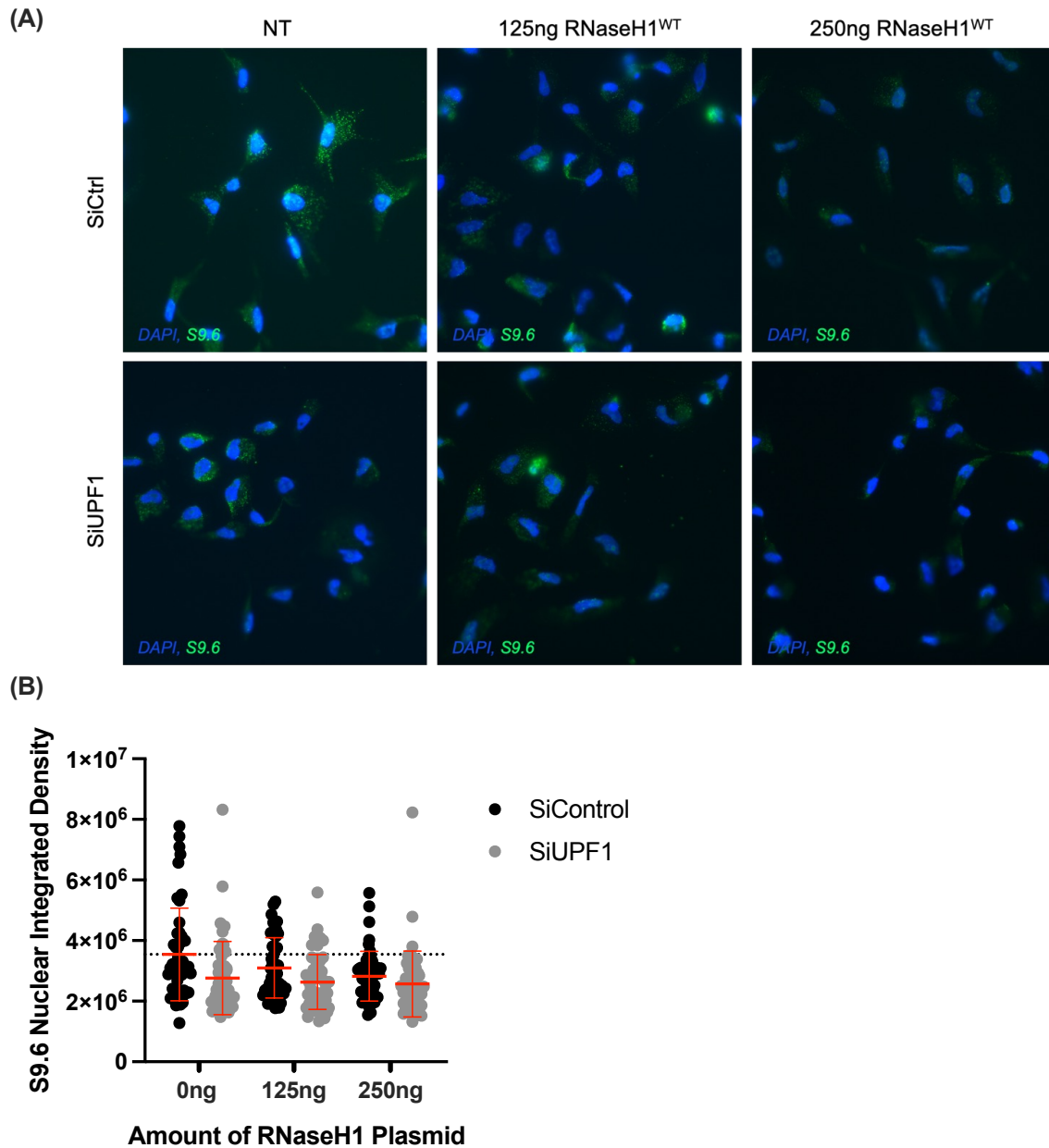


**Figure 5.2.1: Optimisation and validation of RNaseH1 plasmid by immunofluorescence staining for S9.6 in HeLa cells.**

(A) Representative immunofluorescence of HeLa cells transfected with non-targeting SiCtrl or SiUPF1 in combination with increasing amounts of RNaseH1 plasmid, stained for S9.6 and DAPI. (B) Quantification of nuclear S9.6 integrated density. (N=1)

Following this poor staining, we attempted to use a S9.6 staining protocol specifically to try and improve the nuclear signal. However, under the conditions we tested with this new staining protocol we actually observed that RNaseH1 appeared to lead to an increase in S9.6 intensity. This staining also formed no specific foci and was a general

pan-nuclear staining for S9.6 so provided little localisation information (Data not shown).

Nucleolar S9.6 Staining represents rRNA (Smolka *et al.*, 2021). Nucleolar staining is dramatically reduced in S9.6 staining of HeLa cells following siRNA-mediated depletion of UPF1. To attempt to address this we stained for S9.6 in combination with nucleolin to allow for the removal of nucleolar regions from our nuclear masks so we were not quantifying S9.6 foci corresponding to rRNA. Whilst this allowed for the removal of nucleolar staining, we found that due to the relatively high intensity of the nucleoli that it was difficult to visualise the much darker foci that were present in the nucleus. We were able to detect small foci within the nucleus, consistent with the published protocol's staining, however when we came to quantify these, the data was inconsistent with known positive and negative controls which we had included. Importantly, we found that RNaseH1 had little to no effect on S9.6 foci again rendering the data on R-loops unusable. Whilst the staining was indeed improving, we had to move on from these assays and attempt to quantify R-loops in a different manner.

### **5.2.2 Metaphase spreads S9.6**

Having attempted to quantify interphase levels of R-loops through immunostaining of the S9.6 antibody we then turned to metaphase spreads as a potential solution. Since we had been investigating mitotic timing durations, we decided that measuring specifically centromeric R-loops could be an alternative method for assaying the effect that UPF1 was having. It had been shown that R-loops were indeed a key regulatory mechanism at the centromere which regulated cellular timing (Kabeche *et al.*, 2018). For these experiments we utilised the protocol published in Kabeche *et.al.* for the immunostaining of S9.6 on metaphase spreads. Unfortunately, due to time constraints I was unable to optimise the protocol for use with our cell line to reliably produce metaphase spreads that could be used for this analysis.

### **5.2.3 Interphase D210N RNaseH1**

Since we were unable to reliably quantify R-loop levels using the S9.6 antibody we attempted to quantify them using another method. As mentioned, RNaseH1 is routinely used to resolve R-loops as it binds to and degrades RNA specifically present

in DNA-RNA hybrids. For this reason, a mutant RNaseH1<sup>D210N</sup>, specifically a tagged version of RNaseH1 that has no catalytic activity, can be used to measure R-loop abundance and localisation. Since this mutant has no catalytic activity, it binds to RNA present in R-loops but is unable to degrade it resulting in the trapping of the molecule at the R-loop site. This technique has been used for DRIPseq and immunofluorescence, removes non-specific binding that creates problems using S9.6 based approaches and does not require additional RNaseH1 conditions as negative controls.

For these experiments HeLa cells were double-transfected with non-targeting or targeted UPF1 siRNA in combination with a plasmid encoding a V5-tagged RNaseH1<sup>D210N</sup>. Since the plasmid overexpresses RNaseH1 to a significant degree, cells must be pre-extracted prior to fixation to allow for the large soluble fraction of RNaseH1 to be washed out of the nucleus, leaving behind only chromatin-bound RNaseH1. This chromatin-bound fraction can then be detected using anti-V5 antibodies which recognise the small N-terminal tag present on the exogenous RNaseH1 only. Since we are using exogenous RNaseH1 as a reporter system for measuring R-loop abundance it is vital that the reporter is expressed to a similar degree in all conditions tested. To test this, a western blot was carried out on HeLa cells double transfected with non-targeting and UPF1-targeting siRNA in combination with 125ng plasmid encoding V5-RNaseH1<sup>D210N</sup> (see **Figure 5.2.2**). Using a V5 antibody to assess exogenous RNaseH1<sup>D210N</sup> induced expression, we observed that in SiCtrl conditions RNaseH1 was expressed to a significant degree and equally in all three treated conditions. SiUPF1 did indeed result in a reduction in UPF1 protein levels, but we also observed a significant reduction in V5-RNaseH1 levels compared to the SiCtrl condition. This posed an issue with any quantification of RNaseH1<sup>D210N</sup> foci as a reliable measure of R-loop levels. To try and address these problems we wanted to investigate whether the problem could be due to either changes in transfection efficiency as a result of the siRNA or was a specific observation observed following siRNA-mediated depletion of UPF1. We carried out a western once again, assessing UPF1 levels and the level of induced RNaseH1 expression of both a WT and D210N plasmid in combination with SiCtrl, SiUPF1 and SiSOD1. We used two siRNAs against UPF1, one siUPF1 is an alternative siRNA used in studies previous to mine, whilst siUPF1-Res is the engineered siRNA used for my studies that the FLP-

IN lines are resistant against. We also used a SOD1 siRNA which is a siRNA used routinely by another member of our lab, the idea was to test if the phenotype was specific to UPF1 siRNA or just targeting siRNAs in general.

Again, we observed induction of RNaseH1 expression of both WT and D210N RNaseH1 in SiCtrl cells at 125ng of plasmid (see **Figure 5.2.2**). Using the alternative siRNA, we observed clear depletion of UPF1 and again a clear reduction in RNaseH1 levels compared to the SiCtrl conditions, interestingly a similar reduction was also observed following SOD1 siRNA transfection suggesting this could most likely be just a reduction in transfection efficiency. In confirmation of this, increased amounts of RNaseH1 plasmid in combination with SiUPF1-Res resulted in increased induction of expression of WT and D210N RNaseH1 to a similar level seen with SiCtrl. We therefore decided to use 500ng of RNaseH1<sup>D210N</sup> plasmid for transfections in combination with SiUPF1 as this appeared to express to a similar level.

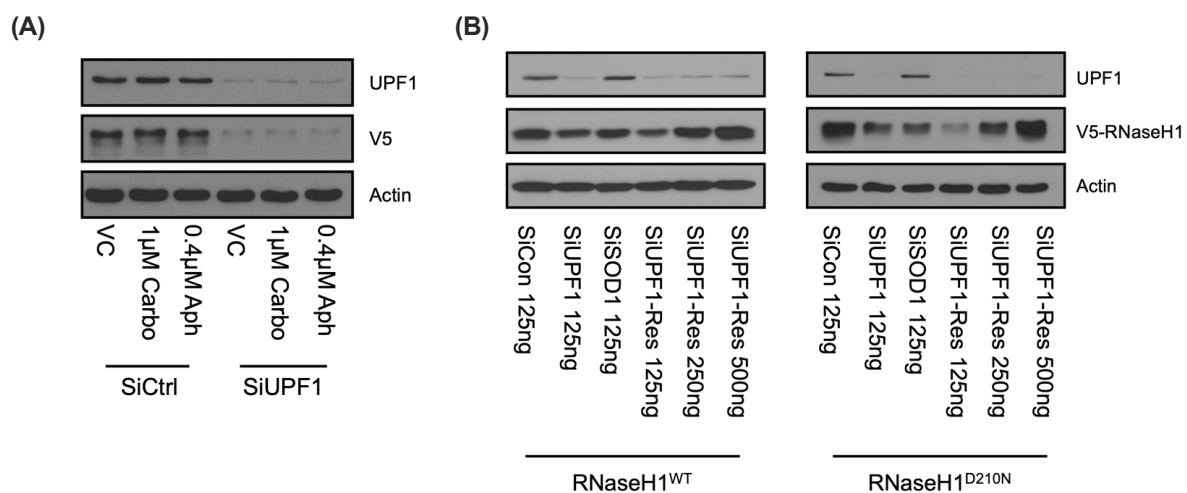


**Figure 5.2.2: Western blot of transfected V5-tagged RNaseH1<sup>D210N</sup> in SiCtrl and SiUPF1 treated HeLa cells**

**(A)** Representative western blot of HeLa cell lysates for UPF1, V5 and actin transfected with non-targeting SiCtrl or SiUPF1 in combination with plasmid encoding RNaseH1<sup>D210N</sup> following treatment with 1μM Carboplatin for 6 hrs or 0.4μM aphidicolin for 24hrs. (N=1) **(B)** Representative western blot of HeLa cell lysates for UPF1, V5 and actin transfected with non-targeting SiCtrl or targeting siUPF1, SiUPF1-Res or SiSOD1 with indicated amount of plasmid encoding RNaseH1<sup>WT</sup> or RNaseH1<sup>D210N</sup>. (N=1)

Since we were now able to induce the expression of our reporter RNaseH1<sup>D210N</sup> to a similar level in all of our conditions we therefore attempted to quantify R-loops by

immunofluorescence using this method (see **Figure 5.2.3A**). We stained for V5 and RPA32 which we hypothesised would be present at R-loop sites in combination with RNaseH1 since R-loops lead to the displacement of ssDNA due to the hybridisation of the other strand to an RNA molecule (see **Figure 5.2.3D**). We did observe some foci that appeared to colocalise though no formal quantification was made of this. Quantification of the number of individual RPA32 and V5 foci per nucleus were made (see **Figure 5.2.3B-C**). We observed relatively few V5 foci in untreated conditions, which appeared to increase following depletion of UPF1. Following treatment with 0.4 $\mu$ M aphidicolin for 24hrs we observed a large increase of V5 foci, consistent with an induction of replication stress and an accumulation of R-loops. However, no obvious change was seen following depletion of UPF1 in combination with replication stress. A similar pattern was observed for RPA32 foci. Few foci were observed in untreated conditions, siRNA-mediated depletion of UPF1 led to a small increase in observable foci. Following treatment with aphidicolin a large increase in RPA32 foci was observed consistent with induction of replication stress, with no obvious change following depletion of UPF1. Unfortunately, we were unable to replicate these results, as in subsequent repeats we observed large levels of background fluorescence that meant we could not reliably quantify the number of nuclear foci.

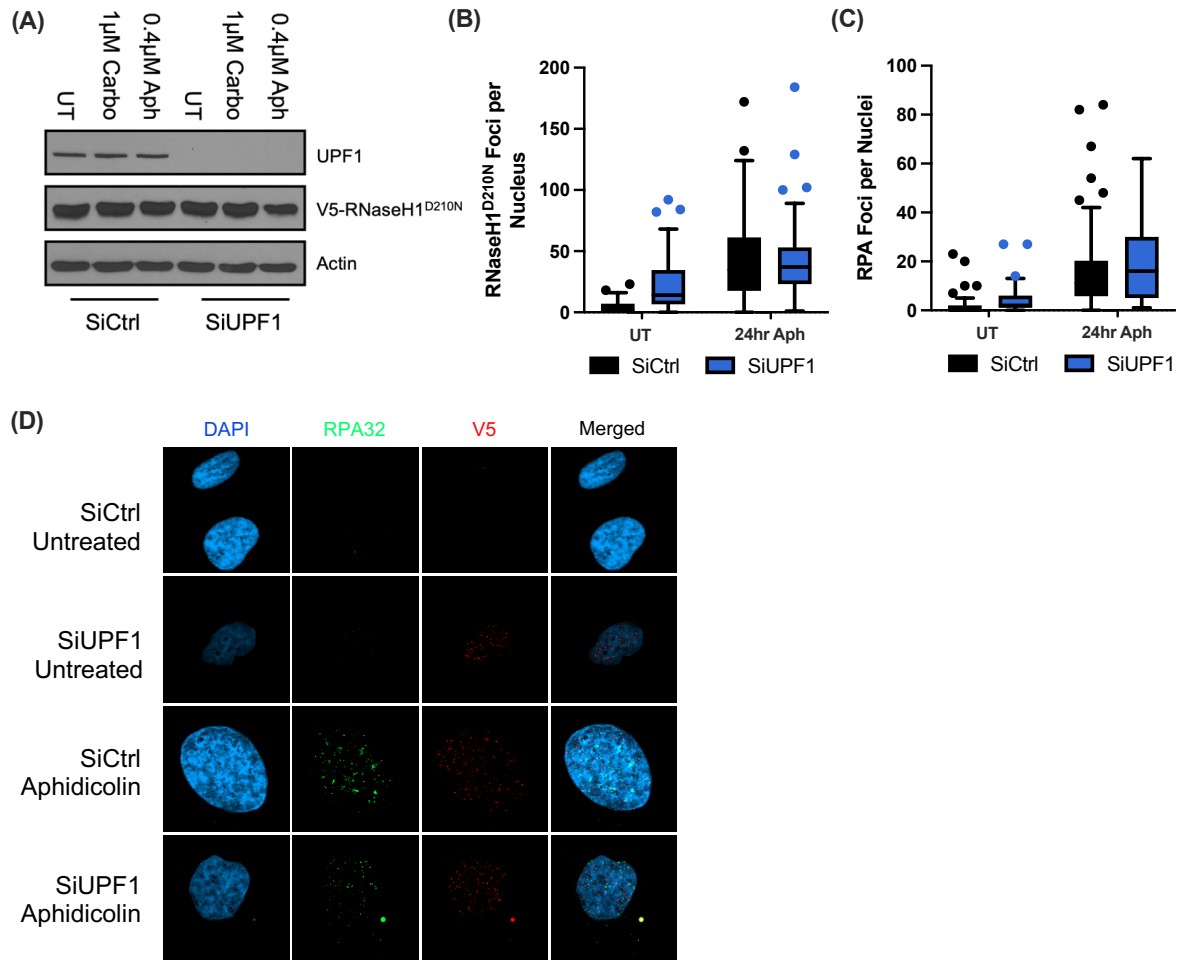


**Figure 5.2.3: Immunofluorescence microscopy for RPA and V5 in HeLa cells transfected with V5-tagged RNaseH1<sup>D210N</sup>.**

**(A)** Representative western blot for UPF1, V5 and Actin of lysates taken of HeLa cells transfected with RNaseH1<sup>D210N</sup> plasmid in combination with non-targeting siRNA and UPF1-targeting siRNAs treated with 1 μM carboplatin for 6hrs or 0.4 μM aphidicolin for 24hrs. **(B-C)** Quantification of V5 or RPA32 nuclear foci respectively. Data illustrated is a Tukey Plot. **(D)** Representative immunofluorescence images of HeLa cells stained for RPA32, V5 and DAPI. (N=1)

### 5.3 Discussion

In chapter 3 we showed that UPF1 is required for promoting a DNA damage or replication stress-dependent mitotic delay, that can be rescued by acute transcriptional inhibition or through overexpression of the R-loop resolving enzyme RNaseH1. We have further shown in chapter 4 that UPF1 depletion appears to result

in spontaneous replication fork stalling, that can be rescued by transcriptional inhibition in the same manner. Together these results suggest UPF1 as mediating a non-canonical function in promoting DNA damage-dependent mitotic delay and safeguarding DNA replication that could be dependent on R-loops.

For this reason, in this chapter, we attempted to quantify R-loop level changes, under the conditions tested in this thesis by immunofluorescence. We began by utilising the well described monoclonal S9.6 antibody that recognises DNA-RNA hybrid structures present in cells (Phillips *et al.*, 2013). This antibody has been used to identify R-loop changes by immunofluorescence, DNA:RNA immunoprecipitation-sequencing (DRIP-seq) and dot blots. The use of this antibody relies on the negative control RNaseH1, which either through induced overexpression or enzymatic degradation is used to degrade the RNA present in R-loops, resulting in their resolution. This control would show that S9.6 changes observed are indeed R-loop specific and not due to off-target effects of the antibody on other dsRNA species. Unfortunately, we were unable to reliably quantify changes in S9.6 in the controls, under the conditions tested in this thesis. Primarily, we observed that S9.6 staining was highly variable between technical repeats even when using different immunofluorescence protocols. In addition to this, RNaseH1 overexpression did not function correctly as a negative control. These observed effects could have been due to cells experiencing significant toxicity as a result of double transfection with the RNaseH1 coding plasmid. However, several studies have also reported problems with the ability of RNaseH1 expression to remove S9.6 specific signal (Smolka *et al.*, 2021). Alternatively, S9.6 staining may have required further optimisation for the cell lines being used.

Problems with the S9.6 antibody have been highlighted previously demonstrating significant off target effects of the antibody to other dsRNA species including primarily ribosomal-RNAs (rRNAs) (Hartono *et al.*, 2018; Smolka *et al.*, 2021). This is likely the main problem that we encountered using the S9.6 antibody, where we observed extremely high intensity staining for S9.6 in the nucleoli, which is due to the presence of rRNA (Smolka *et al.*, 2021). Not only is this staining off-target, but due to its intensity, this makes the imaging of other regions of the nucleus difficult without over saturating the image. We also observed significantly high levels of S9.6 staining in the cytoplasm. Whilst previously this has been suggested to be due to the presence of mitochondria

and associated R-loops, these structures demonstrate limited colocalization (Ginno *et al.*, 2012; Koo *et al.*, 2015; Smolka *et al.*, 2021). The cytoplasmic signalling is now attributed primarily to the presence of several RNA species. Typically in the literature cytoplasmic S9.6 staining is ignored since most studies utilising S9.6 are focused on nuclear changes, even though well-known regulators of R-loops such as SETX and BRCA2 demonstrate to have an effect on cytoplasmic S9.6 staining (Vanoosthuysse, 2018).

As we were unable to reliably measure R-loop changes using the S9.6 monoclonal antibody, we attempted to quantify R-loops utilising a catalytically inactive RNaseH1<sup>D210N</sup> mutant. This method of quantification has also been used previously for both immunofluorescence as well as chromatin immunoprecipitation-sequencing (ChIP-seq) to assess changes in R-loop dynamics across the genome (Ginno *et al.*, 2012; Legros *et al.*, 2014; L. Chen *et al.*, 2017; Mukhopadhyay *et al.*, 2024). It relies on the ability of an exogenously expressed tagged RNaseH1<sup>D210N</sup> to bind to, but not cleave an R-loop. Subsequent pulldown or antibody labelling can then be used to identify regions enriched for R-loop structures. This technique relies on the equal and specific transfection of the exogenous RNaseH1 mutant. It is also important that the RNaseH1 is not overexpressed to a significant degree that would result in a dominant-negative effect in stabilising R-loop structures.

### **5.3.1 UPF1 prevents spontaneous R-loop formation**

From this experiment we observed that UPF1 depletion alone led to a spontaneous increase in R-loop levels marked by RNaseH1<sup>D210N</sup> foci. We also observed that depletion of UPF1 appeared to reduce or have no effect on R-loop levels when combined with aphidicolin treatment. This data supports a role for UPF1 in preventing R-loop accumulation in unperturbed conditions, whilst having an opposite or no effect following DNA replicative stress. It is well known that mRNA processing factors are required for the prevention of spontaneous R-loop formation (Huertas and Andres Aguilera, 2003; Li and Manley, 2005; Mischo *et al.*, 2011; Pfeiffer *et al.*, 2013; Chakraborty, Huang and Hiom, 2018; Cohen *et al.*, 2018; Cristini *et al.*, 2018; Wood *et al.*, 2020), UPF1 is known to interact co-transcriptionally with RNA (Singh *et al.*, 2019; De *et al.*, 2022), this could therefore represent one such mechanism of limiting

nascent RNA rehybridization with template DNA, required for preventing R-loop formation. Alternatively, this result is consistent with UPF1 having a role in promoting the dissociation of R-loop-associated nascent RNAs across the genome and specifically in telomeric regions in unperturbed conditions (Azzalin *et al.*, 2007; Arora *et al.*, 2014; Singh *et al.*, 2019; De *et al.*, 2022). Whether UPF1 is required for the resolution or prevention of R-loops remains to be reputedly determined. In either circumstance, UPF1 depletion appears to drive spontaneous R-loop accumulation which could be a result of or lead to an increase in RNAPII pausing and TRC incidence. As such these obstacles could act as a block to DNA replication fork progression (Rao *et al.*, 2024), as observed in chapter 4. Confirming the dependence of UPF1-deficient replication fork stalling on R-loops is important in confirming this hypothesis.

UPF1 has also been suggested to promote R-loop formation at DSBs induced in sub-telomeric regions to facilitate DNA repair, independently of NMD (Ngo, Grimstead and Baird, 2021). Helicases DDX1 and DHX9 have been demonstrated to promote R-loop formation in this manner to regulate gene expression and to mediate class switching (Chakraborty, Huang and Hiom, 2018; Ribeiro de Almeida *et al.*, 2018). This suggests that UPF1 could have dual functions in R-loop homeostasis in unperturbed and DNA damage conditions. UPF1 could also have a specific function in telomeres that is independent on the role that we are studying here which directly affects DNA replication genome wide. Whilst our data needs repeating to confirm its validity, UPF1 depleted cells under mild replicative stress do show a small reduction in R-loop levels. These observations could infer that UPF1 does promote R-loop formation in such conditions. From chapter 4 we know that UPF1 depletion results in a reduction in transcription-dependent replication fork stalling, following mild replication stress. We hypothesise that this is due to a reduction in TRCs which are usually associated with the formation of R-loop structures, especially in a HO-orientation (Hamperl *et al.*, 2017). Therefore, reduced collisions between the replisome and transcriptional machinery would lead to a reduction in R-loop structures, consistent with this data.

In this chapter of my thesis, we have demonstrated the issues faced when utilising the monoclonal S9.6 antibody for the quantification of DNA-RNA hybrids such as R-loops by immunofluorescence. Though unable to reliably quantify R-loops in this manner, utilisation of an assay to assess the localisation of a catalytically inactive

RNaseH1<sup>D210N</sup> mutant suggests that UPF1 depletion could promote spontaneous R-loop accumulation, though more work is required to validate these findings.

### 5.3.2 Limitations

The use of an exogenous RNaseH1<sup>D210N</sup> mutant for this assay has been proposed to result in the stabilisation of R-loop structures, by preventing their resolution (Chen *et al.*, 2015; Stork *et al.*, 2016). Whilst we observe no problems in mitotic duration or an increase in RPA staining in these experiments, it is most likely that RNaseH1<sup>D210N</sup> is not promoting replication stress or DSBs, but it cannot be entirely ruled out. Overexpression of this protein could also induce problems within the cell due to aggregation or toxicity. To overcome this a negative control, of a mutated form of RNaseH1 which is both catalytically inactive (D210N) but also unable to bind to DNA-RNA hybrids (W43A, K59A, K60A) could be used to rule out any of these affects.

# Chapter 6: Discussion

## 6.1 A novel function or consequence of UPF1 deficiency

In this thesis we have uncovered a novel function of UPF1 in the regulation of mitotic duration following DNA damage as well as DNA replication dynamics in prophase of mitosis and S-phase. We have found that UPF1 is required to prevent cells from exhibiting spontaneous DNA replication fork stalling and DNA damage, that is dependent on active transcription (see **Figure 6.1.1**). UPF1 also potentially prevents an accumulation of R-loops in unperturbed conditions. In the absence of UPF1, cells exposed to mild replicative stress exhibit a reduction in replication fork stalling, most likely due to reduced incidence of either indirect or direct TRCs. Due to reduced replication fork stalling occurring in S-phase, we propose that UPF1-deficient cells are able to completely replicate their DNA, preventing the emergence of UR-DNA associated with mild replicative stress. In line with this, cells deficient for UPF1 do not exhibit DNA replication in prophase of mitosis by the process of MiDAS or DNA damage-dependent mitotic delay. Additionally, RNaseH1 overexpression is known to prevent MiDAS and in this thesis was demonstrated to prevent mitotic delay, suggesting that these two phenotypes could be directly linked (W. Wu *et al.*, 2020; Groelly *et al.*, 2022; Said *et al.*, 2022). Consistent with the hypothesis that UPF1 does not directly promote the process of MiDAS, no increase in signs of UR-DNA in the subsequent G1 phase are observed, marked by 53BP1 nuclear bodies or post-division DNA replication/repair, suggesting that MiDAS is not defective, but not required. Together these results demonstrate a novel function of UPF1 in safeguarding DNA replication from transcriptional replication barriers and fork collapse in unperturbed conditions and suggest that UPF1-deficiency could drive resistance to DNA replication therapies in human cancers by allowing for timely DNA replication even following DNA replication stress.

The working hypothesis is that DNA damage-dependent mitotic delay is most likely a direct or indirect consequence of a necessity for MiDAS in prophase (Wassing *et al.*, 2021). However, UPF1 could have an independent role in the regulation of the centromere, or subsequent kinetochore and SAC function in the presence of replicative stress. It is possible that UPF1 regulates R-loop formation in centromeric

regions through mediating nascent mRNA release. This would in turn affects ATR recruitment through RPA-coated centromeric R-loops which facilitates correct mitotic progression and prevents segregation errors (Kabeche *et al.*, 2018). Damage at centromeric-associated R-loops has also been demonstrated to impair kinetochore integrity (Shih *et al.*, 2022; Malik *et al.*, 2023). BRCA1 associates with centromeric R-loops to facilitate their resolution and mediate CENP-A deposition. Loss of BRCA1 causes R-loop accumulation, increased centromeric transcription, centromeric DSBs and micronuclei formation (Racca *et al.*, 2021). UPF1 could facilitate the resolution of these structures in the same manner. TRC associated R-loops promote centromeric instability following DAXX depletion (Pinto *et al.*, 2024). DAXX has also been associated with kinetochore defects which could cause mitotic delay due to SAC issues (Trier *et al.*, 2023).

The data in this thesis supports a role for UPF1 in preventing the accumulation of co-transcriptional R-loop-associated nascent RNAs, as suggested to occur across the genome in drosophila and yeast and at telomeres in human cells (Azzalin *et al.*, 2007; Arora *et al.*, 2014; Singh *et al.*, 2019; De *et al.*, 2022). These R-loop structures which are negatively regulated by UPF1 represent a potential transcription-dependent replication barrier which could explain the replication fork stalling phenotype observed in unperturbed conditions following loss of UPF1 (see **Figure 6.1.1**). Whilst the direct effect of UPF1-deficiency on global DNA replication has not been previously reported, UPF1-associated factor UPF2 as well as SMG1 modulators SMG8/9 have been implicated in promoting replication fork stalling and TRCs following treatment with an ATR inhibitor in a similar manner that is uncovered for UPF1 in this thesis (Llorca-Cardenosa *et al.*, 2022; O'Leary *et al.*, 2022). Together this provides a basis whereby dysregulation of UPF1 can result in changes in TRC incidence and a manner through which loss of UPF1 can promote transcription-dependent DNA replication fork stalling.

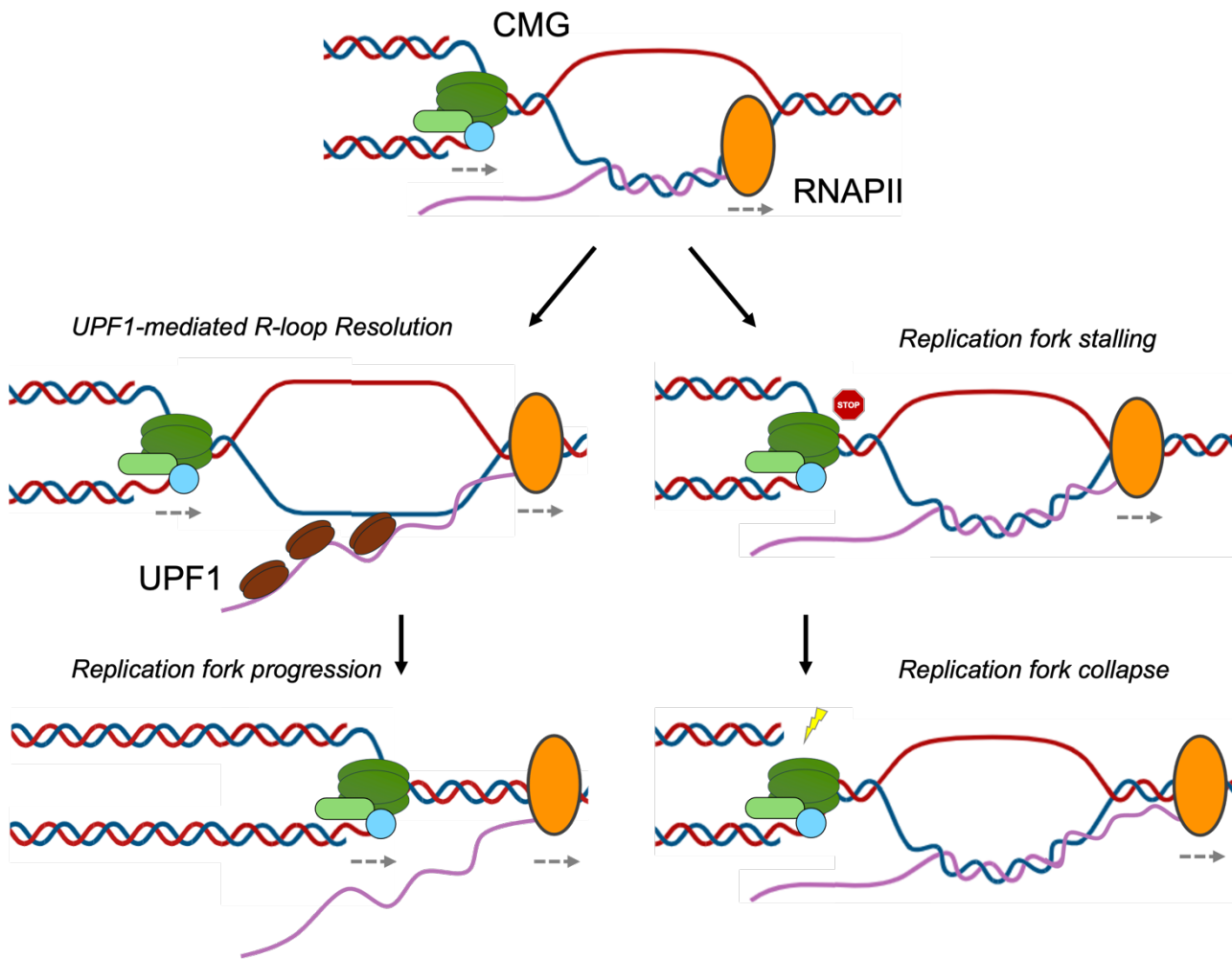


Figure 6.1.1: Proposed model for spontaneous replication fork stalling and DNA damage, following loss of UPF1.

## 6.2 UPF1, a predictive clinical biomarker for replication-targeting chemotherapeutics or a therapeutic target

Oncogenic signalling leads to a global increase in transcription levels in order to support increased rates of proliferation. Oncogene activation-associated increases in RNAPII transcription, referred to as hypertranscription, is associated with an increase in replication stress, replication fork slowing and DNA damage (Kotsantis *et al.*, 2016; Stork *et al.*, 2016; Gorthi *et al.*, 2018). This means that transcription-dependent replication fork stalling is a frequent phenomenon observed in human cancers and targeting it is therapeutically relevant.

Since cells that are deficient for UPF1 show reduced replication fork stalling following DNA replication stress induction, UPF1-deficiency could lead to an increased resistance to anti-cancer therapies that target tumour cells by inflicting DNA replication stress. An accumulation of TRCs and their associated deleterious effects underly treatment response to DNA damaging therapies and checkpoint inhibition (Yang *et al.*, 2024). Loss of UPF1-associated factor UPF2 and SMG8/9 heterodimer which modulates SMG1 drive resistance to ATR inhibition, providing evidence for a role of UPF1-associated factors in driving replication stress sensitivity (Llorca-Cardenosa *et al.*, 2022; O'Leary *et al.*, 2022). Indeed, UPF1 has been demonstrated to be dysregulated among several human cancers including lung adenocarcinoma (LADC), though most of these focused on the role of UPF1 in NMD (Fang *et al.*, 2001; Cao *et al.*, 2017; Han *et al.*, 2020).

Whilst UPF1 deficiency could promote treatment resistance to replication-targeting therapies, the endogenous replication stress induced by UPF1-loss could also drive sensitivity to other therapies. R-loop-associated TRCs have been specifically demonstrated to promote increased sensitivity to PARP inhibitors, effects that are even more significant in HR-deficient tumours (Ye *et al.*, 2021; Jayakumar *et al.*, 2024; Liu *et al.*, 2024; Petropoulos *et al.*, 2024). Since we are most likely observing an increase in TRC incidence, exploring the use of PARP inhibitors in UPF1 deficient cancers could be a promising therapeutic avenue.

### **6.3 Future Work**

From this thesis there are numerous avenues of future work to discover the precise role that UPF1 is playing in the discussed phenotypes. In order to more elegantly demonstrate the function of UPF1 and allow for the assessment of UPF1-depletion and rescue experiments across the cell cycle, development of an auxin degron system targeted to endogenous UPF1 would be desirable (Nishimura *et al.*, 2009). This would allow for the rapid degradation of UPF1 in synchronised populations at specific cell cycle stages, allowing us to demonstrate whether UPF1 is directly involved in S-phase or mitosis, and the respective consequences of UPF1 depletion in one cell cycle phase on another. In order to further exclude the pathway of NMD and general RNA dysregulation following UPF1 depletion, RNA-seq could also be carried out,

specifically to assess whether any key DNA replication or mitotic regulatory factors are dysregulated under conditions of replication stress in the absence of UPF1. Transcripts could be targeted to NMD by alternative splicing events following DNA damage, so assessing splicing isoforms of mitotic regulators would also allow further examination of the role of NMD. As previously described, a general inhibition of NMD following various genotoxic stressors is observed, however we wish to confirm these results with the replicative stress agents we use in this study (Gardner, 2008; Nickless *et al.*, 2017; Ryu *et al.*, 2019; Usuki, Yamashita and Fujimura, 2019). To do this we could use a series of NMD reporter plasmids coding for  $\beta$ -globin constructs that harbour a normal termination codon or a PTC. The quantification of these reporter constructs by qPCR allow us to determine whether NMD efficiency changes. Histone mRNA accumulation in the absence of UPF1 could also lead to changes in DNA replication processes. To determine whether histone mRNA is responsible for the observed phenotypes it will be important to assess changes in histone levels by qPCR and at the protein level by western blot. Determining if any changes in histone deposition occur, we could also carry out immunofluorescence assays. Determining the possible involvement of HMD is an important line of questioning to discover whether the functions observed here and independent of RNA decay pathways attributed to UPF1.

An intriguing line of questioning is to determine the cause of UPF1-depletion induced spontaneous replication fork stalling and DNA damage. In order to assess whether this phenotype is indeed associated with mitotic duration as demonstrated, I would like to assess the relevant involvement of other UPF1-associated factors as carried out in chapter 3 and carry out rescue experiments with UPF1 mutants for all phenotypes observed. Specifically, it would be interesting to determine whether the replication phenotype is dependent on the chromatin-binding ability of UPF1 using the S42 mutants. In addition to this, demonstrating the DNA replication fork stalling and DNA damage is also rescuable by RNaseH1 overexpression would strengthen the proposed model. To this end, proper quantification of R-loop dynamics following UPF1 depletion is also important experimental data. Either repeating S9.6 experiments again or the RNaseH1<sup>D210N</sup> exogenous reporter assay for R-loops. Other methods of R-loop quantification also include dots blots of DNA which has been immunoprecipitated out

using the S9.6 antibody, DRIP-seq for S9.6, ChIP-seq for the RNaseH1<sup>D210N</sup> reporter or DRIP-qPCR for S9.6 at known CFS genes including FRA3B, FRA7B, FRA10C, FRA16D and telomeric binding TERRA. Sequencing techniques have the added benefit of providing precise spatial organisation of R-loops across the genome. Due to their reliance on the precipitation of DNA in most cases they also nullify the off-target effects of the S9.6 antibody on alternative dsRNA structures.

The most obvious cause of replication fork stalling in unperturbed conditions following UPF1 depletion is direct TRCs, which can be quantified by using a proximity ligation assay (PLA), probing for the replisome component PCNA and RNAPII (Ser2), to determine the location of collisions between the two machineries. If the PLA assay demonstrated no clear changes, then I would investigate the possibility that UPF1 promotes indirect DNA replication barriers, potentially due to the existence of R-loop associated nascent mRNAs. This could be investigated by carrying out co-fluorescent in situ hybridisation (Co-FISH), to examine any replisome collisions (marked by PCNA) with known CFS loci or other regions of the genome such as the telomeres and centromeres, which UPF1 has been implicated in regulating. FISH could also be used to confirm the role of UPF1 in promoting release of nascent mRNAs from their transcribed loci. Whilst this has been demonstrated for telomeres and TERRA (Azzalin *et al.*, 2007), it would be interesting to assess other chromosomal loci such as the centromeres. To examine whether this retention of mRNAs occurs and impacts DNA replication, pulse labelling cells with both BrdU to assess ongoing DNA replication as well as 5-EU to assess RNA synthesis, followed by pre-extraction of the cytoplasmic and nuclear soluble fractions, could allow for the visualisation of replication foci which coincide with chromatin-bound nascent mRNA.

Locating the regions of DNA replication fork stalling or DNA damage would provide a wealth of information as to what UPF1 is doing. Techniques such as Chromatin immunoprecipitation sequencing (ChIP-seq), for the DSB marker  $\gamma$ -H2AX, could allow for a genome wide search of whether UPF1 promotes DNA damage at specific genomic loci, or if these events occur randomly. Further analysis of whether UPF1 itself is enriched at specific regions of the genome and mediates any effect on transcription progression could be assessed by DRIP-seq or immunofluorescence for

UPF1 and RNAPII (Ser2) and total respectively. We observed some colocalization of P-UPF1 (S1096) with PCNA and FANCD2 foci, following up on these observations could shed light on how UPF1 is directly involved at stalled replication forks. Not only is the spatial location of this UPF1 depletion-induced DNA damage an important question but also the temporal location. We have shown that UPF1-deficiency promotes DNA replication fork stalling in S-phase and that the UPF1 depletion-induced DNA damage observed is transcription-dependent. Since transcription and DNA replication primarily occur independently these most likely do not coincide, except at large genes and CFSs. Understanding whether this damage is inherited at a specific time in the cell cycle could shed light on this. This could be done by synchronising cell populations and examining whether DSBs, visualised through  $\gamma$ -H2AX by western blots or immunofluorescence are more evident in various cell cycle phases, validated using flow cytometry. An alternative explanation is that UPF1 depletion-induced DNA damage could affect DNA replication and be transcription-dependent is that UPF1 depletion could lead to a de-repression of transcription in S-phase which would drive DNA replication fork stalling. This can be assessed by examining the rate of transcription occurring in S-phase by carrying out immunofluorescence for cells which have been pulse labelled with the uridine analogue 5-Ethynyl-uridine (5-EU), which allows for the detection of ongoing RNA synthesis, and also stain for S-phase markers such as PCNA.

Finally, further understanding why MiDAS does not occur following DNA replicative stress in the absence of UPF1 would reinforce the hypothesis that UPF1 promotes a reduction in UR-DNA following mild replicative stress. To do this, CFS expression could be quantified using metaphase spreads and quantifying visual breaks in chromosomes. Additionally, completing the 53BP1 nuclear body assay and assessing the formation of ultra-fine bridges (UFBs), which allows for the visualisation of UR-DNA during mitosis would allow us to confirm a reduction in UR-DNA. Visualisation of UFBs can be done so by staining for Pich or BLM by immunofluorescence, among other proteins and are evident during spindle pole separation during anaphase or in subsequent G1 cells. To further demonstrate that UPF1 does lead to a reduction in UR-DNA, you could expect UPF1-deficient cells to be more resistant to mild replicative stress. We could assess this effect both in 2D cellular models by clonogenic assay in

CRISPR lines or using UPF1-siRNA or the UPF1 inhibitor, VG1. In addition to this, TRC accumulation is proposed to drive PARP inhibitor sensitivity (Ye *et al.*, 2021; Jayakumar *et al.*, 2024; Liu *et al.*, 2024; Petropoulos *et al.*, 2024). Testing whether this is the case, could show UPF1 as a key therapeutic target, deficiency of which drives treatment sensitivity to PARP inhibition.

# References

- Ahmed-Seghir, S. *et al.* (2023) 'A local ATR-dependent checkpoint pathway is activated by a site-specific replication fork block in human cells', *eLife*. eLife Sciences Publications Ltd, 12. doi: 10.7554/ELIFE.87357.
- Amparo, C. *et al.* (2020) 'Duplex DNA from Sites of Helicase-Polymerase Uncoupling Links Non-B DNA Structure Formation to Replicative Stress', *Cancer Genomics & Proteomics*. International Institute of Anticancer Research, 17(2), pp. 101–115. doi: 10.21873/CGP.20171.
- Amrani, N. *et al.* (2004) 'A faux 3'-UTR promotes aberrant termination and triggers nonsense-mediated mRNA decay', *Nature* 2004 432:7013. Nature Publishing Group, 432(7013), pp. 112–118. doi: 10.1038/nature03060.
- De Antoni, A. *et al.* (2005) 'The Mad1/Mad2 complex as a template for Mad2 activation in the spindle assembly checkpoint', *Current biology: CB*. Curr Biol, 15(3), pp. 214–225. doi: 10.1016/J.CUB.2005.01.038.
- Applequist, S. E. *et al.* (1997) 'Cloning and characterization of HUPF1, a human homolog of the *Saccharomyces cerevisiae* nonsense mRNA-reducing UPF1 protein', *Nucleic Acids Research*. Oxford University Press, 25(4). Available at: <http://www.ncbi.nlm.nih.gov/xrefdb>. (Accessed: 14 November 2021).
- Aria, V. and Yeeles, J. T. P. (2019) 'Mechanism of Bidirectional Leading-Strand Synthesis Establishment at Eukaryotic DNA Replication Origins', *Molecular Cell*. Cell Press, 73(2), pp. 199-211.e10. doi: 10.1016/J.MOLCEL.2018.10.019.
- Ariel, F. *et al.* (2020) 'R-Loop Mediated trans Action of the APOLO Long Noncoding RNA', *Molecular cell*. Mol Cell, 77(5), pp. 1055-1065.e4. doi: 10.1016/J.MOLCEL.2019.12.015.
- Arora, R. *et al.* (2014) 'RNaseH1 regulates TERRA-telomeric DNA hybrids and telomere maintenance in ALT tumour cells', *Nature Communications* 2014 5:1. Nature Publishing Group, 5(1), pp. 1–11. doi: 10.1038/ncomms6220.
- Azzalin, C. M. *et al.* (2007) 'Telomeric repeat-containing RNA and RNA surveillance factors at mammalian chromosome ends', *Science*. American Association for the Advancement of Science, 318(5851), pp. 798–801. doi: 10.1126/SCIENCE.1147182/SUPPL\_FILE/AZZALIN.SOM.PDF.
- Azzalin, C. M. and Lingner, J. (2006) 'The human RNA surveillance factor UPF1 is

required for S phase progression and genome stability', *Current Biology*. Elsevier, 16(4), pp. 433–439. doi: 10.1016/J.CUB.2006.01.018/ATTACHMENT/FE474C14-0200-4AF2-9612-EB88D1F0FD6F/MMC1.PDF.

Balakrishnan, L. and Bambara, R. A. (2013) 'Flap endonuclease 1', *Annual Review of Biochemistry*. Annual Reviews, 82(Volume 82, 2013), pp. 119–138. doi: 10.1146/ANNUREV-BIOCHEM-072511-122603/CITE/REFWORKS.

Balk, B. *et al.* (2013) 'Telomeric RNA-DNA hybrids affect telomere-length dynamics and senescence', *Nature Structural & Molecular Biology* 2013 20:10. Nature Publishing Group, 20(10), pp. 1199–1205. doi: 10.1038/nsmb.2662.

Bandau, S. *et al.* (2024) 'RNA polymerase II promotes the organization of chromatin following DNA replication', *EMBO Reports*. Springer Nature, 25(3), pp. 1387–1414. doi: 10.1038/S44319-024-00085-X/SUPPL\_FILE/44319\_2024\_85\_MOESM14\_ESM.PDF.

Barbier, J. *et al.* (2007) 'Regulation of H-ras Splice Variant Expression by Cross Talk between the p53 and Nonsense-Mediated mRNA Decay Pathways', *Molecular and Cellular Biology*. American Society for Microbiology, 27(20), pp. 7315–7333. doi: 10.1128/MCB.00272-07/SUPPL\_FILE/SUPPLEMENTALMATERIALMCBREVISEDVERSION3.DOC.

Barnes, C. O. *et al.* (2015) 'Crystal structure of a transcribing RNA Polymerase II complex reveals a complete transcription bubble', *Molecular cell*. Cell Press, 59(2), p. 258. doi: 10.1016/J.MOLCEL.2015.06.034.

Baumann, C. *et al.* (2007) 'PICH, a Centromere-Associated SNF2 Family ATPase, Is Regulated by Plk1 and Required for the Spindle Checkpoint', *Cell*. Cell Press, 128(1), pp. 101–114. doi: 10.1016/J.CELL.2006.11.041.

Le Beau, M. M. *et al.* (1998) 'Replication of a Common Fragile Site, FRA3B, Occurs Late in S Phase and is Delayed Further Upon Induction: Implications for the Mechanism of Fragile Site Induction', *Human Molecular Genetics*. Oxford Academic, 7(4), pp. 755–761. doi: 10.1093/HMG/7.4.755.

van den Berg, J. *et al.* (2018) 'A limited number of double-strand DNA breaks is sufficient to delay cell cycle progression', *Nucleic Acids Research*. Oxford University Press, 46(19), p. 10132. doi: 10.1093/NAR/GKY786.

Berti, M. *et al.* (2013) 'Human RECQ1 promotes restart of replication forks reversed by DNA topoisomerase I inhibition', *Nature Structural & Molecular Biology* 2013 20:3. Nature Publishing Group, 20(3), pp. 347–354. doi: 10.1038/nsmb.2501.

Bertolin, A. P., Hoffmann, J. S. and Gottifredi, V. (2020) 'Under-Replicated DNA: The Byproduct of Large Genomes?', *Cancers*. MDPI AG, 12(10), p. 2764. doi: 10.3390/CANCERS12102764.

Bhattacharya, A. *et al.* (2000) 'Characterization of the biochemical properties of the human Upf1 gene product that is involved in nonsense-mediated mRNA decay', *RNA*. Cambridge University Press, 6(9), pp. 1226–1235. doi: 10.1017/S1355838200000546.

Bhowmick, R. *et al.* (2022) 'RAD51 protects human cells from transcription-replication conflicts', *Molecular Cell*. Cell Press, 82(18), pp. 3366-3381.e9. doi: 10.1016/J.MOLCEL.2022.07.010/ASSET/FA1FD870-7AF5-4724-9009-256D94E2362C/MAIN.ASSETS/GR7.JPG.

Bhowmick, R., Minocherhomji, S. and Hickson Correspondence, I. D. (2016) 'RAD52 Facilitates Mitotic DNA Synthesis Following Replication Stress', *Molecular Cell*, 64. doi: 10.1016/j.molcel.2016.10.037.

Bleichert, F., Botchan, M. R. and Berger, J. M. (2017) 'Mechanisms for initiating cellular DNA replication', *Science*. American Association for the Advancement of Science, 355(6327). doi: 10.1126/SCIENCE.AAH6317/ASSET/D9D2B899-B012-46D1-8108-E71A5CA6208F/ASSETS/GRAPHIC/355\_AAH6317\_F5.JPEG.

Blin, M. *et al.* (2018) 'Transcription-dependent regulation of replication dynamics modulates genome stability', *Nature Structural & Molecular Biology* 2018 26:1. Nature Publishing Group, 26(1), pp. 58–66. doi: 10.1038/s41594-018-0170-1.

Blower, M. D. (2016) 'Centromeric Transcription Regulates Aurora-B Localization and Activation', *Cell Reports*. Cell Press, 15(8), pp. 1624–1633. doi: 10.1016/J.CELREP.2016.04.054.

Bobkov, G. O. M., Gilbert, N. and Heun, P. (2018) 'Centromere transcription allows CENP-A to transit from chromatin association to stable incorporation', *Journal of Cell Biology*. The Rockefeller University Press, 217(6), pp. 1957–1972. doi: 10.1083/JCB.201611087.

Boehm, V. *et al.* (2021) 'SMG5-SMG7 authorize nonsense-mediated mRNA decay by enabling SMG6 endonucleolytic activity', *Nature Communications* 2021 12:1. Nature Publishing Group, 12(1), pp. 1–19. doi: 10.1038/s41467-021-24046-3.

Bokhari, A. *et al.* (2018) 'Targeting nonsense-mediated mRNA decay in colorectal cancers with microsatellite instability', *Oncogenesis* 2018 7:9. Nature Publishing Group, 7(9), pp. 1–9. doi: 10.1038/s41389-018-0079-x.

- Bono, F. *et al.* (2006) 'The Crystal Structure of the Exon Junction Complex Reveals How It Maintains a Stable Grip on mRNA', *Cell*. Cell Press, 126(4), pp. 713–725. doi: 10.1016/J.CELL.2006.08.006.
- Bottoni, G. *et al.* (2019) 'CSL controls telomere maintenance and genome stability in human dermal fibroblasts', *Nature Communications*. Nature Publishing Group, 10(1), pp. 1–15. doi: 10.1038/s41467-019-11785-7.
- Brisson, O. *et al.* (2019) 'Transcription-mediated organization of the replication initiation program across large genes sets common fragile sites genome-wide', *Nature Communications* 2019 10:1. Nature Publishing Group, 10(1), pp. 1–12. doi: 10.1038/s41467-019-13674-5.
- Brumbaugh, K. M. *et al.* (2004) 'The mRNA surveillance protein hSMG-1 functions in genotoxic stress response pathways in mammalian cells', *Molecular Cell*. Elsevier, 14(5), pp. 585–598. doi: 10.1016/J.MOLCEL.2004.05.005/ATTACHMENT/9DE72D58-DB8D-4695-B0E4-53ABD7E6CC93/MMC1.PDF.
- Brüning, J. G. and Marians, K. J. (2020) 'Replisome bypass of transcription complexes and R-loops', *Nucleic acids research*. Nucleic Acids Res, 48(18), pp. 10353–10367. doi: 10.1093/NAR/GKAA741.
- Brüning, J. G. and Marians, K. J. (2021) 'Bypass of complex co-directional replication-transcription collisions by replisome skipping', *Nucleic Acids Research*. Oxford University Press, 49(17), p. 9870. doi: 10.1093/NAR/GKAB760.
- Bruno, I. G. *et al.* (2011) 'Identification of a MicroRNA that Activates Gene Expression by Repressing Nonsense-Mediated RNA Decay', *Molecular Cell*. Elsevier, 42(4), pp. 500–510. doi: 10.1016/J.MOLCEL.2011.04.018/ATTACHMENT/59BC08A9-87B2-4E42-9EE4-F0ED15CD583C/MMC3.ZIP.
- Bühler, M. *et al.* (2006) 'EJC-independent degradation of nonsense immunoglobulin- $\mu$  mRNA depends on 3' UTR length', *Nature Structural & Molecular Biology* 2006 13:5. Nature Publishing Group, 13(5), pp. 462–464. doi: 10.1038/nsmb1081.
- Cao, L. *et al.* (2017) 'Human nonsense-mediated RNA decay regulates EMT by targeting the TGF- $\beta$  signaling pathway in lung adenocarcinoma', *Cancer letters*. Cancer Lett, 403, pp. 246–259. doi: 10.1016/J.CANLET.2017.06.021.
- Carastro, L. M. *et al.* (2002) 'Identification of delta helicase as the bovine homolog of HUPF1: demonstration of an interaction with the third subunit of DNA polymerase delta', *Nucleic Acids Research*. Oxford Academic, 30(10), pp. 2232–2243. doi:

10.1093/NAR/30.10.2232.

Castellano-Pozo, M. *et al.* (2013) 'R Loops Are Linked to Histone H3 S10 Phosphorylation and Chromatin Condensation', *Molecular Cell*. Cell Press, 52(4), pp. 583–590. doi: 10.1016/J.MOLCEL.2013.10.006.

Chakrabarti, S. *et al.* (2011) 'Molecular Mechanisms for the RNA-Dependent ATPase Activity of Upf1 and Its Regulation by Upf2', *Molecular Cell*. Cell Press, 41(6), pp. 693–703. doi: 10.1016/J.MOLCEL.2011.02.010.

Chakraborty, P., Huang, J. T. J. and Hiom, K. (2018) 'DHX9 helicase promotes R-loop formation in cells with impaired RNA splicing', *Nature Communications* 2018 9:1. Nature Publishing Group, 9(1), pp. 1–14. doi: 10.1038/s41467-018-06677-1.

Chamieh, H. *et al.* (2007) 'NMD factors UPF2 and UPF3 bridge UPF1 to the exon junction complex and stimulate its RNA helicase activity', *Nature Structural & Molecular Biology* 2008 15:1. Nature Publishing Group, 15(1), pp. 85–93. doi: 10.1038/nsmb1330.

Chan, C. C. *et al.* (2004) 'eIF4A3 is a novel component of the exon junction complex', *RNA*. Cold Spring Harbor Laboratory Press, 10(2), pp. 200–209. doi: 10.1261/RNA.5230104.

Chan, F. L. *et al.* (2012) 'Active transcription and essential role of RNA polymerase II at the centromere during mitosis', *Proceedings of the National Academy of Sciences of the United States of America*. Proc Natl Acad Sci U S A, 109(6), pp. 1979–1984. doi: 10.1073/PNAS.1108705109.

Chan, K. L. *et al.* (2009) 'Replication stress induces sister-chromatid bridging at fragile site loci in mitosis', *Nature Cell Biology* 2009 11:6. Nature Publishing Group, 11(6), pp. 753–760. doi: 10.1038/ncb1882.

Chan, K. L., North, P. S. and Hickson, I. D. (2007) 'BLM is required for faithful chromosome segregation and its localization defines a class of ultrafine anaphase bridges', *EMBO Journal*. John Wiley & Sons, LtdChichester, UK, 26(14), pp. 3397–3409. doi: 10.1038/SJ.EMBOJ.7601777/SUPPL\_FILE/EMBJ7601777-SUP-0007.PDF.

Chang, L. *et al.* (2016) 'Upregulation of SNHG6 regulates ZEB1 expression by competitively binding miR-101-3p and interacting with UPF1 in hepatocellular carcinoma', *Cancer letters*. Cancer Lett, 383(2), pp. 183–194. doi: 10.1016/J.CANLET.2016.09.034.

Chapman, J. H. *et al.* (2024) 'UPF1 ATPase autoinhibition and activation modulate

RNA binding kinetics and NMD efficiency', *Nucleic Acids Research*. Oxford Academic, 52(9), pp. 5376–5391. doi: 10.1093/NAR/GKAE136.

Chappidi, N. *et al.* (2020) 'Fork Cleavage-Religation Cycle and Active Transcription Mediate Replication Restart after Fork Stalling at Co-transcriptional R-Loops', *Molecular Cell*. Cell Press, 77(3), pp. 528-541.e8. doi: 10.1016/j.molcel.2019.10.026.

Chawla, R. *et al.* (2011) 'Human UPF1 interacts with TPP1 and telomerase and sustains telomere leading-strand replication', *The EMBO Journal*. European Molecular Biology Organization, 30(19), p. 4047. doi: 10.1038/EMBOJ.2011.280.

Chedin, F. and Benham, C. J. (2020) 'Emerging roles for R-loop structures in the management of topological stress', *Journal of Biological Chemistry*. Elsevier, 295(14), pp. 4684–4695. doi: 10.1074/JBC.REV119.006364.

Chen, J. *et al.* (2017) 'Identification of a DNA damage–induced alternative splicing pathway that regulates p53 and cellular senescence markers', *Cancer Discovery*. American Association for Cancer Research Inc., 7(7), pp. 766–781. doi: 10.1158/2159-8290.CD-16-0908/333286/AM/IDENTIFICATION-OF-A-DNA-DAMAGE-INDUCED-ALTERNATIVE.

Chen, L. *et al.* (2017) 'R-ChIP Using Inactive RNase H Reveals Dynamic Coupling of R-loops with Transcriptional Pausing at Gene Promoters', *Molecular cell*. NIH Public Access, 68(4), p. 745. doi: 10.1016/J.MOLCEL.2017.10.008.

Chen, P. B. *et al.* (2015) 'R loops regulate promoter-proximal chromatin architecture and cellular differentiation', *Nature Structural & Molecular Biology* 2015 22:12. Nature Publishing Group, 22(12), pp. 999–1007. doi: 10.1038/nsmb.3122.

Cheng, B. and Price, D. H. (2007) 'Properties of RNA polymerase II elongation complexes before and after the P-TEFb-mediated transition into productive elongation', *The Journal of biological chemistry*. J Biol Chem, 282(30), pp. 21901–21912. doi: 10.1074/JBC.M702936200.

Cheng, Z. *et al.* (2007) 'Structural and functional insights into the human Upf1 helicase core', *The EMBO Journal*. European Molecular Biology Organization, 26(1), p. 253. doi: 10.1038/SJ.EMBOJ.7601464.

Cheruiyot, A. *et al.* (2021) 'Nonsense-Mediated RNA Decay Is a Unique Vulnerability of Cancer Cells Harboring SF3B1 or U2AF1 Mutations', *Cancer research*. Cancer Res, 81(17), pp. 4499–4513. doi: 10.1158/0008-5472.CAN-20-4016.

Choe, J. *et al.* (2013) 'Rapid degradation of replication-dependent histone mRNAs largely occurs on mRNAs bound by nuclear cap-binding proteins 80 and 20', *Nucleic*

*Acids Research*. Oxford Academic, 41(2), pp. 1307–1318. doi: 10.1093/NAR/GKS1196.

Choe, J., Ahn, S. H. and Kim, Y. K. (2014) 'The mRNP remodeling mediated by UPF1 promotes rapid degradation of replication-dependent histone mRNA', *Nucleic Acids Research*. Oxford Academic, 42(14), pp. 9334–9349. doi: 10.1093/NAR/GKU610.

Cloutier, S. C. *et al.* (2016) 'Regulated Formation of lncRNA-DNA Hybrids Enables Faster Transcriptional Induction and Environmental Adaptation', *Molecular Cell*. Cell Press, 61(3), pp. 393–404. doi: 10.1016/J.MOLCEL.2015.12.024.

Cohen, S. *et al.* (2018) 'Senataxin resolves RNA:DNA hybrids forming at DNA double-strand breaks to prevent translocations', *Nature Communications* 2018 9:1. Nature Publishing Group, 9(1), pp. 1–14. doi: 10.1038/s41467-018-02894-w.

Collins, K. L. and Kelly, T. J. (1991) 'Effects of T antigen and replication protein A on the initiation of DNA synthesis by DNA polymerase alpha-primase', *Molecular and Cellular Biology*. Informa UK Limited, 11(4), p. 2108. doi: 10.1128/MCB.11.4.2108.

Conti, B. A. and Smogorzewska, A. (2020) 'Mechanisms of direct replication restart at stressed replisomes', *DNA Repair*. Elsevier, 95, p. 102947. doi: 10.1016/J.DNAREP.2020.102947.

Conti, C. *et al.* (2007) 'Replication fork velocities at adjacent replication origins are coordinately modified during DNA replication in human cells', *Molecular Biology of the Cell*. The American Society for Cell Biology, 18(8), pp. 3059–3067. doi: 10.1091/MBC.E06-08-0689/ASSET/IMAGES/LARGE/ZMK0080781550004.JPEG.

Core, L. and Adelman, K. (2019) 'Promoter-proximal pausing of RNA polymerase II: a nexus of gene regulation', *Genes & development*. Genes Dev, 33(15–16), pp. 960–982. doi: 10.1101/GAD.325142.119.

Costa, A. *et al.* (2011) 'The structural basis for MCM2–7 helicase activation by GINS and Cdc45', *Nature Structural & Molecular Biology* 2011 18:4. Nature Publishing Group, 18(4), pp. 471–477. doi: 10.1038/nsmb.2004.

Cristini, A. *et al.* (2018) 'RNA/DNA Hybrid Interactome Identifies DXH9 as a Molecular Player in Transcriptional Termination and R-Loop-Associated DNA Damage', *Cell Reports*. Elsevier B.V., 23(6), pp. 1891–1905. doi: 10.1016/J.CELREP.2018.04.025/ATTACHMENT/7508E0CC-DFBD-4A9C-A5DC-BDFD438B44FD/MMC2.XLSX.

Cristini, A., Gromak, N. and Sordet, O. (2020) 'Transcription-dependent DNA double-strand breaks and human disease', *Molecular & Cellular Oncology*. Taylor and Francis

Ltd., 7(2), p. 1691905. doi: 10.1080/23723556.2019.1691905.

Culbertson, M. R. and Underbrink, K. M. (1980) 'Frameshift Suppression in SACCHAROMYCES CEREVISIAE. II. Genetic Properties of Group II Suppressors', *Genetics*. Oxford University Press, 95(4), p. 833. doi: 10.1093/genetics/95.4.833.

Czaplinski, K. *et al.* (1995) *Purification and characterization of the Upf1 protein: a factor involved in translation and mRNA degradation.*, *RNA*. Available at: [https://rnajournal.cshlp.org/content/1/6/610.abstract?ijkey=b880bcba91753b12c1718153f5cdafb8203d001b&keytype2=tf\\_ipsecsha](https://rnajournal.cshlp.org/content/1/6/610.abstract?ijkey=b880bcba91753b12c1718153f5cdafb8203d001b&keytype2=tf_ipsecsha) (Accessed: 14 November 2021).

Czaplinski, K. *et al.* (1998) 'The surveillance complex interacts with the translation release factors to enhance termination and degrade aberrant mRNAs', *Genes & Development*. Cold Spring Harbor Laboratory Press, 12(11), pp. 1665–1677. doi: 10.1101/GAD.12.11.1665.

Daigaku, Y. *et al.* (2015) 'A global profile of replicative polymerase usage', *Nature Structural & Molecular Biology* 2015 22:3. Nature Publishing Group, 22(3), pp. 192–198. doi: 10.1038/nsmb.2962.

De, S. *et al.* (2022) 'Genome-wide chromosomal association of Upf1 is linked to Pol II transcription in *Schizosaccharomyces pombe*', *Nucleic Acids Research*. Oxford Academic, 50(1), pp. 350–367. doi: 10.1093/NAR/GKAB1249.

Dehghani-Tafti, S. and Sanders, C. M. (2017) 'DNA substrate recognition and processing by the full-length human UPF1 helicase', *Nucleic Acids Research*. Oxford Academic, 45(12), pp. 7354–7366. doi: 10.1093/NAR/GKX478.

DeLisle, A. J. *et al.* (1983) 'Regulation of histone mRNA production and stability in serum-stimulated mouse 3T6 fibroblasts', *Molecular and cellular biology*. Mol Cell Biol, 3(11), pp. 1920–1929. doi: 10.1128/MCB.3.11.1920-1929.1983.

Deng, L. *et al.* (2019) 'Mitotic CDK Promotes Replisome Disassembly, Fork Breakage, and Complex DNA Rearrangements', *Molecular Cell*. Cell Press, 73(5), pp. 915–929.e6. doi: 10.1016/J.MOLCEL.2018.12.021/ATTACHMENT/B92F7B07-DAB7-4E39-8395-14CD75ECD93F/MMC2.PDF.

Dumelie, J. G. and Jaffrey, S. R. (2017) 'Defining the location of promoter-associated R-loops at near-nucleotide resolution using bisDRIP-seq', *eLife*. eLife Sciences Publications, Ltd, 6. doi: 10.7554/ELIFE.28306.

Dutta, A. and Bell, S. P. (1997) 'Initiation of DNA replication in eukaryotic cells', *Annual Review of Cell and Developmental Biology*. Annual Reviews, 13(Volume 13, 1997), pp. 293–332. doi: 10.1146/ANNUREV.CELLBIO.13.1.293/CITE/REFWORKS.

Espert, A. *et al.* (2014) 'PP2A-B56 opposes Mps1 phosphorylation of Knl1 and thereby promotes spindle assembly checkpoint silencing', *The Journal of Cell Biology*. The Rockefeller University Press, 206(7), p. 833. doi: 10.1083/JCB.201406109.

Fabrega, C. *et al.* (2003) 'Structure of an mRNA capping enzyme bound to the phosphorylated carboxy-terminal domain of RNA polymerase II', *Molecular cell*. Mol Cell, 11(6), pp. 1549–1561. doi: 10.1016/S1097-2765(03)00187-4.

Fang, C. *et al.* (2024) 'Ailanthone inhibits non-small cell lung cancer growth and metastasis through targeting UPF1/GAS5/ULK1 signaling pathway', *Phytomedicine*. Urban & Fischer, 128, p. 155333. doi: 10.1016/J.PHYMED.2023.155333.

Fang, L. *et al.* (2001) 'UPF1 increases amino acid levels and promotes cell proliferation in lung adenocarcinoma via the eIF2 $\alpha$ -ATF4 axis', *Journal of Zhejiang University-SCIENCE B*, 23(10), pp. 863–875. doi: 10.1631/jzus.B2200144.

Fatscher, T. *et al.* (2014) 'The interaction of cytoplasmic poly(A)-binding protein with eukaryotic initiation factor 4G suppresses nonsense-mediated mRNA decay', *RNA*. Cold Spring Harbor Laboratory Press, 20(10), pp. 1579–1592. doi: 10.1261/RNA.044933.114.

Fiorini, F. *et al.* (2015) 'Human Upf1 is a highly processive RNA helicase and translocase with RNP remodelling activities', *Nature Communications 2015 6:1*. Nature Publishing Group, 6(1), pp. 1–10. doi: 10.1038/ncomms8581.

Fiorini, F., Boudvillain, M. and Hir, H. Le (2013) 'Tight intramolecular regulation of the human Upf1 helicase by its N- and C-terminal domains', *Nucleic Acids Research*. Oxford University Press, 41(4), p. 2404. doi: 10.1093/NAR/GKS1320.

Fong, C. S. *et al.* (2016) '53BP1 and USP28 mediate p53- dependent cell cycle arrest in response to centrosome loss and prolonged mitosis', *eLife*. eLife Sciences Publications Ltd, 5(2016JULY). doi: 10.7554/ELIFE.16270.

Gabriel, M. *et al.* (2015) 'Role of the splicing factor SRSF4 in cisplatin-induced modifications of pre-mRNA splicing and apoptosis', *BMC Cancer*. BioMed Central Ltd., 15(1), pp. 1–14. doi: 10.1186/S12885-015-1259-0/FIGURES/6.

García-Muse, T. and Aguilera, A. (2016) 'Transcription–replication conflicts: how they occur and how they are resolved', *Nature Reviews Molecular Cell Biology 2016 17:9*. Nature Publishing Group, 17(9), pp. 553–563. doi: 10.1038/nrm.2016.88.

Gardner, L. B. (2008) 'Hypoxic inhibition of nonsense-mediated RNA decay regulates gene expression and the integrated stress response', *Molecular and cellular biology*. Mol Cell Biol, 28(11), pp. 3729–3741. doi: 10.1128/MCB.02284-07.

Garg, P. *et al.* (2004) 'Idling by DNA polymerase delta maintains a ligatable nick during lagging-strand DNA replication', *Genes & development*. Genes Dev, 18(22), pp. 2764–2773. doi: 10.1101/GAD.1252304.

Gartenberg, M. R. and Wang, J. C. (1992) 'Positive supercoiling of DNA greatly diminishes mRNA synthesis in yeast.', *Proceedings of the National Academy of Sciences*. Proceedings of the National Academy of Sciences, 89(23), pp. 11461–11465. doi: 10.1073/PNAS.89.23.11461.

Gatenby, R. *et al.* (2022) 'A SOD1-dependent mitotic DNA damage checkpoint', *bioRxiv*. Cold Spring Harbor Laboratory, p. 2022.10.26.513831. doi: 10.1101/2022.10.26.513831.

Gatenby, R. J. (2022) 'The identification of proteins involved in a novel mitotic DNA damage checkpoint.', *PhD Thesis, University of Sheffield*. Available at: <https://etheses.whiterose.ac.uk/id/eprint/30235/>.

Gellert, M., Lipsett, M. N. and Davies, D. R. (1962) 'Helix formation by guanylic acid', *Proceedings of the National Academy of Sciences of the United States of America*. Proc Natl Acad Sci U S A, 48(12), pp. 2013–2018. doi: 10.1073/PNAS.48.12.2013.

Gewandter, J. S., Bambara, R. A. and O'Reilly, M. A. (2011) 'The RNA surveillance protein SMG1 activates p53 in response to DNA double-strand breaks but not exogenously oxidized mRNA', *Cell Cycle*. Taylor & Francis, 10(15), pp. 2561–2567. doi: 10.4161/CC.10.15.16347.

Ghisays, F. *et al.* (2021) 'RTEL1 influences the abundance and localization of TERRA RNA', *Nature Communications 2021 12:1*. Nature Publishing Group, 12(1), pp. 1–14. doi: 10.1038/s41467-021-23299-2.

Gilchrist, D. A. *et al.* (2008) 'NELF-mediated stalling of Pol II can enhance gene expression by blocking promoter-proximal nucleosome assembly', *Genes & development*. Genes Dev, 22(14), pp. 1921–1933. doi: 10.1101/GAD.1643208.

Ginno, P. A. *et al.* (2012) 'R-Loop Formation Is a Distinctive Characteristic of Unmethylated Human CpG Island Promoters', *Molecular Cell*. Elsevier, 45(6), pp. 814–825. doi: 10.1016/J.MOLCEL.2012.01.017/ATTACHMENT/2CC58E81-606A-47FE-9109-69717CC4BAA3/MMC2.ZIP.

Giunta, S. *et al.* (2021) 'CENP-A chromatin prevents replication stress at centromeres to avoid structural aneuploidy', *Proceedings of the National Academy of Sciences of the United States of America*. National Academy of Sciences, 118(10). doi: 10.1073/PNAS.2015634118/SUPPL\_FILE/PNAS.2015634118.SM01.MP4.

Giunta, S., Belotserkovskaya, R. and Jackson, S. P. (2010) 'DNA damage signaling in response to double-strand breaks during mitosis', *Journal of Cell Biology*. The Rockefeller University Press, 190(2), pp. 197–207. doi: 10.1083/JCB.200911156.

Glover, T. W. *et al.* (1984) 'DNA polymerase  $\alpha$  inhibition by aphidicolin induces gaps and breaks at common fragile sites in human chromosomes', *Human Genetics*. Springer-Verlag, 67(2), pp. 136–142. doi: 10.1007/BF00272988/METRICS.

Glover, T. W., Wilson, T. E. and Arlt, M. F. (2017) 'Fragile Sites in Cancer: More Than Meets the Eye', *Nature reviews. Cancer*. Nature Publishing Group, 17(8), p. 489. doi: 10.1038/NRC.2017.52.

Gong, C. *et al.* (2009) 'SMD and NMD are competitive pathways that contribute to myogenesis: effects on PAX3 and myogenin mRNAs', *Genes & Development*. Cold Spring Harbor Laboratory Press, 23(1), pp. 54–66. doi: 10.1101/GAD.1717309.

Gorthi, A. *et al.* (2018) 'EWS–FLI1 increases transcription to cause R-loops and block BRCA1 repair in Ewing sarcoma', *Nature* 2018 555:7696. Nature Publishing Group, 555(7696), pp. 387–391. doi: 10.1038/nature25748.

Gotham, V. J. B. *et al.* (2016) 'Synthesis and activity of a novel inhibitor of nonsense-mediated mRNA decay', *Organic & Biomolecular Chemistry*. Royal Society of Chemistry, 14(5), p. 1559. doi: 10.1039/C5OB02482J.

Gowravaram, M. *et al.* (2019) 'Insights into the assembly and architecture of a Staufen-mediated mRNA decay (SMD)-competent mRNP', *Nature communications*. Nat Commun, 10(1). doi: 10.1038/S41467-019-13080-X.

Gregersen, L. H. *et al.* (2014) 'MOV10 Is a 5' to 3' RNA helicase contributing to UPF1 mRNA target degradation by translocation along 3' UTRs', *Molecular cell*. Mol Cell, 54(4), pp. 573–585. doi: 10.1016/J.MOLCEL.2014.03.017.

Gressel, S. *et al.* (2017) 'CDK9-dependent RNA polymerase II pausing controls transcription initiation', *eLife*. Elife, 6. doi: 10.7554/ELIFE.29736.

Groelly, F. J. *et al.* (2022) 'Mitotic DNA synthesis is caused by transcription-replication conflicts in BRCA2-deficient cells', *Molecular Cell*. Cell Press, 82(18), pp. 3382-3397.e7. doi: 10.1016/J.MOLCEL.2022.07.011.

Groh, M. *et al.* (2014) 'R-loops Associated with Triplet Repeat Expansions Promote Gene Silencing in Friedreich Ataxia and Fragile X Syndrome', *PLOS Genetics*. Public Library of Science, 10(5), p. e1004318. doi: 10.1371/JOURNAL.PGEN.1004318.

Guenther, M. G. *et al.* (2007) 'A chromatin landmark and transcription initiation at most promoters in human cells', *Cell*. Cell, 130(1), pp. 77–88. doi:

10.1016/J.CELL.2007.05.042.

Guttman, M. *et al.* (2009) 'Chromatin signature reveals over a thousand highly conserved large non-coding RNAs in mammals', *Nature*. *Nature*, 458(7235), pp. 223–227. doi: 10.1038/NATURE07672.

Haberle, V. and Stark, A. (2018) 'Eukaryotic core promoters and the functional basis of transcription initiation', *Nature Reviews Molecular Cell Biology* 2018 19:10. Nature Publishing Group, 19(10), pp. 621–637. doi: 10.1038/s41580-018-0028-8.

Hamperl, S. *et al.* (2017) 'Transcription-Replication Conflict Orientation Modulates R-Loop Levels and Activates Distinct DNA Damage Responses', *Cell*. *Cell*, 170(4), pp. 774–786.e19. doi: 10.1016/J.CELL.2017.07.043.

Hampsey, M. (1998) 'Molecular genetics of the RNA polymerase II general transcriptional machinery', *Microbiology and molecular biology reviews: MMBR*. *Microbiol Mol Biol Rev*, 62(2), pp. 465–503. doi: 10.1128/MMBR.62.2.465-503.1998.

Han, S. *et al.* (2020) 'LncRNA ZFPM2-AS1 promotes lung adenocarcinoma progression by interacting with UPF1 to destabilize ZFPM2', *Molecular oncology*. *Mol Oncol*, 14(5), pp. 1074–1088. doi: 10.1002/1878-0261.12631.

Hansen, K. D. *et al.* (2009) 'Genome-Wide Identification of Alternative Splice Forms Down-Regulated by Nonsense-Mediated mRNA Decay in *Drosophila*', *PLOS Genetics*. Public Library of Science, 5(6), p. e1000525. doi: 10.1371/JOURNAL.PGEN.1000525.

Harrigan, J. A. *et al.* (2011) 'Replication stress induces 53BP1-containing OPT domains in G1 cells', *Journal of Cell Biology*. The Rockefeller University Press, 193(1), pp. 97–108. doi: 10.1083/JCB.201011083.

Hartono, S. R. *et al.* (2018) 'The Affinity of the S9.6 Antibody for Double-Stranded RNAs Impacts the Accurate Mapping of R-Loops in Fission Yeast', *Journal of Molecular Biology*. Academic Press, 430(3), pp. 272–284. doi: 10.1016/J.JMB.2017.12.016.

Heller, R. C. *et al.* (2011) 'Eukaryotic Origin-Dependent DNA Replication In Vitro Reveals Sequential Action of DDK and S-CDK Kinases', *Cell*. *Cell Press*, 146(1), pp. 80–91. doi: 10.1016/J.CELL.2011.06.012.

Hellman, A. *et al.* (2000) 'Replication delay along FRA7H, a common fragile site on human chromosome 7, leads to chromosomal instability', *Molecular and cellular biology*. *Mol Cell Biol*, 20(12), pp. 4420–4427. doi: 10.1128/MCB.20.12.4420-4427.2000.

- Helmrich, A., Ballarino, M. and Tora, L. (2011) 'Collisions between Replication and Transcription Complexes Cause Common Fragile Site Instability at the Longest Human Genes', *Molecular Cell*. Cell Press, 44(6), pp. 966–977. doi: 10.1016/J.MOLCEL.2011.10.013.
- Henriques, T. *et al.* (2013) 'Stable pausing by rna polymerase II provides an opportunity to target and integrate regulatory signals', *Molecular Cell*, 52(4), pp. 517–528. doi: 10.1016/J.MOLCEL.2013.10.001.
- Hewitt, L. *et al.* (2010) 'Sustained Mps1 activity is required in mitosis to recruit O-Mad2 to the Mad1-C-Mad2 core complex', *The Journal of cell biology*. J Cell Biol, 190(1), pp. 25–34. doi: 10.1083/JCB.201002133.
- Le Hir, H. *et al.* (2000) 'The spliceosome deposits multiple proteins 20–24 nucleotides upstream of mRNA exon–exon junctions', *The EMBO Journal*. John Wiley & Sons, Ltd, 19(24), pp. 6860–6869. doi: 10.1093/EMBOJ/19.24.6860.
- Ho, C. K. and Shuman, S. (1999) 'Distinct roles for CTD Ser-2 and Ser-5 phosphorylation in the recruitment and allosteric activation of mammalian mRNA capping enzyme', *Molecular cell*. Mol Cell, 3(3), pp. 405–411. doi: 10.1016/S1097-2765(00)80468-2.
- Hogg, J. R. and Goff, S. P. (2010) 'Upf1 senses 3'UTR length to potentiate mRNA decay', *Cell*. NIH Public Access, 143(3), p. 379. doi: 10.1016/J.CELL.2010.10.005.
- Holt, I. J. (2022) 'R-Loops and Mitochondrial DNA Metabolism', *Methods in Molecular Biology*. Humana Press Inc., 2528, pp. 173–202. doi: 10.1007/978-1-0716-2477-7\_12/FIGURES/3.
- Hong, D., Park, T. and Jeong, S. (2019) 'Nuclear UPF1 Is Associated with Chromatin for Transcription-Coupled RNA Surveillance', *Molecules and Cells*. Korean Society for Molecular and Cellular Biology, 42(7), p. 523. doi: 10.14348/MOLCELLS.2019.0116.
- Van Hooser, A. *et al.* (1998) 'Histone H3 phosphorylation is required for the initiation, but not maintenance, of mammalian chromosome condensation', *Journal of Cell Science*. The Company of Biologists, 111(23), pp. 3497–3506. doi: 10.1242/JCS.111.23.3497.
- Hornig, N. C. D. *et al.* (2002) 'The dual mechanism of separase regulation by securin', *Current biology: CB*. Curr Biol, 12(12), pp. 973–982. doi: 10.1016/S0960-9822(02)00847-3.
- Howes, T. R. L. and Tomkinson, A. E. (2012) 'DNA Ligase I, the Replicative DNA Ligase', *Subcellular Biochemistry*. Springer, Dordrecht, 62, pp. 327–341. doi:

10.1007/978-94-007-4572-8\_17.

Huertas, P. and Aguilera, Andrés (2003) 'Cotranscriptionally formed DNA:RNA hybrids mediate transcription elongation impairment and transcription-associated recombination', *Molecular Cell*. Cell Press, 12(3), pp. 711–721. doi: 10.1016/j.molcel.2003.08.010.

Huertas, P. and Aguilera, Andres (2003) 'Cotranscriptionally Formed DNA:RNA Hybrids Mediate Transcription Elongation Impairment and Transcription-Associated Recombination', *Molecular cell*, 12, pp. 711–721.

Hurst, V. *et al.* (2021) 'A regulatory phosphorylation site on Mec1 controls chromatin occupancy of RNA polymerases during replication stress', *The EMBO Journal*. Springer Science and Business Media LLC, 40(21). doi: 10.15252/EMBJ.2021108439/SUPPL\_FILE/EMBJ2021108439-SUP-0016-SDATAEV.ZIP.

Ilves, I. *et al.* (2010) 'Activation of the MCM2-7 Helicase by Association with Cdc45 and GINS Proteins', *Molecular Cell*. Cell Press, 37(2), pp. 247–258. doi: 10.1016/J.MOLCEL.2009.12.030.

Imamachi, N. *et al.* (2017) 'A GC-rich sequence feature in the 3' UTR directs UPF1-dependent mRNA decay in mammalian cells', *Genome Research*. Cold Spring Harbor Laboratory Press, 27(3), pp. 407–418. doi: 10.1101/GR.206060.116/-/DC1.

Ivanov, A. *et al.* (2016) 'PABP enhances release factor recruitment and stop codon recognition during translation termination', *Nucleic acids research*. Nucleic Acids Res, 44(16), pp. 7766–7776. doi: 10.1093/NAR/GKW635.

Ivanov, P. V. *et al.* (2008) 'Interactions between UPF1, eRFs, PABP and the exon junction complex suggest an integrated model for mammalian NMD pathways', *The EMBO Journal*. John Wiley & Sons, Ltd, 27(5), pp. 736–747. doi: 10.1038/EMBOJ.2008.17.

Jayakumar, S. *et al.* (2024) 'PSIP1/LEDGF reduces R-loops at transcription sites to maintain genome integrity', *Nature Communications 2024 15:1*. Nature Publishing Group, 15(1), pp. 1–14. doi: 10.1038/s41467-023-44544-w.

Jelluma, N. *et al.* (2010) 'Release of Mps1 from kinetochores is crucial for timely anaphase onset', *Journal of Cell Biology*. The Rockefeller University Press, 191(2), pp. 281–290. doi: 10.1083/JCB.201003038/VIDEO-2.

Jeon, J. H. *et al.* (2010) 'Supercoiling induces denaturation bubbles in circular DNA', *Physical Review Letters*. American Physical Society, 105(20), p. 208101. doi:

10.1103/PHYSREVLETT.105.208101/SUPPLEMENTARY.PDF.

Ji, F. *et al.* (2020) 'Genome-wide high-resolution mapping of mitotic DNA synthesis sites and common fragile sites by direct sequencing', *Cell Research*. Springer Nature, 30(11), p. 1009. doi: 10.1038/S41422-020-0357-Y.

Jin, F. F. *et al.* (2023) 'Interaction of E2F3a and CASP8AP2 Regulates Histone Expression and Chemosensitivity of Leukemic Cells', *Journal of Pediatric Hematology/Oncology*. Lippincott Williams and Wilkins, 45(3), pp. E339–E344. doi: 10.1097/MPH.0000000000002558.

Joseph, S. A. *et al.* (2020) 'Time for remodeling: SNF2-family DNA translocases in replication fork metabolism and human disease', *DNA Repair*. Elsevier, 95, p. 102943. doi: 10.1016/J.DNAREP.2020.102943.

Joshi, R. S., Pīa, B. and Roca, J. (2010) 'Positional dependence of transcriptional inhibition by DNA torsional stress in yeast chromosomes', *EMBO Journal*. John Wiley & Sons, Ltd Chichester, UK, 29(4), pp. 740–748. doi: 10.1038/EMBOJ.2009.391/SUPPL\_FILE/EMBJ2009391.REVIEWER\_COMMENTS.PDF.

Kabeche, L. *et al.* (2018) 'A mitosis-specific and R loop-driven ATR pathway promotes faithful chromosome segregation', *Science*. American Association for the Advancement of Science, 359(6371), pp. 108–114. doi: 10.1126/SCIENCE.AAN6490/SUPPL\_FILE/AAN6490\_KABECHE\_SM.PDF.

Kadlec, J. *et al.* (2006) 'Crystal structure of the UPF2-interacting domain of nonsense-mediated mRNA decay factor UPF1', *RNA*. Cold Spring Harbor Laboratory Press, 12(10), pp. 1817–1824. doi: 10.1261/RNA.177606.

Kanaan, J. *et al.* (2018) 'UPF1-like helicase grip on nucleic acids dictates processivity', *Nature Communications 2018 9:1*. Nature Publishing Group, 9(1), pp. 1–9. doi: 10.1038/s41467-018-06313-y.

Kang, S., Warner, M. D. and Bell, S. P. (2014) 'Multiple Functions for Mcm2–7 ATPase Motifs during Replication Initiation', *Molecular Cell*. Cell Press, 55(5), pp. 655–665. doi: 10.1016/J.MOLCEL.2014.06.033.

Kang, Z. *et al.* (2024) 'm6A-modified cenRNA stabilizes CENPA to ensure centromere integrity in cancer cells', *Cell*. Elsevier, 187(21), pp. 6035-6054.e27. doi: 10.1016/J.CELL.2024.08.040.

Kashima, I. *et al.* (2006) 'Binding of a novel SMG-1-Upf1-eRF1-eRF3 complex (SURF) to the exon junction complex triggers Upf1 phosphorylation and nonsense-mediated

mRNA decay', *Genes & development*. Genes Dev, 20(3), pp. 355–367. doi: 10.1101/GAD.1389006.

Kataoka, N. *et al.* (2000) 'Pre-mRNA Splicing Imprints mRNA in the Nucleus with a Novel RNA-Binding Protein that Persists in the Cytoplasm', *Molecular Cell*. Cell Press, 6(3), pp. 673–682. doi: 10.1016/S1097-2765(00)00065-4.

Kaushal, S. *et al.* (2019) 'Sequence and Nuclease Requirements for Breakage and Healing of a Structure-Forming (AT)<sub>n</sub> Sequence within Fragile Site FRA16D', *Cell Reports*. Cell Press, 27(4), pp. 1151-1164.e5. doi: 10.1016/J.CELREP.2019.03.103.

Kaygun, H. and Marzluff, W. F. (2005) 'Regulated degradation of replication-dependent histone mRNAs requires both ATR and Upf1', *Nature Structural & Molecular Biology* 2005 12:9. Nature Publishing Group, 12(9), pp. 794–800. doi: 10.1038/nsmb972.

Khandagale, P., Thakur, S. and Acharya, N. (2020) 'Identification of PCNA-interacting protein motifs in human DNA polymerase  $\delta$ ', *Bioscience Reports*. Portland Press Ltd, 40(4), p. 20200602. doi: 10.1042/BSR20200602/222728.

Kim, M. E. and Burke, D. J. (2008) 'DNA damage activates the SAC in an ATM/ATR-dependent manner, independently of the kinetochore', *PLoS genetics*. PLoS Genet, 4(2). doi: 10.1371/JOURNAL.PGEN.1000015.

Kim, S. *et al.* (2024) 'Polyubiquitinated PCNA triggers SLX4-mediated break-induced replication in alternative lengthening of telomeres (ALT) cancer cells', *Nucleic Acids Research*. Oxford Academic, 52(19), pp. 11785–11805. doi: 10.1093/NAR/GKAE785.

Kim, Y. K. *et al.* (2005) 'Mammalian Staufen1 recruits Upf1 to specific mRNA 3'UTRs so as to elicit mRNA decay', *Cell*. Elsevier B.V., 120(2), pp. 195–208. doi: 10.1016/J.CELL.2004.11.050/ATTACHMENT/94661289-217F-4104-BEEF-5B9B3C2588D1/MMC2.PDF.

Komarnitsky, P., Cho, E. J. and Buratowski, S. (2000) 'Different phosphorylated forms of RNA polymerase II and associated mRNA processing factors during transcription', *Genes & development*. Genes Dev, 14(19), pp. 2452–2460. doi: 10.1101/GAD.824700.

Koo, C. X. G. E. *et al.* (2015) 'RNA polymerase III regulates cytosolic RNA:DNA hybrids and intracellular microRNA expression', *Journal of Biological Chemistry*. American Society for Biochemistry and Molecular Biology Inc., 290(12), pp. 7463–7473. doi: 10.1074/JBC.M115.636365/ASSET/DF83C566-A104-4491-BC08-BB437E18ED64/MAIN.ASSETS/GR9.JPG.

- Koseoglu, M. M., Dong, J. and Marzluff, W. F. (2010) 'Coordinate regulation of histone mRNA metabolism and DNA replication', *Cell Cycle*. Taylor & Francis, 9(19), pp. 3857–3863. doi: 10.4161/CC.9.19.13300.
- Kotsantis, P. *et al.* (2016) 'Increased global transcription activity as a mechanism of replication stress in cancer', *Nature Communications* 2016 7:1. Nature Publishing Group, 7(1), pp. 1–13. doi: 10.1038/ncomms13087.
- Kotsantis, P. *et al.* (2020) 'RTEL1 Regulates G4/R-Loops to Avert Replication-Transcription Collisions', *Cell reports*. Cell Rep, 33(12). doi: 10.1016/J.CELREP.2020.108546.
- Kumagai, A. *et al.* (2010) 'Treslin Collaborates with TopBP1 in Triggering the Initiation of DNA Replication', *Cell*. Elsevier B.V., 140(3), pp. 349–359. doi: 10.1016/j.cell.2009.12.049.
- Kumagai, A. *et al.* (2011) 'Direct regulation of Treslin by cyclin-dependent kinase is essential for the onset of DNA replication', *Journal of Cell Biology*. The Rockefeller University Press, 193(6), pp. 995–1007. doi: 10.1083/JCB.201102003.
- Kumar, C. *et al.* (2021) 'The interplay of RNA:DNA hybrid structure and G-quadruplexes determines the outcome of R-loop-replisome collisions', *eLife*. eLife Sciences Publications Ltd, 10, p. e72286. doi: 10.7554/ELIFE.72286.
- Kurosaki, T. *et al.* (2014) 'A post-translational regulatory switch on UPF1 controls targeted mRNA degradation', *Genes & Development*. Cold Spring Harbor Laboratory Press, 28(17), pp. 1900–1916. doi: 10.1101/GAD.245506.114.
- Lalonde, M. *et al.* (2021) 'Consequences and Resolution of Transcription–Replication Conflicts', *Life* 2021, Vol. 11, Page 637. Multidisciplinary Digital Publishing Institute, 11(7), p. 637. doi: 10.3390/LIFE11070637.
- Landsverk, H. B. *et al.* (2020) 'WDR82/PNUTS-PP1 Prevents Transcription-Replication Conflicts by Promoting RNA Polymerase II Degradation on Chromatin', *Cell reports*. Cell Rep, 33(9). doi: 10.1016/J.CELREP.2020.108469.
- Lang, K. S. *et al.* (2017) 'Replication-Transcription Conflicts Generate R-Loops that Orchestrate Bacterial Stress Survival and Pathogenesis', *Cell*. Cell Press, 170(4), pp. 787-799.e18. doi: 10.1016/J.CELL.2017.07.044/ATTACHMENT/F4B3DC86-6376-4705-9FA2-1CF30B2BB963/MMC1.PDF.
- Lang, K. S. and Merrikh, H. (2021) 'Topological stress is responsible for the detrimental outcomes of head-on replication-transcription conflicts', *Cell Reports*. Elsevier B.V., 34(9), p. 108797. doi:

10.1016/J.CELREP.2021.108797/ATTACHMENT/01A8417B-A807-4C09-A018-A71741CAAF0D/MMC2.PDF.

Langer, L. M. *et al.* (2024) 'UPF1 helicase orchestrates mutually exclusive interactions with the SMG6 endonuclease and UPF2', *Nucleic Acids Research*. Oxford Academic, 52(10), pp. 6036–6048. doi: 10.1093/NAR/GKAE323.

Lee, Y. *et al.* (2004) 'MicroRNA genes are transcribed by RNA polymerase II', *The EMBO journal*. EMBO J, 23(20), pp. 4051–4060. doi: 10.1038/SJ.EMBOJ.7600385.

Leeds, P. *et al.* (1991) 'The product of the yeast UPF1 gene is required for rapid turnover of mRNAs containing a premature translational termination codon.', *Genes & Development*. Cold Spring Harbor Laboratory Press, 5(12a), pp. 2303–2314. doi: 10.1101/GAD.5.12A.2303.

Legros, P. *et al.* (2014) 'RNA Processing Factors Swd2.2 and Sen1 Antagonize RNA Pol III-Dependent Transcription and the Localization of Condensin at Pol III Genes', *PLOS Genetics*. Public Library of Science, 10(11), p. e1004794. doi: 10.1371/JOURNAL.PGEN.1004794.

Letessier, A. *et al.* (2011) 'Cell-type-specific replication initiation programs set fragility of the FRA3B fragile site', *Nature*. Nature, 470(7332), pp. 120–124. doi: 10.1038/NATURE09745.

Lew, J. E., Enomoto, S. and Berman, J. (1998) 'Telomere Length Regulation and Telomeric Chromatin Require the Nonsense-Mediated mRNA Decay Pathway', *Molecular and Cellular Biology*. American Society for Microbiology, 18(10), pp. 6121–6130. doi: 10.1128/MCB.18.10.6121/FORMAT/EPUB.

Lewis, B. P., Green, R. E. and Brenner, S. E. (2003) 'Evidence for the widespread coupling of alternative splicing and nonsense-mediated mRNA decay in humans', *Proceedings of the National Academy of Sciences of the United States of America*. National Academy of Sciences, 100(1), pp. 189–192. doi: 10.1073/PNAS.0136770100/SUPPL\_FILE/6770TABLE1.TXT.

Li, C. *et al.* (2020) 'TOP1 $\alpha$ , UPF1, and TTG2 regulate seed size in a parental dosage-dependent manner', *PLOS Biology*. Public Library of Science, 18(11), p. e3000930. doi: 10.1371/JOURNAL.PBIO.3000930.

Li, L. *et al.* (2024) 'Loss of Fbxo45 in AT2 cells leads to insufficient histone supply and initiates lung adenocarcinoma', *Cell Death & Differentiation 2024*. Nature Publishing Group, pp. 1–21. doi: 10.1038/s41418-024-01433-z.

Li, N. *et al.* (2018) 'Structure of the origin recognition complex bound to DNA

- replication origin', *Nature* 2018 559:7713. Nature Publishing Group, 559(7713), pp. 217–222. doi: 10.1038/s41586-018-0293-x.
- Li, X. and Manley, J. L. (2005) 'Inactivation of the SR Protein Splicing Factor ASF/SF2 Results in Genomic Instability', *Cell*. Cell Press, 122(3), pp. 365–378. doi: 10.1016/J.CELL.2005.06.008.
- Li, X. Z. *et al.* (2013) 'An ancient transcription factor initiates the burst of piRNA production during early meiosis in mouse testes', *Molecular cell*. Mol Cell, 50(1), pp. 67–81. doi: 10.1016/J.MOLCEL.2013.02.016.
- Li, Y. *et al.* (2022) 'LncRNA SNHG5 promotes the proliferation and cancer stem cell-like properties of HCC by regulating UPF1 and Wnt-signaling pathway', *Cancer Gene Therapy* 2022. Nature Publishing Group, pp. 1–11. doi: 10.1038/s41417-022-00456-3.
- Liang, K. *et al.* (2015) 'Mitotic Transcriptional Activation: Clearance of Actively Engaged Pol II via Transcriptional Elongation Control in Mitosis', *Molecular Cell*. Cell Press, 60(3), pp. 435–445. doi: 10.1016/J.MOLCEL.2015.09.021/ATTACHMENT/84BFF6A2-F1D8-494E-AE43-D247CC2427BE/MMC6.PDF.
- Ligasová, A. and Koberna, K. (2021) 'Strengths and Weaknesses of Cell Synchronization Protocols Based on Inhibition of DNA Synthesis', *International Journal of Molecular Sciences*. MDPI, 22(19), p. 10759. doi: 10.3390/IJMS221910759.
- Lilley, D. M. (1980) 'The inverted repeat as a recognizable structural feature in supercoiled DNA molecules', *Proceedings of the National Academy of Sciences of the United States of America*. Proc Natl Acad Sci U S A, 77(11), pp. 6468–6472. doi: 10.1073/PNAS.77.11.6468.
- Lischetti, T. *et al.* (2014) 'The internal Cdc20 binding site in BubR1 facilitates both spindle assembly checkpoint signalling and silencing', *Nature communications*. Nat Commun, 5. doi: 10.1038/NCOMMS6563.
- Liu, H. *et al.* (2015) 'Mitotic Transcription Installs Sgo1 at Centromeres to Coordinate Chromosome Segregation', *Molecular cell*. Mol Cell, 59(3), pp. 426–436. doi: 10.1016/J.MOLCEL.2015.06.018.
- Liu, J., Ali, M. and Zhou, Q. (2020) 'Establishment and evolution of heterochromatin', *Annals of the New York Academy of Sciences*. John Wiley & Sons, Ltd, 1476(1), pp. 59–77. doi: 10.1111/NYAS.14303.
- Liu, L. F. and Wang, J. C. (1987) 'Supercoiling of the DNA template during

transcription.’, *Proceedings of the National Academy of Sciences*. Proceedings of the National Academy of Sciences, 84(20), pp. 7024–7027. doi: 10.1073/PNAS.84.20.7024.

Liu, Z. S. *et al.* (2024) ‘R-Loop Accumulation in Spliceosome Mutant Leukemias Confers Sensitivity to PARP1 Inhibition by Triggering Transcription–Replication Conflicts’, *Cancer Research*. American Association for Cancer Research Inc., 84(4), pp. 577–597. doi: 10.1158/0008-5472.CAN-23-3239/730129/AM/R-LOOP-ACCUMULATION-IN-SPLICEOSOME-MUTANT.

Llorca-Cardenosa, M. J. *et al.* (2022) ‘SMG8/SMG9 Heterodimer Loss Modulates SMG1 Kinase to Drive ATR Inhibitor Resistance’, *Cancer Research*. American Association for Cancer Research Inc., 82(21), pp. 3962–3973. doi: 10.1158/0008-5472.CAN-21-4339/709910/P/SMG8-SMG9-HETERODIMER-LOSS-MODULATES-SMG1-KINASE.

Loh, B., Jonas, S. and Izaurralde, E. (2013) ‘The SMG5–SMG7 heterodimer directly recruits the CCR4–NOT deadenylase complex to mRNAs containing nonsense codons via interaction with POP2’, *Genes & Development*. Cold Spring Harbor Laboratory Press, 27(19), pp. 2125–2138. doi: 10.1101/GAD.226951.113.

Lopes, J. *et al.* (2011) ‘G-quadruplex-induced instability during leading-strand replication’, *EMBO Journal*. John Wiley & Sons, Ltd Chichester, UK, 30(19), pp. 4033–4046. doi: 10.1038/EMBOJ.2011.316/SUPPL\_FILE/EMBJ2011316.REVIEWER\_COMMENTS.PDF.

Lukas, C. *et al.* (2011) ‘53BP1 nuclear bodies form around DNA lesions generated by mitotic transmission of chromosomes under replication stress’, *Nature Cell Biology* 2011 13:3. Nature Publishing Group, 13(3), pp. 243–253. doi: 10.1038/ncb2201.

Luo, H. *et al.* (2022) ‘HOTTIP-dependent R-loop formation regulates CTCF boundary activity and TAD integrity in leukemia’, *Molecular Cell*. Cell Press, 82(4), pp. 833–851.e11. doi: 10.1016/J.MOLCEL.2022.01.014.

Macheret, M. *et al.* (2020) ‘High-resolution mapping of mitotic DNA synthesis regions and common fragile sites in the human genome through direct sequencing’, *Cell Research* 2020 30:11. Nature Publishing Group, 30(11), pp. 997–1008. doi: 10.1038/s41422-020-0358-x.

Malik, K. K. *et al.* (2023) ‘MLL methyltransferases regulate H3K4 methylation to ensure CENP-A assembly at human centromeres’, *PLOS Biology*. Public Library of Science,

21(6), p. e3002161. doi: 10.1371/JOURNAL.PBIO.3002161.

Marchal, C., Sima, J. and Gilbert, D. M. (2019) 'Control of DNA replication timing in the 3D genome', *Nature reviews. Molecular cell biology*. Nat Rev Mol Cell Biol, 20(12), pp. 721–737. doi: 10.1038/S41580-019-0162-Y.

Martínez-Balbás, M. A. *et al.* (1995) 'Displacement of sequence-specific transcription factors from mitotic chromatin', *Cell*. Cell Press, 83(1), pp. 29–38. doi: 10.1016/0092-8674(95)90231-7.

Massé, E. and Drolet, M. (1999) 'Escherichia coli DNA topoisomerase I inhibits R-loop formation by relaxing transcription-induced negative supercoiling', *The Journal of biological chemistry*. J Biol Chem, 274(23), pp. 16659–16664. doi: 10.1074/JBC.274.23.16659.

Masuda-Sasa, T., Imamura, O. and Campbell, J. L. (2006) 'Biochemical analysis of human Dna2', *Nucleic Acids Research*. Oxford Academic, 34(6), pp. 1865–1875. doi: 10.1093/NAR/GKL070.

Matsuoka, S. *et al.* (2007) 'ATM and ATR substrate analysis reveals extensive protein networks responsive to DNA damage', *Science*. American Association for the Advancement of Science, 316(5828), pp. 1160–1166. doi: 10.1126/SCIENCE.1140321/SUPPL\_FILE/MATSUOKA.SOM.PDF.

McCann, J. J. *et al.* (2023) 'Participation of ATM, SMG1, and DDX5 in a DNA Damage-Induced Alternative Splicing Pathway', <https://doi.org/10.1667/RADE-22-00219.1>. Radiation Research Society, 199(4), pp. 406–421. doi: 10.1667/RADE-22-00219.1.

McNulty, S. M., Sullivan, L. L. and Sullivan, B. A. (2017) 'Human Centromeres Produce Chromosome-Specific and Array-Specific Alpha Satellite Transcripts that Are Complexed with CENP-A and CENP-C', *Developmental Cell*. Cell Press, 42(3), pp. 226-240.e6. doi: 10.1016/J.DEVCEL.2017.07.001/ATTACHMENT/8F3700DE-F9BA-46B0-A9E0-21B7E79EAB84/MMC1.PDF.

Meaux, S. A., Holmquist, C. E. and Marzluff, W. F. (2018) 'Role of oligouridylation in normal metabolism and regulated degradation of mammalian histone mRNAs', *Philosophical Transactions of the Royal Society B: Biological Sciences*. The Royal Society, 373(1762). doi: 10.1098/RSTB.2018.0170.

Medghalchi, S. M. *et al.* (2001) 'Rent1, a trans-effector of nonsense-mediated mRNA decay, is essential for mammalian embryonic viability', *Human Molecular Genetics*. Oxford Academic, 10(2), pp. 99–105. doi: 10.1093/HMG/10.2.99.

Mei, Q. *et al.* (2017) 'Regulation of DNA replication-coupled histone gene expression',

- Oncotarget*. Impact Journals, 8(55), pp. 95005–95022. doi: 10.18632/ONCOTARGET.21887.
- Mejlvang, J. *et al.* (2014) 'New histone supply regulates replication fork speed and PCNA unloading', *The Journal of Cell Biology*, 204(1), p. 29. doi: 10.1083/JCB.201305017.
- Mena, A. L., Lam, E. W. F. and Chatterjee, S. (2010) 'Sustained Spindle-Assembly Checkpoint Response Requires De Novo Transcription and Translation of Cyclin B1', *PLOS ONE*. Public Library of Science, 5(9), p. e13037. doi: 10.1371/JOURNAL.PONE.0013037.
- Merrikh, H. *et al.* (2011) 'Co-directional replication–transcription conflicts lead to replication restart', *Nature 2011 470:7335*. Nature Publishing Group, 470(7335), pp. 554–557. doi: 10.1038/nature09758.
- Meryet-Figuere, M. *et al.* (2014) 'Temporal separation of replication and transcription during S-phase progression', *Cell cycle (Georgetown, Tex.)*. Cell Cycle, 13(20), pp. 3241–3248. doi: 10.4161/15384101.2014.953876.
- Minocherhomji, S. *et al.* (2015) 'Replication stress activates DNA repair synthesis in mitosis', *Nature*. Nature, 528(7581), pp. 286–290. doi: 10.1038/NATURE16139.
- Mirkin, S. M. *et al.* (1987) 'DNA H form requires a homopurine-homopyrimidine mirror repeat', *Nature*. Nature, 330(6147), pp. 495–497. doi: 10.1038/330495A0.
- Mischo, H. E. *et al.* (2011) 'Yeast Sen1 helicase protects the genome from transcription-associated instability', *Molecular cell*. Mol Cell, 41(1), pp. 21–32. doi: 10.1016/J.MOLCEL.2010.12.007.
- Mocanu, C. *et al.* (2022) 'DNA replication is highly resilient and persistent under the challenge of mild replication stress', *Cell Reports*. Elsevier B.V., 39(3). doi: 10.1016/J.CELREP.2022.110701/ATTACHMENT/934A0B4B-54E1-4CE3-8A7C-70F9E6A6C774/MMC1.PDF.
- Moreno, S. P. *et al.* (2019) 'Mitotic replisome disassembly depends on TRAIIP ubiquitin ligase activity', *Life science alliance*. Life Sci Alliance, 2(2). doi: 10.26508/LSA.201900390.
- Morris, D. P., Michelotti, G. A. and Schwinn, D. A. (2005) 'Evidence that phosphorylation of the RNA polymerase II carboxyl-terminal repeats is similar in yeast and humans', *The Journal of biological chemistry*. J Biol Chem, 280(36), pp. 31368–31377. doi: 10.1074/JBC.M501546200.
- Morrison, O. and Thakur, J. (2021) 'Molecular Complexes at Euchromatin,

Heterochromatin and Centromeric Chromatin', *International Journal of Molecular Sciences* 2021, Vol. 22, Page 6922. Multidisciplinary Digital Publishing Institute, 22(13), p. 6922. doi: 10.3390/IJMS22136922.

Moyer, S. E., Lewis, P. W. and Botchan, M. R. (2006) 'Isolation of the Cdc45/Mcm2-7/GINS (CMG) complex, a candidate for the eukaryotic DNA replication fork helicase', *Proceedings of the National Academy of Sciences of the United States of America*. National Academy of Sciences, 103(27), pp. 10236–10241. doi: 10.1073/PNAS.0602400103/SUPPL\_FILE/02400TABLE2.PDF.

Mukhopadhyay, P. *et al.* (2024) 'Approaches for Mapping and Analysis of R-loops', *Current Protocols*. John Wiley & Sons, Ltd, 4(4), p. e1037. doi: 10.1002/CPZ1.1037.

Müller, B. *et al.* (2007) 'DNA-activated protein kinase functions in a newly observed S phase checkpoint that links histone mRNA abundance with DNA replication', *The Journal of Cell Biology*. The Rockefeller University Press, 179(7), p. 1385. doi: 10.1083/JCB.200708106.

Musacchio, A. and Salmon, E. D. (2007) 'The spindle-assembly checkpoint in space and time', *Nature reviews. Molecular cell biology*. Nat Rev Mol Cell Biol, 8(5), pp. 379–393. doi: 10.1038/NRM2163.

Naim, V. *et al.* (2013) 'ERCC1 and MUS81–EME1 promote sister chromatid separation by processing late replication intermediates at common fragile sites during mitosis', *Nature Cell Biology* 2013 15:8. Nature Publishing Group, 15(8), pp. 1008–1015. doi: 10.1038/ncb2793.

Natsume, T. and Tanaka, T. U. (2010) 'Spatial regulation and organization of DNA replication within the nucleus', *Chromosome research : an international journal on the molecular, supramolecular and evolutionary aspects of chromosome biology*. Chromosome Res, 18(1), pp. 7–17. doi: 10.1007/S10577-009-9088-0.

Ngo, G. H. P., Grimstead, J. W. and Baird, D. M. (2021) 'UPF1 promotes the formation of R loops to stimulate DNA double-strand break repair', *Nature Communications* 2021 12:1. Nature Publishing Group, 12(1), pp. 1–15. doi: 10.1038/s41467-021-24201-w.

Nickless, A. *et al.* (2017) 'p38 MAPK inhibits nonsense-mediated RNA decay in response to persistent DNA damage in noncycling cells', *Journal of Biological Chemistry*. Elsevier, 292(37), pp. 15266–15276. doi: 10.1074/JBC.M117.787846.

Nishimura, K. *et al.* (2009) 'An auxin-based degron system for the rapid depletion of proteins in nonplant cells', *Nature Methods* 2009 6:12. Nature Publishing Group, 6(12), pp. 917–922. doi: 10.1038/nmeth.1401.

Nitta, M. *et al.* (2004) 'Spindle checkpoint function is required for mitotic catastrophe induced by DNA-damaging agents', *Oncogene* 2004 23:39. Nature Publishing Group, 23(39), pp. 6548–6558. doi: 10.1038/sj.onc.1207873.

Novais-Cruz, M. *et al.* (2018) 'Mitotic progression, arrest, exit or death relies on centromere structural integrity, rather than de novo transcription', *eLife*. eLife Sciences Publications Ltd, 7. doi: 10.7554/ELIFE.36898.

O'Leary, P. C. *et al.* (2022) 'Resistance to ATR Inhibitors Is Mediated by Loss of the Nonsense-Mediated Decay Factor UPF2', *Cancer Research*. American Association for Cancer Research (AACR), 82(21), pp. 3950–3961. doi: 10.1158/0008-5472.CAN-21-4335/709911/P/RESISTANCE-TO-ATR-INHIBITORS-IS-MEDIATED-BY-LOSS.

Oh, J. M. and Myung, K. (2022) 'Crosstalk between different DNA repair pathways for DNA double strand break repairs', *Mutation Research/Genetic Toxicology and Environmental Mutagenesis*. Elsevier, 873, p. 503438. doi: 10.1016/J.MRGENTOX.2021.503438.

Ohnishi, T. *et al.* (2003) 'Phosphorylation of hUPF1 induces formation of mRNA surveillance complexes containing hSMG-5 and hSMG-7', *Molecular cell*. Mol Cell, 12(5), pp. 1187–1200. doi: 10.1016/S1097-2765(03)00443-X.

Oricchio, E. *et al.* (2006) 'ATM is Activated by Default in Mitosis, Localizes at Centrosomes and Monitors Mitotic Spindle Integrity', *Cell Cycle*. Taylor & Francis, 5(1), pp. 88–92. doi: 10.4161/CC.5.1.2269.

Palacios, I. M. *et al.* (2004) 'An eIF4AIII-containing complex required for mRNA localization and nonsense-mediated mRNA decay', *Nature* 2004 427:6976. Nature Publishing Group, 427(6976), pp. 753–757. doi: 10.1038/nature02351.

Pan, Q. *et al.* (2025) 'The SETDB1-PC4-UPF1 post-transcriptional machinery controls periodic degradation of CENPF mRNA and maintains mitotic progression', *Cell Death & Differentiation* 2025. Nature Publishing Group, pp. 1–15. doi: 10.1038/s41418-025-01465-z.

Panayotatos, N. and Wells, R. D. (1981) 'Cruciform structures in supercoiled DNA', *Nature*. Nature, 289(5797), pp. 466–470. doi: 10.1038/289466A0.

Park, S. H. *et al.* (2021) 'Locus-specific transcription silencing at the FHIT gene suppresses replication stress-induced copy number variant formation and associated replication delay', *Nucleic Acids Research*. Oxford Academic, 49(13), pp. 7507–7524. doi: 10.1093/NAR/GKAB559.

Paul, P. K. *et al.* (2016) 'Histone chaperone ASF1B promotes human  $\beta$ -cell

proliferation via recruitment of histone H3.3', *Cell Cycle*. Taylor & Francis, 15(23), pp. 3191–3202. doi: 10.1080/15384101.2016.1241914.

Paulsen, R. D. *et al.* (2009) 'A genome-wide siRNA screen reveals diverse cellular processes and pathways that mediate genome stability', *Molecular cell*. Mol Cell, 35(2), pp. 228–239. doi: 10.1016/J.MOLCEL.2009.06.021.

Pedersen, R. T. *et al.* (2015) 'TopBP1 is required at mitosis to reduce transmission of DNA damage to G1 daughter cells', *Journal of Cell Biology*. The Rockefeller University Press, 210(4), pp. 565–582. doi: 10.1083/JCB.201502107.

Petermann, E. *et al.* (2010) 'Hydroxyurea-Stalled Replication Forks Become Progressively Inactivated and Require Two Different RAD51-Mediated Pathways for Restart and Repair', *Molecular Cell*. Cell Press, 37(4), pp. 492–502. doi: 10.1016/J.MOLCEL.2010.01.021.

Petermann, E., Lan, L. and Zou, L. (2022) 'Sources, resolution and physiological relevance of R-loops and RNA–DNA hybrids', *Nature Reviews Molecular Cell Biology* 2022 23:8. Nature Publishing Group, 23(8), pp. 521–540. doi: 10.1038/s41580-022-00474-x.

Petropoulos, M. *et al.* (2024) 'Transcription–replication conflicts underlie sensitivity to PARP inhibitors', *Nature* 2024 628:8007. Nature Publishing Group, 628(8007), pp. 433–441. doi: 10.1038/s41586-024-07217-2.

Pfeiffer, V. *et al.* (2013) 'The THO complex component Thp2 counteracts telomeric R-loops and telomere shortening', *The EMBO Journal*. John Wiley & Sons, Ltd, 32(21), pp. 2861–2871. doi: 10.1038/EMBOJ.2013.217.

Phatnani, H. P. and Greenleaf, A. L. (2006) 'Phosphorylation and functions of the RNA polymerase II CTD', *Genes & development*. Genes Dev, 20(21), pp. 2922–2936. doi: 10.1101/GAD.1477006.

Phillips, D. D. *et al.* (2013) 'The sub-nanomolar binding of DNA–RNA hybrids by the single-chain Fv fragment of antibody S9.6', *Journal of Molecular Recognition*. John Wiley & Sons, Ltd, 26(8), pp. 376–381. doi: 10.1002/JMR.2284.

Pinto, L. M. *et al.* (2024) 'DAXX promotes centromeric stability independently of ATRX by preventing the accumulation of R-loop-induced DNA double-stranded breaks', *Nucleic Acids Research*. Oxford Academic, 52(3), pp. 1136–1155. doi: 10.1093/NAR/GKAD1141.

Poli, J. *et al.* (2016) 'Mec1, INO80, and the PAF1 complex cooperate to limit transcription replication conflicts through RNAPII removal during replication stress',

*Genes & development*. *Genes Dev*, 30(3), pp. 337–354. doi: 10.1101/GAD.273813.115.

Pomerantz, R. T. and O'Donnell, M. (2008) 'The replisome uses mRNA as a primer after colliding with RNA polymerase', *Nature* 2008 456:7223. Nature Publishing Group, 456(7223), pp. 762–766. doi: 10.1038/nature07527.

Pommier, Y. *et al.* (2022) 'Human topoisomerases and their roles in genome stability and organization', *Nature Reviews Molecular Cell Biology* 2022 23:6. Nature Publishing Group, 23(6), pp. 407–427. doi: 10.1038/s41580-022-00452-3.

Poole, L. A. and Cortez, D. (2017) 'Functions of SMARCAL1, ZRANB3, and HLTF in maintaining genome stability', *Critical Reviews in Biochemistry and Molecular Biology*. Taylor & Francis, 52(6), pp. 696–714. doi: 10.1080/10409238.2017.1380597.

Porro, A. *et al.* (2010) 'Molecular dissection of telomeric repeat-containing RNA biogenesis unveils the presence of distinct and multiple regulatory pathways', *Molecular and cellular biology*. *Mol Cell Biol*, 30(20), pp. 4808–4817. doi: 10.1128/MCB.00460-10.

Porro, A. *et al.* (2014) 'Functional characterization of the TERRA transcriptome at damaged telomeres', *Nature Communications* 2014 5:1. Nature Publishing Group, 5(1), pp. 1–13. doi: 10.1038/ncomms6379.

Primorac, I. *et al.* (2013) 'Bub3 reads phosphorylated MELT repeats to promote spindle assembly checkpoint signaling', *eLife*. eLife Sciences Publications, Ltd, 2(2), p. 1030. doi: 10.7554/ELIFE.01030.

Primorac, I. and Musacchio, A. (2013) 'Panta rhei: The APC/C at steady state', *Journal of Cell Biology*. The Rockefeller University Press, 201(2), pp. 177–189. doi: 10.1083/JCB.201301130.

Promonet, A. *et al.* (2020) 'Topoisomerase 1 prevents replication stress at R-loop-enriched transcription termination sites', *Nature Communications* 2020 11:1. Nature Publishing Group, 11(1), pp. 1–12. doi: 10.1038/s41467-020-17858-2.

Racca, C. *et al.* (2021) 'BRCA1 prevents R-loop-associated centromeric instability', *Cell Death & Disease* 2021 12:10. Nature Publishing Group, 12(10), pp. 1–11. doi: 10.1038/s41419-021-04189-3.

Rao, S. *et al.* (2024) 'Senataxin RNA/DNA helicase promotes replication restart at co-transcriptional R-loops to prevent MUS81-dependent fork degradation', *Nucleic Acids Research*. Oxford Academic, 52(17), pp. 10355–10369. doi: 10.1093/NAR/GKAE673.

Ray Chaudhuri, A. *et al.* (2012) 'Topoisomerase I poisoning results in PARP-mediated

replication fork reversal', *Nature Structural & Molecular Biology* 2012 19:4. Nature Publishing Group, 19(4), pp. 417–423. doi: 10.1038/nsmb.2258.

Razin, S. V. *et al.* (2011) 'Transcription factories in the context of the nuclear and genome organization', *Nucleic acids research*. Nucleic Acids Res, 39(21), pp. 9085–9092. doi: 10.1093/NAR/GKR683.

Rehwinkel, J. *et al.* (2005) 'Nonsense-mediated mRNA decay factors act in concert to regulate common mRNA targets', *RNA*. Cold Spring Harbor Laboratory Press, 11(10), pp. 1530–1544. doi: 10.1261/RNA.2160905.

Reuswig, K. U. *et al.* (2022) 'Unscheduled DNA replication in G1 causes genome instability and damage signatures indicative of replication collisions', *Nature Communications* 2022 13:1. Nature Publishing Group, 13(1), pp. 1–20. doi: 10.1038/s41467-022-34379-2.

Ribeiro de Almeida, C. *et al.* (2018) 'RNA Helicase DDX1 Converts RNA G-Quadruplex Structures into R-Loops to Promote IgH Class Switch Recombination', *Molecular Cell*. Cell Press, 70(4), pp. 650-662.e8. doi: 10.1016/J.MOLCEL.2018.04.001.

Rivera-Mulia, J. C. and Gilbert, D. M. (2016) 'Replication timing and transcriptional control: beyond cause and effect-part III', *Current opinion in cell biology*. Curr Opin Cell Biol, 40, pp. 168–178. doi: 10.1016/J.CEB.2016.03.022.

Rojas, P. *et al.* (2024) 'Genome-wide identification of replication fork stalling/pausing sites and the interplay between RNA Pol II transcription and DNA replication progression', *Genome Biology*. BioMed Central Ltd, 25(1), pp. 1–28. doi: 10.1186/S13059-024-03278-8/FIGURES/5.

Ruiz-Gutierrez, N. *et al.* (2025) 'RNA anchoring of Upf1 facilitates recruitment of Dcp2 in the NMD decapping complex', *Nucleic Acids Research*. Oxford Academic, 53(5), pp. 13–14. doi: 10.1093/NAR/GKAF160.

Ryu, I. *et al.* (2019) 'eIF4A3 Phosphorylation by CDKs Affects NMD during the Cell Cycle', *Cell Reports*. Cell Press, 26(8), pp. 2126-2139.e9. doi: 10.1016/J.CELREP.2019.01.101.

Said, M. *et al.* (2022) 'FANCD2 promotes mitotic rescue from transcription-mediated replication stress in SETX-deficient cancer cells', *Communications Biology* 2022 5:1. Nature Publishing Group, 5(1), pp. 1–13. doi: 10.1038/s42003-022-04360-2.

Sanchez, A. *et al.* (2020) 'Transcription-replication conflicts as a source of common fragile site instability caused by BMI1-RNF2 deficiency', *PLoS Genetics*. Public Library

of Science, 16(3), p. e1008524. doi: 10.1371/JOURNAL.PGEN.1008524.

Santos-Pereira, J. M. and Aguilera, A. (2015) 'R loops: new modulators of genome dynamics and function', *Nature Reviews Genetics* 2015 16:10. Nature Publishing Group, 16(10), pp. 583–597. doi: 10.1038/nrg3961.

Saponaro, M. *et al.* (2014) 'RECQL5 controls transcript elongation and suppresses genome instability associated with transcription stress', *Cell*. Elsevier B.V., 157(5), pp. 1037–1049. doi: 10.1016/J.CELL.2014.03.048/ATTACHMENT/521B3ED4-2068-43DB-A839-F4CA30B02F3C/MMC5.PDF.

Shih, H. T. *et al.* (2022) 'DNMT3b protects centromere integrity by restricting R-loop-mediated DNA damage', *Cell Death & Disease* 2022 13:6. Nature Publishing Group, 13(6), pp. 1–14. doi: 10.1038/s41419-022-04989-1.

Šiková, M. *et al.* (2020) 'The torpedo effect in *Bacillus subtilis*: RNase J1 resolves stalled transcription complexes', *The EMBO Journal*. Springer Science and Business Media LLC, 39(3). doi: 10.15252/EMBJ.2019102500/SUPPL\_FILE/EMBJ2019102500-SUP-0018-SDATAEV.ZIP.

Silva, B. *et al.* (2021) 'TERRA transcription destabilizes telomere integrity to initiate break-induced replication in human ALT cells', *Nature Communications* 2021 12:1. Nature Publishing Group, 12(1), pp. 1–12. doi: 10.1038/s41467-021-24097-6.

Sinai, M. I. T. *et al.* (2019) 'AT-dinucleotide rich sequences drive fragile site formation', *Nucleic Acids Research*. Oxford Academic, 47(18), pp. 9685–9695. doi: 10.1093/NAR/GKZ689.

Singh, A. K. *et al.* (2019) 'The RNA helicase UPF1 associates with mRNAs co-transcriptionally and is required for the release of mRNAs from gene loci', *eLife*. eLife Sciences Publications Ltd, 8. doi: 10.7554/ELIFE.41444.

Singh, R. K. *et al.* (2009) 'Histone levels are regulated by phosphorylation and ubiquitylation-dependent proteolysis', *Nature Cell Biology* 2009 11:8. Nature Publishing Group, 11(8), pp. 925–933. doi: 10.1038/ncb1903.

Singh, R. K., Paik, J. and Gunjan, A. (2011) *Histones: Dosage and Degradation, Epigenetics: A Reference Manual*. Available at: <https://www.caister.com/hsp/abstracts/epigenetics/09.html> (Accessed: 26 March 2025).

Skourti-Stathaki, K., Kamieniarz-Gdula, K. and Proudfoot, N. J. (2014) 'R-loops induce repressive chromatin marks over mammalian gene terminators', *Nature* 2014

516:7531. Nature Publishing Group, 516(7531), pp. 436–439. doi: 10.1038/nature13787.

Smits, V. A. J. *et al.* (2000) 'Polo-like kinase-1 is a target of the DNA damage checkpoint', *Nature Cell Biology* 2000 2:9. Nature Publishing Group, 2(9), pp. 672–676. doi: 10.1038/35023629.

Smolka, J. A. *et al.* (2021) 'Recognition of RNA by the S9.6 antibody creates pervasive artifacts when imaging RNA:DNA hybrids', *The Journal of cell biology*. J Cell Biol, 220(6). doi: 10.1083/JCB.202004079.

Snow, B. E. *et al.* (2003) 'Functional Conservation of the Telomerase Protein Est1p in Humans', *Current Biology*. Cell Press, 13(8), pp. 698–704. doi: 10.1016/S0960-9822(03)00210-0.

Sollier, J. *et al.* (2014) 'Transcription-Coupled Nucleotide Excision Repair Factors Promote R-Loop-Induced Genome Instability', *Molecular Cell*. Cell Press, 56(6), pp. 777–785. doi: 10.1016/j.molcel.2014.10.020.

Sonneville, R. *et al.* (2019) 'TRAIP drives replisome disassembly and mitotic DNA repair synthesis at sites of incomplete DNA replication', *eLife*. eLife Sciences Publications Ltd, 8. doi: 10.7554/ELIFE.48686.

Spies, J. *et al.* (2019) '53BP1 nuclear bodies enforce replication timing at under-replicated DNA to limit heritable DNA damage', *Nature Cell Biology* 2019 21:4. Nature Publishing Group, 21(4), pp. 487–497. doi: 10.1038/s41556-019-0293-6.

St Germain, C., Zhao, H. and Barlow, J. H. (2021) 'Transcription-Replication Collisions—A Series of Unfortunate Events', *Biomolecules* 2021, Vol. 11, Page 1249. Multidisciplinary Digital Publishing Institute, 11(8), p. 1249. doi: 10.3390/BIOM11081249.

Stodola, J. L. and Burgers, P. M. (2017) 'Mechanism of Lagging-Strand DNA Replication in Eukaryotes', *Advances in Experimental Medicine and Biology*. Springer, Singapore, 1042, pp. 117–133. doi: 10.1007/978-981-10-6955-0\_6.

Stojic, L. *et al.* (2020) 'A high-content RNAi screen reveals multiple roles for long noncoding RNAs in cell division', *Nature Communications* 2020 11:1. Nature Publishing Group, 11(1), pp. 1–21. doi: 10.1038/s41467-020-14978-7.

Stolz, R. *et al.* (2019) 'Interplay between DNA sequence and negative superhelicity drives R-loop structures', *Proceedings of the National Academy of Sciences of the United States of America*. Proc Natl Acad Sci U S A, 116(13), pp. 6260–6269. doi: 10.1073/PNAS.1819476116.

- Stork, C. T. *et al.* (2016) 'Co-transcriptional R-loops are the main cause of estrogen-induced DNA damage', *eLife*. eLife Sciences Publications Ltd, 5(AUGUST). doi: 10.7554/ELIFE.17548.
- Stracker, T. H. (2024) 'Regulation of p53 by the mitotic surveillance/stopwatch pathway: implications in neurodevelopment and cancer', *Frontiers in Cell and Developmental Biology*. Frontiers Media SA, 12, p. 1451274. doi: 10.3389/FCELL.2024.1451274/ENDNOTE.
- Strobino, M. *et al.* (2020) 'Loss of histone H3.3 results in DNA replication defects and altered origin dynamics in *C. elegans*', *Genome Research*. Cold Spring Harbor Laboratory Press, 31(12), pp. 1740–1751. doi: 10.1101/GR.260794.120/-/DC1.
- Sugimoto, N. *et al.* (2018) 'Genome-wide analysis of the spatiotemporal regulation of firing and dormant replication origins in human cells', *Nucleic Acids Research*. Oxford Academic, 46(13), pp. 6683–6696. doi: 10.1093/NAR/GKY476.
- Sullivan, K. D. *et al.* (2009) 'Knockdown of SLBP results in nuclear retention of histone mRNA', *RNA*. Cold Spring Harbor Laboratory Press, 15(3), pp. 459–472. doi: 10.1261/RNA.1205409.
- Šviković, S. *et al.* (2019) 'R-loop formation during S phase is restricted by PrimPol-mediated repriming', *The EMBO journal*. EMBO J, 38(3). doi: 10.15252/EMBJ.201899793.
- Técher, H. *et al.* (2013) 'Replication Dynamics: Biases and Robustness of DNA Fiber Analysis', *Journal of Molecular Biology*. Academic Press, 425(23), pp. 4845–4855. doi: 10.1016/J.JMB.2013.03.040.
- Thangavel, S. *et al.* (2015) 'DNA2 drives processing and restart of reversed replication forks in human cells', *Journal of Cell Biology*. The Rockefeller University Press, 208(5), pp. 545–562. doi: 10.1083/JCB.201406100.
- Thompson, R. *et al.* (2015) 'An Inhibitor of PIDDosome Formation', *Molecular Cell*. Cell Press, 58(5), pp. 767–779. doi: 10.1016/J.MOLCEL.2015.03.034/ATTACHMENT/580F0F94-6E76-4E8B-A36A-5F6B8A70BC3D/MMC1.PDF.
- Torres-Rosell, J. *et al.* (2007) 'Anaphase onset before complete DNA replication with intact checkpoint responses', *Science*. American Association for the Advancement of Science, 315(5817), pp. 1411–1415. doi: 10.1126/SCIENCE.1134025/SUPPL\_FILE/TORRES-ROSSELL.SOM.PDF.
- Treangen, T. J. and Salzberg, S. L. (2011) 'Repetitive DNA and next-generation

sequencing: computational challenges and solutions', *Nature reviews. Genetics*. Nat Rev Genet, 13(1), pp. 36–46. doi: 10.1038/NRG3117.

Trier, I. *et al.* (2023) 'ATR protects centromere identity by promoting DAXX association with PML nuclear bodies', *Cell Reports*. Cell Press, 42(5), p. 112495. doi: 10.1016/J.CELREP.2023.112495.

Trivigno, D. *et al.* (2013) 'Regulation of protein translation initiation in response to ionizing radiation', *Radiation Oncology*. BioMed Central, 8(1), pp. 1–12. doi: 10.1186/1748-717X-8-35/FIGURES/8.

Tuduri, S. *et al.* (2009) 'Topoisomerase I suppresses genomic instability by preventing interference between replication and transcription', *Nature cell biology*. Nat Cell Biol, 11(11), pp. 1315–1324. doi: 10.1038/NCB1984.

Turchick, A. *et al.* (2023) 'Selective inhibition of ATM-dependent double-strand break repair and checkpoint control synergistically enhances the efficacy of ATR inhibitors', *Molecular Cancer Therapeutics*. American Association for Cancer Research Inc., 22(7), pp. 859–872. doi: 10.1158/1535-7163.MCT-22-0685/726037/AM/SELECTIVE-INHIBITION-OF-ATM-DEPENDENT-DOUBLE.

Turton, D. (2014) 'The functional analysis of Upf1 in S-phase progression and genome stability', (January).

Uchiyama, M. and Wang, T. S.-F. (2004) 'The B-Subunit of DNA Polymerase  $\alpha$ -Primase Associates with the Origin Recognition Complex for Initiation of DNA Replication', *Molecular and Cellular Biology*. Taylor & Francis, 24(17), pp. 7419–7434. doi: 10.1128/MCB.24.17.7419-7434.2004.

Unterholzner, L. and Izaurralde, E. (2004) 'SMG7 Acts as a Molecular Link between mRNA Surveillance and mRNA Decay', *Molecular Cell*. Cell Press, 16(4), pp. 587–596. doi: 10.1016/J.MOLCEL.2004.10.013.

Usuki, F., Yamashita, A. and Fujimura, M. (2019) 'Environmental stresses suppress nonsense-mediated mRNA decay (NMD) and affect cells by stabilizing NMD-targeted gene expression', *Scientific Reports 2019 9:1*. Nature Publishing Group, 9(1), pp. 1–15. doi: 10.1038/s41598-018-38015-2.

Valenzisi, P. *et al.* (2024) 'WRNIP1 prevents transcription-associated genomic instability', *eLife*. eLife Sciences Publications Ltd, 13. doi: 10.7554/ELIFE.89981.

Valton, A. L. and Prioleau, M. N. (2016) 'G-Quadruplexes in DNA Replication: A Problem or a Necessity?', *Trends in Genetics*. Elsevier Ltd, 32(11), pp. 697–706. doi: 10.1016/J.TIG.2016.09.004/ASSET/9D21A987-E726-486B-A1D4-

FB5B18976747/MAIN.ASSETS/GR5.SML.

Vanoosthuyse, V. (2018) 'Strengths and Weaknesses of the Current Strategies to Map and Characterize R-Loops', *Non-Coding RNA 2018, Vol. 4, Page 9*. Multidisciplinary Digital Publishing Institute, 4(2), p. 9. doi: 10.3390/NCRNA4020009.

Voineagu, I. *et al.* (2009) 'Replisome stalling and stabilization at CGG repeats, which are responsible for chromosomal fragility', *Nature Structural & Molecular Biology 2009 16:2*. Nature Publishing Group, 16(2), pp. 226–228. doi: 10.1038/nsmb.1527.

Van Vugt, M. A. T. M. *et al.* (2010) 'A Mitotic Phosphorylation Feedback Network Connects Cdk1, Plk1, 53BP1, and Chk2 to Inactivate the G2/M DNA Damage Checkpoint', *PLOS Biology*. Public Library of Science, 8(1), p. e1000287. doi: 10.1371/JOURNAL.PBIO.1000287.

Wada, T. *et al.* (1998) 'DSIF, a novel transcription elongation factor that regulates RNA polymerase II processivity, is composed of human Spt4 and Spt5 homologs', *Genes & development*. Genes Dev, 12(3), pp. 343–356. doi: 10.1101/GAD.12.3.343.

Waga, S. and Stillman, B. (1998) 'The DNA replication fork in eukaryotic cells', *Annual review of biochemistry*. Annu Rev Biochem, 67, pp. 721–751. doi: 10.1146/ANNUREV.BIOCHEM.67.1.721.

Wahba, L. *et al.* (2011) 'RNase H and Multiple RNA Biogenesis Factors Cooperate to Prevent RNA:DNA Hybrids from Generating Genome Instability', *Molecular Cell*. Cell Press, 44(6), pp. 978–988. doi: 10.1016/J.MOLCEL.2011.10.017.

Wahba, L., Gore, S. K. and Koshland, D. (2013) 'The homologous recombination machinery modulates the formation of RNA-DNA hybrids and associated chromosome instability', *eLife*, 2013(2). doi: 10.7554/ELIFE.00505.

Wan, Y. *et al.* (2015) 'Splicing function of mitotic regulators links R-loop-mediated DNA damage to tumor cell killing', *Journal of Cell Biology*. The Rockefeller University Press, 209(2), pp. 235–246. doi: 10.1083/JCB.201409073.

Wang, I. X. *et al.* (2018) 'Human proteins that interact with RNA/DNA hybrids', *Genome Research*. Cold Spring Harbor Laboratory Press, 28(9), pp. 1405–1414. doi: 10.1101/GR.237362.118.

Wang, J. *et al.* (2021) 'Persistence of RNA transcription during DNA replication delays duplication of transcription start sites until G2/M', *Cell reports*. Cell Rep, 34(7). doi: 10.1016/J.CELREP.2021.108759.

Wang, Q. *et al.* (2011) 'G-quadruplex formation at the 3' end of telomere DNA inhibits its extension by telomerase, polymerase and unwinding by helicase', *Nucleic Acids*

*Research*. Oxford Academic, 39(14), pp. 6229–6237. doi: 10.1093/NAR/GKR164.

Wang, X. *et al.* (2020) 'Long noncoding RNA MACC1-AS1 promotes the stemness of non-small cell lung cancer cells through promoting UPF1-mediated destabilization of LATS1/2', *Environmental toxicology*. Environ Toxicol, 35(9), pp. 998–1006. doi: 10.1002/TOX.22936.

Wassing, I. E. *et al.* (2021) 'The RAD51 recombinase protects mitotic chromatin in human cells', *Nature Communications 2021 12:1*. Nature Publishing Group, 12(1), pp. 1–17. doi: 10.1038/s41467-021-25643-y.

Weng, Y., Czaplinski, K. and Peltz, S. W. (1996) 'Genetic and biochemical characterization of mutations in the ATPase and helicase regions of the Upf1 protein', *Molecular and Cellular Biology*. American Society for Microbiology, 16(10), pp. 5477–5490. doi: 10.1128/MCB.16.10.5477.

Whitfield, M. L. *et al.* (2000) 'Stem-loop binding protein, the protein that binds the 3' end of histone mRNA, is cell cycle regulated by both translational and posttranslational mechanisms', *Molecular and cellular biology*. Mol Cell Biol, 20(12), pp. 4188–4198. doi: 10.1128/MCB.20.12.4188-4198.2000.

Whitfield, M. L. *et al.* (2004) 'SLBP is associated with histone mRNA on polyribosomes as a component of the histone mRNP', *Nucleic Acids Research*. Oxford Academic, 32(16), pp. 4833–4842. doi: 10.1093/NAR/GKH798.

Williams, S. L. *et al.* (2023) 'Replication-induced DNA secondary structures drive fork uncoupling and breakage', *The EMBO Journal*. Springer Science and Business Media LLC, 42(22). doi: 10.15252/EMBJ.2023114334/SUPPL\_FILE/EMBJ2023114334-SUP-0004-TABLEEV2.XLSX.

Wilson, M. D. *et al.* (2013) 'Proteasome-Mediated Processing of Def1, a Critical Step in the Cellular Response to Transcription Stress', *Cell*. Cell Press, 154(5), pp. 983–995. doi: 10.1016/J.CELL.2013.07.028.

Wilson, T. E. *et al.* (2015) 'Large transcription units unify copy number variants and common fragile sites arising under replication stress', *Genome Research*. Cold Spring Harbor Laboratory Press, 25(2), pp. 189–200. doi: 10.1101/GR.177121.114.

Wittmann, J., Hol, E. M. and Jäck, H.-M. (2006) 'hUPF2 Silencing Identifies Physiologic Substrates of Mammalian Nonsense-Mediated mRNA Decay', *Molecular and Cellular Biology*. American Society for Microbiology, 26(4), pp. 1272–1287. doi: 10.1128/MCB.26.4.1272-1287.2006/SUPPL\_FILE/SUPPLEMENT\_FIGURE1\_WITTMANN\_ET\_AL.ZIP.

Wood, M. *et al.* (2020) 'TDP-43 dysfunction results in R-loop accumulation and DNA replication defects', *Journal of Cell Science*. Company of Biologists, 133(20). doi: 10.1242/JCS.244129.

Wu, C. *et al.* (2020) 'Poly(A)-Binding Protein Regulates the Efficiency of Translation Termination', *CellReports*, 33, p. 108399. doi: 10.1016/j.celrep.2020.108399.

Wu, W. *et al.* (2020) 'RTEL1 suppresses G-quadruplex-associated R-loops at difficult-to-replicate loci in the human genome', *Nature structural & molecular biology*. Nat Struct Mol Biol, 27(5), pp. 424–437. doi: 10.1038/S41594-020-0408-6.

Wu, W. *et al.* (2023) 'Mitotic DNA synthesis in response to replication stress requires the sequential action of DNA polymerases zeta and delta in human cells', *Nature Communications 2023 14:1*. Nature Publishing Group, 14(1), pp. 1–17. doi: 10.1038/s41467-023-35992-5.

Xiao, M. *et al.* (2022) 'Dual-functional significance of ATM-mediated phosphorylation of spindle assembly checkpoint component Bub3 in mitosis and the DNA damage response', *Journal of Biological Chemistry*. American Society for Biochemistry and Molecular Biology Inc., 298(3). doi: 10.1016/J.JBC.2022.101632/ATTACHMENT/94ED2CE6-9796-4868-AB7C-56AC2D955744/MMC1.PDF.

Yamada, T. *et al.* (2006) 'P-TEFb-mediated phosphorylation of hSpt5 C-terminal repeats is critical for processive transcription elongation', *Molecular cell*. Mol Cell, 21(2), pp. 227–237. doi: 10.1016/J.MOLCEL.2005.11.024.

Yamagishi, Y. *et al.* (2012) 'MPS1/Mph1 phosphorylates the kinetochore protein KNL1/Spc7 to recruit SAC components', *Nature cell biology*. Nat Cell Biol, 14(7), pp. 746–752. doi: 10.1038/NCB2515.

Yamaguchi, Y. *et al.* (1999) 'NELF, a multisubunit complex containing RD, cooperates with DSIF to repress RNA polymerase II elongation', *Cell*. Cell, 97(1), pp. 41–51. doi: 10.1016/S0092-8674(00)80713-8.

Yamamoto, T. M. *et al.* (2005) 'APC/C-Cdc20-mediated degradation of cyclin B participates in CSF arrest in unfertilized *Xenopus* eggs', *Developmental biology*. Dev Biol, 279(2), pp. 345–355. doi: 10.1016/J.YDBIO.2004.12.025.

Yang, Y. *et al.* (2024) 'Transcription and DNA replication collisions lead to large tandem duplications and expose targetable therapeutic vulnerabilities in cancer', *Nature Cancer 2024 5:12*. Nature Publishing Group, 5(12), pp. 1885–1901. doi: 10.1038/s43018-024-00848-4.

- Ye, B. J. *et al.* (2021) 'PARP1-mediated PARylation of TonEBP prevents R-loop-associated DNA damage', *DNA Repair*. Elsevier, 104, p. 103132. doi: 10.1016/J.DNAREP.2021.103132.
- Yeeles, J. T. P. *et al.* (2017) 'How the Eukaryotic Replisome Achieves Rapid and Efficient DNA Replication', *Molecular Cell*. Cell Press, 65(1), p. 105. doi: 10.1016/J.MOLCEL.2016.11.017.
- Yesbolatova, A. *et al.* (2020) 'The auxin-inducible degron 2 technology provides sharp degradation control in yeast, mammalian cells, and mice', *Nature Communications* 2020 11:1. Nature Publishing Group, 11(1), pp. 1–13. doi: 10.1038/s41467-020-19532-z.
- Ying, S. *et al.* (2013) 'MUS81 promotes common fragile site expression', *Nature Cell Biology* 2013 15:8. Nature Publishing Group, 15(8), pp. 1001–1007. doi: 10.1038/ncb2773.
- Yu, K. *et al.* (2003) 'R-loops at immunoglobulin class switch regions in the chromosomes of stimulated B cells', *Nature Immunology* 2003 4:5. Nature Publishing Group, 4(5), pp. 442–451. doi: 10.1038/ni919.
- Yuan, H. *et al.* (2025) 'LINC00626 drives tamoxifen resistance in breast cancer cells by interaction with UPF1', *Scientific Reports* 2025 15:1. Nature Publishing Group, 15(1), pp. 1–17. doi: 10.1038/s41598-025-86287-2.
- Yuan, Z. *et al.* (2016) 'Structure of the eukaryotic replicative CMG helicase suggests a pumpjack motion for translocation', *Nature Structural & Molecular Biology* 2016 23:3. Nature Publishing Group, 23(3), pp. 217–224. doi: 10.1038/nsmb.3170.
- Zellweger, R. *et al.* (2015) 'Rad51-mediated replication fork reversal is a global response to genotoxic treatments in human cells', *The Journal of cell biology*. J Cell Biol, 208(5), pp. 563–579. doi: 10.1083/JCB.201406099.
- Zhai, Y. and Tye, B. K. (2017) 'Structure of the MCM2-7 Double Hexamer and Its Implications for the Mechanistic Functions of the Mcm2-7 Complex', *Advances in Experimental Medicine and Biology*. Springer, Singapore, 1042, pp. 189–205. doi: 10.1007/978-981-10-6955-0\_9.
- Zhang, H. and Freudenreich, C. H. (2007) 'An AT-Rich Sequence in Human Common Fragile Site FRA16D Causes Fork Stalling and Chromosome Breakage in *S. cerevisiae*', *Molecular Cell*. Cell Press, 27(3), pp. 367–379. doi: 10.1016/J.MOLCEL.2007.06.012.
- Zhang, Z. *et al.* (2016) 'Rapid dynamics of general transcription factor TFIIB binding

during preinitiation complex assembly revealed by single-molecule analysis', *Genes & development*. *Genes Dev*, 30(18), pp. 2106–2118. doi: 10.1101/GAD.285395.116.

Zheng, L. *et al.* (2003) 'Phosphorylation of stem-loop binding protein (SLBP) on two threonines triggers degradation of SLBP, the sole cell cycle-regulated factor required for regulation of histone mRNA processing, at the end of S phase', *Molecular and cellular biology*. *Mol Cell Biol*, 23(5), pp. 1590–1601. doi: 10.1128/MCB.23.5.1590-1601.2003.

Zhou, Y. *et al.* (2019) 'UPF1 inhibits the hepatocellular carcinoma progression by targeting long non-coding RNA UCA1', *Scientific Reports 2019 9:1*. Nature Publishing Group, 9(1), pp. 1–8. doi: 10.1038/s41598-019-43148-z.

# Appendix

(A)	Untreated			1 $\mu$ M Carboplatin		
	SiCtrl	SiUPF1	SiUPF2	SiCtrl	SiUPF1	SiUPF2
UT SiCtrl		0.8712	0.4851	<0.0001	0.8153	0.8836
UT SiUPF1			0.9749	<0.0001	>0.9999	>0.9999
UT SiUPF2				<0.0001	0.9891	0.9700
1 $\mu$ M Carboplatin SiCtrl					<0.0001	<0.0001
1 $\mu$ M Carboplatin SiUPF1						>0.9999

(B)	Untreated			1 $\mu$ M Carboplatin		
	SiCtrl	SiUPF3b	SiSTAU1	SiCtrl	SiUPF3b	SiSTAU1
UT SiCtrl		>0.9999	0.9547	0.0023	0.0059	0.0005
UT SiUPF3b			0.8954	0.0016	0.0042	0.0004
UT SiSTAU1				0.0089	0.0241	0.0017
1 $\mu$ M Carboplatin SiCtrl					0.9897	0.9026
1 $\mu$ M Carboplatin SiUPF3b						0.6073

Figure A1: Table of p-values for One-way ANOVA analysis of live cell microscopy in Figure 3.2.2.

(C)	Untreated					1 $\mu$ M Carboplatin				
	SiCtrl	SiSMG1	SiSMG5	SiSMG6	SiUPF1/ SiSMG6	SiCtrl	SiSMG1	SiSMG5	SiSMG6	SiUPF1/ SiSMG6
UT SiCtrl		0.0027	>0.9999	0.0002	0.8839	0.0012	0.0037	0.0003	<0.0001	0.9911
UT SiSMG1			0.0076	<0.0001	0.0640	<0.0001	>0.9999	<0.0001	<0.0001	0.0222
UT SiSMG5				<0.0001	0.9881	0.0004	0.0105	0.0001	<0.0001	>0.9999
UT SiSMG6					<0.0001	0.9911	<0.0001	>0.9999	0.9984	<0.0001
UT SiUPF1/SiSMG6						<0.0001	0.0849	<0.0001	<0.0001	>0.9999
1 $\mu$ m Carboplatin SiCtrl							<0.0001	0.9997	0.7674	0.0002
1 $\mu$ M Carboplatin SiSMG1								<0.0001	<0.0001	0.0300
1 $\mu$ M Carboplatin SiSMG5									0.9775	<0.0001
1 $\mu$ M Carboplatin SiSMG6										<0.0001

(D)	Untreated		1 $\mu$ M Carboplatin	
	SiCtrl	SiBubR1	SiCtrl	SiBubR1
UT SiCtrl		<0.0001	<0.0001	<0.0001
UT SiBubR1			<0.0001	0.0673
1 $\mu$ M Carboplatin SiCtrl				<0.0001
1 $\mu$ M Carboplatin SiBubR1				

Figure A2: Table of p-values for One-way ANOVA analysis of live cell microscopy in Figure 3.2.2 continued.

Condition			Untreated								1µM Carboplatin							
UPF1 Variant			WT		R843C		S42A		S42E		WT		R843C		S42A		S42E	
SiRNA			C	U	C	U	C	U	C	U	C	U	C	U	C	U	C	U
Untreated	WT	C	>0.9999	>0.9999	>0.9999	>0.9999	0.9995	>0.9999	>0.9999	<0.0001	>0.9999	<0.0001	0.9987	<0.0001	>0.9999	<0.0001	>0.9999	
		U		>0.9999	>0.9999	>0.9999	0.9991	>0.9999	>0.9999	<0.0001	>0.9999	<0.0001	0.9978	<0.0001	>0.9999	<0.0001	>0.9999	
	R843C	C			>0.9999	>0.9999	>0.9999	0.9999	>0.9999	<0.0001	>0.9999	<0.0001	>0.9999	<0.0001	>0.9999	<0.0001	>0.9999	
		U				>0.9999	0.9996	>0.9999	>0.9999	<0.0001	>0.9999	<0.0001	0.9991	<0.0001	>0.9999	<0.0001	>0.9999	
	S42A	C					>0.9999	0.9931	>0.9999	<0.0001	0.9993	<0.0001	>0.9999	<0.0001	>0.9999	<0.0001	0.9944	
		U						0.9749	0.9991	0.0001	0.9955	<0.0001	>0.9999	<0.0001	0.9993	<0.0001	0.9787	
	S42E	C							>0.9999	<0.0001	>0.9999	<0.0001	0.9607	<0.0001	>0.9999	<0.0001	>0.9999	
		U								<0.0001	>0.9999	<0.0001	0.9978	<0.0001	>0.9999	<0.0001	>0.9999	
	1µM Carboplatin	WT	C								<0.0001	>0.9999	0.0001	0.9413	<0.0001	0.9983	<0.0001	
			U									<0.0001	0.9915	<0.0001	>0.9999	<0.0001	>0.9999	
R843C		C										<0.0001	0.9896	<0.0001	>0.9999	<0.0001		
		U											<0.0001	0.9983	<0.0001	0.9660		
S42A		C												<0.0001	>0.9999	<0.0001		
		U													<0.0001	>0.9999		
S42E		C														<0.0001		

Figure A3: Table of p-values for One-way ANOVA analysis of live cell microscopy in Figure 3.2.3C.

Condition			Untreated								1µM Carboplatin							
UPF1 Variant			WT		R843C		S42A		S42E		WT		R843C		S42A		S42E	
SiRNA			C	U	C	U	C	U	C	U	C	U	C	U	C	U	C	U
Untreated	WT	C	>0.9999	0.9981	0.9944	<0.0001	0.0005	0.9896	0.9896	0.0271	0.0044	0.0049	0.9966	0.0004	0.0008	0.0033	0.9934	
		U		>0.9999	0.9996	<0.0001	0.0002	0.9990	0.9990	0.0135	0.0021	0.0023	0.9998	0.0002	0.0004	0.0016	0.9995	
	R843C	C			>0.9999	<0.0001	<0.0001	>0.9999	>0.9999	0.0013	0.0002	0.0002	>0.9999	<0.0001	<0.0001	0.0001	>0.9999	
		U				<0.0001	<0.0001	>0.9999	>0.9999	0.0009	0.0001	0.0001	>0.9999	<0.0001	<0.0001	<0.0001	>0.9999	
	S42A	C					>0.9999	<0.0001	<0.0001	0.7537	0.9862	0.9819	<0.0001	>0.9999	>0.9999	0.9934	<0.0001	
		U						<0.0001	<0.0001	0.9738	>0.9999	>0.9999	<0.0001	>0.9999	>0.9999	>0.9999	<0.0001	
	S42E	C							>0.9999	0.0007	0.0001	0.0001	>0.9999	<0.0001	<0.0001	<0.0001	>0.9999	
		U								0.0007	0.0001	0.0001	>0.9999	<0.0001	<0.0001	<0.0001	>0.9999	
	1µM Carboplatin	WT	C									>0.9999	>0.9999	0.0011	0.9591	0.9910	>0.9999	0.0009
			U										>0.9999	0.0002	0.9999	>0.9999	>0.9999	0.0001
		R843C	C											0.0002	0.9998	>0.9999	>0.9999	0.0001
			U												<0.0001	<0.0001	0.0001	>0.9999
S42A		C													>0.9999	>0.9999	<0.0001	
		U														>0.9999	<0.0001	
S42E		C															<0.0001	

Figure A4: Table of p-values for One-way ANOVA analysis of live cell microscopy in Figure 3.2.3D.

Condition			Untreated						1 $\mu$ M Carboplatin					
Inhibitor			VC		ATRi		ATMi		VC		ATRi		ATMi	
SiRNA			C	U	C	U	C	U	C	U	C	U	C	U
Untreated	VC	C	>0.9999	<0.0001	>0.9999	0.5799	0.2224	0.0038	>0.9999	0.0001	>0.9999	<0.0001	0.2401	
		U		<0.0001	>0.9999	0.5331	0.1951	0.0032	<0.9999	<0.0001	>0.9999	<0.0001	0.2112	
	ATRi	C			0.0002	0.0135	0.0605	0.8776	<0.0001	>0.9999	<0.0001	0.2167	0.0550	
		U				0.8384	0.4425	0.0110	0.9989	0.0003	>0.9999	<0.0001	0.4691	
	ATMi	C						>0.9999	0.3590	0.3357	0.0191	0.5892	<0.0001	>0.9999
		U						0.7611	0.1019	0.0825	0.2282	<0.0001	>0.9999	
1 $\mu$ M Carboplatin	VC	C							0.0014	0.9294	0.0040	0.0065	0.7356	
		U								<0.0001	>0.9999	<0.0001	0.1113	
	ATRi	C									0.0001	0.1659	0.0752	
		U										<0.0001	0.2462	
	ATMi	C											<0.0001	
		U												<0.0001

Figure A5: Table of p-values for One-way ANOVA analysis of live cell microscopy in Figure 3.2.5B.

(C)			Untreated				1 $\mu$ M Carboplatin			
			RNaseH1 <sup>D210N</sup>		RNaseH1 <sup>WT</sup>		RNaseH1 <sup>D210N</sup>		RNaseH1 <sup>WT</sup>	
			SiCtrl	SiSUPF1	SiCtrl	SiSUPF1	SiCtrl	SiSUPF1	SiCtrl	SiSUPF1
Untreated	D210N	SiCtrl	0.9997	>0.9999	0.9626	<0.0001	0.6969	0.9985	0.9813	
		SiUPF1		0.9951	0.9989	<0.0001	0.9155	>0.9999	0.9998	
	WT	SiCtrl			0.8942	<0.0001	0.5497	0.9875	0.9340	
		SiUPF1				<0.0001	0.9972	0.9998	>0.9999	
Carboplatin	D210N	SiCtrl					<0.0001	<0.0001	<0.0001	
		SiUPF1						0.9497	0.9920	
	WT	SiCtrl							>0.9999	

Figure A6: Table of p-values for One-way ANOVA analysis of live cell microscopy in Figure 3.2.6A.

			Untreated				1 $\mu$ M Carboplatin			
			VC		2 $\mu$ g/ml Amanitin		VC		2 $\mu$ g/ml Amanitin	
			SiCtrl	SiSUPF1	SiCtrl	SiSUPF1	SiCtrl	SiSUPF1	SiCtrl	SiSUPF1
Untreated	VC	SiCtrl		>0.9999	>0.9999	>0.9999	<0.0001	>0.9999	0.1487	>0.9999
		SiUPF1			0.9973	>0.9999	<0.0001	>0.9999	0.0893	>0.9999
	Amanitin	SiCtrl				>0.9999	0.0004	0.9952	0.7895	>0.9999
		SiUPF1					0.0001	>0.9999	0.3640	>0.9999
Carboplatin	VC	SiCtrl					<0.0001	0.0286	<0.0001	
		SiUPF1						0.0792	>0.9999	
	Amanitin	SiCtrl							0.2246	

Figure A7: Table of p-values for One-way ANOVA analysis of live cell microscopy in Figure 3.2.6B.

			Untreated				1 $\mu$ M Carboplatin			
			$\alpha$ -Amanitin		RNaseH1		$\alpha$ -Amanitin		RNaseH1	
			-	+	D210N	WT	-	+	D210N	WT
Untreated	$\alpha$ -Amanitin	-		>0.9999	0.9991	>0.9999	0.0030	>0.9999	0.0008	0.9999
		+			0.9784	0.9964	0.0014	0.9981	0.0004	0.9915
	RNaseH1	D210N				>0.9999	0.0086	>0.9999	0.0021	>0.9999
		WT					0.0053	>0.9999	0.0013	>0.9999
Carboplatin	$\alpha$ -Amanitin	-					0.0046	0.9951	0.0065	
		+						0.0012	>0.9999	
	RNaseH1	D210N							0.0016	

Figure A8: Table of p-values for One-way ANOVA analysis of live cell microscopy in Figure 3.2.7A.

			Untreated				1 $\mu$ M Carboplatin			
			$\alpha$ -Amanitin		RNaseH1		$\alpha$ -Amanitin		RNaseH1	
			-	+	D210N	WT	-	+	D210N	WT
Untreated	$\alpha$ -Amanitin	-	0.0001	0.0409	0.0003	>0.9999	0.0003	0.6776	0.0002	
		+		<0.0001	0.9975	<0.0001	0.9992	<0.0001	>0.9999	
	RNaseH1	D210N			<0.0001	0.0675	<0.0001	0.5983	<0.0001	
		WT				0.0002	>0.9999	<0.0001	>0.9999	
Carboplatin	$\alpha$ -Amanitin	-					0.0002	0.8221	0.0001	
		+						<0.0001	>0.9999	
	RNaseH1	D210N							<0.0001	

Figure A9: Table of p-values for One-way ANOVA analysis of live cell microscopy in Figure 3.2.7B.

			Untreated				1 $\mu$ M Carboplatin			
			$\alpha$ -Amanitin		RNaseH1		$\alpha$ -Amanitin		RNaseH1	
			-	+	D210N	WT	-	+	D210N	WT
Untreated	$\alpha$ -Amanitin	-	0.0121	0.9772	0.0048	0.8130	0.0093	>0.9999	0.0039	
		+		0.0044	0.9863	0.0025	>0.9999	0.0121	0.9593	
	RNaseH1	D210N			0.0019	0.9987	0.0035	0.9772	0.0016	
		WT				0.0011	0.9980	0.0048	>0.9999	
Carboplatin	$\alpha$ -Amanitin	-					0.0020	0.8130	0.0009	
		+						0.0093	0.9897	
	RNaseH1	D210N							0.0039	

Figure A10: Table of p-values for One-way ANOVA analysis of live cell microscopy in Figure 3.2.7C.

G1		RPE <sup>WT</sup>			RPE <sup>UPF1 KO</sup>		
		Untreated	4hrs 0.4μM Aphidicolin	24hrs 0.4μM Aphidicolin	Untreated	4hrs 0.4μM Aphidicolin	24hrs 0.4μM Aphidicolin
RPE <sup>WT</sup>	Untreated		>0.9999	0.0005	0.8125	0.2287	0.0906
	4hrs 0.4μM Aphidicolin			0.0004	0.8853	0.2900	0.0688
	24hrs 0.4μM Aphidicolin				<0.0001	<0.0001	0.0643
RPE <sup>UPF1 KO</sup>	Untreated					0.8428	0.0114
	4hrs 0.4μM Aphidicolin						0.0017

Figure A11: Table of p-values for One-way ANOVA analysis of G1 population changes in Figure 4.2.7.

Early S-Phase		RPE <sup>WT</sup>			RPE <sup>UPF1 KO</sup>		
		Untreated	4hrs 0.4μM Aphidicolin	24hrs 0.4μM Aphidicolin	Untreated	4hrs 0.4μM Aphidicolin	24hrs 0.4μM Aphidicolin
RPE <sup>WT</sup>	Untreated		0.0900	0.9192	0.5263	0.9975	0.8010
	4hrs 0.4μM Aphidicolin			0.0177	0.0048	0.0437	0.5305
	24hrs 0.4μM Aphidicolin				0.9652	0.9935	0.2935
RPE <sup>UPF1 KO</sup>	Untreated					0.7708	0.0889
	4hrs 0.4μM Aphidicolin						0.5600

Figure A12: Table of p-values for One-way ANOVA analysis of Early S-phase population changes in Figure 4.2.7.

Mid-Late S-Phase		RPE <sup>WT</sup>			RPE <sup>UPF1 KO</sup>		
		Untreated	4hrs 0.4μM Aphidicolin	24hrs 0.4μM Aphidicolin	Untreated	4hrs 0.4μM Aphidicolin	24hrs 0.4μM Aphidicolin
RPE <sup>WT</sup>	Untreated		>0.9999	0.1037	0.9464	0.7544	0.1988
	4hrs 0.4μM Aphidicolin			0.0807	0.9760	0.8315	0.1572
	24hrs 0.4μM Aphidicolin				0.0243	0.0109	0.9979
RPE <sup>UPF1 KO</sup>	Untreated					0.9962	0.0490
	4hrs 0.4μM Aphidicolin						0.0219

Figure A13: Table of p-values for One-way ANOVA analysis of Mid-Late S-phase population changes in Figure 4.2.7.

G2		RPE <sup>WT</sup>			RPE <sup>UPF1 KO</sup>		
		Untreated	4hrs 0.4μM Aphidicolin	24hrs 0.4μM Aphidicolin	Untreated	4hrs 0.4μM Aphidicolin	24hrs 0.4μM Aphidicolin
RPE <sup>WT</sup>	Untreated		0.0258	<0.0001	>0.9999	0.1647	>0.9999
	4hrs 0.4μM Aphidicolin			<0.0001	0.0267	0.8604	0.0366
	24hrs 0.4μM Aphidicolin				<0.0001	<0.0001	<0.0001
RPE <sup>UPF1 KO</sup>	Untreated					0.1698	>0.9999
	4hrs 0.4μM Aphidicolin						0.2250

Figure A14: Table of p-values for One-way ANOVA analysis of G2 population changes in Figure 4.2.7.

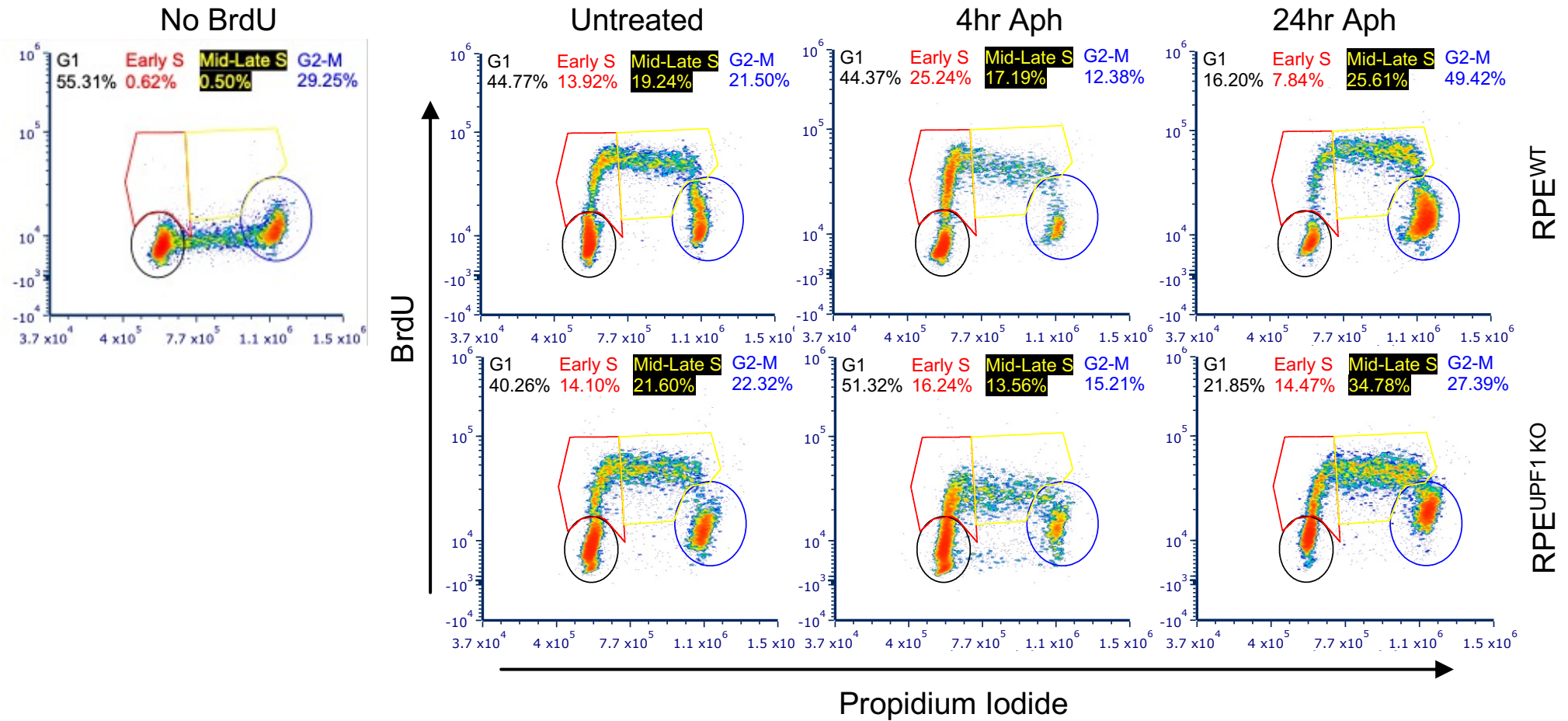


**Figure A15: FACS Gating for Figure 4.2.7.**

Representative FACS plots for Propidium Iodide staining vs BrdU staining in RPE<sup>WT</sup> and RPE<sup>UPF1 KO</sup> cells treated without and with 0.4 $\mu$ M aphidicolin for 4hrs or 24hrs. Gating examples can be seen on all plots. A negative control of cells not incubated with BrdU was used to define non-S-Phase populations.

$\gamma$ -H2AX (S139)		RPE <sup>WT</sup>				RPE <sup>UPF1 KO</sup>			
		Untreated	100 $\mu$ M DRB	0.4 $\mu$ M Aphidicolin	0.4 $\mu$ M Aphidicolin + 100 $\mu$ M DRB	Untreated	100 $\mu$ M DRB	0.4 $\mu$ M Aphidicolin	0.4 $\mu$ M Aphidicolin + 100 $\mu$ M DRB
RPE <sup>WT</sup>	Untreated		0.9626	0.9699	>0.9999	0.0097	0.7584	0.0004	0.0156
	100 $\mu$ M DRB			0.5015	0.9695	0.0013	0.2240	<0.0001	0.0021
	0.4 $\mu$ M Aphidicolin				0.9632	0.0644	0.9986	0.0023	0.0998
	0.4 $\mu$ M Aphidicolin + 100 $\mu$ M DRB					0.0090	0.7371	0.0003	0.0144
RPE <sup>UPF1 KO</sup>	Untreated					0.1800	0.6677	>0.9999	
	100 $\mu$ M DRB						0.0071	0.2634	
	0.4 $\mu$ M Aphidicolin							0.5247	

Figure A16: Table of p-values for One-way ANOVA analysis of  $\gamma$ -H2AX protein changes in Figure 4.2.10.

Phospho-Chk1 (Ser345)		RPE <sup>WT</sup>				RPE <sup>UPF1 KO</sup>			
		Untreated	100 $\mu$ M DRB	0.4 $\mu$ M Aphidicolin	0.4 $\mu$ M Aphidicolin + 100 $\mu$ M DRB	Untreated	100 $\mu$ M DRB	0.4 $\mu$ M Aphidicolin	0.4 $\mu$ M Aphidicolin + 100 $\mu$ M DRB
RPE <sup>WT</sup>	Untreated		0.9996	0.0082	0.1855	>0.9999	>0.9999	0.0282	0.3656
	100 $\mu$ M DRB			0.0049	0.1041	>0.9999	>0.9999	0.0162	0.2134
	0.4 $\mu$ M Aphidicolin				0.2991	0.0060	0.0055	0.9519	0.1488
	0.4 $\mu$ M Aphidicolin + 100 $\mu$ M DRB					0.1296	0.1192	0.7963	0.9984
RPE <sup>UPF1 KO</sup>	Untreated						>0.9999	0.0199	0.2629
	100 $\mu$ M DRB							0.0184	0.2428
	0.4 $\mu$ M Aphidicolin								0.5047

Figure A17: Table of p-values for One-way ANOVA analysis of P-Chk1 (Ser345) protein changes in Figure 4.2.10.

Phospho-RNAPII CTD (Ser2)		RPE <sup>WT</sup>				RPE <sup>UPF1 KO</sup>			
		Untreated	100 $\mu$ M DRB	0.4 $\mu$ M Aphidicolin	0.4 $\mu$ M Aphidicolin + 100 $\mu$ M DRB	Untreated	100 $\mu$ M DRB	0.4 $\mu$ M Aphidicolin	0.4 $\mu$ M Aphidicolin + 100 $\mu$ M DRB
RPE <sup>WT</sup>	Untreated		0.0001	0.5540	<0.0001	0.0030	<0.0001	0.0014	<0.0001
	100 $\mu$ M DRB			0.0049	0.2895	0.7046	0.1414	0.8926	0.0482
	0.4 $\mu$ M Aphidicolin				<0.0001	0.1164	<0.0001	0.0578	<0.0001
	0.4 $\mu$ M Aphidicolin + 100 $\mu$ M DRB					0.0146	0.9997	0.0309	0.9589
RPE <sup>UPF1 KO</sup>	Untreated						0.0061	>0.9999	0.0019
	100 $\mu$ M DRB							0.0129	0.9984
	0.4 $\mu$ M Aphidicolin								0.0040

Figure A18: Table of p-values for One-way ANOVA analysis of P-RNAPII CTD (Ser2) protein changes in Figure 4.2.10.